STATUS OF THESIS

Title of thesis: DEVELOPMENT OF POLYETHERETHERKETONE/MULTIWALLED CARBON NANOTUBES NANOCOMPOSITES WITH DIFFERENT IONIC LIQUIDS FOR HUMAN BONE TRANSPLANTATION

I AQEEL AHMAD

hereby allow my thesis to be placed at the Information Resource Center (IRC) of Universiti Teknologi PETRONAS (UTP) with the following conditions:

1. The thesis becomes the property of UTP
2. The IRC of UTP may make copies of the thesis for academic purposes only.
3. This thesis is classified as

☐ Confidential

☑ Non-confidential

If this thesis is confidential, please state the reason:

The contents of the thesis will remain confidential for ___________ years.

Remarks on disclosure:

Endorsed by

Aqeel Ahmad

Signature of Author

Moniruzzaman

Dr. MUHAMMAD MONIRUZZAMAN
Associate Professor
Chemical Engineering Department
Universiti Teknologi PETRONAS

Signature of Supervisor

Permanent address: Khan town, Mohallah
Sharif Pura, Kamoke, Gujranwala, Punjab,
Pakistan

Name of Supervisor
AP Dr Muhammad Moniruzzaman

Date : 01-07-2022

Date : 14/7/2022

UNIVERSITI TEKNOLOGI PETRONAS

DEVELOPMENT OF POLYETHERETHERKETONE/MULTIWALLED CARBON NANOTUBES NANOCOMPOSITES WITH DIFFERENT IONIC LIQUIDS FOR HUMAN BONE TRANSPLANTATION

by

AQEEL AHMAD

The undersigned certify that they have read, and recommend to the Postgraduate Studies Programme for acceptance this thesis for the fulfillment of the requirements for the degree stated.

Signature: Moniruzzaman
Dr. MUHAMMAD MONIRUZZAMAN
Associate Professor
Chemical Engineering Department
Universiti Teknologi PETRONAS
14/7/2022

Main Supervisor: Assoc. Prof. Dr Muhammad Moniruzzaman

Signature: 15.07.2022

Co-Supervisor: Assoc. Prof. Dr Nurlidia Mansor

Signature:

Head of Department: Assoc. Prof. Ir Dr Abd Halim Shah bin Maulud

Date: 15/7/2022

DEVELOPMENT OF POLYETHERETHERKETONE/MULTIWALLED CARBON NANOTUBES NANOCOMPOSITES WITH DIFFERENT IONIC LIQUIDS FOR HUMAN BONE TRANSPLANTATION

by

AQEEL AHMAD

A Thesis

Submitted to the Postgraduate Studies Programme

as a Requirement for the Degree of

DOCTOR OF PHILOSOPHY

CHEMICAL ENGINEERING

UNIVERSITI TEKNOLOGI PETRONAS

BANDAR SERI ISKANDAR,

PERAK

JULY 2022

DECLARATION OF THESIS

Title of thesis DEVELOPMENT OF POLYETHERETHERKETONE/MULTIWALLED CARBON NANOTUBES NANOCOMPOSITES WITH DIFFERENT IONIC LIQUIDS FOR HUMAN BONE TRANSPLANTATION

I AQEEL AHMAD

hereby declare that the thesis is based on my original work except for quotations and citations which have been duly acknowledged. I also declare that it has not been previously or concurrently submitted for any other degree at UTP or other institutions.

Witnessed by

Aqeel Ahmad

Signature of Author

Moniruzzaman
Dr. MUHAMMAD MONIRUZZAMAN
Associate Professor
Chemical Engineering Department
Universiti Teknologi PETRONAS

Signature of Supervisor

Permanent address: Khan town, near masjid
Ayesha, Kamoke, Gujranwala, Punjab,
Pakistan

Name of Supervisor
AP Dr Muhammad Moniruzzaman

Date : 01-07-2022

Date : 14/7/2022

DEDICATION

To my beloved Parents,

Sister and Brothers.

ACKNOWLEDGEMENTS

"In The Name of ALLAH, The Most Beneficent, The Most Merciful"

All praises and thanks to ALLAH, the Most Beneficent, the Most Merciful, and His countless blessings be upon His Prophet Muhammad (PBUH). Without His help, it would have been impossible to complete this project and compile this thesis.

I would like to express my heartfelt appreciation and gratitude to my research supervisor, Assoc. Prof. Dr Muhammad Moniruzzaman, for providing me with the opportunity to work with his research team at the Centre for Research in Ionic Liquids (CORIL), as well as for his sincere guidance, advice, support, and encouragement throughout this research work. I would like to thank my co-supervisor, Assoc. Prof. Dr Nurlidia Bt Mansor, for her attention and assistance in my research project. She had always been eager to listen and resolve the issues throughout this research project. I would definitely feel an honour to thank my field supervisors, Prof. Dr Tanveer Iqbal and Assoc. Prof Dr Hamayoun Mahmood for their help in conducting experiments in their research lab (Pakistan), valuable suggestions and comments. Particularly, for their help and technical guidance for the preparation of polymer composites.

I wish to extend my appreciation to all the staff of chemical engineering department for their technical and moral helps during my postgraduate studies. I would like to acknowledge the financial support and research facilities provided by Universiti Teknologi PETRONAS (UTP) and Higher Education Commission, Pakistan. I would like to thank all my friends, Dr Zia ul Mustafa, Dr Waqas Yaqub, Dr Rizwan Safdar, Sajid Mumtaz, Muhammad Nawaz, and Dr Mansoor ul Hassan, for their love and motivation which enabled me to boost up my confidence level for achieving this goal.

Finally, I would like to thank my family members and friends for their continuous support, encouragement, love and faith in me, which helped me to accomplish my graduate studies within stipulated time frame and their prayers for my success.

ABSTRACT

Polyetheretherketone (PEEK) is a high-performance semicrystalline thermoplastic polymer with excellent chemical and thermal stability that has been widely used in the biomedical field as a substitute for human cortical bone. However, low bioactivity and weak mechanical properties restrict the use of PEEK in orthopedic implants. Reinforcement of PEEK by nanoparticles such as hydroxyapatite (HA) and multiwalled carbon nanotubes (MWCNTs), is a technique that has the potential to prepare PEEK composites with enhanced properties. Nevertheless, the homogenous dispersion of MWCNTs in the polymer matrix is a primary processing challenge. The present study reports an environmentally friendly approach for homogeneous MWCNTs dispersion in PEEK composites by using ionic liquids (ILs) with different loadings via melt-blending and compression molding techniques. To examine the effect of ILs on PEEK composites, optical microscope, FESEM, DSC, TGA, nanoindenter and UTM analysis were performed. Moreover, the effect of HA on biological properties, and thermal degradation kinetics of PEEK composites were also explained. ILs provoked a uniform MWCNTs dispersion in PEEK, as confirmed by FESEM and optical micrographs. The thermal properties including decomposition temperature and percentage crystallinity of PEEK composites with the employed ILs were enhanced. PEEK composites containing 1 wt% of 1-butyl-3-methylimidazolium hydrogen sulphate ([BMIM]HSO_4) exhibited 37 % and 6.33 % increase in elastic modulus and tensile strength, respectively. The Alamar blue assay investigation confirmed that inclusion of HA to PEEK composites improved the cells viability (more than 80 %). Also, the effectiveness of PEEK composites with and without ILs was modelled using Coats-Redfern, Broido and Horowitz-Metzger models, and it was discovered that a 3-8 % rise in the activation energy of ILs treated composites was found. The considerable improvements indicated that ILs-based approaches could be a novel, green, and promising processing method for uniform MWCNTs dispersion in PEEK for prospective biological applications.

ABSTRAK

Polyetheretherketone (PEEK) ialah polimer termoplastik semikristalin berprestasi tinggi dengan kestabilan kimia dan haba yang sangat baik yang telah digunakan secara meluas dalam bidang bioperubatan sebagai pengganti tulang kortikal manusia. Walau bagaimanapun, kurangnya bioaktiviti yang rendah serta sifat mekanikal yang lemah menyekat penggunaan PEEK dalam implan ortopedik. Pengukuhan PEEK oleh nanopartikel seperti hidroksiapatit (HA) dan tiub nano karbon berbilang dinding (MWCNTs), adalah satu teknik yang berpotensi untuk menyediakan komposit PEEK dengan sifat yang dipertingkatkan. Meskipun demikian, penyebaran homogen MWCNT dalam matriks polimer adalah cabaran pemprosesan yang utama. Kajian ini melaporkan pendekatan yang mesra alam sekitar untuk penyebaran MWCNT homogen dalam komposit PEEK dengan menggunakan cecair ionik (IL) dengan beban yang berbeza melalui teknik pengacuan leburan dan mampatan. Untuk mengkaji kesan IL pada komposit PEEK, mikroskop optik, FESEM, DSC, TGA, nanoindenter dan analisis UTM telah dilakukan. Selain itu, kesan HA ke atas sifat biologi, dan kinetik degradasi haba komposit PEEK turut dijelaskan. IL mencetuskan penyebaran MWCNT yang seragam dalam PEEK, seperti yang disahkan oleh FESEM dan mikrograf optik. Sifat terma termasuk suhu penguraian dan peratusan kehabluran komposit PEEK dengan IL yang digunakan telah dipertingkatkan. Komposit PEEK yang mengandungi 1% berat 1-butil-3-methylimidazolium hidrogen sulfat ([BMIM]HSO_4) masing-masing menunjukkan peningkatan 37 % dan 6.33 % dalam modulus elastik dan kekuatan tegangan. Siasatan ujian biru Alamar mengesahkan bahawa kemasukan HA ke komposit PEEK meningkatkan daya maju sel (lebih daripada 80%). Selain itu, keberkesanan komposit PEEK dengan dan tanpa IL telah dimodelkan menggunakan model Coats-Redfern, Broido dan Horowitz-Metzger, dan didapati bahawa peningkatan 3-8% dalam tenaga pengaktifan komposit yang dirawat IL telah ditemui. Penambahbaikan yang ketara menunjukkan bahawa pendekatan berasaskan IL boleh menjadi kaedah pemprosesan yang baru, hijau, dan menjanjikan penyebaran MWCNT seragam dalam PEEK untuk aplikasi biologi prospektif.

TABLE OF CONTENT

ABSTRACT vii
ABSTRAK viii
LIST OF FIGURES xiv
LIST OF TABLES xviii
LIST OF ABBREVIATIONS xx
CHAPTER 1 INTRODUCTION 1
  1.1 Overview 1
  1.2 Background 1
  1.3 Problem Statement 4
  1.4 Research Objectives 6
  1.5 Hypothesis 6
  1.6 Scope of research 7
  1.7 Thesis outline 8
  1.8 Summary 9
CHAPTER 2 LITERATURE REVIEW 10
  2.1 Overview 10
  2.2 Polyetheretherketone (PEEK) 10
  2.3 Motivation for use of PEEK in composite preparation 12
  2.4 Current methods to promote PEEK bioactivity 13
    2.4.1 Surface modification 13
      2.4.1.1 Physical Treatment 14
      2.4.1.2 Chemical Treatment 15
    2.4.2 Surface coatings 18
    2.4.3 Bioactive PEEK composites 21
      2.4.3.1 PEEK/HA composites with nano-sized fillers 26
  2.5 Carbon nanofillers: Responsible for high mechanical strength 28
    2.5.1 Carbon nanotubes, classification, and significance 29
    2.5.2 Polymer/carbon nanotubes composites 32
    2.5.3 Modification of polymers with carbon nanotubes 33
      2.5.3.1 Covalent functionalization of CNTs with polymers 34

2.5.3.2 Non-covalent functionalization of CNTs with polymers.........36

2.6 Ionic liquid assisted fabrication of Polymer/MWCNTs composites...............53

2.6.1 Ionic liquids and their properties...53

2.6.2 Ionic liquid properties and processing affecting MWCNTs dispersion...57

2.6.2.1 Cationic and anionic structures..57

2.6.2.2 Particle size and loadings..58

2.6.3 MWCNTs Dispersion in ILs for polymer composites preparation.....58

2.7 Polymer composites processing approach..66

2.7.1 Internal Mixer..66

2.8 Thermal degradation kinetics of polymers and inorganic fillers.....................68

2.9 Summary..75

CHAPTER 3 RESEARCH METHODOLOGY 78

3.1 Overview..78

3.2 Materials 78

3.2.1 Polyetheretherketone (PEEK) 80

3.2.2 Multiwalled carbon nanotubes (MWCNTs).......................................81

3.2.3 Ionic Liquids (ILs) 81

3.2.4 Hydroxyapatite (HA)..83

3.2.5 Dimethylformamide (DMF)...83

3.3 Preparation of PEEK/MWCNTs and PEEK/MWCNTs/IL composites..........83

3.4 PEEK/MWCNTs/nHA/ILs composites..84

3.4.1 Preparation of PEEK/MWCNTs/nHA composites (without IL).........85

3.4.2 Preparation of PEEK/MWCNTs/nHA/ILs composites (with ILs)......85

3.4.3 Preparation of PEEK composite pellets 89

3.4.4 Hot-press molding to prepare PEEK composites................................90

3.5 Characterization of prepared PEEK-MWCNTs/nHA/ILs composites............93

3.5.1 Optical microscope (OM)..94

3.5.2 Field-emission scanning electron microscopy (FESEM)....................95

3.5.3 Differential scanning calorimetry (DSC) 95

3.5.4 Thermogravimetric analysis (TGA)..96

3.5.5 Nanoindentation 96

3.5.6 Universal testing machine (UTM) 96
3.5.7 Proliferation Analysis 97
3.5.7.1 Alamar Blue Assay 97
3.5.7.2 In vitro degradation study 98
3.5.8 Statistical Analysis 98
3.6 Calculation of thermal activation energy 98
3.7 Summary 99
CHAPTER 4 RESULTS AND DISCUSSION 101
4.1 Overview 101
4.2 Effect of organic solvent and ionic liquid on the properties of PEEK composites 101
4.2.1 The MWCNTs dispersion in PEEK composites 101
4.2.2 The thermal properties of PEEK composites 104
4.2.3 The mechanical properties of PEEK composites 106
4.3 Effect of ionic liquids with different amounts on the properties of PEEK composites 110
4.3.1 Effect of [EMIM]Ac and [BMIM]HSO_4 on the MWCNTs dispersion in PEEK composites 110
4.3.2 Effect of [EMIM]HSO_4 and [BMIM]Ac on the MWCNTs dispersion in PEEK composites 114
4.3.3 Effect of [EMIM]Ac and [BMIM]HSO_4 on thermal properties of PEEK composites 119
4.3.4 Effect of [EMIM]HSO_4 and [BMIM]Ac on thermal properties of PEEK composites 124
4.3.5 Effect of [EMIM]Ac and [BMIM]HSO_4 on mechanical properties of PEEK composites 129
4.3.6 Effect of [EMIM]HSO_4 and [BMIM]Ac on mechanical properties of PEEK composites 135
4.3.7 Effect of [EMIM]Ac and [BMIM]HSO_4 on the biological properties of PEEK composites 139
4.3.8 Effect of [EMIM]HSO_4 and [BMIM]Ac on the biological properties of PEEK composites 143

4.3.9 Effect of [EMIM]Ac and [BMIM]HSO_4 on thermal degradation kinetic of PEEK composites 147
4.3.10 Effect of [EMIM]HSO_4 and [BMIM]Ac on thermal degradation kinetic of PEEK composites 152
4.4 Summary 158
CHAPTER 5 CONCLUSIONS AND RECOMMENDATIONS 160
5.1 Conclusions 160
5.2 Recommendations 162
Appendix A 184
Appendix B 187

LIST OF FIGURES

Figure 1.1: Structure of PEEK [2] 2

Figure 2.1: PEEK, an ultra-high performance polymer [64] 11

Figure 2.2: Some of the applications of PEEK [68, 69] 12

Figure 2.3: Some of the current strategies to improve the bioactivity of PEEK [18] .. 13

Figure 2.4: MTT assay results for PEEK/MWCNTs/HA composites [1] 24

Figure 2.5: (A) SEM image of Hap and (B) EDX result of Hap [126] 25

Figure 2.6: Cell viability of PEEK and its nanocomposites [55] 27

Figure 2.7: Single-walled carbon nanotubes b) Multiwalled carbon nanotubes [15, 139] 30

Figure 2.8: Some applications of CNTs [149] 32

Figure 2.9: Different methods for preparation of polymer composites [30, 31] 34

Figure 2.10: Schematic diagram of the solution processing approach [148, 170] 39

Figure 2.11: Different steps in the preparation of a polymer composite by solution mixing [170] 40

Figure 2.12: Schematic diagram of the melt mixing approach [148] 46

Figure 2.13: Flowchart describes the major steps of melt blending of polymer composite [170] 47

Figure 2.14: The π-π interactions between PEEK and CF [68] 48

Figure 2.15: MWCNTs agglomeration in PEEK/BG composites [34] 49

Figure 2.16: The number of articles published in the past decade (Source: ScienceDirect, keywords (Polymer composites; Ionic liquid), June 2021) 53

Figure 2.17: Most frequently used cations and anions for polymer composites [211] 54

Figure 2.18: Important characteristics of ILs [211] 56

Figure 2.19: Schematic diagram of different interactions between CMI and MWCNT [48] 59

Figure 2.20: The CNTs and IL@CNTs distribution in DMF solvent [47] 61

Figure 2.21: Top and bottom view of rotor geometrics of the internal mixer [250] 67

Figure 3.1: Overall research flow chart for the development of PEEK/MWCNTs nanocomposite 79

Figure 3.2: Chemical structures of used ILs 82
Figure 3.3: Chemical structure of DMF 83
Figure 3.4: General steps involved in the preparation of PEEK nanocomposite 84
Figure 3.5: Polymer-filler interactions after using DMF and IL 84
Figure 3.6: Schematic representation of the steps to prepare PEEK-MWCNTs/nHA/ILs composites 87
Figure 3.7: a) Internal mixer machine used in the current study b) PEEK pellets obtained from the internal mixer 90
Figure 3.8: a) Compression molding machine used in the current study b) Final product for characterization 93
Figure 3.9: Characterization of prepared PEEK composites 94
Figure 3.10: Procedure used to calculate activation energy of PEEK composites 99
Figure 4.1: a) Optical micrographs of neat PEEK b) PEEK/MWCNTs c) PEEK/MWCNTs/IL at 50 mm magnification 102
Figure 4.2: Mapping of pure PEEK (a, b), PEEK/MWCNTs (c, d, e), PEEK/MWCNTs/IL (f, g, h) 103
Figure 4.3: FESEM images of PEEK (a), PEEK/MWCNTs (b), PEEK/MWCNTs/IL (c) at X500 103
Figure 4.4: Thermogravimetric (TG) curves for the PEEK, PEEK/MWCNTs, PEEK/MWCNTs/IL at 10 °C/min 105
Figure 4.5: Heating (a) and cooling (b) curves of differential scanning calorimetry (DSC) for PEEK and its nanocomposites at 10 °C/min. 106
Figure 4.6: Indentation load-displacement curves for the PEEK, PEEK/MWCNTs, and PEEK/MWCNTs/IL 107
Figure 4.7: Elastic Modulus as a function of contact depth for PEEK nanocomposites. 108
Figure 4.8: Stress-Strain curves of a) PEEK and its nanocomposites 109
Figure 4.9: PEEK composites micrographs obtained from optical microscope a) Without IL, b-e) [EMIM]Ac based composites, f-i) [BMIM]HSO_4 based composites 112
Figure 4.10: FESEM images of a) without IL, b-e) [EMIM]Ac based PEEK nanocomposites, f-i) [BMIM]HSO_4 based composites at 500X 113

Figure 4.11: Mapping and EDX of PEEK nanocomposites a-d) Without IL e-h) [EMIM]Ac based PEEK nanocomposites, i-l) [BMIM]HSO_4 based PEEK composites 114

Figure 4.12: EDX images a) without IL b) [EMIM]Ac based PEEK nanocomposites c) [BMIM]HSO_4 based PEEK composites 114

Figure 4.13: PEEK composites micrographs obtained from optical microscope a) Without IL, b-e) [EMIM]HSO_4 based composites, f-i) [BMIM]Ac based composites 116

Figure 4.14: FESEM images of a) without IL, b-e) [EMIM]HSO_4 based composites, f-i) [BMIM]Ac based composites at 500X 118

Figure 4.15: Mapping of PEEK nanocomposites a-d) Without IL e-h) [EMIM] HSO_4 based PEEK composites i-l) [BMIM]Ac based PEEK composites 118

Figure 4.16: EDX analysis of PEEK nanocomposites a) Without IL b) [EMIM] HSO_4 based PEEK composites c) [BMIM]Ac based PEEK composites 119

Figure 4.17: TGA curves of PEEK composites without and with different amounts of a) [EMIM]Ac and b) [BMIM]HSO_4 at 10 °C/min 120

Figure 4.18: Cooling and heating curves of PEEK-based composites at 10 °C/min a) Cooling curves of [EMIM]Ac based composites b) Cooling curves of [BMIM]HSO_4 based composites c) Heating curves of [EMIM]Ac based composites d) Heating curves of [BMIM]HSO_4 based PEEK 123

Figure 4.19: TGA curves of PEEK composites without and with different amounts of a) [EMIM]HSO_4 and b) [BMIM]Ac at 10 °C/min 125

Figure 4.20: Cooling and heating curves of PEEK-based composites at 10 °C/min a) Cooling curves of [EMIM]HSO_4 based composites b) Cooling curves of [BMIM]Ac based composites c) Heating curves of [EMIM]HSO_4 based composites d) Heating curves of [BMIM]Ac based PEEK composites 128

Figure 4.21: Load-displacement curves of PEEK-based composites with different loadings of a) [EMIM]Ac b) [BMIM]HSO_4 130

Figure 4.22: Elastic modulus profiles of PEEK-based composites with different loadings of a) [EMIM]Ac b) [BMIM]HSO_4 132

Figure 4.23: Stress-strain profiles of PEEK-based composites with different loadings of a) [EMIM]Ac b) [BMIM]HSO_4 134

Figure 4.24: Load-displacement curves of PEEK-based composites with different loadings of a) [EMIM]HSO_4 b) [BMIM]Ac 136
Figure 4.25: Elastic modulus profiles of PEEK-based composites with different loadings of a) [EMIM]HSO_4 b) [BMIM]Ac 137
Figure 4.26: Stress-strain profiles of PEEK-based composites with different loadings of a) [EMIM]HSO_4 b) [BMIM]Ac 139
Figure 4.27: Cells viability of [EMIM]Ac and [BMIM]HSO_4 based PEEK composites 141
Figure 4.28: EDX analysis of a) pure PEEK b) without IL c) 1 wt % of [BMIM]HSO_4 d) 1 wt % of [EMIM]Ac 143
Figure 4.29: Cells viability of [EMIM]HSO_4 and [BMIM]Ac based PEEK composites 144
Figure 4.30:EDX analysis of a) pure PEEK b) without IL c) 1 wt % of [EMIM]HSO_4 d) 1 wt % of [BMIM]Ac 147
Figure 4.31: Coats-Redfern plots of PEEK composites with various amounts of ILs a) [BMIM]HSO_4 b) [EMIM]Ac 149
Figure 4.32: Broido plots of PEEK composites with various amounts of ILs a) [BMIM]HSO_4 b) [EMIM]Ac 150
Figure 4.33: Horowitz-Metzger plots of PEEK composites with various amounts of ILs a) [BMIM]HSO_4 b) [EMIM]Ac 152
Figure 4.34: Coats-Redfern plots of PEEK composites with various amounts of ILs a) [EMIM]HSO_4 b) [BMIM]Ac 153
Figure 4.35: Broido plots of PEEK composites with various amounts of ILs a) [EMIM]HSO_4 b) [BMIM]Ac 155
Figure 4.36: Horowitz-Metzger plots of PEEK composites with various amounts of ILs a) [EMIM]HSO_4 b) [BMIM]Ac 157

LIST OF TABLES

Table 2.1: General properties of PEEK [2, 30] 11

Table 2.2: Comparison of different approaches for biological performance of PEEK 16

Table 2.3: Different types of bioactive materials [104] 20

Table 2.4: The biological assessment of PEEK 22

Table 2.5: Comparison between MWCNTs and SWCNTs [140, 141] 31

Table 2.6: Mechanical properties of CNTs [147, 148] 33

Table 2.7: Different methods for preparing PEEK/MWCNTs composites 37

Table 2.8: PEEK/MWCNTs composites prepared by solution mixing approach 43

Table 2.9: PEEK/MWCNTs composites prepared with melt mixing 50

Table 2.10: Properties of ILs for polymer composites 55

Table 2.11: Polymer composites prepared by IL-modified CNTs 62

Table 2.12: Advantages of internal mixer for the processing of polymer composites [167] 67

Table 2.13: Polymer composites using internal mixer 68

Table 2.14: Thermal degradation kinetics models for polymer composites. 71

Table 3.1: Material and chemicals used for the fabrication of PEEK composites 80

Table 3.2: Physicochemical properties of ILs 82

Table 3.3: PEEK composites prepared in this study 88

Table 3.4: Overview of operational parameters for several stages in the fabrication of PEEK nanocomposites 92

Table 4.1: The thermal properties of PEEK and its nanocomposites 106

Table 4.2: The mechanical properties of PEEK and its nanocomposites 110

Table 4.3: Thermal properties of [BMIM]HSO_4 and [EMIM]Ac based PEEK composites 124

Table 4.4: Thermal properties of [EMIM]HSO_4 and [BMIM]Ac based PEEK composites 129

Table 4.5: Mechanical properties of [BMIM]HSO_4 and [EMIM]Ac based PEEK composites 134

Table 4.6: Mechanical properties of [EMIM]HSO_4 and [BMIM]Ac based PEEK composites...139
Table 4.7: Cells viability of PEEK composites made with [EMIM]Ac and [BMIM]HSO_4 141
Table 4.8: Cells viability of PEEK composites with [EMIM]HSO_4 and [BMIM]Ac 145
Table 4.9: Kinetic parameters of [BMIM]HSO_4 and [EMIM]Ac based PEEK composites...152
Table 4.10: Kinetic parameters of [EMIM]HSO_4 and [BMIM]Ac based PEEK composites...158

LIST OF ABBREVIATIONS

PEEK	Polyetheretherketone
ICI	Imperial chemical industries
HA/HAP	Hydroxyapatite
CNTs	Carbon nanotubes
MWCNTs	Multi-walled carbon nanotubes
SWCNTs	Single-walled carbon nanotubes
CNFs	Carbon nanofibers
MMT	Montmorillonite
ILs	Ionic liquids
[EMIM]Ac	1-ethyl-3-methylimidazolium acetate
[EMIM]HSO_4	1-ethyl-3-methylimidazolium hydrogen sulphate
[BMIM]Ac	1-butyl-3-methylimidazolium acetate
[BMIM]HSO_4	1-butyl-3-methylimidazolium hydrogen sulphate
ANAB	Accelerated neutral atom beam
TCPS	Tissue culture polystyrene
RF	Radiofrequency
hFOB	Human fetal osteoblast cells
SBF	Stimulated body fluid
BG	Bioactive glass
PVC	Polyvinyl chloride
SLS	Selective laser sintering
TCP	Tricalcium-phosphate
Sr	Strontium
NHOst	Normal human osteoblast
BIC	Bone implant contact
SMA	Styrene-maleic anhydride
ATRP	Atom transfer radical polymerization
SDS	Sodium dodecyl sulfate
NMP	N-methyl pyrrolidone

PMMA	Polymethylmethacrylate
PE	Polyethylene
PS	Polystyrene
PP	Polypropylene
WC	Tungsten carbide
CMI	1-carboxyethyl-3-methyl-imidazolium bis(trifluoromethyl sulfonyl)imide
CR	Polychloroprene
SBR	Styrene-butadiene rubber
PVDF	Poly(vinylidene fluoride)
T_g	Glass transition temperature
T_m	Melting temperature
T_c	Crystallization temperature
[Bmim][Cl]	1-butyl-3-methylimidazolium chloride
[Emim][dep]	1-ethyl-3-methyl-imidazolium diethyl phosphate
[Ch][DHP]	2-hydroxy-ethyl-trimethyl ammonium dihydrogen phosphate
BMI	1-butyl 3-methyl imidazolium bis(trifluoromethyl sulfonyl)imide
[OMIM]BF$_4$	1-octyl, 3-methylimidazolium tetrafluoroborate
[EPIL]BF$_4$	N-methylimidazole-3-epoxy imidazolium tetrafluoroborate
[HMIM]PF$_6$	1-hexyl-3-methylimidazolium hexafluorophosphate
[BMIM]PF$_6$	1-butyl-3-methylimidazolium hexafluorophosphate
[AMIM]Cl	1-allyl-3-methyl imidazolium chloride
EMIT	1-ethyl-3-methyl imidazolium thiocyanate
MOIC	1-methyl-3-octylimidazolium chloride
[HEMIM]BF	1-hydroxyethyl-3-methylimidazolium tetrafluoroborate
[VEIM][BF$_4$	1-vinyl-3-ethylimidazolium tetrafluoroborate

[EMIM][TF_2N]	1-ethyl-3-methylimidazolium bis(trifluoromethyl sulfonyl)imide
[AEIM]Br	3-aminoethyl imidazolium bromide
CNCs	Cellulose nanocrystals
HDPE	High density polyethylene
BIIR	Bromo-butyl rubber
E_a	Apparent activation energy
α	Decomposition factor
A	Frequency or pre-exponential factor
β	Heating rate
R	Universal gas constant
X_c	Percentage crystallinity
ASTM	American Society for Testing and Materials
DMEM	Dulbecco’s Minimal Essential Medium
FBS	Fetal Bovine Serum
PBS	Phosphate buffer solution
ΔH_m	Melting enthalpy
T_d	Decomposition temperature
R^2	Regression coefficient

CHAPTER 1
INTRODUCTION

1.1 Overview

In this chapter, the background of the study is described. The significance of PEEK polymer, with a particular emphasis on biomedical applications, is discussed, as well as challenges and concerns about biological and mechanical characteristics. Furthermore, the problem statement, research objectives, and scope of the study are provided.

1.2 Background

In recent years, polymers have received augmented significance because of their lightweight, reasonable cost, ease of handling, and good processability. They are widely used in a broad range of applications, including packaging, coatings, storage, electronics, optical, and biological implant materials [1]. Among polymers, polyetheretherketone (PEEK) is a high-performance semicrystalline (30-35%) thermoplastic polymer with a rigid benzene ring, flexible ether bonds, and carbonyl groups, as shown in Figure 1.1. This configuration makes the polymer thermally stable even at a high temperature (usually over 300 ^{o}C) [2]. Since its commercialization, this polymer has found widespread use in different industries, including pharmaceutical, chemical, aerospace, automobiles, telecommunication, and biomedical applications, especially for human bone fixation devices [3]. Despite these outstanding features, a mismatch of mechanical properties and biological inertness (limited capability to join with bone tissues) compared to human bone retards its biomedical engineering applications [4-7].

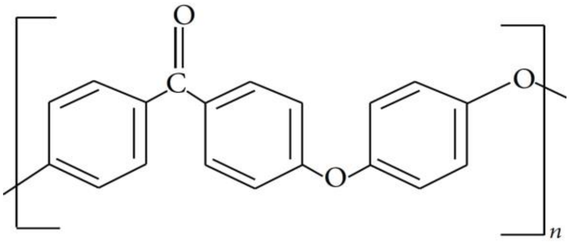

Figure 1.1: Structure of PEEK [2]

The biological characteristics of PEEK polymer can be altered by including a variety of biomaterials [8, 9]. Hydroxyapatite (HA) is the most commonly utilized bioactive material as a PEEK coating because of its similarity to human bone minerals. The HA is calcium phosphate-based bioceramic with the chemical formula $Ca_{10}(PO_4)_6(OH)_2$) [10]. The approaches to incorporate PEEK with the HA are surface coating [11], surface modification [12] and composite preparations [13]. Among these, the most practical and useful technique is polymeric composite material manufacturing [14, 15]. Composite materials are classified as materials composed of two or more constituent phases with substantially different physical or chemical properties that remain distinct and separate within the structure. The overall properties of a composite are superior to those of the individual components. Composites are made up of a continuous phase called the matrix (polymer) and a distributed phase called the reinforcement [16, 17]. It was worth noting that the addition of HA to PEEK [18, 19] enhanced the functional integration of human cells line with the synthesized composites. Nevertheless, the mechanical properties were reduced with the introduction of HA into PEEK [20].

Polymer composites with improved mechanical features are becoming more popular in high-performance applications, including aerospace, automotive industries, and biomedical engineering applications. In particular, the mechanical performance of PEEK composites was enhanced by using different reinforcement fillers such as nano SiO_2 [21], montmorillonite (MMT) [22], carbon fibres (CFs) [23], multi-walled carbon nanotubes (MWCNTs) [24, 25] and graphene [26]. Conversely, MWCNTs are prioritized over other nanofillers due to their low cost, large surface area, negligible toxicity, bone-tissue compatibility, outstanding mechanical and thermal properties, and low mass density (1.3–2.1 g/cm^3), making them excellent nanofillers for large scale industrialization to improve the properties of polymeric composites [27-29]. In recent years, PEEK/MWCNTs composites have been prepared through two different strategies, covalent functionalization [30], and non-covalent functionalization [31]. In the first method, chemical reactions are involved, which is time-consuming, expensive and cause damage to the CNTs surface [15]. In comparison, non-covalent functionalization methods are eco-friendly and do not change the CNTs characteristics, and they interact with the polymers via π-π interactions and van der Waals forces [32, 33]. In non-covalent functionalization, preparation of composites via solution mixing [34, 35], and melt blending [1, 24, 27, 36] is involved. The solution mixing method is the most common strategy for preparing CNTs-polymer composites in which a suitable solvent (the solvent can dissolve polymer matrix) is used for the dispersion of CNTs by magnetic stirring or ultrasonication. After magnetic stirring, CNTs are combined with the polymer at a specific temperature, and the solvent is evaporated in the vacuum oven [15, 35, 37]. Whereas, in the melt mixing method, thermoplastic polymers are heated above their melting point for the fabrication of CNTs-polymer composites by several processes such as extrusion [24, 38], internal mixer [39], injection molding [34] and compression molding [35]. In addition, this method is best suited for polymers which are insoluble in common organic solvents. However, several studies have been reported in which PEEK/MWCNTs composites were prepared via solution mixing and melt blending methods; the homogenous and precise dispersion of MWCNTs in PEEK still presents significant challenges because of low dispersibility, high aspect ratio (ca. 300–1000) and agglomeration of MWCNTs in the PEEK polymer. Recently, the use of ionic liquids (ILs) for effective MWCNTs dispersion in polymeric composites could be an alternative method.

The growing interest in ILs primarily from the increased awareness of their possible applications in "green chemistry," with a corresponding focus on the dispersion of MWCNTs into different polymers. Generally, ILs consist of an organic cation (usually an alkyl-substituted imidazolium) and an inorganic/organic anion. The melting temperature of ILs is usually less than 100 °C, and they remain liquid across a wide temperature range (usually up to 400 °C). The length and symmetry of alkyl-substituted groups, as well as the degree of delocalization of anion charge, are all factors that influence the physical, chemical, and biological properties of ILs [40, 41]. The physicochemical characteristics of ILs can be easily tuned by making appropriate changes to the cation and anion structures [42]. Ionic liquids with extremely low vapor pressure, high solvation interactions, and outstanding chemical and thermal stability, are the prime candidates for homogenous MWCNTs dispersion into polymer matrices [41, 43]. In particular, ILs containing imidazolium-based cations and hydrogen sulfate/acetate-based anions are believed to be non-toxic and cost effective [44-46]. Over the past few years, ILs have comprehensively been studied as a promising alternative to flammable, hazardous, toxic and highly volatile organic solvents for polymer composites [47], in which filler distribution have been investigated [48, 49].

1.3 Problem Statement

PEEK is a polyaromatic ultra-high performance thermoplastic polymer that is a viable option to be used in various engineering applications such as aerospace, electronics and biomedical, especially for the substitution of human bone implants because of its excellent biocompatibility, radiolucency, chemical resistance, and mechanical characteristics similar to those of human bone [50]. The elastic modulus (4 GPa) and tensile strength (80 MPa) of PEEK are comparable to that of human cortical bone (7-12 GPa, 85-100 MPa), which is suitable for a bone implant. However, PEEK demonstrates two serious shortcomings. When PEEK is utilized in body implants, it has been linked to inadequate bone union [51]. In fact, PEEK is a biologically inert polymer that is incapable of promoting bone-implant integration due to the lack of a chemical connection between the implants and human bone tissues. Secondly, pure PEEK cannot satisfy the stringent criteria for weight-bearing bone fracture replacement devices since the mechanical characteristics of unfilled PEEK are close (lower limit) to those of human cortical bone [52].

PEEK materials can be made more bioactive by including various bioactive compounds, such as hydroxyapatite (HA) [53]. Surface modification, surface coatings, and composites preparation are some of the methods that can be used to treat HA in PEEK. The PEEK/HA composites [53, 54] provoked considerably better bioactive characteristics than those of pure PEEK but at the sacrifice of the mechanical properties

[55]. The incorporation of HA into PEEK results in interfacial debonding between the PEEK matrix and the HA, resulting in nanocomposite with weak mechanical properties. To enhance mechanical performance, it has been shown that reinforcing PEEK with a variety of nanofillers such as multiwalled carbon nanotubes (MWCNTs) is advantageous owing to their large surface area, low density, and higher tensile attributes [24]. It is discovered that the characteristics of PEEK/MWCNTs are strongly reliant on the homogeneous dispersion of MWCNTs in PEEK. Multiple techniques, including solution mixing [56], compounding and injection molding [7], as well as covalent and non-covalent modification [57] have been used to improve the MWCNTs distribution in various polymeric matrices. However, MWCNTs have a significant proclivity for agglomeration and entanglement as a result of Van der Walls forces, high aspect ratio, and the lack of active sites on their surface to promote filler-matrix interactions [58]. Therefore, using ionic liquids (ILs) to disperse MWCNTs effectively in polymeric composites could be an alternative approach [59].

It is thereby required to build a novel, environmentally acceptable, and efficient pretreatment technique capable of dispersing MWCNTs into the polymer matrix. ILs are low vapor pressure tunable solvents with strong solvation interactions and good thermal stability, rendering appropriate alternatives for homogenous MWCNTs distribution in the polymer matrices [41, 48]. ILs can accelerate the interactions of MWCNTs with the polymer matrix, resulting in improved filler dispersion [58]. ILs have been utilized in numerous polymer processing methods to develop polymer/MWCNTs composites for multiple applications. Nevertheless, no research has been conducted on the use and optimization of the quantity of ILs for the fabrication of PEEK/MWCNTs composites for biomedical applications.

After treating MWCNTs with ILs, thermal degradation kinetics is critical for the logical design of molding and thermoplastic processing methods for the manufacturing of PEEK/MWCNTs/nHA/ILs composites. The thermal kinetics must be predicted in order to design the impact of ILs-treated MWCNTs on PEEK composites. Nonetheless, no discussion of kinetic modelling of the thermal degrading behavior of PEEK/MWCNTs/nHA/ILs composites has been found in the literature.

1.4 Research Objectives

The main objective of the present work is to explore the effect of ILs modified MWCNTs on the preparation of PEEK nanocomposite. In this approach, the specific objectives are:

1. To investigate the effect of IL and organic solvent on MWCNTs dispersion in the PEEK nanocomposites.

2. To synthesize and compare the properties of PEEK/MWCNTs/nHA nanocomposites by using ILs treated MWCNTs by melt blending and compression molding processes.

3. To evaluate the biocompatibility and cells viability of fabricated PEEK/MWCNTs/ILs nanocomposites incorporated with nanohydroxyapatite (nHA).

4. To assess the effect of ILs modified MWCNTs on the thermal degradation kinetics of the PEEK nanocomposites by adopting the activation energy approach.

1.5 Hypothesis

The development of environmentally friendly approach could greatly influence the biological and physical characteristics of PEEK/MWCNTs/nHA/ILs nanocomposites for biomedical applications. The addition of HA and MWCNTs could enhance the biocompatibility and elastic modulus of PEEK composites. IL as a designer solvent can be utilized to disperse MWCNTs in PEEK polymer for improving the tensile strength and elastic modulus of synthesized PEEK composites for human bone substitution. Thermal degradation kinetics models could provide the understanding of the logical design of molding and thermoplastic processing methods for the manufacturing of PEEK/MWCNTs/nHA/ILs composites.

1.6 Scope of research

This thesis aims to investigate the effect of ILs on the MWCNTs dispersion into PEEK as a promising 'green' approach for the fabrication of PEEK nanocomposites incorporated with nHA.

The dispersion of MWCNTs into PEEK was investigated by using IL, [EMIM]HSO_4 (1 wt %) and DMF (1 wt %). The strong interactions between IL-modified MWCNTs and PEEK provoked that IL could be a benign and environmentally friendly solvent for polymer composites. The MWCNTs distribution in PEEK was examined by optical microscope and field-emission scanning electron microscope (FESEM).

Four ILs (0-2 wt %) containing different alkyl chain length imidazolium-based cations with hydrogen sulphate and acetate-based anions were used in this work due to their high dissolution capability for PEEK and provided advantages of cost [45, 46, 60]. PEEK nanocomposites were also produced utilizing the standard solvent dimethylformamide (DMF, 1 wt %) [30, 61] for effective implementation and comparison of IL capabilities. To investigate the impact of ILs modifications on the dispersion of MWCNTs (1 wt %) [62] for the development of PEEK nanocomposites containing nHA (10 wt %) [63], as well as to evaluate morphological, thermal, and mechanical properties before and after ILs modification.

Further, a conventional nanocomposite manufacturing approach was followed that involves the physical mixing of MWCNTs and ionic liquids by using agate mortar followed by magnetic stirring. After adding PEEK and nHA powder into IL-modified MWCNTs, the formulations were melt blended at 350 ℃ in the internal mixer and compounded in compression molding at 390 °C. The cells viability and biocompatibility of ILs based PEEK/MWCNTs nanocomposites was compared with non-IL and DMF based PEEK nanocomposites.

The work continued by measuring the biocompatibility of the PEEK/MWCNTs/nHA nanocomposite prepared with the different ILs and compared with the human bone cortical bone. Besides, the effect of ILs modified MWCNTs on the thermal degradation kinetics of PEEK composites using Coat-Redfern, Broido and Horowitz-Metzger approaches was also established.

1.7 Thesis outline

This thesis is divided into five chapters, each of which contains the following information:

Chapter 1: The PEEK/MWCNTs/nHA based composites with use of ILs and their background, also including problem statement and existing technological challenges, objectives, and approaches of this research work as well as thesis outline.

Chapter 2: Literature Review, which covers the present role of PEEK in biomedical engineering applications, existing strategies for PEEK/HA composites to improve the biological and mechanical properties, and the need of homogenous MWCNTs dispersion in polymers with the introduction of ionic liquids as innovative solvents. Recent research reports on the kinetic analysis of thermal degradation of PEEK nanocomposites using the activation energy method are also included.

Chapter 3: Research Methodology; the detailed experimental steps to prepare nanocomposites, including modification of MWCNTs by ILs, physical mixing of PEEK and nHA powder, ultrasonication, and processing of nanocomposites by melt blending and compression molding processes are included. Particularly, various PEEK nanocomposites characterization approaches, as well as the calculation of properties of prepared nanocomposites, are listed.

Chapter 4: The findings of morphological, thermal, mechanical, and biological characterizations of untreated and ILs-treated PEEK nanocomposites are discussed. The effect of ILs on the thermal degradation kinetics of PEEK nanocomposites on the activation energy approach has also been explored.

Chapter 5: This chapter summarizes the conclusions of the current study and suggestions for the potential research.

1.8 Summary

The use of PEEK-based nanocomposites has received increased attraction in different engineering applications, especially in biomedical field for human bone replacement, due to the concerns of low mechanical properties and the inert nature of pure PEEK polymer. The MWCNTs agglomeration impedes the effective interaction of MWCNTs with the polymer matrix. The effective strategy for fabricating PEEK nanocomposites with homogenous MWCNTs dispersion is an important and challenging task. Various pretreatment methods for homogenous MWCNTs dispersion into polymer matrices are currently under practiced and remains challenging. Therefore, the development of a new, cost-effective and environmentally benign pretreatment technology for efficient MWCNTs dispersion is required. ILs have emerged as a promising and environmentally friendly alternative solvent for the uniform distribution of MWCNTs. The main goal of this research is to determine the impact of ILs on the morphological, thermal, mechanical, and biological characteristics of PEEK/MWCNTs/nHA nanocomposites.

CHAPTER 2

LITERATURE REVIEW

2.1 Overview

This chapter covers the overview of PEEK polymer in the biomedical uses. The challenges and available methods to improve the biological and mechanical properties of PEEK composites are explained in this chapter. The advantages of using ILs in the polymer composites for MWCNTs dispersion are highlighted in detail. In later sections, an overview of thermal degradation kinetics of polymer composites is provided.

2.2 Polyetheretherketone (PEEK)

PEEK is a ultra-high performance semicrystalline thermoplastic polymer (shown in Figure 2.1) with a rigid benzene ring, flexible ether bonds, and carbonyl groups [64]. This configuration makes the polymer thermally stable even at a high temperature (usually over 300 ^{o}C) [2]. The general properties of PEEK polymer are given in Table 2.1. Johnson et al.(1967) [65] registered the first attempt to prepare PEEK by polycondensation of bisphenolate with activated dihalides in Dimethyl sulfoxide (DMSO) with sodium hydroxide (NaOH) as a basis. Due to crystallinity and the subsequent insolubility of polymers in DMSO, high molecular weight polymers were difficult to develop. To evade the solubility problem, Attwood and Rose [66] used diphenyl sulfone as a solvent and polymerized near the melting point. Later on, it was commercialized by Imperial Chemical Industries (ICI) in the early 1990s with the unique combination of high chemical stability, excellent mechanical properties, and flame retardance [2, 67]. PEEK has been used in a broad variety of applications since its commercialization, from the chemical process industry to the electronics, telecommunications, transportation sectors (automobile, aeronautics, and aerospace), and in biomedical engineering applications, as shown in Figure 2.2 [68, 69].

Table 2.1: General properties of PEEK [2, 30]

Property	Value
Solubility in water	Insoluble
Specific gravity	1.30
Melting point	343 ℃
Glass transition temperature	143 ℃
Thermal stability	Stable at room temperature
Crystallinity	30-35%
Tensile strength	80 MPa
Elastic modulus	4 GPa

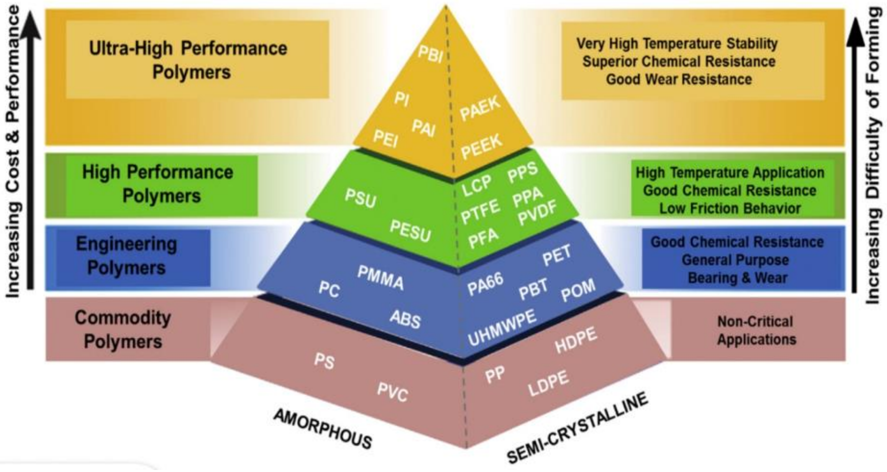

Figure 2.1: PEEK, an ultra-high performance polymer [64]

Many reports have been published in the last few decades on the structural [68], thermal [70], and mechanical [71] characteristics of this linear aromatic polymer. The following are the features [72, 73] of this high-performance material:

- Chemical and hydrolysis resistant: Insoluble in conventional solvents, provides outstanding resistance to both organic and inorganic liquids.
- Wear resistance: superb tribological properties under a variety of environments.
- Radiation resistance: It can withstand heavy doses of gamma radiation.
- High-temperature reliability: At temperatures up to 300°C, outstanding mechanical properties are maintained.

- Electrical: Superior electrical performance that is consistent at a higher temperature and frequency spectrum.

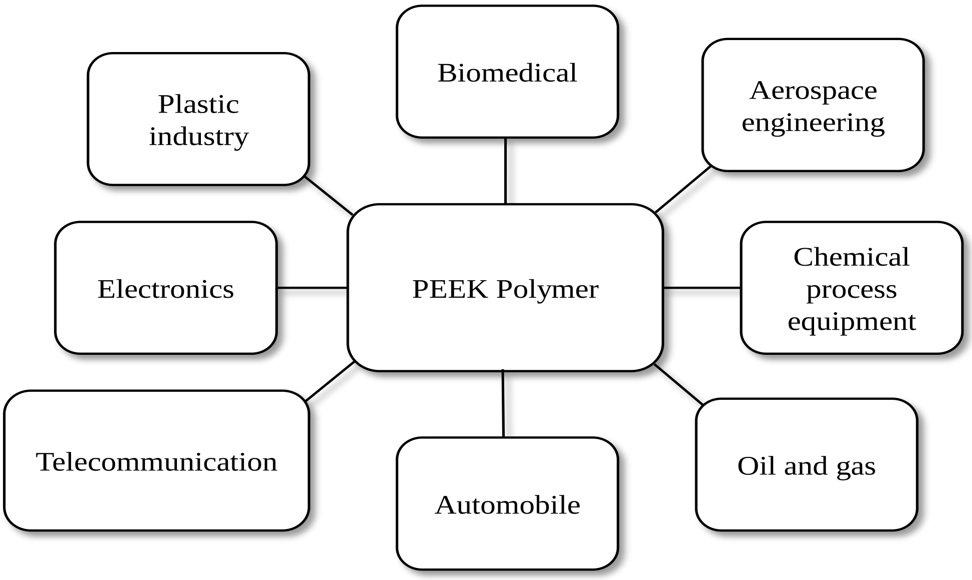

Figure 2.2: Some of the applications of PEEK [68, 69]

2.3 Motivation for use of PEEK in composite preparation

PEEK has been extensively used in various biomedical engineering applications, especially for load-bearing hip implants, bone fixation devices and human cortical bone because of its elastic modulus resembling human bone, non-toxic behavior, and excellent radiolucency [50, 74]. Despite these excellent features, PEEK is bio-inert and cannot functionally integrate with the surrounding bone tissues upon implantation [75]. In other words, the PEEK biocompatibility with the living host: natural bone is poor. The term “biocompatibility” referring the capacity of a material to perform with an adequate host response in a given condition. It can be seen as a relationship between the host and the bioactive material [76]. The lack of bone attachment at the implant surface may trigger a vicious loop of implant micromotion and inflammation, ultimately resulting in fibrous layer thickening, osteolysis (bone loss and degradation), and implant loosening [77-79]. Therefore, the optimization of PEEK bioactivity is a major obstacle that must be overcome in order to fully understand the potential benefits. In the last decades, several strategies (Figure 2.3) have been used to enhance to biological performance of PEEK, including surface coatings, composites processing, and their comparison is illustrated in Table 2.2.

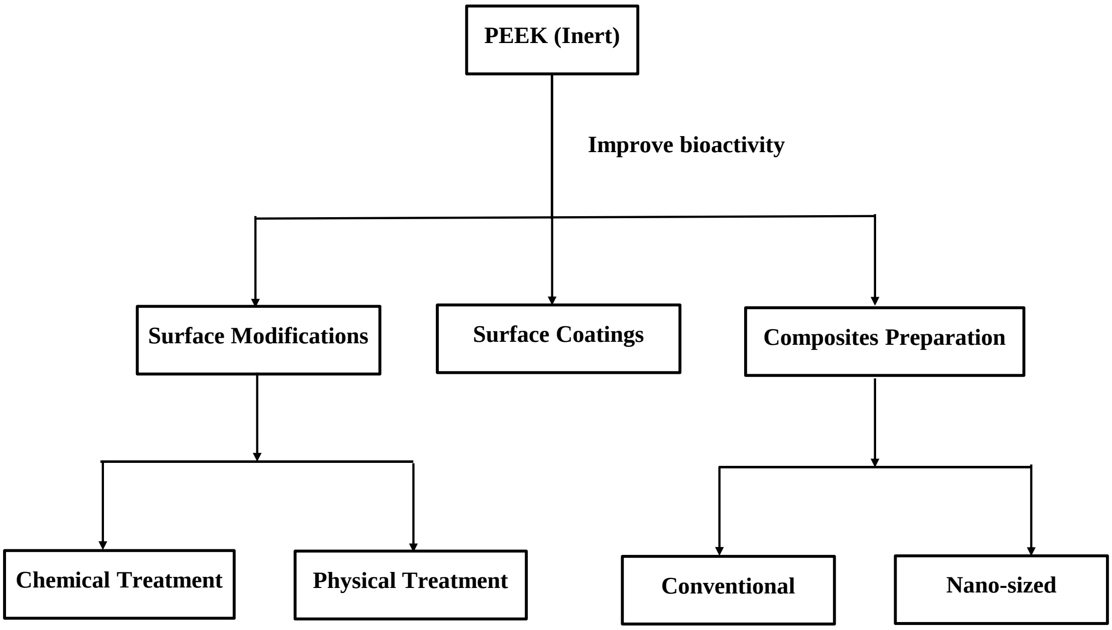

Figure 2.3: Some of the current strategies to improve the bioactivity of PEEK [18]

2.4 Current methods to promote PEEK bioactivity

Because of the poor functional integration of PEEK and widespread use, developing procedures to encourage biocompatibility with the bone and underlying tissue is of considerable science and clinical importance. The surface and bulk modifications via chemical and physical treatments, as well as composite preparation, are currently used. The aim of these treatments is to have a more desirable relationship at the bone-implant interface, as the implant surface is vital for osseointegration [80].

2.4.1 Surface modification

It is well established that micrometer and nanometer seized features can improve the surface properties such as osseointegration of orthopedic implants [81]. In fact, for subsequent cell adhesion and proliferation, substrate surface properties are sometimes more important than surface chemistry [82]. Studies have shown that high surface roughness has been shown to be critical for the long-term osseointegration of implants [79]. The PEEK polymer also exhibited a differentiated response as compared to machined and injection molded samples [83]. Despite the fact that PEEK is still physically and chemically intact, it may be modified by physical or chemical treatments. The plasma modifications (such as oxygen (O_2) plasma, ammonia (NH_4) plasma, nitrogen and oxygen (N_2/O_2) plasma, methane and oxygen (CH_4/O_2) plasma, oxygen and argon (O_2/Ar) plasma, ammonia/argon (NH_4/Ar) plasma, and hydrogen/argon (H_2/Ar) plasma) and accelerated neutral atom beam (ANAB) plasma are the most widely employed physical treatments. In chemical modifications, wet chemistry or sulfonation treatments are generally used for enhancing the bioactivity od PEEK.

2.4.1.1 Physical Treatment

Plasmas are ionized gases generated by excitation with electro-magnetic waves in a closed reactor device comprising a low-pressure gas mixture [84]. The reactive particles produced in this way can interfere with the surface of the biomaterial deposited in the reactor, modifying its physical and chemical surface characteristics while retaining the mechanical, electrical, and optical properties unchanged [85]. Briem et al. (2005) studied the proliferation and separation of primary fibroblasts and osteoblasts on plasma-treated PEEK using two plasma processes. They discovered that the osteogenic behavior of cells grown on treated PEEK was similar to that of tissue culture polystyrene (TCPS), and that plasma modification methods could be used to reliably stimulate and inhibit cell proliferation [84]. In another study, the bioactivity of PEEK was increased by treating it with N_2/O_2 low-pressure plasma by Ha et al.(1997) [12]. On the surface of plasma-treated PEEK, a carbonate-containing calcium phosphate coating with a thickness of up to 50 μm was produced after 24 days of exposure in calcium and phosphate-saturated solution. The cell viability of plasma-treated and calcium phosphate coated PEEK was slightly higher than that of untreated PEEK.

Awaja et al. (2012) [51] used radiofrequency (RF) plasma with a mixture of CH_4/O_2 to modify the PEEK surface. They discovered that CH_4/O_2 gas treatment increased bond intensity considerably over untreated samples. They also observed the formation of oxygen-rich nanofilms on PEEK with high surface energy using a plasma immersion ion implantation and deposition (PIII&D) strategy with a CH_4/O_2 gas mixture, which significantly enhanced cell adhesion. Waser-Althaus et al. (2012) [86] treated the PEEK surface with O_2/Ar or NH_4 plasma. They found that plasma-treated PEEK increased the adipose tissue-derived mesenchymal stem cells (adMSC) adhesion, proliferation, and osteogenic differentiation and revealed that osteogenic differentiation was based on plasma strength. Khoury et al. (2013) [87] used the ANAB technique to improve the surface biocompatibility of PEEK without changing the surface composition or including bioactive substances. The cell proliferation assay and microscopy revealed that ANAB-treated PEEK promoted the growth of human fetal osteoblast cells (hFOB) relative to untreated PEEK in vitro.

2.4.1.2 Chemical Treatment

The chemically modifying PEEK with wet surface chemistry has resulted in a number of surface-functionalized PEEK. Several studies have shown that wet chemical treatment can improve the bioactivity of PEEK. Different PEEK surface chemistry modifications to PEEK-ONa, PEEK-OH, PEEK-F and PEEK-OH ($CFCl_3$) have shown a reduced water contact angle of the implant and thus an improvement in PEEK bioactivity [88]. The wet chemical processing strategy was used utilized as a pre-treatment to improve apatite formation through immersion in stimulated body fluid (SBF). The impact of NaOH pre-treatments on PEEK apatite formation in SBF revealed that NaOH pre-treatments increased the growth of the apatite coating layer [89]. A 3D porous and nano-structured network with bio-functional groups was generated on PEEK by sulfonation and subsequent water immersion to prepare two types of sulfonation-treated PEEK (SPEEK) samples (SPEEK-W (water immersed and rinsing after sulfonation)) and SPEEK-WA (SPEEK-W with more acetone rinsing)) [90]. The findings indicated that SPEEK-WA was found to induce the pre-osteoblast functions such as proliferation, initial cell adhesion, increased osseointegration and strong bone-implant bonding ability. Recently, the chemical deposition method was used to deposit HA crystalline particles on the surface of PEEK through plasma spraying [91]. The

Table 2.2: Comparison of different approaches for biological performance of PEEK

Methods to improve PEEK bioactivity	Benefits	Drawbacks	Ref.
Pure PEEK	Non-toxic Excellent corrosion resistance Elastic modulus close to bone	Biological inert	[92-94]
Physical Treatment	The most commonly used approach In this strategy, the bioactivity of PEEK is enhanced without affecting/decreasing the mechanical and electrical properties. In this method, the cell adhesion, biocompatibility, and osteointegration can be significantly increased.	A non-uniform (amorphous) HA-coated layer deposited on PEEK.	[18, 95, 96]
Chemical Treatment	The formation and growth of the apatite	The chemical methods are rarely	[18, 19, 91]

	layer on PEEK were enhanced.	employed for PEEK modification. Alter and weaken the surface and structure of the polymers. The mechanical characteristics of the substance were lowered as the surface chemistry of the material changed.	
Surface Coatings	Create a rough and porous surface for cells viability.	It was difficult to deposit HA crystalline on the PEEK surface for a long duration. Some surface coating methods were not used because of the low melting point of PEEK. Irregular coating thickness.	[19, 97-99]

		Inhomogeneous melting of HA at 2000 °C.	
PEEK-HA composites/nanocomposites	The biological activity and elastic modulus were boosted.	The mechanical properties of PEEK-mHA composites were reduced as compared to those of pure PEEK. The mechanical characteristics of the PEEK were lowered by increasing the nHA concentration. The agglomeration of HA particles.	[13, 53, 100-102]

results such as deposition of HA coating, strong chemical bonding between HA and PEEK, enhanced surface roughness, and an increase in the wettability of the treated samples were reported.

2.4.2 Surface coatings

There are many approaches for depositing the bioactive material on PEEK, including plasma spraying, vacuum deposition, dip coating, and immersion in SBF [103]. The bioactive materials (Table 2.3) including, hydroxyapatite (HA), bioactive glass (BG), and tricalcium phosphate (TCP), have been deposited on the surface of

PEEK to enhance cells proliferation and biocompatibility [104]. They generate a good response at the interface among the living tissues and the implant in the biological environment, resulting the strong bonding. BG is the inorganic bioactive material with four components including SiO_2, CaO, Na_2O and P_2O_5 that has been used in implant materials. The essential characteristics of bioactive glasses that generate appropriate applicants for bone tissue application, are their capability to improve revascularization, osteoblast adhesion, and enzyme process. On the other side, BG is brittle which have limited toughness and cannot be used in the bulk form for the load bearing implantations[104]. Tricalcium phosphate (TCP) ($Ca_3(PO_4)_2$) is a member of calcium-phosphate ceramics. TCP are highly bioactive ceramics which form bone-like apatite on their surface in vivo and bond to living tissues via the apatite layer formation. Nevertheless, they have poor mechanical properties and fracture toughness, not being suitable for load bearing implantation[104].

Hydroxyapatite is the most commonly utilized bioactive material as a PEEK coating because of its similarity to human bone minerals. The HA is calcium phosphate-based bioceramic with the chemical formula $Ca_{10}(PO_4)_6(OH)_2$) [10]. It was reported in many studies (Table 2.4) that the HA modification has successfully enhanced the biocompatibility, osteointegration, and bioactivity of PEEK [105, 106]. Lee et al. (2013) [11] produced HA-coated PEEK using a cold spray technique and examined its bioactivity in vitro and in vivo. In vitro studies revealed that HA-coated PEEK increased the adhesion and viability as compared to uncoated PEEK. For in vivo experiments, the authors used micro-computed tomography (micro-CT) and histomorphometry analysis to show that HA-coated PEEK cylinders facilitated implant osteointegration with the bone tissue in a rabbit ilium model. Barkarmo et al. (2019) [44] used a spin coating technique to fabricate nanocrystalline HA-coated PEEK cylinder implants and implanted them into the femurs of rabbits with non-coated cylinders as controls. The mean bone-implant interaction in nano-HA coated PEEK cylinders was higher than in uncoated cylinders, suggesting that nano-HA coated PEEK had stimulated the osteointegration. The PEEK polymer is bioinert, and the development of a HA coating layer on it after immersion in an aqueous solution is low. The PEEK surface is combined with Mg as a bioactive additive to manufacture PEEK/Mg composite, which allows for better deposition of the HA coating layer in an aqueous solution. In contrast to pure PEEK, the HA coating layer developed on the surface of the PEEK/Mg composite exhibits enhanced in vitro bioactivity with more associated MC3T3-E1 cells [107].

Table 2.3: Different types of bioactive materials [104]

Type of Biomaterial	Benefits	Drawbacks
Hydroxyapatite (HA)	Similarity to human bone minerals Can increase the bioactivity of PEEK Increase cells proliferation	
Bioactive Glass (BG)	Can enhance osteoblast adhesion and revascularization	Brittle which has limited toughness
Tricalcium Phosphate (TCP)	Used to create bone-like apatite layer	Poor mechanical and fracture toughness

The degree of crystallization of the HA coating is one of the challenges of HA deposition on PEEK. The HA coating layer should be crystalline for long-term orthopedic and dental implant durability due to the low solubility of crystalline HA in water. However, the coated HA is generally amorphous, requiring a further heat treatment step. The annealing process at 600 °C or above for at least one hour is a conventional heat treatment for crystallization of the HA coating layer. The standard annealing process cannot be utilized to crystallize the HA layer on the PEEK surface due to the low melting point of PEEK (343°C).

This issue has been solved using three different approaches. The first method involves using a microwave to heat the HA coating layer only. This approach relies on the electromagnetic absorption properties of HA coating and the PEEK transparency to electromagnetic properties [108]. The second approach, laser-induced crystallization, employs a short pulse length to heat just a thin coating of the surface [109]. Hydrothermal annealing is the third approach that has been proposed. In this approach, the coating layer is subjected to saturated steam at 200 ℃ or lower temperature in a high-pressure vessel, which produced excellent results for the crystallization of the HA coating layer [110, 111]. Even with the use of these approaches, the HA coating layer crystallization issue was one of the greatest challenges for PEEK coating because of its heat-sensitive characteristics [110].

2.4.3 Bioactive PEEK composites

As previously explained, one of the ways for increasing the bioactivity of PEEK implants is to compound with bioactive material. In the polymer composites technique, different materials, including hydroxyapatite (HA), bioactive glass (BG), and calcium silicate (CS) have been used to boost the biological activity of polymers [112]. Several studies have been conducted to explore the impact of HA on the biocompatibility and biological performance of PEEK composites (PEEK/HA). The most common application is load-bearing implants [113], although various studies (Table 2.4) have been conducted to demonstrate the possibility of manufacturing three-dimensional porous scaffold PEEK/HA for tissue engineering [114, 115] and cervical spinal fusion cages [116]. PEEK/HA composites were prepared with 0-40 vol % HA to analyze the effect of HA on the bioactivity of PEEK using melt compounding and injection molding processes. The biocompatibility and functional integration of PEEK was boosted, and the authors proposed that filler matrix bonding is essential for improvements of the biological performance [13, 100].

Table 2.4: The biological assessment of PEEK

Bioactive PEEK	Bioactive materials	Processing Technique	Biological activity/Mechanical Properties	Ref.
PEEK/CS	Calcium Silicate	Plasma treatment	A layer containing carbonate with calcium phosphate	[12]
PEEK	Surface modification by methane and oxygen plasma	Plasma treatment	The maximum bonding strength was achieved.	[51, 117]
PEEK	Surface modification by oxygen and ammonia plasma	Plasma treatment	Changed the PEEK surface chemistry and topography for osteogenic differentiation	[86]
PEEK/OH		Chemical treatment	Improved the biocompatibility of PEEK	[88]
PEEK/HA	HA	Chemical deposition	The wettability and bioactivity of PEEK/HA were increased.	[91]
PEEK/HA	HA	Cold spray technology	PEEK-HA enhanced the bifunctionality and osteointegration	[11, 118]

PEEK/Mg/HA	HA	Compression molding	Enhanced biocompatibility without sacrificing the mechanical properties	[107]
PEEK/HA	HA	Selective laser sintering	The cells viability to PEEK was improved	[115]
PEEK/HA	HA	Compounding and injection molding	The elastic modulus of PEEK/HA was calculated within the range of human cortical bone	[13]
PEEK/Sr/HA	HA	Compression molding	Strontium modified hydroxyapatite (Sr-HA) enhanced the PEEK bioactivity	[119]
PEEK/HA	HA	Surface Coating	The mean bone-implant contact (BIC) percentage was significantly higher	[97, 120, 121]
PEEK/HA	HA	In situ synthesis	PEEK/HA showed satisfactory biological results without compromising the mechanical properties	[122]

In another study, bioactive PEEK/HA composites were prepared using solvent-based extrusion and compression molding processes to control the biological characteristics for bone tissue engineering scaffolds. The results showed that PEEK/HA composites exhibited a good interface and excellent biocompatibility between the HA and PEEK matrix [123]. In a vivo study, bioactive materials can generate a bone-like apatite coating on their surfaces, and this apatite layer may bond to the bone. Thus, the capacity of a material to generate apatite layer on its interface in a simulated body fluid

(SBF) with ion concentrations nearly equal to that of human blood plasma was examined [112]. The SBF bioactivity experiment on HA/PEEK composites with varied volume fractions up to 40%, which were made by combining PEEK and HA powders, compaction, and sintering, and revealed that the HA layer formation for the composite with a larger HA volume fraction percentage of HA [124]. Zhang et al. (2009) used primary human osteoblast cells to assess cell adhesion, morphology, proliferation, and differentiation after fabricating HA/PEEK composites using the selective laser sintering (SLS) process. In comparison to thermanox (TMX) and polyvinyl chloride (PVC), they discovered that SLS-treated HA/PEEK promoted osteoblast development and revealed that composites with increased HA content displayed improved cell growth and osteogenic differentiation [125].

Liu et al. (2016) [1] used melt blending to incorporate HA and MWCNTs into PEEK to improve the biological and mechanical characteristics of PEEK composites. The cellular metabolic activity (MTT) was employed to determine the viability of the cells, and it was found in Figure 2.4 that PEEK/(0.93 percent MWCNTs) and PEEK/(1.86 percent MWCNTs) composites displayed greater cell metabolic activity than pure PEEK. After introduction of HA into the PEEK/MWCNTs composites, significant effects were seen; cell survival and biocompatibility were greatly increased compared to those of pure PEEK.

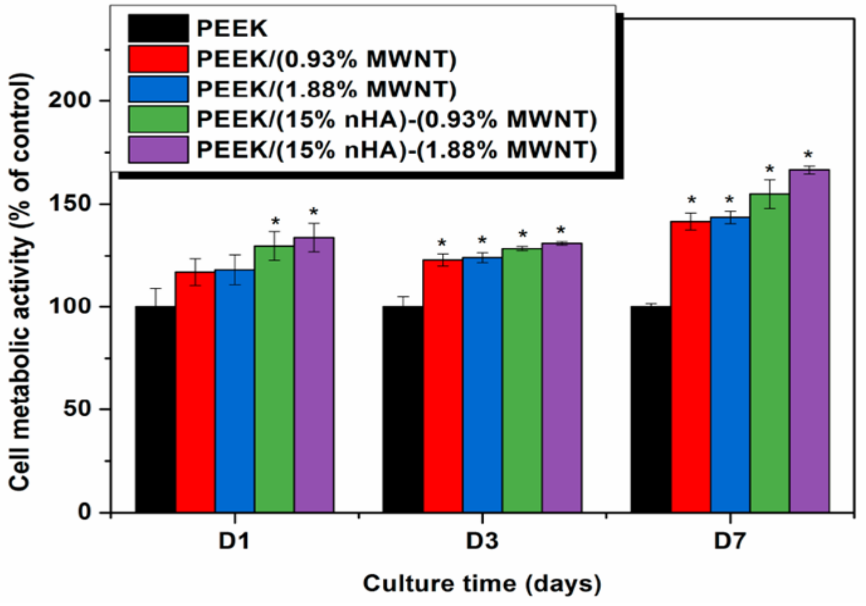

Figure 2.4: MTT assay results for PEEK/MWCNTs/HA composites [1]

Ma et al. (2013) employed an in situ synthetic technique to effectively create a HA/PEEK composite with good bonding between the PEEK matrix and hydroxyapatite fillers. The in situ synthesized composite materials were shown to have high biocompatibility without toxicity or compromising mechanical performance [122]. The Invibio has introduced “PEEK-OPTIMA HA enhanced polymer,” a HA-filled PEEK compound containing microscale HA particles for use in implants. PEEK-OPTIMA HA augmented biomaterial was introduced with good mechanical properties and performance, biocompatibility, elastic modulus comparable to cortical bone, reduced stress shielding, and a high degree of radiolucency that allowed for clear fusion evaluation. In a pre-clinical in vivo investigation, employing a sheep model, Invibio "PEEK-OPTIMA HA enhanced polymer" revealed improved bone apposition within four weeks after implantation as compared to PEEK-OPTIMA® Natural [18].

Maheshwari et al. (2014) [126] fabricated and evaluated polycaprolactone/polyvinyl alcohol/hydroxyapatite nanoparticles (PCL/PVA/HAp) scaffolds for bone tissue regeneration application. The structural, thermal, and biological properties of the prepared scaffolds were determined. The composition and Ca/P ratio of HAp was found out using Energy Dispersive X-ray analysis (EDX) for analyzing the biocompatibility and the results showed that the HAp particles had a Ca/P ratio of 1.62 (Figure 2.5B), very close to natural bone.

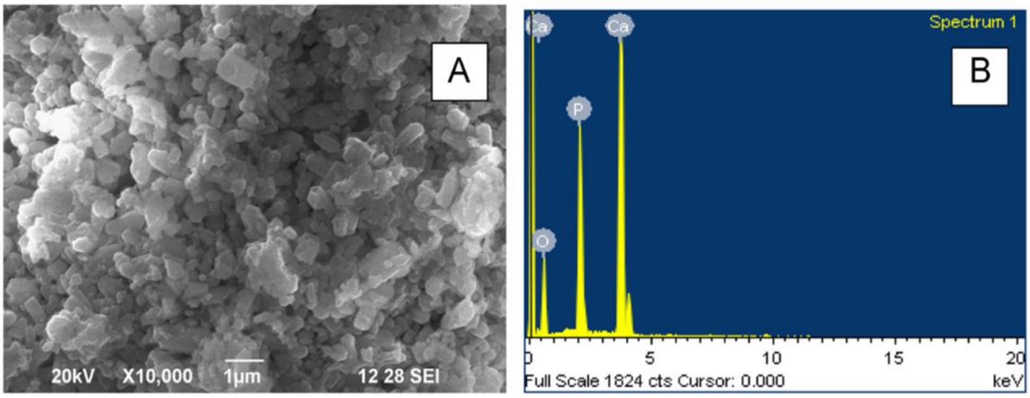

Figure 2.5: (A) SEM image of Hap and (B) EDX result of Hap [126]

Other bioactive materials, such as strontium with hydroxyapatite (Sr-HA), calcium silicate, glass fibres, bioglass, and β-tricalcium-phosphate (β-TCP), were also employed to generate bioactive PEEK composites. By using a compression molding process, Wong et al. (2009) [119] synthesized Sr-HA/PEEK composites with Sr-HA concentration varying from 15–30 vol%. Based on a qualitative evaluation of apatite production in SBF and a quantitative evaluation of MG-63 cell-mediated mineralization using alizarin red staining in vitro, Sr-HA surpassed HA in improving the bioactivity of the composite. Kim et al. (2009) [127] manufactured a calcium silicate-modified PEEK composite (CS/PEEK) with 0–50 vol % CS and soaked specimens in SBF with pure PEEK as a control. With the exception of pure PEEK, all of the CS modified composites induced apatite coating on their surfaces, indicating the ability to attach to living bone. The mechanical characteristics of the samples after immersion in SBF did not substantially decrease compared to those samples that were not subjected to SBF. Petrovic et al. (2006) [128] investigated the impact on normal human osteoblast (NHOst) cells of PEEK with 5, 10, 20, and 40% wt. % β-TCP produced by injection molding. The findings revealed that NHOst cells growing on β-TCP/PEEK had lower proliferation rates than those growing on pure PEEK, but that β-TCP/PEEK had no concentration-dependent reduction in cell proliferation when compared to pure PEEK. Von Wilmowsky [129] also discovered that β-TCP/PEEK had reduced cell viability and proliferation when compared to pure PEEK. These authors speculated that the inhibitory impact of β-TCP/PEEK on cell growth might be due to a change in the pH of the cell culture medium caused by the breakdown of the β-TCP molecule. Therefore, further research was needed to fully comprehend the effects of β-TCP/PEEK on osteoblasts. According to some studies, increasing the volume percentage of HA in the HA/PEEK composite enhanced the biological activity but decreased its mechanical strength and strain at the fracture point because of debonding between the PEEK and HA composites [13, 63, 102].

2.4.3.1 PEEK/HA composites with nano-sized fillers

Due to debonding between the HA filler and the PEEK matrix, conventional HA/PEEK composites may not be able to withstand long-term critical loading, and material scientists have used nanotechnology to solve this issue. Li et al. (2012) [130] used powder processing and sintering to make HA/PEEK nanocomposites, and they discovered that this new HA/PEEK nanocomposite had good mechanical characteristics and a high surface HA content. The findings of SBF immersion, cell adhesion, and proliferation in vitro indicated that the biocompatibility of PEEK/HA nanocomposites was boosted compared to those of pure polymer matrix. The PEEK/HA nanocomposites were recently fabricated using integrated solvent-based extrusion with the purpose of optimizing the biological and mechanical characteristics of the composites [131]. The researchers discovered that PEEK/HA composites had good biocompatibility, yields and compressive strength within the range of human cortical bone, making them suitable for load-bearing applications.

The structural, mechanical, and biological characteristics of highly porous polyetheretherketone (PEEK)/hydroxyapatite (HA) nanocomposite scaffolds reinforced with carbon fibre (CF) and carbon nanotubes (CNTs) were examined in detail [55]. In biological tests, cytotoxicity and cell viability of the prepared PEEK composites were evaluated as presented in Figure 2.6. It was worth noting that the prepared composites were non-toxic, and the biocompatibility was significantly enhanced in comparison to those of pure PEEK. The findings indicated that PEEK/HA nanocomposites containing CF and CNTs are a viable choice for bone scaffolding and other tissue engineering applications.

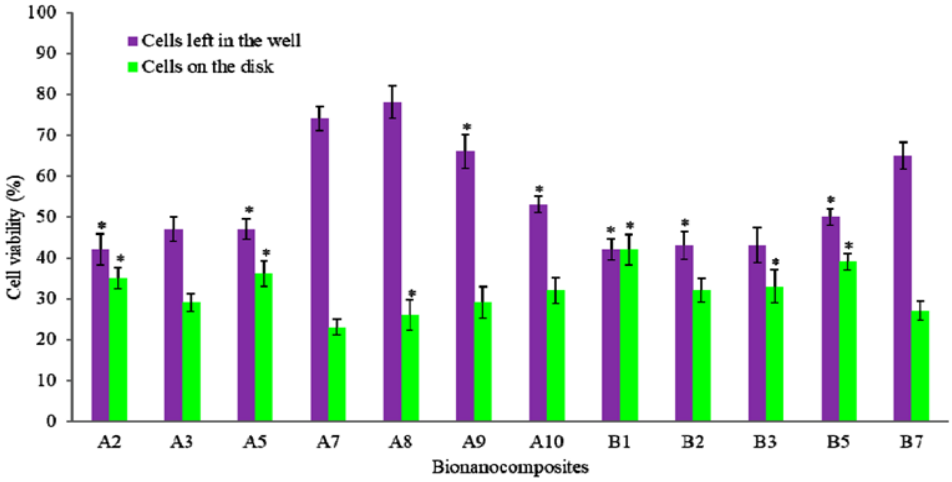

Figure 2.6: Cell viability of PEEK and its nanocomposites [55]

Ma et al. (2014) [132] developed PEEK/nHA nanocomposites by vibrating a ball mill and then injection molding process. They discovered that adding 40 wt % (21.5 vol %) nHA to PEEK increases the elastic modulus to 4.6 GPa. The elastic modulus of the prepared nanocomposites was substantially lower than the bottom limit for cortical bone modulus, i.e., 7 GPa. Recently, PEEK/nHA nanocomposites were prepared by using 4.4-21.5 vol % nHA for improving the bioactivity and mechanical properties [101]. The findings demonstrated that increasing the nHA content had enhanced the tensile strength and modulus of elasticity of PEEK-based nanocomposites. PEEK/nHA nanocomposites, on the other hand, were very brittle, with just 0.63 % fracture elongation. Because of their brittleness, PEEK/nHA nanocomposites were found to be inappropriate for use in load-bearing implants. To address this issue, different inorganic fillers were employed to enhance the mechanical properties of different polymer nanocomposites [1].

Among the several existing ways for modifying and enhancing the biological activity of PEEK, we concentrate on the fabrication of PEEK/HA composites by melt blending due to its simplicity of design and practicality. On the other side, when HA was coupled with PEEK through surface coatings/modifications, a non-uniform (amorphous) HA coated layer formed on the PEEK surface, altering the surface and mechanical characteristics of the polymers. In the recent literature, it was observed that the biological and mechanical properties of PEEK/HA composites were improved. However, the perfect control of the mechanical characteristics of the produced PEEK/HA composites is difficult to obtain. As a result, studies have continued to produce a variety of PEEK ternary composites, the most prominent of which is PEEK/MWCNTs/nHA.

2.5 Carbon nanofillers: Responsible for high mechanical strength

The effectiveness of the composites can be defined by their type, quantity, orientation, and alignment. Carbon nanofillers are defined as fillers with a carbon content of at least 92 wt % [133]. Polymer composites with carbon-based nanofillers have several potential uses, including electronics, fuel cells, transportation, and biomedical applications. The carbon-based nanofillers, such as carbon nanotubes (CNTs) and carbon nanofibers (CNFs), can increase the mechanical characteristics of polymer composites as well as their electrical and thermal conductivities [134, 135].

The commercially available carbon nanofillers based on their structure are categorized into three groups; General purpose (GP), high-performance (HP) and activated carbon fibres (ACF). The amorphous and symmetric structure, poor tensile strength, and relatively low cost are the characteristics that belong to the general purpose. Their uses are sealing materials, electrically charged materials, heating elements, filters, and as a reinforcement in concrete. The high-performance type can be utilized in many industries as the effective fillers in different kinds of materials, such as plastics, metals, and ceramics due to their high strength and modulus. And, the activated carbon fibers possess low strength and modulus, as well as a significant number of open micro pores that serve as adsorption sites.

2.5.1 Carbon nanotubes, classification, and significance

Carbon nanotubes (CNTs) have received a lot of interest among all the carbon nanofillers because of their excellent mechanical and electrical qualities as well as their ease of processing. Although, Iijima [136] is generally associated with discovering CNTs, Roger Bacon [137]reported the synthesis of carbon nanotubes as early as 1960. There are also reports from the 1950s catalysis literature to eliminate unwanted fibrous carbon deposits. Although nanotubes were not discovered in his studies, it was possible that they were present as a by-product when he utilized the electric arc technique to manufacture graphite whiskers. Some previous literature showed the development of carbon tubular structures when Endo was involved in hydrocarbon decomposition in 1976 [138]. However, in 1991 Iijima found the graphical tube structure of CNTs in the arc discharge equipment used in the production of C60 and other fullerenes.

The CNTs are the cylindrical structures of carbon atoms that are covalently bonded. They resemble the graphitic platelet, which are wrapped in smooth cylinders. Hemifullerenes are often used to cover the ends of cylinders in CNTs. There are two types of carbon nanotubes (CNTs) based on the number of stacked graphitic layers: single-walled carbon nanotubes (SWCNTs) and multi-walled carbon nanotubes (MWCNTs), as presented in Figure 2.7.

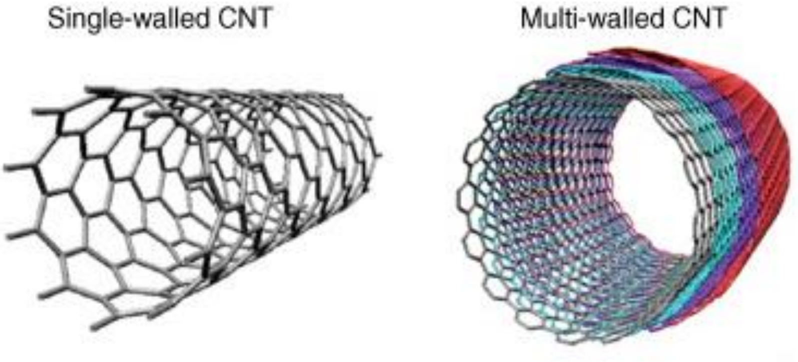

Figure 2.7: Single-walled carbon nanotubes b) Multiwalled carbon nanotubes [15, 139]

In MWCNTs, multiple rolled layers of graphite are placed coaxially around a central hollow core with van der Waals forces connecting subsequent layers, while a single sheet graphene cylinder is used in SWCNTs [15, 139]. The MWCNTs have an outer diameter that varies depending on the number of graphene layers and is typically between 10-50 nm, which is around ten times that of SWCNTs. MWCNTs have an inner diameter that is generally half of their outer diameter. Because of the smaller diameter and larger surface area, SWCNTs agglomerate more readily than MWCNTs and may build ropes or oriented bundles of SWCNTs. As a result, the cost of pure SWCNTs is often higher than that of MWCNTs, and their comparison is listed in Table 2.5 [140, 141]. In certain cases, the lengths of single and multi-wall carbon nanotubes may vary from a few micrometers to a few centimeters [142]. The resulting CNTs may differ greatly in terms of geometrical characteristics, such as diameter, aspect ratio, and entanglement, and crystalline perfection, including crystallization and purity, depending on their fabrication technique, which can significantly affect their properties [143].

Table 2.5: Comparison between MWCNTs and SWCNTs [140, 141]

Single-walled carbon nanotubes (SWCNTs)	Multi-walled carbon nanotubes (MWCNTs)
It is simple to characterize and evaluate	Complicated structure
Single graphene layer	Multiple graphene layers
Malleable and easily twisted	Not easily twisted
Need catalyst for the synthesis	Cannot prepared without catalyst
Difficult to disperse	Less agglomeration capability
Purity is a problem	Purity is high
30-50 wt. % with chemical vapor deposition (CVP) method	35-90 wt. % with CVP method
Up to 80% via arc discharge method	
Low mechanical strength	High mechanical strength
During functionalization, the risk of a defect is higher	When using the arc-discharged approach, the chances of a defect are reduced
It is difficult to synthesize in large volume	MWCNTs need easy processing to manufacture in large quantities

The CNTs with the associated materials and their applications have received augmented attention in the last two decades. CNTs possess a high degree of flexibility, chemical robustness [144], thermal stability even at more than 1000 ℃ temperature [145], a low mass density, and a high aspect ratio (usually >1000), whereas several experimental results suggested that these materials have extraordinarily high mechanical properties including tensile strength and elastic modulus [146]. The mechanical characteristics of CNTs [147, 148] are compared to those of other extensively used engineering materials and are enlisted in Table 2.6. It can be observed that CNTs have a substantially higher elastic modulus (E) and tensile strength than the most easily accessed materials. Because of these excellent features, CNTs have been used in a wide range of applications, including electronic devices, sensors, and biosensors, as well as transistors, batteries, hydrogen storage cells, and electrical shielding [149], and shown in Figure 2.8.

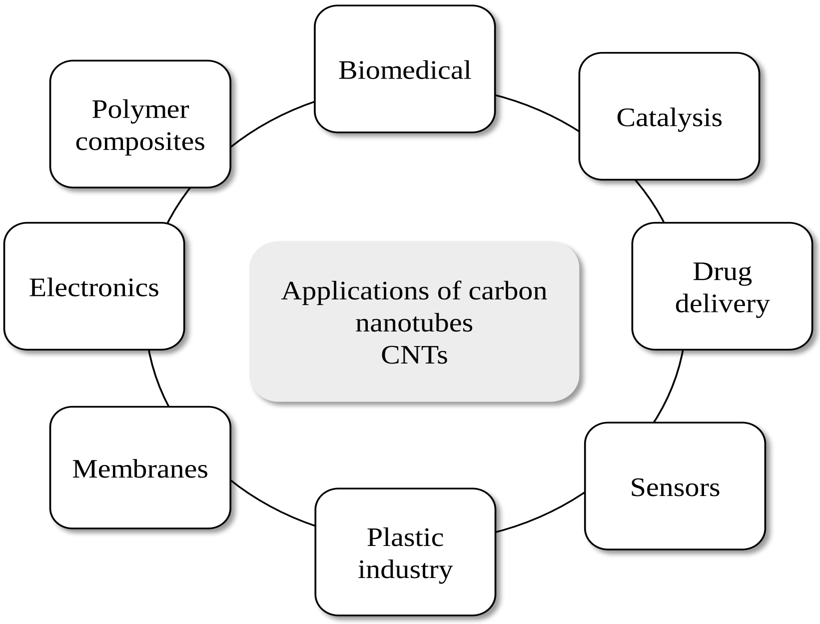

Figure 2.8: Some applications of CNTs [149]

2.5.2 Polymer/carbon nanotubes composites

The multifunctional characteristics of MWCNTs, particularly their superior mechanical strength, make them the ideal reinforcing agent in different engineering applications, especially for human bone fixation devices. The PEEK-HA composites have already been used in biomedical applications, with mechanical characteristics being sacrificed [1, 13, 132]. The MWCNTs can be introduced into PEEK-HA composites to boost their mechanical characteristics which are comparable to that of human cortical bone. The addition of even a small amount of carbon nanotubes has been shown to produce major changes in the mechanical performance of the nanocomposites. In 1994, after the first polymer nanocomposites with the reinforcement of CNTs by Ajayan [150], different researchers had been experimenting with a variety of approaches for producing CNT polymer nanocomposites, including covalent and non-covalent functionalization of CNTs [15].

Table 2.6: Mechanical properties of CNTs [147, 148]

Fiber Material	Specific Density (g/cm^3)	Elastic Modulus (TPa)	Tensile strength (GPa)
CNTs	1.3-2	1	10
High strength steel	7.8	0.2	<10
Carbon fiber	1.7-2	0.2-0.6	0.3-2.4
Quartz	2.3	0.07	3.4
Boron	2.5	0.4	3.5
Glass fiber	2.5	0.07-0.08	4.8

The addition of even a small amount of carbon nanotubes has been shown to produce major changes in the mechanical performance of the nanocomposites. In 1994, after the first polymer nanocomposites with the reinforcement of CNTs by Ajayan [150], different researchers had been experimenting with a variety of approaches for producing CNT polymer nanocomposites, including covalent and non-covalent functionalization of CNTs [15].

2.5.3 Modification of polymers with carbon nanotubes

The polymer modification with CNTs can be categorized into two classes: covalent and non-covalent functionalization between the CNTs and the polymer as shown in Figure 2.9 and their comparison is explained in Table 2.7. The covalent functionalization is concerned with the chemical bonding (grafting) of polymers to CNTs, in which strong chemical bonds are formed between nanotubes and polymers.

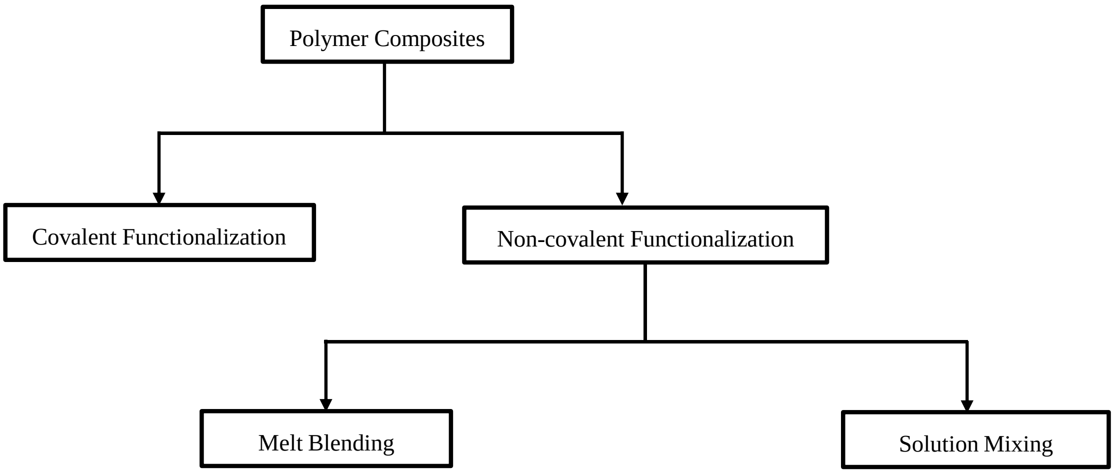

Figure 2.9: Different methods for preparation of polymer composites [30, 31]

2.5.3.1 Covalent functionalization of CNTs with polymers

Based on the construction of polymers, there are two major methods for covalent modifications of CNTs. The "grafting to" method needs manufacturing a polymer with a certain molecular weight that is ended with reactive groups or radical precursors. The polymer chain is then linked to the nanotubes surface through addition reactions in the second step [151]. The drawback of this strategy is that the grafted polymer content is restricted due to poor reactivity and the strong steric hindrance of macromolecules [152]. On the other hand, the "grafting from" method involves generating polymers from CNT surfaces by in situ polymerizations of monomers induced by chemical species adsorbed on the sidewalls and edges of the CNTs. This type of polymerization is an example of a surface-initiated polymerization process. Because of the strong reactivity of monomers, this approach allows for efficient, controlled, designable, and customizable grafting [15].

Diez-Pascual et al. (2010) [153] synthesized a hydroxyl polyetheretherketone derivative (PEEK-OH) which was covalently grafted to the acid-treated CNTs surface through a one-step process involving the activation of the carboxylic groups and a two-stage process involving acylation of the nanotubes with thionyl chloride resulting in a grafting degree of about 12 %. Zehua et al. (2008) [154] grafted the styrene-maleic anhydride copolymer (SMA) on MWCNTs and then incorporated the modified material into the polyvinyl chloride (PVC) matrix. The mechanical tests revealed considerable improvements in impact strength and elongation at break. The major drawback of this technique is that initial polymer chain binding sterically inhibits the migration of subsequent macromolecules to the CNT surface, resulting in a low grafting density. Additionally, only polymers with reactive functional groups are allowed to be employed [15].

The “grafting from” method includes polymerizing monomers from surface-derived initiators on CNTs. These initiators are covalently linked via small-molecule functionalization reactions such as acid-defect group chemistry and CNTs sidewall functionalization [155]. The benefit of the “grafting from” strategy is that polymer growth is not hindered by steric hindrance, enabling high molecular weight polymeric materials to be grafted effectively. The introduction of an atom transfer radical polymerization (ATRP) initiator onto the CNTs surface was used to graft the styrene-co-acrylonitrile (SAN) copolymer from MWCNTs [156]. For comparison, polystyrene and polyacrylonitrile-grafted MWCNTs were produced. The quantity of PS, SAN, and PAN covalently bound to MWCNTs were determined as 63.4, 45.5, and 64.5 wt. %, respectively. The glass transition temperature of the grafted polymer was increased significantly, showing that the chains were better immobilized because of adsorption on to CNTs. The limitation of this approach is that it requires precise control of initiator and substrate quantities, as well as the conditions necessary for the polymerization process [15].

2.5.3.1.1 Limitations of covalent functionalization

- Chemical reactions are involved.
- It is time consuming method.
- Expensive and cause damage to the surface of the CNTs.
- In this approach, the dispersed filler is not adapted for higher temperature [121].
- It cannot be conducted without using environmentally unfriendly strong acids or oxidants [48].

2.5.3.2 Non-covalent functionalization of CNTs with polymers

The CNTs functionalization by chemical procedures not only causes damage to varying degrees, limiting CNTs reinforcement, but it is also difficult to commercialize because of their complex procedures. Many researchers are becoming interested in non-covalent modification since it is more practical than covalent modification [157, 158]. The dispersion of noncovalently modified CNTs in the polymer is mainly accomplished by van der Waals forces, π-π interactions, and hydrogen bonding among the polymer, surfactant, and the surface of CNTs [159]. The non-covalent approach enables different groups to adsorb on the surface of CNTs without disrupting the CNTs surface structure. As a result, non-covalent surface treatment using different surfactants or polymers is often employed in the formulation of aqueous or organic solutions having a high weight fraction of homogenously distributed CNTs. The non-covalent aggregates have been effectively formed using surface-active compounds like sodium dodecyl sulfate (SDS) or benzylalkonium chloride [160, 161].

CNTs are incorporated into different polymeric host matrices using a variety of synthesis processes [162-164]. With certain compromises in the properties, one may select the appropriate processing technique for a specific scenario based on the thermal or mechanical characteristics of the matrix polymer, ease of synthesis from suitable monomers, desired composite performance indices, and cost limitations.

2.5.3.2.1 Solution Processing

The most common method to fabricate CNT-based polymer nanocomposites is solution processing which uses vigorous agitation (e.g., refluxing, mechanical stirring, vigorous shaking, bath/probe sonication) to aid rigorous and thorough mixing of CNTs with polymer in a solvent to enhance nanotube de-bundling and dispersion inside the polymer matrix [163, 165]. It is worth noting that this approach is only confined to the solvent-soluble polymers.

Table 2.7: Different methods for preparing PEEK/MWCNTs composites

Type of Methods	Benefits	Drawbacks	Ref.
Covalent Functionalization	This method is used to increase the adhesion and chemical properties of composites. This method is effective for homogenous CNTs dispersion. The covalent functionalization on composites was used in this approach to prevent functional group incompatibility with polymer matrices.	In this approach, chemical reactions are involved. It is a time-consuming method. Expensive and cause damage to the surface of the fillers. In this approach, the dispersed filler is not adapted for higher temperature. It cannot be conducted without using environmentally unfriendly strong acids or oxidants. CNTs Re-agglomeration in the polymer matrix.	[33, 48, 121, 165]
Non-covalent Functionalization	This strategy is eco-friendly and does not change the CNTs characteristics. It is related to the physical adsorption of polymers to the surface of CNTs and has no effect on the final structural properties of the material.	In this method, CNTs agglomerates are produced because of their poor dispersibility.	[15, 41]

	In this method, strong π-cation interactions with the inorganic fillers are involved. This method is used to boost the thermomechanical performance properties of the composites.		
Solution Mixing	This is the most common strategy for preparing polymer composites. The suitable and cheap conventional solvents are used for the dispersion of fillers in polymer matrices.	In this method, upon solvent removal, the intercalated/exfoliated structure/re-agglomeration remains, resulting in polymer composites. The effective removal of the solvents is still challenging.	[15, 166, 167]
Melt Mixing	This method is environmentally benign because of the absence of organic solvents. It is compatible with industrial applications. This approach is suitable for polymers that are insoluble in common solvents and, therefore, cannot be processed using solution techniques.	In this method, CNTs are re-agglomerated. This approach is successful at low CNTs concentrations since the viscosity of nanocomposites increased with greater CNT loadings.	[15, 168, 169]

The general procedure is dispersing CNTs in the suitable solvent and combining them with the polymer solution is shown in Figure 2.10 [148, 170], and other steps, including film casting and solvent evaporation, producing a nanocomposite film/sheet behind, are displayed in Figure 2.11. The selection of solvents is mostly determined by the solubility of the polymer matrix. Additionally, the solvents for CNTs and polymer distribution could be the same or different, but they must be capable of allowing intimate mixing between phases. In many applications, CNTs are not dispersed separately; instead, they are introduced immediately to the polymer solution, followed by vigorous stirring before film casting. The main disadvantage of using high power ultrasonication or shear mixing for a prolonged period is that it might result in tube lengthening, which weakens the composite characteristics. The boiling point of the dispersant or solvent has been discovered to have a significant influence on the characteristics of nanocomposites that have been produced [171]. The low-boiling point (i.e., quick evaporating or drying) solvents are recommended because they are easier to remove from the solution-casted nanocomposites.

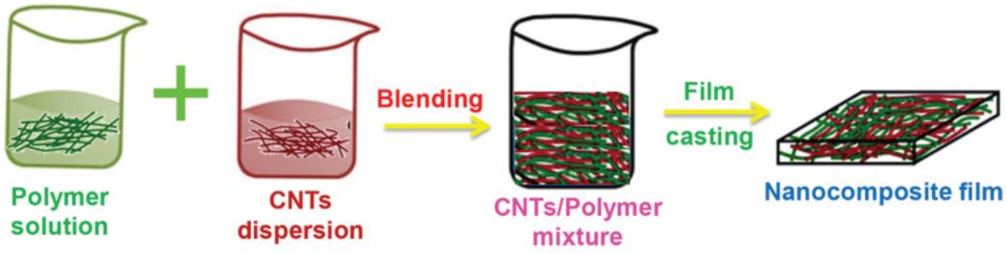

Figure 2.10: Schematic diagram of the solution processing approach [148, 170]

On the other hand, the solvents with higher boiling points are harder to remove and tend to get stuck in the solidifying/curing mass. An entrapped solvent may hinder the curing processes (in thermosetting polymers) or serve as a softener (in thermoplastic polymers), affecting electrical, thermal, and mechanical performance. Also, attempts to remove the solvent and avoid evaporation-induced void formation add to the complexity and expense of the system by requiring the use of regulated heating, vacuum/pressure, and other components [172]. Another issue with solution processing is that the slow evaporation of solvent allows enough time for CNTs to re-agglomerate and settle differentially, which result the inhomogeneous CNT dispersion in the matrix and poor properties. The solvent evaporation rate constraints may be overcome by gradually pouring a CNT/polymer nanocomposite dispersion over a revolving substrate (spin coating) [173] or on a drop casting [174]. The spin coating method is confined to thin films (a few nanometers thick) that cannot be pulled away from the substrate, while drop-casting method has problems with uniform drying throughout the thickness and a significant risk of void formation. Another effective technique uses coagulation of CNT/polymer distribution by pouring it into the excess of non-solvent, resulting in quick polymer chain precipitation and rapid entrapment of CNTs (without allowing CNTs to diffuse and settle) [175, 176].

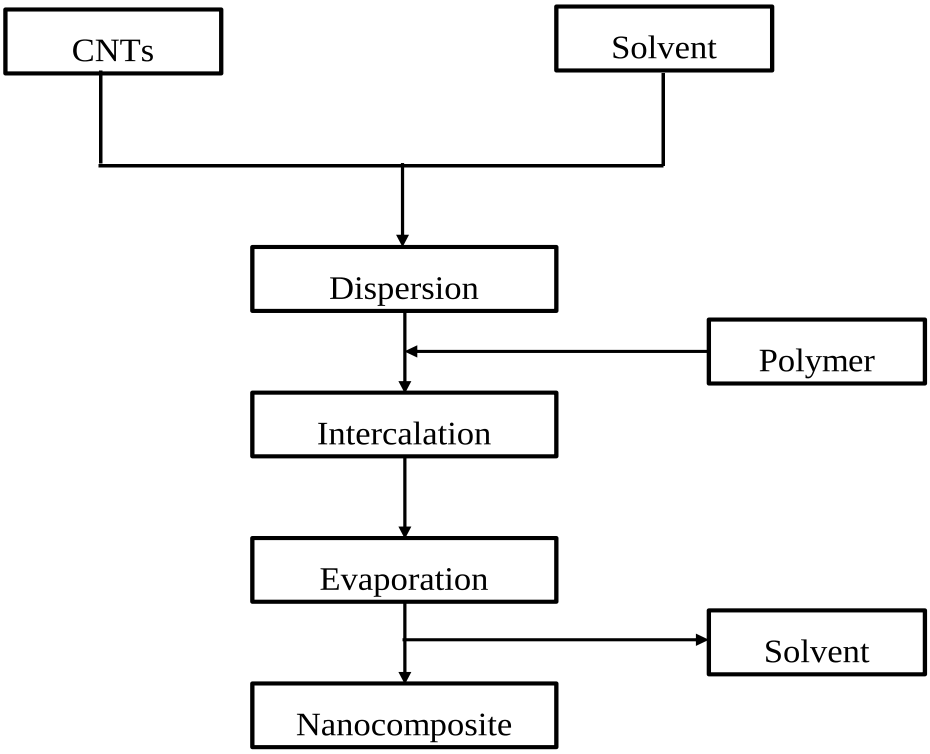

Figure 2.11: Different steps in the preparation of a polymer composite by solution mixing [170]

Because of the various benefits of this approach, many investigations on PEEK-MWCNTs composites have been described in the literature (Table 2.8). PEEK/ZrO_2 coated MWCNTs have been prepared using Brabender Plasticoder to improve the mechanical and thermal properties [177]. The authors revealed that at below glass transition temperature, the storage modulus of the composites rises gradually with the addition of wrapped MWCNTs, indicating the stiffening impact of these MWCNTs.

Because of the homogenous MWCNTs dispersing ability combined with a stronger PEEK–MWCNTs interfacial adhesion, the notable modulus enhancement reported in the PEEK/ZrO_2 wrapped MWCNTs nanocomposite should be associated to a more efficient load transfer from the matrix to the fillers.

The mechanical characteristics and biological functioning of PEEK/HA composites with 0-1 wt. % functionalized CNTs were examined [178]. The nanocomposites were manufactured through melt blending by dispersing MWCNTs uniformly in the PEEK employing ethanol as a solvent. The findings of mechanical and biological investigations revealed that elastic modulus and biological performance (cell attachment) were enhanced, and the synthesized composites were encouraged for use as an implant material.

The flexible PEEK/MWCNTs nanocomposites were successfully synthesized employing GENIOPLAST PELLET S (GPPS), a high-temperature lubricant for uniform MWCNTs dispersion in PEEK [179]. The GPPS has efficiently reduced the melt viscosity of PEEK and improved the MWCNTs dispersion inside it, allowing PEEK composites with improved mechanical characteristics. Importantly, the thermal stability (degradation temperature with 5% mass loss was 586 °C) and mechanical characteristics (tensile strength = 101 MPa) were recorded. Based on these findings, this method was suggested for improving MWCNTs dispersion in PEEK.

Lin et al. (2019) [180] used bulk conjugated carbazole side chains (PAK-Cz) as a solubilizer to investigate the interfacial compatibility of PEEK and CNTs. PAK-Cz has the benefits of ease of manufacture, cheap cost, excellent thermostability, and excellent solubility in N-methyl pyrrolidone (NMP). As predicted, all of these composites outperformed the pure PEEK material and the MWCNTs/PEEK (no solubilizer) composites in terms of mechanical performance, tensile strength, flexural strength, and simultaneous toughening effect. These findings indicate that PAK-Cz is a potential solubilizer material for CNT/PEEK composites.

The biocompatible PEEK/BG/MWCNTs ternary composite scaffold was successfully fabricated through compounding and injection-molding processes, and their mechanical properties were investigated [34]. It was noted that the mechanical properties of PEEK/BG/MWCNTs were vastly superior to the binary PEEK/BG composites. Because of the excellent interfacial bonding between MWCNTs and the PEEK matrix, as well as the homogeneous distribution of nanotubes across the composite, MWCNTs may penetrate into and entangle with the polymer matrix leading to increase the modulus and strength. Moreover, it was found that MWCNTs in composite further promoted cell metabolic vitality and osteogenic differentiation of osteoblast cells.

A unique coprecipitation-compounding and injection-molding approach were used to effectively produce biocompatible MWCNTs/PEEK nanocomposites comprising 1–10 wt. % MWCNTs using sodium dodecyl sulfate (SDS) as a solvent for uniform MWCNTs. The mechanical characteristics of MWCNTs in PEEK polymer were enhanced by their homogenous dispersion and tight adhesion, which were similar to those of human cortical bone. Additionally, the researchers demonstrated that strong π-π interactions between the extended π-conjugated core of PEEK polymer chains and the sides of MWCNTs increased the amount of MWCNTs in the polymer [7].

To enhance the mechanical characteristics of hydroxyapatite–polyetheretherketone (HAP–PEEK) composites for bone tissue engineering, a nano-sandwich scaffold was constructed by mixing two-dimensional graphene nanosheets (GNSs) with one-dimensional carbon nanotubes (CNTs) [20]. The long tubular CNTs in these nano-sandwich composites penetrated the graphene interlayers and resisted aggregation, enhancing the contact area between the MWCNTs and PEEK. In comparison with HAP-PEEK, the compressive strength and modulus of the PEEK-HAP-GNSs-MWCNTs have been enhanced 63.58 % and 56.54%, respectively. Moreover, after immersion into simulated body fluid, apatite layers were produced on the scaffolded surface, and the cells adhered across the scaffold surface, showing high viability and differentiation. This finding suggests that HAP–PEEK scaffolds augmented with GNSs and CNTs are a potential bone tissue engineering alternative.

Table 2.8: PEEK/MWCNTs composites prepared by solution mixing approach

Composite	Processing Technique	Key Results	References
PEEK/MWCNTs	Solution Mixing	Elastic modulus 2.10 GPa Tensile strength 85 MPa	[181]
PEEK/CNFs		The elasticity was maximum at 2 % CNFs	[182]
PEEK/CNTs		Poor dispersion between PEEK and CNTs	[183]
PEEK/MWCNTs/BG		Satisfactory mechanical properties with high degree of bioactivity	[184]
PEEK/MWCNTs/GO		High mechanical and thermal stability	[185]
PEEK/MWCNTs		Enhanced compatibility between MWCNTs and PEEK.	[30]
PEEK/MWCNTs/HA/GNSs		Apatite layer formation with modulus of 4.79 GPa	[20]

PEEK/MWCNTs/BG		MWCNTs enhanced the cells viability in the prepared composites	[34]
PEEK/MWCNTs		Better mechanical performance	[180]
PEEK/MWCNTs/PES		High thermal stability and good mechanical properties	[179]
PEEK/MWCNTs	Solution Mixing	Effect MWCNTs debundling and disentanglement in PEEK	[177]
PEEK/MWCNTs/HA		13 % improvements in elastic modulus MWCNTs helped to promote cells attachments and biocompatibility of PEEK and HA Agglomeration and bundling are caused by higher filler concentrations.	[178]
PEEK/MWCNTs		The MWCNTs dispersion, thermal stability and	[25]

mechanical properties were higher at 1 % MWCNTs.

MWCNTs agglomeration at 2%.

2.5.3.2.1.1 Limitations to use solution processing

- The inclusion of high boiling point surfactant/solvent imposes the inevitable restriction of surfactant retention in the nanocomposites, impairing their thermal and mechanical characteristics [186].

- The trapped solvent may obstruct the curing process (in thermosets) or serve as a softener (in thermoplastics), weakening the electrical, thermal, or mechanical characteristics. Also, attempts to remove the solvent and avoid the development of evaporation-generated voids add to the complexity and expense of the process by necessitating the use of controlled heating, vacuum/pressure, and other equipment [187].

- The slow evaporation of the solvent allows ample time for CNTs to re-agglomerate and settle differentially, resulting in inhomogeneous CNTs dispersion in the matrix and the observation of non-uniform and poor characteristics.

2.5.3.2.2 Melt Mixing

Melt processing is regarded as a promising method for producing thermoplastic matrices based CNTs/polymer composites owing to its cheap cost and suitability for large-scale fabrication for industrial uses. The elevated temperatures are used to melt the receptor thermoplastic matrix polymers, forming a viscous liquid that is designed to flow [163, 188]. High shear forces are generated by the molten polymer flow, which facilitates partial debundling of CNTs and their dispersion within the matrix. Melt blending has three main benefits: it is more customizable because the polymer does not need to be dissolved; it is compatible with traditional industrial operations like extrusion, internal mixer, injection, and blow molding, generating large-scale applications; and it is environmentally benign because organic solvents are not used [14].

In general, melt processing can be achieved in two stages. It involves melt blending of polymer with CNTs nanoparticles using high shear forces in an extruder or internal mixer. The extended mixing intervals often result in better dispersion of the nanotube bundles. The bulk samples can be subsequently prepared using a variety of methods, including compression or injection molding, depending on the ultimate morphology/shape of the nanocomposite [189]. The schematic flowchart for melt blending can be seen in Figure 2.12 [148].

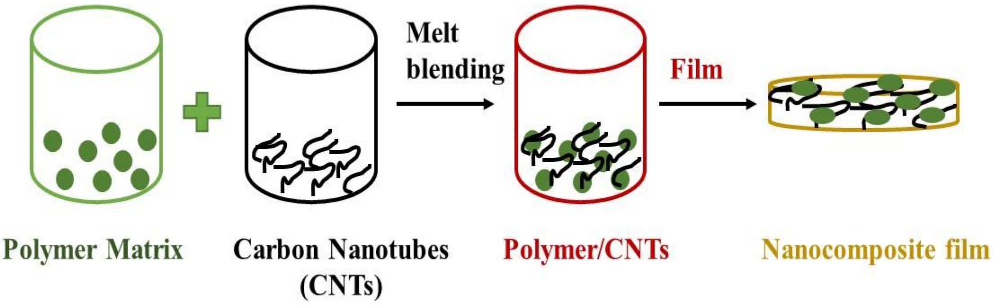

Figure 2.12: Schematic diagram of the melt mixing approach [148]

Recently, melt mixing/blending was effectively used to disperse carbon nanotubes (CNTs) inside a variety of thermoplastic matrices, polyamide 6 [190], polymethylmethacrylate(PMMA) [191], polyethylene(PE) [192], polystyrene(PS) [193], and polypropylene(PP) [194]. PEEK has been combined with CNTs to develop polymer nanocomposites with improved thermal and mechanical characteristics as compared to neat polymers since the introduction of CNTs as a high-performance nanofiller, as seen in Table 2.9. The flowchart for basic steps involved in melt blending is shown in Figure 2.13 [170].

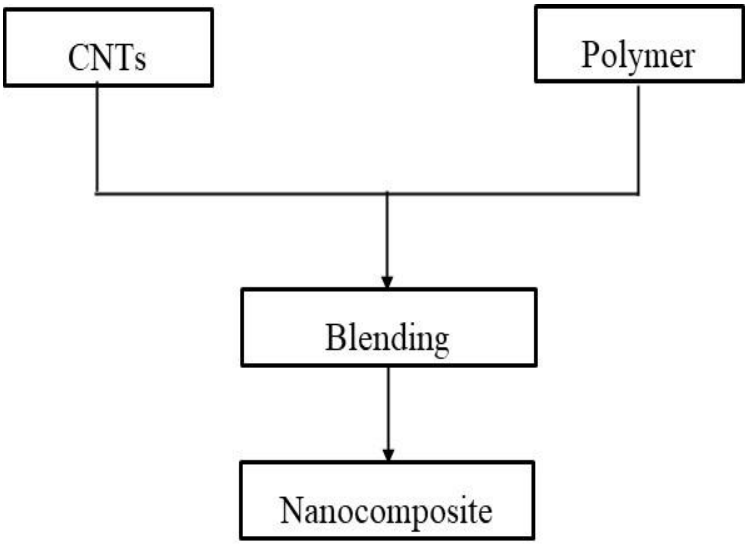

Figure 2.13: Flowchart describes the major steps of melt blending of polymer composite [170]

The PEEK/MWCNTs and PEEK/MWCNTs/tungsten carbide (WC) nanocomposites were prepared using a twin-screw extruder with different volume percentages of MWCNTs and WC [24]. The comparative morphological, thermal and mechanical properties were evaluated. The addition of nanofillers enhanced the thermal and mechanical performance of the nanocomposites. The increase in the temperature where the maximal degradation occurs and the improvement in the initiation of degradation temperature were indications of the resistance provided by the nanofillers in polymer nanocomposites. The incorporation of nanofillers to PEEK composites also improved the mechanical characteristics (stiffness and rigidity).

The compounding and injection molding processes were used to manufacture MWCNTs filled PEEK nanocomposites with filler loadings ranging from 0.5 to 5 wt % [27]. The homogeneous distribution of CNTs inside the matrix indicated an exceptionally high strain at rupture (up to 140 %) and enhanced elastic modulus. The authors discovered that the nanotubes served as a confining agent for the polymer chain, preventing it from moving freely.

The agglomeration of nanofillers, such as CNTs in the PEEK matrix remains a difficult task owing to the inert nature of PEEK towards organic solvents [195]. The MMT (organically modified montmorillonite) was used as a second filler to promote the dispersion of CNTs in the PEEK matrix and to improve the mechanical characteristics and minimize the material costs. The melt-blended PEEK/CNTs/MMT nanocomposites enhanced the dispersion capacity of CNTs in the PEEK, and the findings showed that elastic modulus was 23.3 % greater than pure PEEK at 0.5 wt % CNTs and MMT. In summary, the addition of MMT as an additional filler has a reinforcing impact on PEEK by enhancing CNT dispersion in the matrix.

The poor wettability of carbon fibre (CF) and inert PEEK resulted in weak interfacial adhesion, which limited the application potential of PEEK/CF composites [68]. PEEK/CF composites were developed by grafting hydroxylated PEEK on MWCNTs and modifying the interface among PEEK and CF. The interfacial adhesion was enhanced by the π-π interactions (as illustrated in Figure 2.14 [68]) between the aromatic rings of each component. The mechanical strength of PEEK/CF nanocomposites was improved as a consequence of these strong interactions.

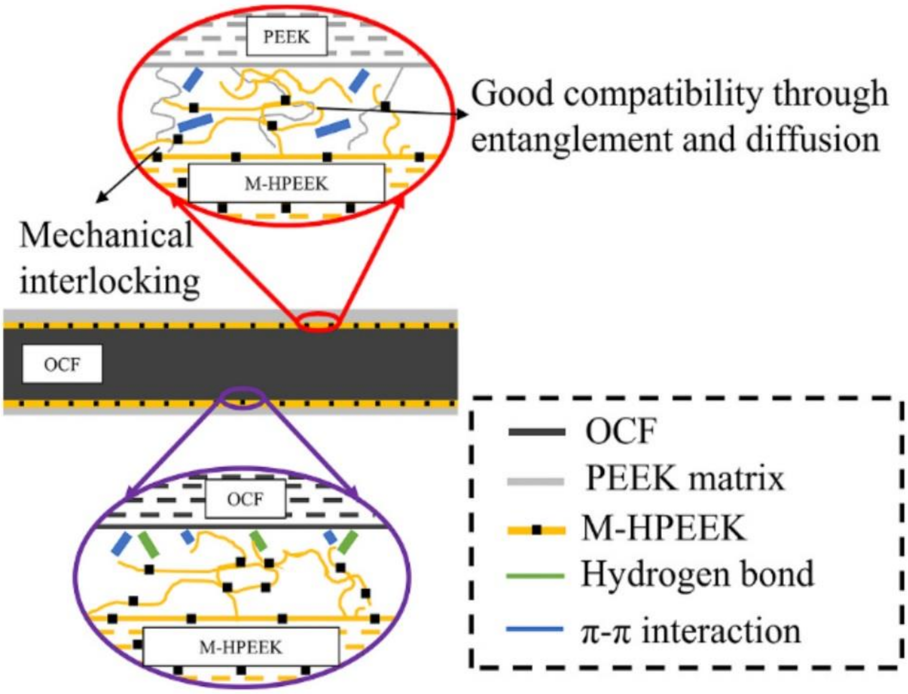

Figure 2.14: The π-π interactions between PEEK and CF [68]

PEEK foams with various HA, CF, and CNTs nanoparticles were produced using the cast melting and salt porogen leaching manufacturing methods [196]. The inclusion of HA, CF, and CNTs substantially improved the elastic modulus and yield strength of materials when compared to base PEEK. The introduction of 0.5 wt % CNTs to the PEEK/20 wt % HA composite resulted 186 % increments in compression modulus. However, incorporating a large quantity of carbon particles into PEEK, decreased the mechanical characteristics owing to carbon particle agglomeration, which acted as a stress enhancer.

In another study, the MWCNTs were intended to be incorporated into PEEK/BG to develop a composite of PEEK/BG/MWCNTs using compounding and injection-molding methods [34]. The PEEK/BG/MWCNTs composites with improved mechanical characteristics and good biocompatibility were obtained by combining the benefits of BG and MWCNTs. At 6 wt % of MWCNTs in PEEK composites, the highest elastic modulus value (6.1 GPa) was achieved as compared to plain polymer (4 GPa). The authors discovered that the aggregation of MWCNTs (Figure 2. 15) in PEEK/BG composites, as well as their low elastic modulus compared to human cortical bone (7 GPa), limited its use as a bone repair biomaterial.

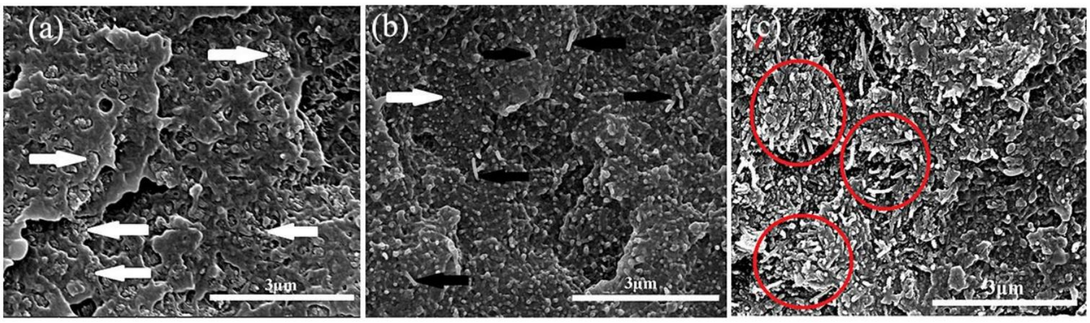

Figure 2.15: MWCNTs agglomeration in PEEK/BG composites [34]

The amounts and dispersion of MWCNTs are the key parameters to boost the thermal and mechanical properties of the PEEK/MWCNTs nanocomposites using melt mixing techniques. A twin-screw extruder was used to produce PEEK/MWCNTs nanocomposites with improved mechanical characteristics [197]. The MWCNTs were homogeneously distributed in the PEEK matrix, as revealed by transmission electron microscopy (TEM) images. By adding up to 17 wt % CNTs to the produced composites, the tensile elastic modulus was increased linearly. At 17 wt % MWCNTs, the maximum modulus (50 % higher than pure PEEK) was achieved. The obtained value of elastic modulus was 6.6 GPa which was lower than those of human cortical bone (7 GPa). The

Table 2.9: PEEK/MWCNTs composites prepared with melt mixing

Polymer Composite	Filler loading (%)	Fabrication technique	Key results	Ref.
PEEK/MWCNTs	0 -15	Extrusion	The elastic modulus of the composites increased by 89 %.	[198]
PEEK/CNTs/PEI	0-1%	Extrusion	An increase in decomposition temperature (18 °C) than pure PEEK. 35 % higher modulus values than neat PEEK.	[199]
PEEK/MWCNTs	2- 17	Extrusion	Formation of MWCNTs agglomeration	[200]
PEEK/MWCNTs	0-17	Extrusion	Elastic modulus was 6GPa	[197]
PEEK/MWCNTs/ CNF	0.5-5	Internal mixer	Improved mechanical properties	[201]
PEEK/CNTs/PS (Polysulfones)	-	Extrusion	CNTs agglomeration at higher contents	[169]
PEEK/MWCNTs	0-5	Extrusion	Better mechanical properties	[37]

PEEK/CNTs/PS (Polysulfones)		Extrusion	Enhanced thermal and mechanical stability	[202]
PEEK/CNTs	0.1-0.9	Extrusion and hot press	CNTs aggregates bigger than 2μm	[203]
PEEK/CNTs	0.1-0.9	Extrusion and hot press	CNTs agglomerates with 65nm diameter	[38]
PEEK/MWCNTs	9-15	Injection molding	Considerable high mechanical properties	[204]
PEEK/CNTs	0.1-1	Internal mixer and hot press	Good MWCNTs dispersion	[62]
PEEK/CNTs	0.1-2	Haake Rheocord	Small amounts of fillers are effective.	[205]
PEEK/CNTs/HA/GNS	0-10		56.54 % increased elastic modulus	[20]
PEEK/MWCNTs	0-5	Haake MiniJet	Improvement in thermal degradation temperature	[206]
PEEK/MWCNTs/HA	0-3	Extrusion	MWCNTs agglomeration	[1]
PEEK/MWCNTs	0.5-5	Compounding and injection molding	Maximum elastic modulus was 2.9 GPa	[27]
PEEK/MWCNTs	0-1.5	Extrusion	Higher mechanical properties than pure PEEK matrix	[24]

PEEK/MWCNTs/ MMT	0.5	Injection molding	23.3 % greater elastic modulus than pure PEEK	[195]
PEEK/CNTs	1-10	Extrusion	Thermal stability decreased because of heterogenous nucleators.	[207]
PEEK/CNTs	0.1-1	Compression molding	Elastic modulus range (4.6-5.1 GPa)	[69]
PEEK/CNTs	0.1-2		CNTs agglomeration	[25]

authors recommended that novel and environmentally friendly approaches should be employed to promote the distribution of MWCNTs in PEEK polymer matrix for increasing the required properties.

2.5.3.2.2.1 Limitations to use melt processing

Although melt mixing technique is simple but some issues that hindered it from being used in different polymer composite processing applications.

- The strong shear force and increased temperature must be appropriately handled to prevent nanocomposites from deteriorating. While, significant shear forces aid in the dispersion of carbon nanotubes, they can also result in undesired CNTs fragmentation or polymer chain scission [148].

- It is not well designed for the fabrication of polymer composite having a higher amount of CNTs (> 5 wt %) [208]. Likewise, the inclusion of larger concentrations of CNTs significantly increases the viscosity and MWCNTs agglomeration in the polymer composites, rendering extrusion or internal mixer very challenging.

To overcome the aforementioned limitations, researchers are focusing on the use of ionic liquids (ILs) as possible solvents or dispersing agents for the synthesis of polymer composites owing to their outstanding physicochemical characteristics. Over the past decade, more than 1845 papers have been published, demonstrating the significance of utilizing ILs in polymer composites synthesis. Indeed, as illustrated in Figure 2.16, studies on the preparation of polymer composites employing ILs is growing linearly.

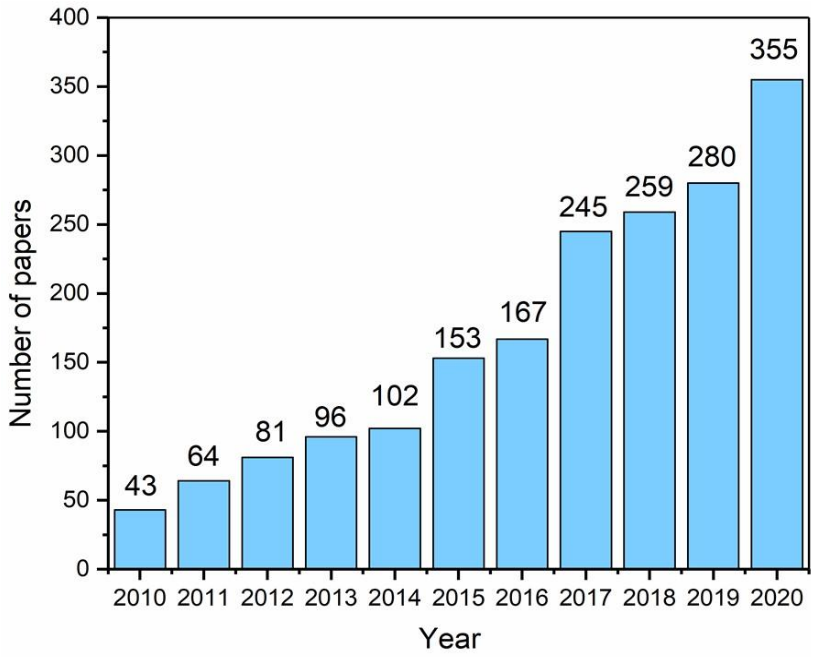

Figure 2.16: The number of articles published in the past decade (Source: ScienceDirect, keywords (Polymer composites; Ionic liquid), June 2021)

2.6 Ionic liquid assisted fabrication of Polymer/MWCNTs composites

2.6.1 Ionic liquids and their properties

ILs are mainly composed of an organic cation and an inorganic anion. The alkyl-substituted imidazolium, quaternary ammonium, or pyridinium ions are the most common cations. The melting point of ILs is generally below 100 °C, and they stay liquids over a broad temperature range (around 400 °C). In 1914, Walden [209] developed the first IL, ethyl ammonium nitrate, and in the 1970s-1980s, by combining aluminum halides with the imidazolium halides, the 1st generation ILs (alkyl imidazolium halogen aluminate) were synthesized [210]. The cationic structure (e.g., the length and geometry of alkyl-substituted groups), as well as the degree of anion charge delocalization, determine the chemical, physical, and biological properties of ILs [46]. The physicochemical characteristics of ILs may be readily adjusted by altering the structure of the anions and cations. As a result, the properties of ILs include a broad range of values and are very difficult to generalize. Zhang et al. (2006) collected a detailed database on the physical characteristics of ILs, comprising viscosity, melting point, and density [42]. The Figure 2.17 illustrates some of the most frequently used ILs cations and anions for fabrication of polymer composites and the properties of ILs are shown in Table 2.10.

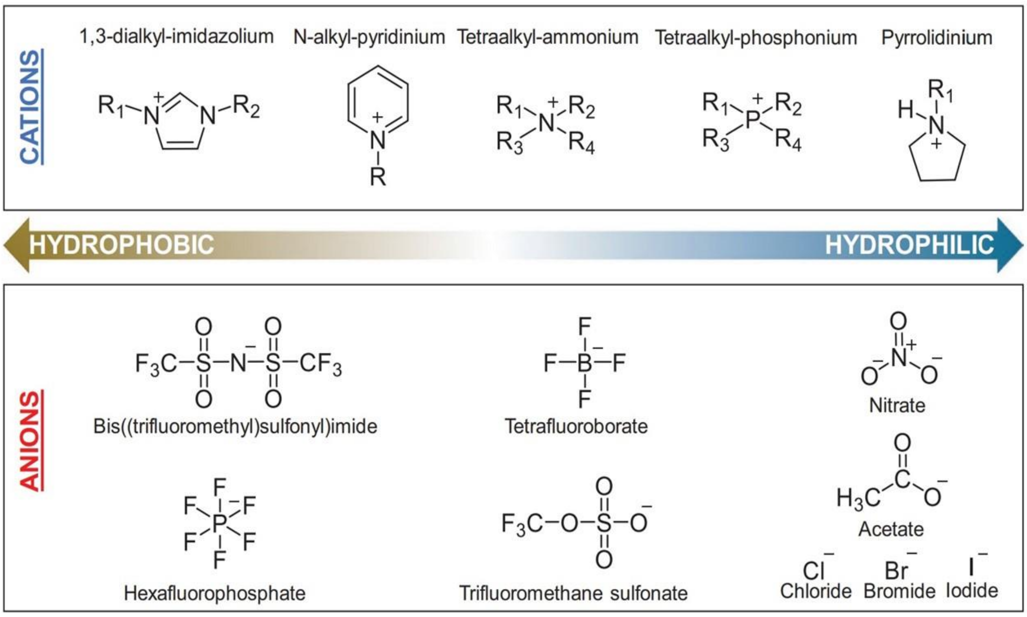

Figure 2.17: Most frequently used cations and anions for polymer composites [211]

ILs are categorized as extremely polar solvents on their solvation properties. The partitioning, solvatochromic dyes, and fluorescence probe techniques have been used to obtain knowledge on the ILs polarity [212]. Also, several empirical and semiempirical polarity measurements have been used to estimate and compare the solubility of polymers in ILs with their polarities, including the Hansen solubility parameters [213], COSMO-RS [214], and Kamlet-Taft [215]polarity technique.

Table 2.10: Properties of ILs for polymer composites

Property	Description	Ref.
Intermolecular interactions	ILs are likely to interact with polymers in a variety of ways, including π-π interactions, hydrogen bonding, and van der Waals interactions.	[216]
Miscibility of ILs with other solvents	There is no universal rule. Certain polar solvents, such as ketones and lower alcohols, are miscible with it, while others, such as ethyl acetate and hexane, are not.	[217]
Solubility in water	Two types of ILs: hydrophilic (water-miscible) and hydrophobic (water-immiscible)	[218]
Thermal performance	ILs are extremely stable solvents, having thermal stability up to 440°C and just 5-10% degradation. As a result, ILs are excellent high-temperature solvents for making polymer composites.	[211, 219]

The majority of conventional solvents are thermally resistant at high temperatures for relatively short periods; prolonged exposure often results in undesired breakdown [220]. On the other hand, it is well recognized that ILs are thermally stable up to 440 °C. The thermal stability of ILs is determined by the strength of their hydrocarbon bonds. It is noted that ILs with a greater transfer of protons decompose prematurely before achieving their boiling points at temperatures of between 100 °C and 360 °C [221]. Due to their bond strength arising from resonance stabilization [222], ILs containing alkylammonium, imidazolium and a variety of many other heterocyclic cations are categorized as the most stable ILs. It is well proven that anionic components contribute significantly more to the thermal properties of ILs than their cationic counterparts. In addition, the hydrophilic nature of the anions causes a reduction in the thermal characteristics of the ILs [223].

Ionic liquids are considered to be appropriate for a wide variety of intermolecular interactions, including π-π interactions, hydrogen bonding, and van der Waals interactions among polymers and fillers. Such strong matrix-filler interactions improve the interfacial adhesion and contribute to significantly enhance the composite characteristics such as filler dispersion, thermal stability and mechanical strength [211]. ILs possess a low vapor pressure (negligible), which is generally lower than the degradation temperature, as well as a high conductivity (~10^3-10^2 cm^{-1}) [224] times greater than organic solvents. Moreover, because of their high solubility and miscibility with a wide variety of compounds (organic/inorganic/polymeric materials), ILs with these unique properties (Figure 2.18) can be used in lieu of conventional organic solvents [225]in a number of techniques, including organic reactions, catalysis, extraction, and separation, thereby supporting the implementation of green chemistry and clean technologies [226].

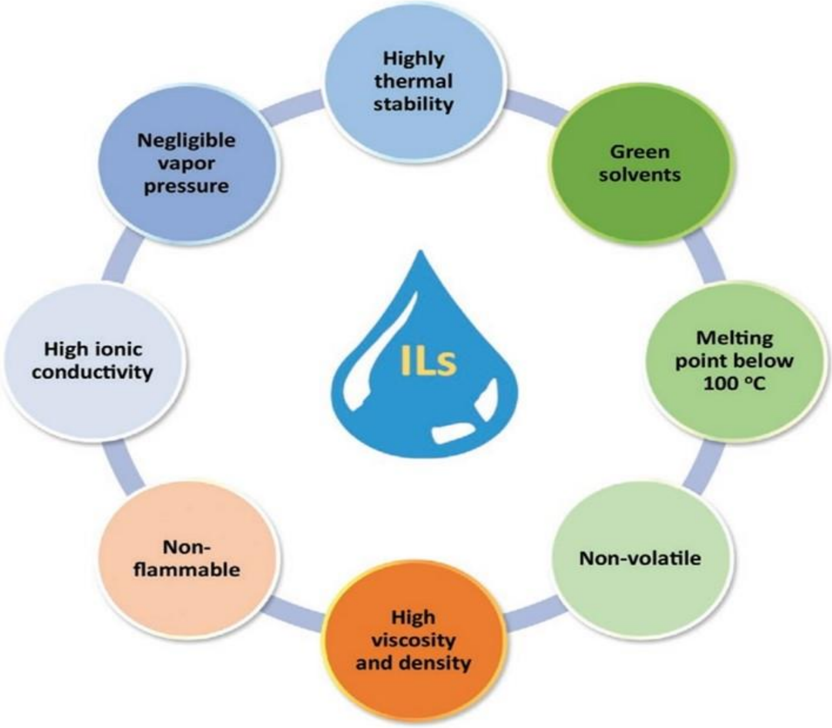

Figure 2.18: Important characteristics of ILs [211]

2.6.2 Ionic liquid properties and processing affecting MWCNTs dispersion

2.6.2.1 Cationic and anionic structures

The most extensively studied ILs for polymer composites are incorporated with imidazolium-based cations due to aromatic nature of delocalized π-π electrons. The cations having heterocyclic aromatic functionality, such as imidazolium (hydrophobic), were also shown to have a greater capacity to distribute inorganic fillers in polymer composites [227]. Furthermore, ILs containing non-aromatic cyclic cations such as piperidinium or pyrrolidinium are ineffective in dispersing CNTs in the polymer nanocomposites [228]. Imidazolium based ILs with HSO_4 and acetate anions have extensively been employed for the dissolution and dispersion of various polymeric materials and are also attractive from a cost perspective [45, 46]. Moreover, increasing the chain length of a cation in a specific IL increases the dispersion of CNTs into the polymer matrices because of stronger π-π interactions between imidazolium ring and π-electronic nanotubes. Fang et al. (2018) [58] extensively examined the impact of alkyl chain lengths ranging from C4 to C6. Interestingly, IL with a longer alkyl chain (C6) exhibited improved dispersion and higher thermal stability.

The importance of anions in dispersing inorganic fillers (CNTs) into polymer matrices has been shown in fundamental investigations. It was demonstrated that anions (such as [OAc] and [Cl]) with exceptional hydrogen bond basicity have a greater capacity for dispersing inorganic fillers into polymers [46, 229]. The basicity value has a significant effect on the distribution and dissolution of different fillers in polymers. In comparison, anions having low basicity are ineffective for polymers and filler [230]. Additionally, ILs containing HSO_4 as an anion have a substantial influence on the characteristics (morphology) of polymer composites and are economically viable anions. Indeed, since bigger anion sizes have a lower capacity for hydrogen bond formation, increasing the anionic size significantly reduces the dissolving ability of ILs [231]. The effect of IL anion on polymer composites is entirely determined by its hydrogen-bond basicity since IL anions contribute significantly to the breakdown of inter- and intramolecular hydrogen bonding [232].

2.6.2.2 Particle size and loadings

The novel nanomaterials with unique characteristics have been developed as a result of recent advances in nanotechnology research. In general, nanomaterials have superior physicochemical characteristics to their micron-sized equivalents [1]. To improve the surface characteristics of polymers containing ILs, such as the dispersion of inorganic fillers, small-sized particles are essential [218]. In this regard, the most significant variables in achieving uniform distribution are the sizes of polymer matrices and inorganic fillers. According to Ke et al. (2017) [233], PVDF/CNTs nanocomposites were fabricated using IL as a dispersant to ensure homogeneous dispersion of CNTs. The dispersion of CNTs in PVDF was significantly enhanced with the help of IL. This phenomenon was ascribed to strong surface adhesion between the nano-sized carbon nanotubes and IL, which may enable the CNTs in correctly dispersing on PVDF. Additionally, IL-assisted CNTs had a significantly higher mean molecular weight than the untreated sample. Likewise, the modified MWCNTs demonstrated increased thermomechanical stability on comparing to the samples that were not pretreated [234].

The concentrations and quantities of ILs and MWCNTs used in the preparation of polymer composites are also critical characteristics. In this respect, Subramaniam et al. (2011) [235] studied the impact of different concentrations of IL on the mechanical and electrical properties of polychloroprene rubber (CR) nanocomposites containing MWCNTs and proposed the optimal weight ratio (MWCNTs: IL) for achieving the best properties. It was also discovered that increasing the IL loading caused the mechanical characteristics of the composite to deteriorate. The examples show that using nano-sized fillers with optimum amounts of ILs and inorganic fillers to facilitate the fabrication of CNT-based polymer nanocomposites may be a very useful and cost-effective method.

2.6.3 MWCNTs Dispersion in ILs for polymer composites preparation

Numerous research has recently concentrated on utilizing ILs to pretreat CNTs for polymeric composites, demonstrating the tremendous potential of IL as a solvent.

Because of their particular structure, ILs have distinctive solubility properties in comparison to other polar molecular and conventional organic solvents. This section gives a quick summary of how to produce various polymer composites using MWCNTs distributed by ILs. Table 2.11 shows the features of environmentally friendly composites made from CNTs that have been pretreated with ILs.

The role of IL, 1-carboxyethyl-3-methyl-imidazolium bis(trifluoromethyl sulfony)imide (CMI), on polymer filler interactions, filler distribution, thermal stability, and mechanical characteristics of polychloroprene (CR)/MWCNTs composites was investigated [48]. The non-covalent functionalization of MWCNTs/CMI was attributed to the strong interaction, which included the cation-π and π-π stacking interactions, and other potential interfacial properties between CMI and MWCNT, as shown in Figure 2.19. The tensile strength was enhanced from 12.4 MPa to 18.2 MPa as a result of these interactions with decreased filler agglomeration.

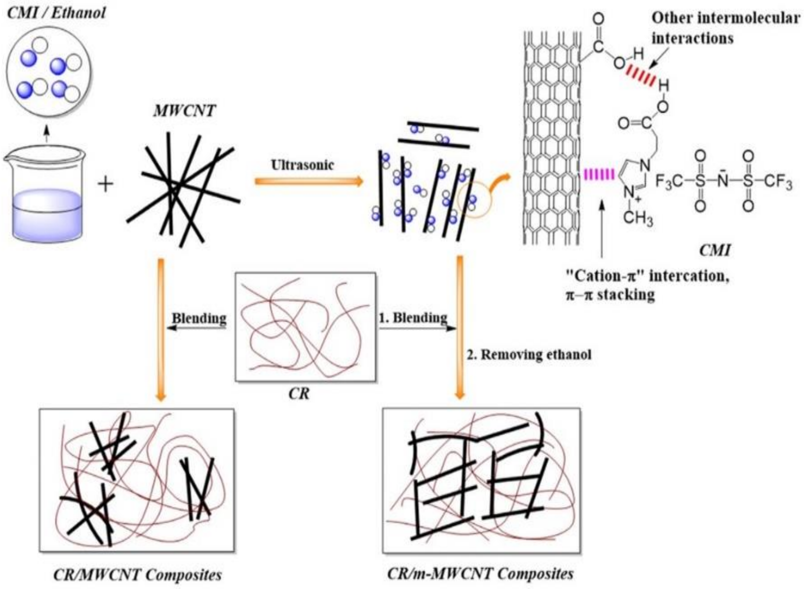

Figure 2.19: Schematic diagram of different interactions between CMI and MWCNT [48]

Abraham and coworkers (2018) produced well-dispersed, durable, and mechanically stable MWCNTs-styrene-butadiene rubber (SBR) composites using a melt mixing method with the use of an IL as dispersant [49]. They investigated the dispersion and mechanical characteristics of MWCNTs in SBR. The tensile experiments demonstrated that the mechanical reinforcement was enhanced as a result of appropriate CNTs distribution in the SBR matrix. It was shown that the well-settled MWCNTs increased the tensile strength to 318 % over the pure polymer.

A new method for manufacturing extremely piezo-resistive and robust poly(vinylidene fluoride) (PVDF)-based polymer nanocomposites was developed by adjusting the interactions among the polymer matrix and CNTs through the use of an IL as an interfacial linker/modifier [233]. The pretreatment of CNTs with IL substantially enhanced their macro-dispersion in the PVDF matrix. It was discovered that when the IL content increased, the agglomerates shrink in size and the area ratio of remaining aggregates (A_{agg}) reduced substantially. For instance, the nanocomposite 10IL-2CNTs displayed an A_{agg} of about 0.2 %, which was approximately 23 times less than the A_{agg} of the reference nanocomposite (4.8 %). TEM also confirmed the findings from the microscope, indicated that IL-pretreated CNTs exhibited reasonably uniform dispersion in PVDF, despite the presence of a few small entangled CNTs.

The addition of plain CNTs and IL-coated carbon nanotubes (IL@CNTs) to synthesized PVDF nanocomposites by extrusion and injection molding methods [47]. The morphological and microstructure analysis revealed that the IL@CNTs had superior dispersion than the CNTs in the PVDF nanocomposites, as can be seen in Figure 2.20. It was worth mentioning that all PVDF/IL@CNTs samples had a high melting point compared to PVDF/CNTs samples with the same CNTs concentration. The significant nucleation effects provided by the CNTs into PVDF were attributed to these improvements in the melting point.

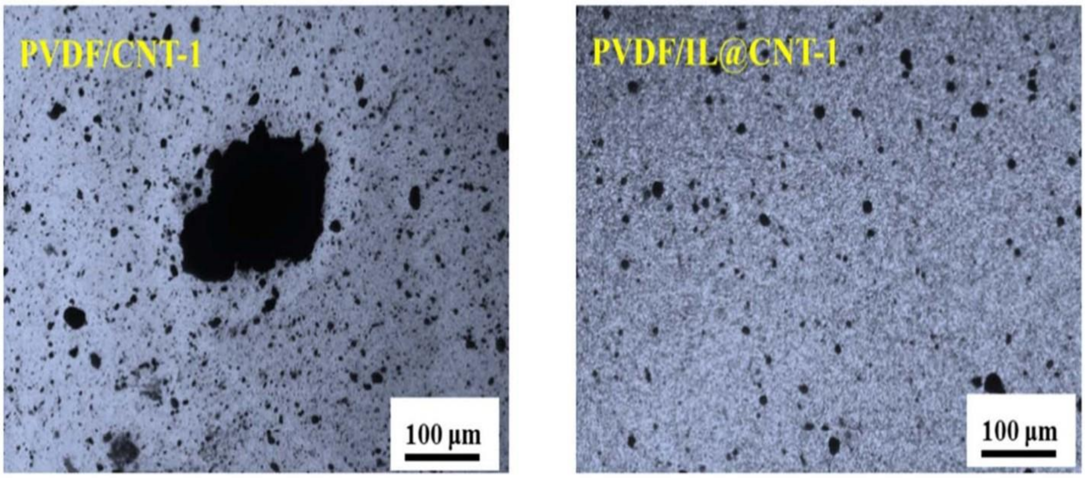

Figure 2.20: The CNTs and IL@CNTs distribution in DMF solvent [47]

The impact of IL/MWCNTs on the mechanical, thermal, and electrical characteristics of PMMA nanocomposites was explored [236]. The mechanical properties, including tensile strength and elastic modulus of PMMA composites, were estimated. The tensile strength and modulus were determined to be 46.52 MPa and 2.25 GPa at 0.5 wt % IL/MWCNTs, respectively, which were 119 % and 58 % higher than pure PMMA. This is because of the significant π or π-π interactions between the IL/MWCNTs and the polymer matrix, which inhibited the polymer chain mobility from deteriorating.

Amit and coworkers combined MWCNTs with IL to facilitate their dispersion in the PVDF matrix, and the PVDF composites were synthesized by melt blending [237]. The FESEM and TEM images showed that the IL-bound MWCNTs were uniformly distributed throughout the PVDF matrix. MWCNTs/ILs were shown to be an effective nucleating cites for PVDF crystallization in the differential scanning calorimetry (DSC) investigation. The glass transition temperature (T_g) was progressively raised in accordance with the amount of MWCNTs/IL. The Young's modulus was also improved (77 % higher at 1 wt % IL than those without IL) with the concentration of MWCNTs/IL, and the findings indicated that at their low concentrations, they followed a parallel alignment to the film surface.

Table 2.11: Polymer composites prepared by IL-modified CNTs

Polymer Composite	Ionic liquid	Loading (%)	Processing approach	Key results	Ref.
Epoxy-MWCNT	$[EPIL]BF_4$	0-2	Internal mixer and hot press	π-π interactions	[238]
Epoxy-MWCNTs	Phosphonium based IL (PPIL)	5	Speed mixer	Excellent MWCNTs dispersion	[59]
Epoxy-CNTs	$[OMIM]BF_4$	1.5		Showed synergistic effects between epoxy resin matrix and IL-modified CNTs	[239]
PS-MWCNTs	Phosphonium based IL	5	Melt mixing	Higher thermal stability due to the strong interactions between IL and MWCNTs	[33]
SSBR-CNTs	BMI	5	Hot press	π-π stacking interactions and plasticization effects of IL	[240]
PC-MWCNTs	CMI	0-8	Hydraulic press	46 % improvements in tensile strength Plasticization effects at higher amounts of IL	[48]

PC-MWCNTs	BMI	1-20	Hot press	50 % increments in elastic modulus Physical (cation-pi/pi-pi) interactions	[241]
PMMA-CNTs	[BMIM]PF$_6$ [HMIM]PF$_6$	10	Internal mixer	Strong interactions between [HMIM]PF$_6$ and CNTs because of longer alkyl chain length	[58]
PMMA-MWCNTs	[BMIM]PF$_6$	0-10	Batch mixer and hot press	IL acted as an effective compatibilizer, and plasticizer. Thermal decomposition temperature was improved.	[242]
PS-PMMA-PC-CNTs	[OMIM]BF$_4$	0.5	Grinding and ultrasounds	Decomposition temperature increased (5 %) than those of pure PMMA	[243]
PAI-MWCNTs	Imidazolium based IL	5-15	Melt mixing	Homogenous MWCNTs dispersion	[244]

SBR-MWCNTs	[AMIM]Cl, EMIT, MOIC	1	Compounding	Enhanced dispersion and superior mechanical properties	[245]
SBR-MWCNTs	[BMIM]Cl	0-30	Melt mixing	Strong interface between IL-MWCNTs and SBR matrix	[49]
SBR-MWCNTs	[BMIM]Cl	1-10	Melt mixing	Strong cation-π interactions	[246]
PU-MWCNTs	[HEMIM]BF	8.56 g	Hot plate	Higher thermal and mechanical properties with low amounts of MWCNTs in the composites	[247]
PVDF-CNTs	[VEIM]BF_4	10	Internal mixer and hot press	Homogenously dispersed CNTs in PVDF 3.6 % improvements in crystallization temperature Plasticization effects of IL	[234]
PVDF-CNTs	[BMIM]PF_6	1-5	Compression molding	Strong PVDF-CNTs bonding by IL	[233]

				Uniform CNT dispersion in PVDF	
PVDF-CNTs	[BMIM]PF$_6$	1-5	Melt compounding	Improved interfacial interactions between PVDF matrix and filler.	[47]
PVDF-MWCNTs	[BMIM]PF$_6$	0-5	Batch mixer	IL:CNTs (1:1) (w/w) is the optimum ratio for higher thermal properties	[43]
PVDF-MWCNTs	[EMIM][TF$_2$N]	1-5	Extrusion	Cation-π interaction Enhanced thermal and mechanical performance	[248]
PVDF-MWCNTs	[AEIM]Br	0-1	Melt blending	Young's modulus increased from 1.3 to 2.5 GPa Tensile strength (300 % higher than those of pure PVDF)	[237]

For tissue engineering applications, IL/PVDF nanocomposite having multiple ILs, 1-butyl-3-methylimidazolium chloride [Bmim][Cl], and 2-hydroxy-ethyl-trimethyl ammonium dihydrogen phosphate [Ch][DHP] were developed [249]. It was discovered that adding [Bmim][Cl] and [Ch][DHP] to the mixture enhanced the PVDF crystallization. The thermal and mechanical characteristics of the composites were also improved by the presence of the ILs. Also, the non-cytotoxicity of the IL/PVDF nanocomposite films and the proliferation of C2C12 cells proved the potential of the composites for muscle regeneration methods.

2.7 Polymer composites processing approach

2.7.1 Internal Mixer

Internal mixers have been effectively used for high and low viscosity environments in the polymer composite industry, where high-power mixing is needed for masticating and compounding processes. The general objective is to introduce solid and/or liquid components into a plastic or rubber matrix. The additives or inorganic fillers (aggregated nanoparticles or droplets trapped together by surface tension) should be detached, decreased in size, and dispersed equally throughout the matrix: There are two kinds of mixing that occur: extensive mixing and intense mixing. Extensive (also known as distributive) mixing is responsible for the spatial distribution of the individual particles within the polymeric matrix. Intensive (also known as dispersive) mixing is responsible for separating and reducing the particle size of the additives. Table 2.12 summarizes some of the advantages of internal mixers for polymer composites.

The maximum dispersion of inorganic fillers into polymers is obtained by choosing the appropriate equipment and process parameters. Internal mixers with intermeshing and tangential rotors are designed nowadays and mixing performance is highly dependent on the rotor design. In the enclosed mixing chamber, the spiral-shaped rotors spin in opposite directions at the same speed or at varying speeds to maintain the material circulating, as shown in Figure 2.21. The space between the rotor blades and the chamber walls causes the mixture to be sheared vigorously. A hopper is used to load materials, and a batch is contained inside the mixing chamber by an air-operated piston in the feed neck. The discharge door enables the mixture to be unloaded quickly and efficiently at the completion of the mixing process.

Table 2.12: Advantages of internal mixer for the processing of polymer composites [167]

Processing Technique	Advantages
Internal Mixer	Most efficient technique, since no solvent is required
	Highly compatible for the insoluble polymers
	Environmentally benign approach
	It is suitable for the current industrial processes
	An efficient method for dispersing inorganic additives in the polymer nanocomposites

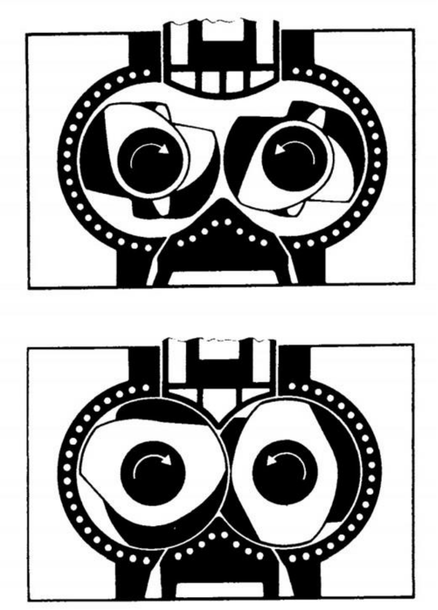

Figure 2.21: Top and bottom view of rotor geometrics of the internal mixer [250]

Table 2.13: Polymer composites using internal mixer

Filler	Polymer	Internal mixer processing condition	Ref.
Cellulose nanocrystals (CNCs)	Thermoplastic starch	115 °C, 8 min	[251]
CNTs	Polyethylene	180 °C, 10 min	[252]
CNTs	Natural rubber	60 °C	[253]
CNTs	PVDF	190 °C, 3 min	[254]
Lignin	Poly(lactic) acid	180 °C, 10 min	[255]
Silicon carbide	PEEK	365 °C, 5 min	[256]
Cellulose nanofibers (CNFs)	PMMA	175 °C, 15 min	[257]

Numerous research has been conducted on the fabrication of polymer composites using the internal mixer method, as shown in Table 2.13. Fang et al. (2018) [58] presented the fabrication of PMMA based composites by employing CNTs. The composites with various amounts of CNTs were produced immediately by melt blending at 170 °C for 5 min at 50 rpm in the internal mixer. The mechanical properties of PEEK-HA composites have been examined after the dispersion of CNTs in the polymer matrix [178]. The PEEK/HA/CNTs composites were prepared by using the internal mixer and the authors claimed that the higher mechanical properties were achieved because of the uniform MWCNTs distribution in the polymer composites.

2.8 Thermal degradation kinetics of polymers and inorganic fillers

Multiwalled carbon nanotubes are the potential and most popular inorganic fillers for the fabrication of thermoplastic polymer composite with enhanced thermal and mechanical properties. The detailed understanding of thermal stability and the investigation of thermal decomposition kinetics under pyrolytic environments through various kinetics models (Table 2.14) are essential for the processing and using MWCNTs fibres as raw materials in the fabrication of polymer composites. It is crucial to understand and anticipate the kinetic parameters of thermal degradation of polymer nanocomposites in order to develop molding and processing methods effectively [258, 259]. Furthermore, determining the activation energy of fillers enables precise prediction of their behavior under a variety of thermo-molding circumstances, which is very beneficial for their processing with a variety of thermoplastic polymer composites [260].

The thermogravimetric analysis was used to determine the thermal degradation kinetics of epoxy and epoxy/silica nanoparticle nanocomposites at a temperature ranging from 25 °C to 600 °C employing a single heating rate of 10 °C/min in an inert environment [261]. At various conversion ranges, the kinetic parameters such as activation energy, pre-exponential factor, and thermodynamic properties were measured at different amounts of silica nanoparticles. With increasing the silica nanoparticle concentration, the thermodynamic parameters (activation energy, frequency factor, and rate constant) were improved because of the strong bonding between the filler and the polymer matrix.

Li et al. (2019) [262] used the Coats-Redfern technique to investigate the thermal degradation and kinetics of a micro-encapsulated red phosphorus /high density polyethylene (MRP/HDPE) nanocomposite at various heating rates. The findings showed that the activation energy (Ea) of the 4 % MRP/HDPE composite was greater than that of pure HDPE and that the inclusion of MRP increased the thermal resilience and delayed its thermal disintegration. By adding MRP as the filler, the degradation process of HDPE was altered, resulting in a reduction in the decomposition rate.

The melt blending method was used to manufacture polyetherimide (PEI)-MWCNTs nanocomposites, and the surface of MWCNTs was modified by acid and plasma treatments [263]. The thermal degradation kinetics of PEI/MWCNTs composites was investigated extensively using the Coats-Redfern method. The activation energy was increased by 699 KJ/mol at 2 wt% MWCNTs, implying the improved thermal degradation stability. The enhanced thermal resistance of PEI composites was attributed to the improved interfacial interactions of the polymer with the employed filler.

Recently, the effect of IL-assisted pretreatment on the decomposition kinetics of oil palm biomass-derived biocomposites using thermoplastic starch as the polymer matrix was investigated [264]. Before fabricating thermo-molded composite panels, oil palm frond (OPF) fiber was pretreated with ILs, 1-butyl-3-methyl-imidazolium chloride ([Bmim][Cl]) and 1-ethyl-3-methyl-imidazolium diethylphosphate ([Emim][dep]). To estimate the activation energy, several kinetic models were explored, including the Coats-Redfern approach. When compared to untreated composites, the findings showed that composites produced with ILs pretreatment had a 10–125 % greater activation energy. The increased activation energy indicated that the fibres were more thermally stable and had greater fibre-polymer phase adhesion.

The thermal stability of bromo-butyl rubber (BIIR) nanocomposites was enhanced by employing a solution compounding technique after including ILs modified graphene oxide (GO-ILs) [265]. The values of activation energy of the produced composites were determined employing the Kissinger and Flynn–Wall–Ozawa techniques. The addition of IL-modified GO significantly improved the thermal performance of the BIIR nanocomposites. At 4 wt % of GO-ILs, the activation energy of BIIR nanocomposites was 27 % higher than the pure matrix because of the significant interfacial adhesion between GO and the rubber.

Conversely, by modelling thermogravimetry analysis data for lignocellulosic Spartium junceum (jute) fibre-based biocomposites, the Broido model was used to estimate the activation energy [266]. To improve the fire resistance of the composite material, the fibres were processed with montmorillonite nano clay prior to composite development. The model fitting was carried out between 340 and 400 °C since this temperature range exhibited the quickest decomposition phase for all biocomposites. Biocomposites prepared with NaOH treated fibres (reference sample) showed a greater value of activation energy of 224.16 kJ/mol than composites reinforced with montmorillonite nano clay (156.59 kJ/mol). It was suggested that the interactions between the fibre and the matrix were the primary factor affecting the thermal properties of fabricated biocomposites.

Table 2.14: Thermal degradation kinetics models for polymer composites.

Kinetic model	Expression	Plot	Ref.
Coats-Redfern	$\ln\left(\frac{-\ln(1-\alpha)}{T^2}\right)=\ln\frac{AR}{\beta E_a}-\frac{E_a}{RT}$ and α is, $\alpha=\frac{m_0-m}{m_0-m_f}$ Where m_o, m_f, and m are initial mass, final mass, and mass at a temperature. α= decomposition factor A=frequency or pre-exponential factor (s^{-1}) E_a= apparent activation energy (J/mol) β= heating rate R= universal gas constant (8.3145 J/mol K) n= order of reaction (s^{-1})	$\ln\left(\frac{-\ln(1-\alpha)}{T^2}\right)$ vs $1000/T$	[267]
Broido	$\ln\ln\left(\frac{1}{\alpha}\right)=-\frac{E_a}{RT}+\pi$ and α is, $\alpha=\frac{w_t-w_f}{w_0-w_f}$ Where w_o, w_f, w_t are weight at initial, final, and at a temperature α= decomposition factor E_a= apparent activation energy (J/mol)	$\ln\ln\left(\frac{1}{\alpha}\right)$ vs 1000/T	[268]

	R= universal gas constant (8.3145 J/mol K)		
Horowitz-Metzger	$\ln\left\{\ln\left(\frac{w_0}{w_t}\right)\right\} = \frac{E_a\theta}{RT_{max}^2}$ θ = T-T_{max} T= temperature at any time t T_{max}=temperature at which decomposition rate was highest E_a= apparent activation energy (J/mol) R= universal gas constant (8.3145 J/mol K)	$\ln\left\{\ln\left(\frac{w_0}{w_t}\right)\right\}$ vs θ	[269, 270]

Using the ecologically benign 1-butyl-3-methyl-imidazolium chloride (BmimCl) ionic liquid, green nanocomposites comprising cellulose/exfoliated graphite nanosheets with lower filler loadings were synthesized [271]. The thermal properties of the fabricated nanocomposites were evaluated employing the Broido method. When 0.75 wt% GNS treated with ILs was added to the nanocomposites, the activation energy was increased to 15.31 kJ/mol from 13.2 KJ/mol of the pure cellulose. The increment in the activation energy values of the manufactured composites indicated that they were more thermally stable than the pure films. This supported the fact that ILs-GNS inclusion influenced the morphology of regenerated cellulose composite crystals.

Similarly, MWCNTs-reinforced polylactide (PLA) composites were injection molded onto a microneedle pattern mold [272]. The Horowitz-Metzger model was used to examine the impact of MWCNTs on thermal characteristics. The interactions between PLA and MWCNTs, as well as the physical barrier provided by the MWCNTs, increased the activation energy values of the produced composites. Pure PLA had the activation energy of 21.3 KJ/mole, which was increased to 30.1 KJ/mole for PLA/MWCNTs composites.

The biodegradable ternary blended films of polyvinyl alcohol (PVA) and biomaterials (corn starch and pectin) were fabricated using the solution casting technique with water as a solvent to enhance the thermomechanical stabilities [273].

The tensile characteristics of blend films were improved, and blends with a starch/pectin ratio of 1:5 had a tensile strength (18.85 MPa) as well as the maximum elongation at break (516 %). Additionally, it was also observed that the activation energies of the prepared blends were substantially increased owing to the strong interactions provided by the biomaterials with the PVA.

Overall, the activation energy of thermal decomposition is a useful tool for examining the impact of IL-modified CNTs on the thermal properties and resultant bond strengths of the composite materials. Thus, the activation energy of thermal decomposition kinetics for a composite material may reveal the macroscopic characteristics of the composite, which are usually determined by the intrinsic qualities of the components, which are mostly influenced by their chemical composition. Especially, the estimation of activation energy through the proper model-fitting of thermal decomposition of untreated and ILs-treated nanocomposites may offer insight into the influence of ILs introduction in the filler-polymer interactions during the melt blending operation. The filler-polymer interactions are among the most important factors that determine activation energies pre and post modification, and it may be a significant indicator of the effectiveness of IL addition in the fabrication of polymer nanocomposites. Based on this, it was suggested that the activation energy of thermal degradation might be a useful approach for determining the kinetics of thermal decomposition and the resultant bond energies because of the interactions of different materials throughout the melt blending process.

The rate of decomposition ($\frac{d\alpha}{dt}$) of polymer nanocomposites can be expressed using the equation below [274].

$$\frac{d\alpha}{dt} = A\,e^{-\frac{E_a}{RT}}(1-\alpha)^n \qquad (2.1)$$

The terms A, E_a, and α are frequency factor/pre-exponential factor (s^{-1}), apparent activation energy (J/mol), and decomposition factor, respectively. The below formula can be employed to determine the value of α.

$$\alpha = \frac{m_0 - m_t}{m_0 - m_f} \qquad (2.2)$$

Where m_o, m_f, and m_t are initial, final, and given masses at a temperature.

Equation for a linear heating rate (β) is,

$$\frac{d\alpha}{dT} = \frac{A}{\beta} e^{-\frac{E_a}{RT}} (1-\alpha)^n \qquad (2.3)$$

Or

$$\int_0^{\alpha} \frac{d\alpha}{(1-\alpha)^n} = \frac{A}{\beta} \int_0^{T} e^{-\frac{E_a}{RT}} dT \qquad (2.4)$$

After integration, equation (2.4) is,

$$\frac{1-(1-\alpha)^{1-n}}{1-n} = \frac{ART^2}{\beta E_a} e^{-\frac{E_a}{RT}} \left(1 - \frac{2RT}{E_a}\right) \qquad (2.5)$$

Logarithmic form of equation (2.5) is,

$$\ln\left(\frac{1-(1-\alpha)^{1-n}}{T^2(1-n)}\right) = \ln\left(\frac{AR}{\beta E_a} - \frac{2RT}{E_a}\right) - \frac{E_a}{RT} \qquad (2.6)$$

As, $\left(1 - \frac{2RT}{E_a}\right) \ll 1$, so simplified form of equation (2.6) is,

$$\ln\left(\frac{1-(1-\alpha)^{1-n}}{T^2(1-n)}\right) = \ln\left(\frac{AR}{\beta E_a}\right) - \frac{E_a}{RT} \qquad (2.7)$$

or

$$\ln\left(\frac{-\ln(1-\alpha)}{T^2}\right) = \ln\left(\frac{AR}{\beta E_a}\right) - \frac{E_a}{RT} \qquad (2.8)$$

Equation (2.8) is called Coats-Redfern model for a single order of a reaction [267]. The plots of ln $\left(\frac{-\ln(1-\alpha)}{T^2}\right)$ and 1/T give the straight line with the slope $(-\frac{E_a}{R})$ and the activation energy of the composites can be calculated (equation 2.9):

$$E_a = -R \times \text{slope} \qquad (2.9)$$

Broido [268] proposed the following formula (Equation 2.3), which may be employed to determine the activation energy of thermal decomposition of polymer composites using TGA data.

$$\ln\ln\left(\frac{1}{\alpha}\right) = -\frac{E_a}{RT} + \pi \qquad (2.10)$$

Where π is a constant.

For a single heating rate, the Equation (2.10) provides a straight line with slope $(-\frac{E_a}{R})$ after plotting $\ln\ln\left(\frac{1}{\alpha}\right)$ vs 1/T and the activation energy can be determined:

$$E_a = -R \times \text{slope} \qquad (2.11)$$

Similarly, the equation for Horowitz-Metzger [269] can be obtained from the Equation (2.3) for thermal degradation kinetics of polymer composites.

$$\ln\ln\left(\frac{w_0}{w_t}\right) = \frac{E_a\theta}{RT_{max}^2} \qquad (2.12)$$

Where w_0 and w_t are initial weight and weight at a given temperature, $\theta = T - Ts$, θ is variable auxiliary temperature, T is the degradation temperature with time and T_{max} is maximum decomposition temperature (peak temperature). The kinetic energy can be calculated from the below equation obtained after plotting $\ln\ln\left(\frac{w_0}{w_t}\right)$ and θ. The mathematical equations for the thermal decomposition kinetic models are described in Table 2.14.

$$E_a = R \times \text{slope} \times T_{max}^2 \qquad (2.13)$$

2.9 Summary

PEEK is a high-performance thermoplastic with superior thermal and chemical characteristics. It is extensively used in the medical technology, energy, and chemical industries. When employed in biomedical industries, PEEK has additional advantages, such as the capability to be sterilized repeatedly and to be easily molded through machining. Nevertheless, PEEK is usually bioinert in the absence of further surface coatings or modifications. Therefore, in order to make it a better option for biomaterial applications, its bioactivity must be enhanced.

Hydroxyapatite (HA) is a biocompatible and biodegradable substance, and it may establish a strong interaction with the surrounding bone tissues. The inclusion of HA to PEEK is expected to enhance the biological characteristics of composites used in bone tissue engineering. Today, a variety of methods exist to alter the PEEK surface with HA. These methods are divided into four broad classifications: physical, chemical, surface coating, and composites preparation. However, the incorporation of HA to the PEEK matrix would reduce the mechanical properties of scaffolds, particularly in extremely porous structures.

MWCNTs have been broadly applied as efficient reinforcing fillers in a wide variety of thermoset and thermoplastic polymers for the purpose of enhancing the mechanical properties of the composites. Additionally, MWCNTs are usually nontoxic and biocompatible due to their ability to encourage osteoblast adhesion and proliferation on the polymer composites surfaces. Despite these advantageous properties, the agglomeration of CNTs in a polymer matrix has proved to be problematic because of their large aspect ratio. Multiple approaches have been used to enhance the dispersion of CNTs in polymer matrices, including covalent (chemical, surface modifications) and non-covalent functionalization (solution mixing, melt mixing). The most practical approach for tuning the interfacial characteristics of CNTs by using physical interactions is a non-covalent modification (melt mixing), which can prevent CNTs aggregation. In this method, the commonly available organic solvents (DMF, NMP, acetone etc.) have been employed for breaking the CNTs bundles in the polymer composites. However, the key issue of CNTs agglomerations is still uncertain in the polymer/CNTs/HA composites.

To address the aforementioned impediment, an efficient polymer/CNTs interface linker is needed. Ionic liquids (ILs) are composed of an organic cation and an inorganic anion and typically have a melting point of less than 100 °C. The cationic structure of ILs, as well as the degree of anion charge delocalization, influence their chemical, physical, and biological properties. Particular ILs (low cost and high power of dissolution in the polymer matrices) have an exceptional ability to distribute and break down CNTs bundles into polymer matrices, consequently improving the necessary characteristics. To fully develop the polymer composites, it is necessary to modify the inorganic filler with the ILs for excellent CNTs distribution. Among the many polymer processing methods, internal mixer and compression molding are well-known and often used in the fabrication of polymer filler composites.

The investigation of thermal decomposition kinetics under pyrolytic conditions, as well as a comprehensive understanding of thermal stability, are particularly important for the processing and use of ILs-modified CNTs in bioactive polymeric composite materials. It is critical to understand and estimate the thermal degradation kinetics of the polymer composites in order to develop reasonable molding and thermoplastic processing methods.

CHAPTER 3

RESEARCH METHODOLOGY

3.1 Overview

This chapter discusses the materials and methods for modifying multi-walled carbon nanotubes using ILs (ILs/MWCNTs), as well as the different phases involved in the manufacturing of bioactive PEEK nanocomposites using ILs/MWCNTs in combination with PEEK and hydroxyapatite (HA). The equipment used to fabricate the nanocomposites and the evaluation of untreated and IL-treated PEEK composites with the various characterization techniques are briefly described.

The overall research flow chart for the development of PEEK/MWCNTs composites via internal mixer and compression molding processes is depicted in Figure 3.1. Broadly, the experimental procedure could be divided into four parts: (1) effectiveness of IL and organic solvent for MWCNTs dispersion (2) fabrication and characterization of PEEK/MWCNTs composites (3) evaluation of biological properties and finally (4) thermal degradation kinetics.

3.2 Materials

The following chemicals and materials were employed in this research to manufacture polymer nanocomposites for the purpose of studying human bone regeneration in biomedical applications. All the chemicals were of analytical quality and were used without further processing. Table 3.1 summarizes some of the most significant physicochemical characteristics of the materials and chemicals employed in this research.

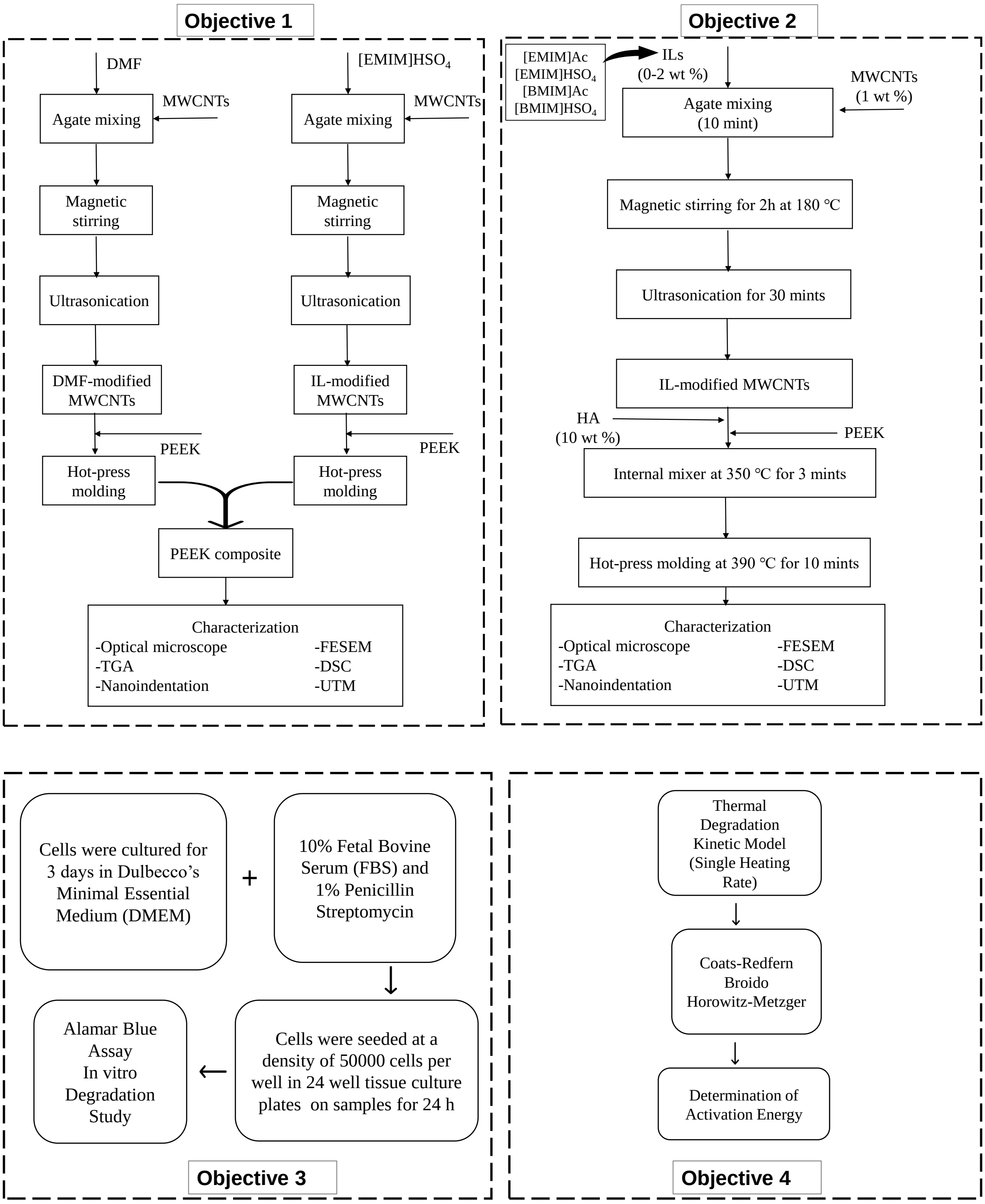

Figure 3.1: Overall research flow chart for the development of PEEK/MWCNTs nanocomposite

Table 3.1: Material and chemicals used for the fabrication of PEEK composites

Chemical Name	Purity (%)	Size	Brand
PEEK	99	37 µm	Huaian, China
MWCNTs	97	15 nm	Ugent, Malaysia
[EMIM]Ac	98	-	Sigma Aldrich
[EMIM]HSO_4	95	-	Sigma Aldrich
[BMIM]Ac	96	-	Sigma Aldrich
[BMIM]HSO_4	95	-	Io-li-tec
nHA	99.7	20-50 nm	Huaian, China
DMF	99.8	-	Sigma Aldrich
Silicone spray	-	-	Allopar
Mold release wax	99	-	Honey wax
Teflon paper	99.9	-	Local

3.2.1 Polyetheretherketone (PEEK)

The PEEK powder (particle size 400 microns and molecular mass of a repeating unit: 288.31 g/mol) was collected from Huaian RuanKe Plastics, China. The ultimate choice of the polymer for composite fabrication is a basic requirement. For long-term utilization in the human bone replacement, the polymer should have superior mechanical and biological characteristics. PEEK being an attractive thermoplastic polymer for bone regeneration with elastic modulus close to human bone [34, 178] and fulfilling required criteria was selected as the base polymer.

3.2.2 Multiwalled carbon nanotubes (MWCNTs)

The MWCNTs (15 nm in diameter, 5 μm length) were purchased by Ugent Tech Sdn. Bhd, Malaysia. Inorganic fillers are most often employed to improve the thermal, mechanical, and other basic characteristics of polymeric materials. The MWCNTs are the preferred reinforcing filler for biomedical applications because to their non-toxic nature and high biocompatibility with surrounding bone structures after implantation[20, 29].

3.2.3 Ionic Liquids (ILs)

The four imidazolium ILs with distinct alkyl chain length and anions, 1-ethyl-3-methylimidazolium acetate ([EMIM]Ac), 1-ethyl-3-methylimidazolium hydrogen sulphate ([EMIM]HSO_4), 1-butyl-3-methylimidazolium acetate ([BMIM]Ac), and 1-butyl-3-methylimidazolium hydrogen sulphate ([BMIM]HSO_4) were taken from Sigma-Aldich, Germany and their chemical structures are displayed in Figure 3.2. ILs are environmentally friendly and designer solvents which exhibit numerous solvation interactions with the polymers in comparison to volatile organic solvents. They are employed in polymer composites to facilitate the stronger interactions of the filler with the polymer matrix. ILs are regarded as the primary driving factor for strong filler-polymer interactions, which led to the homogeneous dispersion of MWCNTs in numerous polymer matrices. Based on these insights, ILs have been employed for the first time to disperse MWCNTs in PEEK composites for improved thermomechanical characteristics for human bone substitution. The imidazolium cations (which are most successful in polymer composites)[211, 219], as well as acetate[45] and hydrogen sulfate[46, 60], are considered appealing anions due to their cheap cost and strong solvation interactions with the polymers. Table 3.2 summarizes some critical physicochemical characteristics of the ILs utilized in this research.

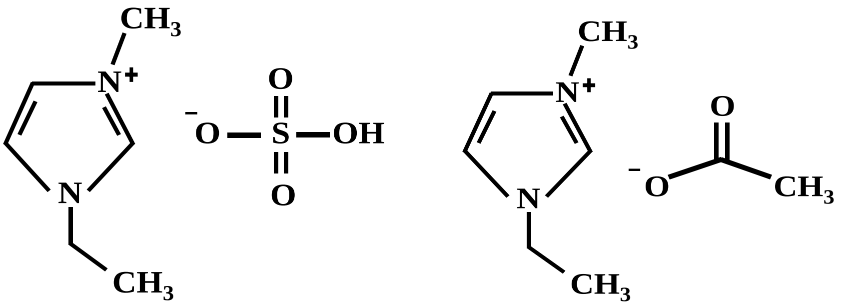

a) [EMIM]HSO_4 b) [EMIM]Ac

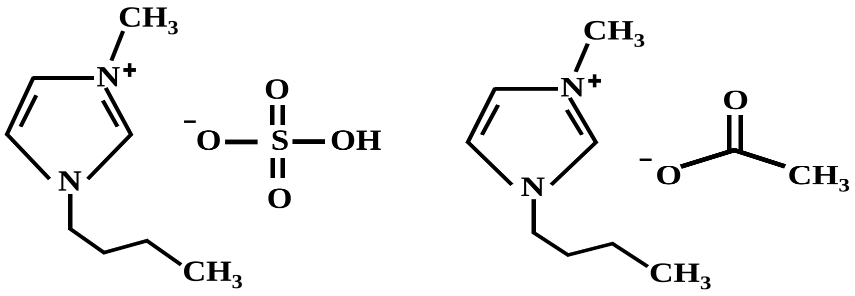

c) [BMIM]HSO_4 d) [BMIM]Ac

Figure 3.2: Chemical structures of used ILs

Table 3.2: Physicochemical properties of ILs

Property	[EMIM]Ac	[EMIM]HSO_4	[BMIM]Ac	[BMIM]HSO_4
CAS No	143314-17-4	412009-61-1	284049-75-8	262297-13-2
Molecular mass (g/gmol)	170.21	208.24	198.26	236.29
Density (g/cm^3)	1.28	1.367	1.1	1.27
Viscosity (Pa. s)	0.162	0.798	0.484	1.049
Decomposition temperature (°C)	224	359	212	340

3.2.4 Hydroxyapatite (HA)

The nanohydroxyapatite (nHA, purity 98.7%) was received from Huaian RuanKe Plastics, China. The nHA is calcium phosphate-based bioceramic with chemical formula $Ca_{10}(PO_4)_6(OH)_2$)[10] used to enhance the biocompatibility and biological characteristics of the polymer composites.

3.2.5 Dimethylformamide (DMF)

DMF (purity 99.8 %) was purchased from Sigma-Aldich, Germany and its chemical structure is shown in Figure 3.3. The DMF seems to be significant in the debundling and separation of CNTs into individual CNTs. It is conceivable that DMF first adsorbs on the CNTs, reducing their van der Waals affinity[275].

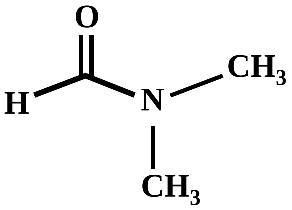

Figure 3.3: Chemical structure of DMF

3.3 Preparation of PEEK/MWCNTs and PEEK/MWCNTs/IL composites

PEEK, PEEK/MWCNTs (employing conventional organic solvent dimethylformamide), and PEEK/MWCNTs/IL (using [EMIM][HSO_4]) composites were synthesized via compression molding method and the summary of the basic steps and amounts of the used materials are illustrated in Table 3.3. MWCNTs were modified with DMF in PEEK/MWCNTs composites, while PEEK/MWCNTs/IL composites were prepared using IL-assisted MWCNTs. The experimental method for producing PEEK/MWCNTs and PEEK/MWCNTs/IL composites were broadly subdivided into two stages, as shown in Figure 3.1 (objective 1) and the summary of the basic steps is explained in Figure 3.4. The schematic representation of possible polymer-filler interactions after the incorporation of DMF and IL are illustrated in Figure 3.5.

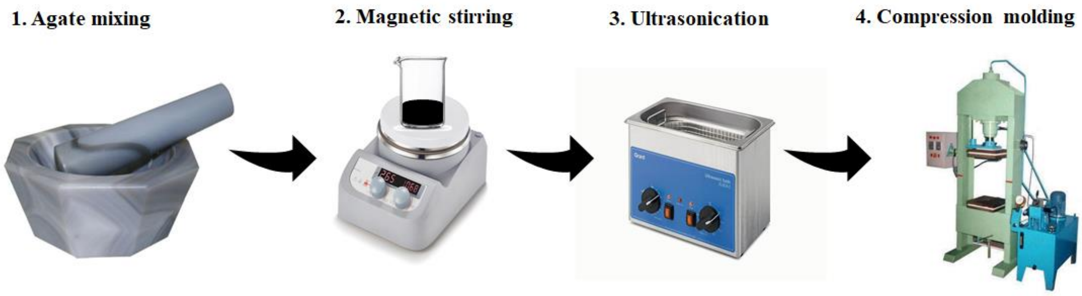

Figure 3.4: General steps involved in the preparation of PEEK nanocomposite

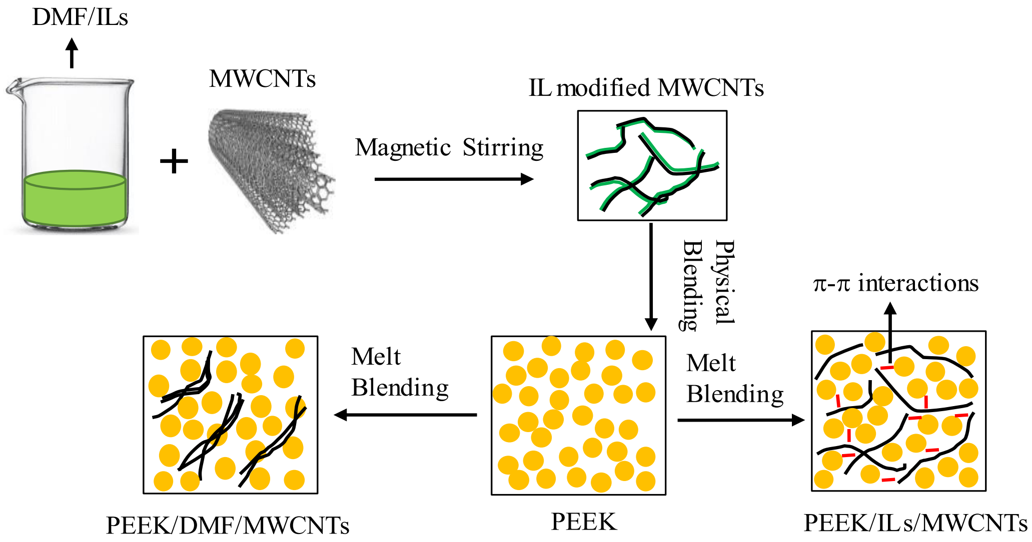

Figure 3.5: Polymer-filler interactions after using DMF and IL

3.4 PEEK/MWCNTs/nHA/ILs composites

The purpose of this research is to determine the possibility of producing bioactive PEEK/MWCNTs/nHA/ILs composites by employing ILs supported MWCNTs. The primary objective was to utilize ILs to ensure homogeneous MWCNTs dispersion in PEEK/MWCNTs/nHA/ILs composites for improvements in the mechanical and biological properties of the final composite materials. Four ILs containing imidazolium-based cations were selected for this purpose in this research as pretreatment for MWCNTs. Indeed, ILs having imidazolium-based cations offer better dissolving properties for a range of polymeric materials and have been shown to be more dissolvable than ILs containing other cationic groups such as morpholium, piperidium, and pyrrolidinium [40, 49, 58, 219].

On the other hand, it is thought that the anionic component is mainly important for the stronger interactions of IL with MWCNTs. Ionic liquids comprising hydrogen sulfate and acetate anions outperformed other anionic classes such as PF_6, BF_4, and $MeSO_4$ in terms of polymeric material dissolving. Interestingly, ILs with hydrogen sulfate and acetate anions are cheap and economical than other groups [46, 60, 276-278]. Hence, ILs comprising hydrogen sulfate and acetate-based anions have been extensively applied in polymeric materials to enhance fibre-polymer interactions.

3.4.1 Preparation of PEEK/MWCNTs/nHA composites (without IL)

The preparation of PEEK/MWCNTs/nHA composites includes the following steps (i) physically mixing of filler with solvent, (ii) adding polymer and biomaterial in the filler/solvent solution and (iii) composite sheets obtained after melt mixing and compression molding. 1 wt % of DMF and MWCNTs were physically mixed in an agate mortar for 10 min, followed by magnetic stirring for 2 h at 180 °C. The mixture was then degassed for 30 mints in a sonication bath (Transonic Digital S, Elma®). After that, PEEK and nHA (10 wt %) were added in a homogenized solution of MWCNTs/DMFs. The PEEK/MWCNTs/nHA composites pellets were successfully obtained from the internal mixer (Madina engineering materials, Pakistan) after melt mixing at 350 °C for 3 min with a rotating speed of 80 rpm and the composite sheets were prepared in the compression molding (Madina Engineering materials, Pakistan) at 390 °C and at 20 MPa for 10 min.

3.4.2 Preparation of PEEK/MWCNTs/nHA/ILs composites (with ILs)

To synthesize IL-modified MWCNTs, the MWCNTs were combined with each of four ILs (1-ethyl-3-methylimidazolium acetate (EMIM]Ac)/1-ethyl-3-methylimidazolium hydrogen sulfate ([EMIM]HSO_4)/1-butyl-3-methylimidazolium acetate ([BMIM]Ac)/1-butyl-3-methylimidazolium hydrogen sulfate([BMIM]HSO_4)) in an agate mortar for 10 min at room temperature, followed by magnetic stirring for 2 h at 180 °C (Figure 3.1; objective 2). The weight percentage of IL to MWCNTs varies between 0:1 and 2:1. After that, IL modified MWCNTs were mixed with nHA (10 wt %) and PEEK powder and homogenized by ultrasonication for 30 min. The PEEK/MWCNTs/nHA/ILs composites were successfully produced in the internal mixer at 350 °C for 3 min with a rotating speed of 80 rpm. The internal mixer pellets were melt compounded in the hydraulic press at 390 °C and at 20 MPa for 10 min. The detailed schematic diagram of preparing PEEK composites was shown in Figure 3.6.

A total of twenty (20) polymer composites were prepared and classified into four (4) composites groups as illustrated in Table 3.3. Firstly, a reference polymeric composite comprised entirely of PEEK was synthesized. Secondly, a polymeric composite (PEEK/MWCNTs) based on an organic solvent (1 wt % DMF) was produced. Thirdly, ionic liquid (1 wt % of [EMIM]HSO_4 (1-ethyl-3-methylimidazolium hydrogen sulfate)) was employed to manufacture PEEK/MWCNTs/IL composites for comparison to pure PEEK and PEEK/MWCNTs composites. This IL ([EMIM]HSO_4) was chosen for the comparative study in order to investigate the effect of IL on PEEK/MWCNTs composites due to its anion, which has the potential to form stronger physical interactions with the PEEK polymer [238]. 1 wt % of IL (EMIMHSO_4) was employed since at this composition, optimum thermomechanical properties in polymer composites were achieved. Additionally, this type of IL is inexpensive and has significant solvation interactions with the polymers [238]. Lastly, four imidazolium-based ILs (1-ethyl-3-methylimidazolium acetate ([EMIM]Ac), 1-ethyl-3-methylimidazolium hydrogen sulfate ([EMIM]HSO_4), 1-butyl-3-methylimidazolium acetate ([BMIM]Ac), 1-butyl-3-methylimidazolium hydrogen sulfate ([BMIM]HSO_4) with various amounts (0.5, 1, 1.5 and 2 wt %) were used to fabricate PEEK/MWCNTs/nHA/ILs composites. The MWCNTs (1 wt %) and nHA (10 wt %) were also introduced in the composites for improving their mechanical properties and biological performance, respectively. Based on literature, 1 wt % of MWCNTs [24, 25], 10 wt % of HA [5, 178] and 0-2 wt % of ILs [43, 242] were chosen since at this compositions, they exhibited superior thermomechanical characteristics in polymer composites.

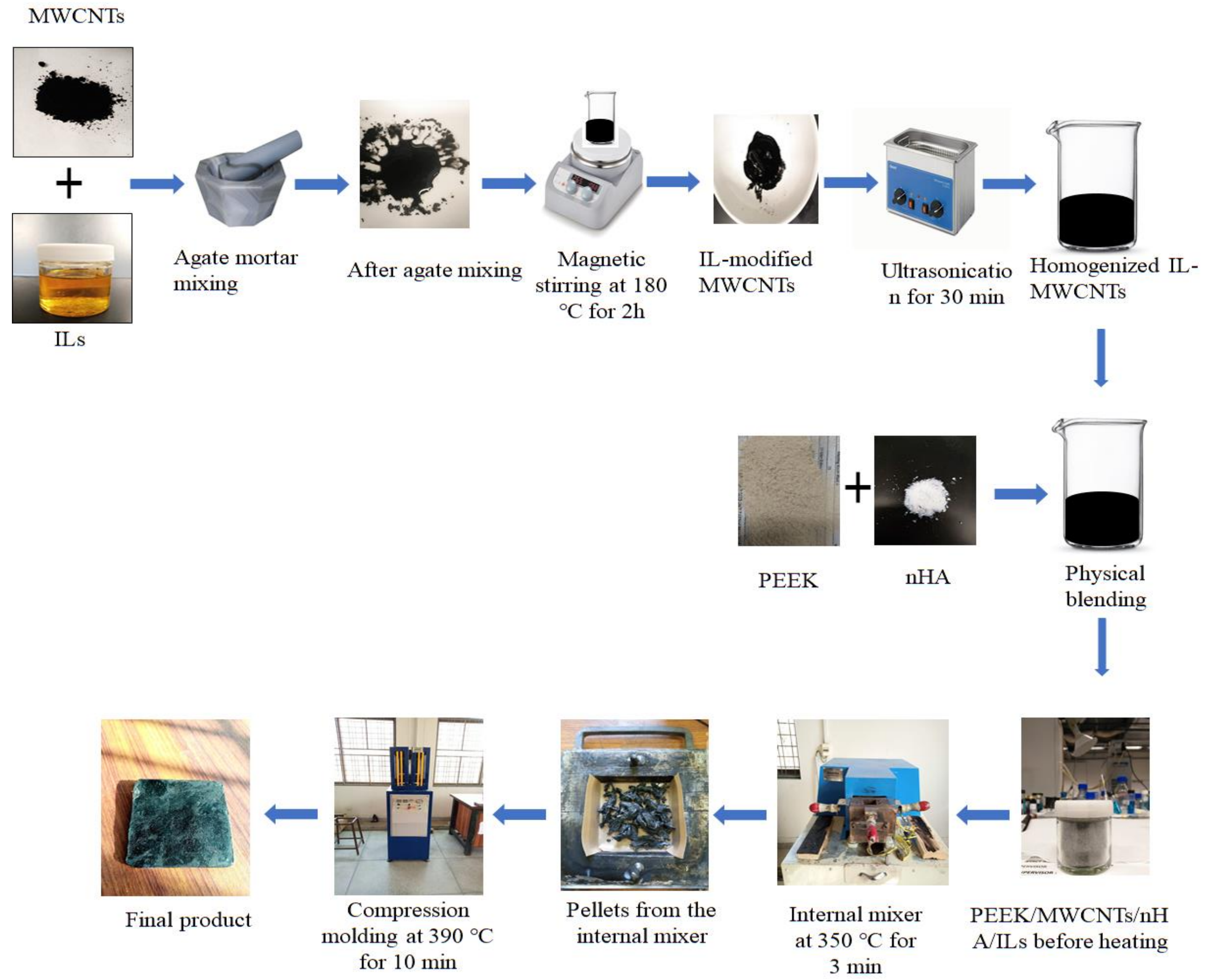

Figure 3.6: Schematic representation of the steps to prepare PEEK-MWCNTs/nHA/ILs composites

Table 3.3: PEEK composites prepared in this study

Composite type	Sample Code	PEEK (wt%)	MWCNTs (wt%)	nHA (wt%	DMF (wt%)	[EMIM] Ac (wt%)	[EMIM] HSO_4 (wt%)	[BMIM] Ac (wt%)	[BMIM] HSO_4 (wt%)
Pure PEEK	S1	100	-	-	-	-	-	-	-
PEEK/MWCNTs	S2	100-MWCNTs-DMF	1	-	1	-	-	-	-
PEEK/MWCNTs/IL	S3	100-MWCNTs-IL	1	-	-	-	1	-	-
PEEK/MWCNTs/nHA	S4	100-MWCNTs-nHA	1	10	1	-	-	-	-
PEEK/MWCNTs/ nHA/ILs ([EMIM]Ac)	S5	100-(MWCNTs+ILs +nHA) wt %	1	10	-	0.5	-	-	-
	S6				-	1	-	-	-
	S7				-	1.5	-	-	-
	S8				-	2	-	-	-
PEEK/MWCNTs/ nHA/ILs ([EMIM]HSO_4)	S9	100-(MWCNTs+ILs +nHA) wt %	1	10	-	-	0.5	-	
	S10				-	-	1	-	-
	S11				-	-	1.5	-	-
	S12				-	-	2	-	-
PEEK/MWCNTs/ nHA/ILs ([BMIM]Ac)	S13	100-(MWCNTs+ILs +nHA) wt %	1	10	-	-	-	0.5	-
	S14				-	-	-	1	-
	S15				-	-	-	1.5	-
	S16				-	-	-	2	-
PEEK/MWCNTs/ nHA/ILs ([BMIM]HSO_4)	S17	100-(MWCNTs+ILs +nHA) wt %	1	10	-	-	-	-	0.5
	S18				-	-	-	-	1
	S19				-	-	-	-	1.5
	S20				-	-	-	-	2

3.4.3 Preparation of PEEK composite pellets

Internal mixers are widely recognized as one of the most flexible and fast mixing equipment available with high throughput. Two parallel rotors with "flight" or "nogs" are used in the working portion of the internal mixer to revolve against one another in a cylindrical enclosure, and these rotors are operated by motor and gear. Dispersion is usually accomplished in the small area around the rotor, and the chamber wall, where the circulation is uniform and shear stress is considerable. It also assists in the assimilation and distributional mixing of components. The breadth of the rotors tip has a significant effect on both the total shear and the time of the material spends inside the high shear zone [279]. By estimating its volume and contrasting it to the overall free volume of the mixing chamber, the quantity of material flowing through this zone may be determined. The rolling bank volume relies on the film thickness and the speed of the rotor: The volume of the rolling bank decreases as the rotor speed increases, and an increasing amount of material fills the area behind the rotor tip [280]. Figure 3.7 a) shows the used internal mixer in this study.

In order to be successful in dispersion, the shear stress inside the clearance between the flying tip and the chamber wall must exceed a critical value, which is the stress needed to break the agglomerates. If the shear force is significantly greater than the critical stress, only those aggregates with their longitudinal direction perpendicular to the streamlines that are oriented to the linear flow in the clearance will break. Without additional dispersive or distributive impact, the residual agglomerates will eventually align with the flow [281, 282]. The stress in the clearance between both the chamber wall and flight tip is dependent on the width and depth of the channel [283]: the higher shear force varies inversely with the clearance between the chamber wall and flight tip, creating the shear stress extremely sensitive to clearance variations and necessitating very narrow clearances for elevated shear stresses [281].

First of all, the internal mixer was heated to 350 °C and set the rotor speed to 80 rpm. The predetermined amount (14 g) of the sample was put into the sample area and heated for 3 mints. The spinning rotor ensured that the sample was adequately mixed with each component distributed evenly to prepare homogenized PEEK composite pellets. The internal mixer was turned off once the required time was elapsed, and the molten material was extracted from the rotors using a spatula. The pellets were produced when the sample was removed and air-cooled to room temperature, as illustrated in Figure 3.7 b).

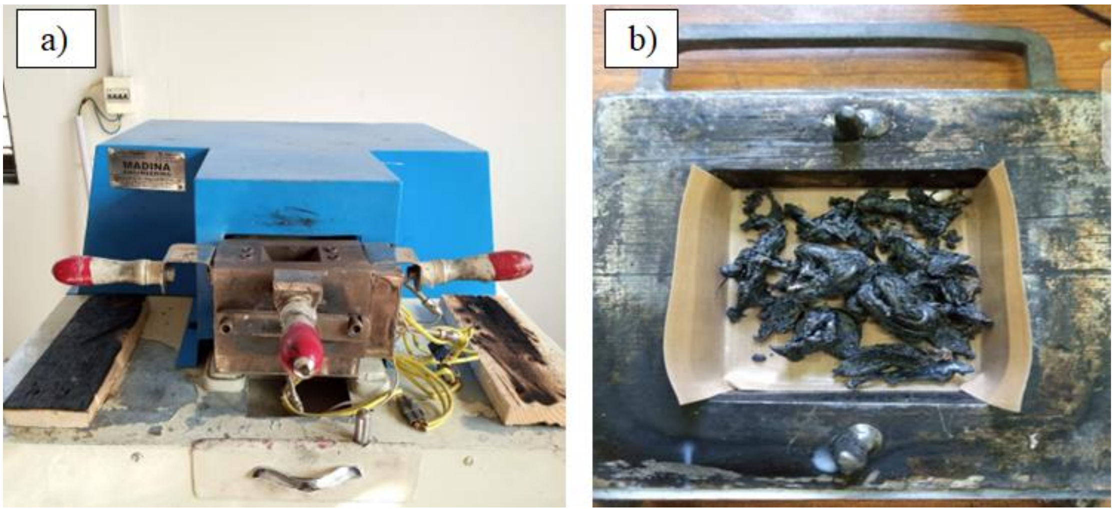

Figure 3.7: a) Internal mixer machine used in the current study b) PEEK pellets obtained from the internal mixer

3.4.4 Hot-press molding to prepare PEEK composites

The final stage to prepare PEEK composites sheets from the internal mixer pellets is hot-press molding. Evidently, a broad range of thermoplastic polymers have been used in hot-press molding for the development of polymer-filler based nanocomposite materials. For this, mild steel molds with standard specifications based on modified ASTM D638 [284] were employed to fabricate PEEK composites. This standard covers the testing of polymer-based composites with inorganic fillers [35, 285].

A predetermined amount of PEEK/MWCNTs/nHA/ILs was injected into the female section of the mold at a mass flux of 0.2411 gcm^{-2} with interior dimensions of 7.62 cm × 7.62 cm. The target density (Table 3.4) of the final composite sheet with specifications of 7.62 cm × 7.62 cm × 0.2 cm would be 1.21 gcm^{-3} using the value of mass flux distribution.

Volume of final composite = 7.62 cm × 7.62 cm × 0.2 cm= 11.613 cm^3

If, the required density= 1.21 gcm^{-3}

Then, mass of compounded mixture =volume × density = 11.613 cm^3× 1.21 gcm^{-3}

= 14 g

Further, cross-section area of the mold = 7.62 cm × 7.62 cm= 58.0644 cm^2

So, mass flux distribution= 14 g/58.0644 cm^2 = 0.2411 gcm^{-2}

The resulting density of polymer composites is essential since it has a huge effect on the thermomechanical and other characteristics of the nanocomposites. Thus, nanocomposites made of MWCNTs and IL-modified MWCNTs were synthesized at the same target density allowing for the study of the impact of IL-modified MWCNTs on the characteristics of nanocomposites to be conducted independently.

The adhesion of the final products with the interior walls of the mold after cooling and reducing the pressure is a frequent and inconvenient problem that generally results in the breaking of the molded specimen during the thermo-molding stage. This issue is particularly acute for the nanocomposites, which include thermoplastic polymers as matrices. While mold ejector pins and mold release wax are employed to circumvent this issue, these methods generally operate effectively for thermosetting polymer-based composites but fail miserably when used to thermoplastic polymer-based composites. To address this problem, we used a modified Teflon paper as a mold-releasing agent which is impervious to high pressure of several bars and temperature of up to 420 °C.

Following that, the mold was closed and put onto the pre-heated plates of the compression molding machine (Madina engineering materials, Pakistan) (Figure 3.8a). The mold was then thermally compressed for 10 min at 390 °C and 20 MPa. It should be remembered that during the molding of thermoplastic-based composite materials, the mold cannot be released immediately after 10 min of compression but must be cooled to room temperature while maintaining pressure in order to prevent spoiling of the molten polymer in the mold [286]. The summary of the operational conditions used during the manufacturing of PEEK nanocomposites is explained in Table 3.4. For further characterization, the final product (Figure 3.8b) was wrapped in plastic bags and placed in airtight boxes.

Table 3.4: Overview of operational parameters for several stages in the fabrication of PEEK nanocomposites

Process	Operating parameters
DMF modified MWCNTs	MWCNTs = 1 wt%
	DMF =1 wt%
	Conditions = 140 °C, 2h, 400 rpm
ILs modified MWCNTs	MWCNTs = 1 wt%
	ILs = 0.5,1.0, 1.5, 2.0 wt%
	Conditions = 180 °C, 2 h, 400 rpm
Bioactive PEEK composites before melt blending	nHA= 10 wt%
	PEEK (wt%) = 100 - (MWCNTs+ILs+nHA) wt%
PEEK/MWCNTs/nHA/ILs pellets in the internal mixer	Conditions = 350 °C, 3 min, 80 rpm
	Target density = 1.21 g cm^{-3}
	Mass flux distribution = 0.2411 g cm^{-2}
PEEK/MWCNTs/nHA/ILs sheets in the compression molding	Sheet dimensions = 7.62 cm × 7.62 cm × 0.2 cm
	Mold material = Mild steel
	Conditions = 390 °C, 10 min, 20 MPa

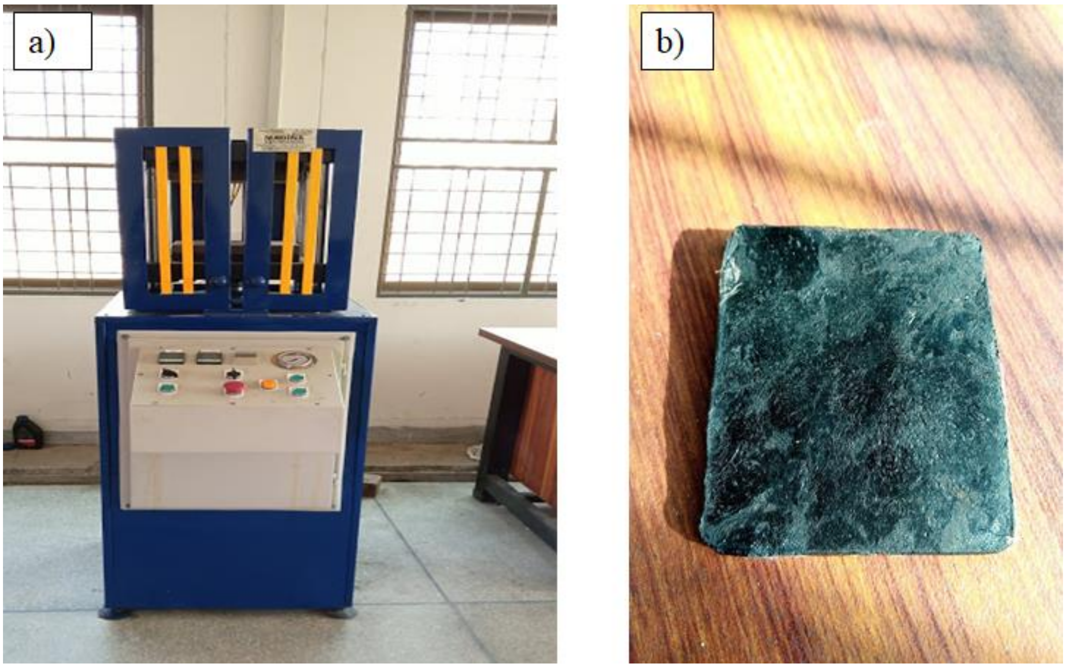

Figure 3.8: a) Compression molding machine used in the current study b) Final product for characterization

3.5 Characterization of prepared PEEK-MWCNTs/nHA/ILs composites

To examine the impact of MWCNTs and ILs-modified MWCNTs on the characteristics of PEEK/MWCNTs/nHA/ILs nanocomposites, multiple characterization techniques (Figure 3.9), including morphological study, thermal stability evaluation, mechanical performance, and cells viability investigation were performed. The next section provides an overview of various characterization techniques.

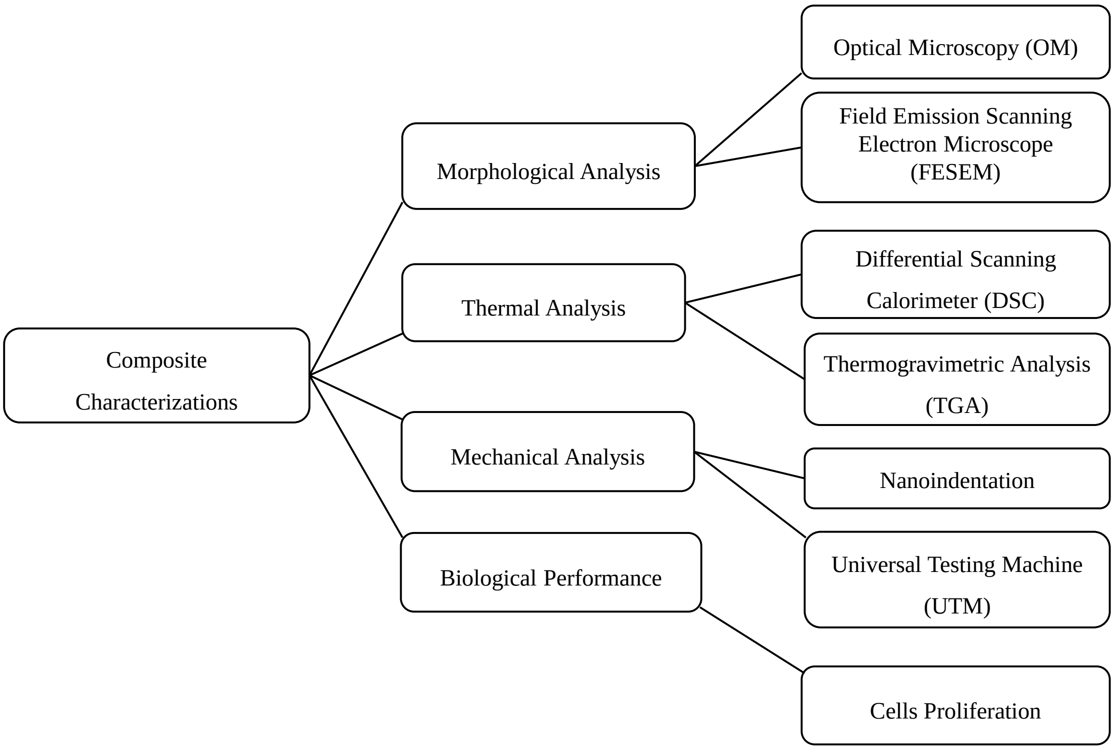

Figure 3.9: Characterization of prepared PEEK composites

3.5.1 Optical microscope (OM)

Optical microscopy (OM) is widely utilized as a viable technique for determining the morphology of an inorganic filler in the various polymer matrices. The OM, also known as the "light optical microscope," is a kind of microscope that magnifies pictures of tiny materials using visible light and a lens system. It is performed to determine the nanoparticles dispersibility inside the polymer matrix, which is essential for high mechanical characteristics of nanocomposites. The size of MWCNTs aggregates in PEEK composites prepared with and without ILs modifications was determined with the Dino-lite microscope bought from AnMo Electronics Co. Taiwan (AD4113ZT Dino-lite). The dimensions of the testing sample were 1 cm × 1 cm × 0.2 cm. Optical microscope is effective for 0-250 mm magnification range.

3.5.2 Field-emission scanning electron microscopy (FESEM)

The field-emission scanning electron microscopy (FESEM) has become a comprehensive technique for capturing images of the microstructures of the used materials in the composites. FESEM has been usually conducted in a high vacuum environment since gas molecules attempt to influence the electron beam and the released secondary and backscattered electrons employed for imaging. The morphologies and mapping of the produced PEEK composites were investigated by FESEM/Energy Dispersive X-Ray (SUPRA 55VP, Germany). FESEM images were obtained at a magnification of 500X using double-faced tape to adhere the composites on metal stubs with sample size of 1 cm × 1 cm × 0.2 cm. Prior to imaging, specimens were coated with gold-palladium by a sputter coater.

3.5.3 Differential scanning calorimetry (DSC)

The determination of phase transition temperature (melting point, T_m) and crystallinity of thermoplastic polymer composites with homogenous MWCNTs dispersion is regarded to be one of the primary parameters. Differential scanning calorimetry (DSC; Q2000 USA) was used to evaluate the melting point and crystallization temperature of PEEK composites. A sample weighing about 5–10 mg [287] was heated at a rate of 10 °C/min from ambient temperature to 400 °C in a nitrogen environment. After 5 min at the isothermal temperature, the specimens were cooled to 40 °C at a rate of 10 °C/min. Using the below formula (Equation 3.1), the degree of crystallinity (X_c) of PEEK and its nanocomposites was calculated.

$$x_c = \frac{\Delta H_m}{\Delta H_0(1-\phi)} \times 100 \qquad (3.1)$$

Where, ΔH_m is melting enthalpy and (ΔH_0) is heat of fusion of a 100 % crystalline PEEK sample (130 J/g), and Φ is the mass percent of the MWCNTs in the PEEK nanocomposites [2].

3.5.4 Thermogravimetric analysis (TGA)

The capacity of a composite material to maintain necessary properties such as strength, hardness, or elasticity at the operating temperatures is referred to as thermal stability. Therefore, it is always necessary to investigate the thermal degradation properties of polymeric composites. The thermogravimetric analysis (TGA Q600; TA) was used to determine the thermal decomposition behaviour of the produced PEEK nanocomposites. The specimens (5-10 mg) were heated up to 800 ℃ at 10 ℃/min. Simultaneously, an inert environment was produced to avoid undesired oxidation using pure nitrogen (10 mL/min) as carrier gas. To maximize moisture evaporation, the samples were vacuum dried overnight at 100 °C. In general, a change in thermal properties is recorded during TGA measurement in terms of % mass loss as a function of temperature. The decomposition temperature of the samples was obtained from the TGA curves.

3.5.5 Nanoindentation

Polymeric composites would have a wide range of engineering applications, but only if they have the desired mechanical characteristics. For most applications, mechanical properties, particularly mechanical strength and elastic modulus, are the most important of all the chemical and physical characteristics of polymer composites. Nanoindentation is a technique for determining the nanomechanical characteristics and machinability of polymeric materials. The elastic modulus and load-displacement curves of prepared PEEK composites (1 cm × 1 cm × 0.2 cm) were obtained from the nanoindentation (NANO INDENTER® (supplied by Zwick/Roell)) at Poisson ratio 0.5 with the QCMS modulus-hardness method. The nanoindentation tests were conducted with a maximum indentation force (100 mN) and displacement (70 μm) with a 20 sec hold time.

3.5.6 Universal testing machine (UTM)

The tensile test is a basic material evaluation that includes stressing a sample in uniaxial tension till failure to determine the association in between tensile stress and the tensile strain**.** Tensile tests can be used to determine a variety of mechanical characteristics, which include tensile strength, total elongation, and elastic modulus. To examine the effect of ILs modified MWCNTs and plain MWCNTs on the mechanical properties (tensile strength and elastic modulus) of PEEK composites by using Zwick-Roell Amsler HA-50 UTM (Universal Testing Machine) and employing the modified standard test method of ASTM D638. The initial clamping length and crosshead speed were set at 70 mm and 5 mm/min, respectively, with a preload of 5 KN.

3.5.7 Proliferation Analysis

Biocompatibility of the pure PEEK and synthesized PEEK/MWCNTs/nHA/ILs scaffolds was determined using the murine fibroblast cell line NIH3T3. The cells were cultured for 3 days in Dulbecco’s Minimal Essential Medium (DMEM) with 10% Fetal Bovine Serum (FBS) and 1% Penicillin Streptomycin till confluence (Figure 3.4; objective 3). At 80% confluence the cells were trypsinized and centrifuged to remove trypsin and re-suspended in DMEM for subsequent plating. The cells were seeded at a density of 50000 cells per well in 24 well tissue culture plates and allowed to adhere for 24 hours before adding 1μg/ml of each type of the samples. The dimensions of the testing sample were 1 cm × 1 cm × 0.2 cm.

3.5.7.1 Alamar Blue Assay

To evaluate the cell attachment and viability, Alamar blue absorbance measurements were taken after 24 h. A redox indicator changing from oxidized (blue) to a reduced (red) form due to activity of dehydrogenase enzyme inside the metabolically active cells was analyzed by Alamar blue testing. The cell seeded samples were washed by phosphate buffer solution (PBS) prior to adding 0.5 mL of Alamar blue solution (Sigma Aldrich, UK) (saturated 1:10 with phosphate buffer solution) and incubated at 37 °C for 4 h. The absorbance readings were recorded at 570 nm using a fluorescence plate reader (Bio Rad, UK, PR4100 Absorbance Microplate Reader).

3.5.7.2 In vitro degradation study

The initial weight of dry samples (w_1) was determined prior to incubation in two distinct aquatic environments. For time period (6 months), the sample tubes were incubated in phosphate buffer solution (PBS) and lysozyme solution (1 mg/mL) in PBS at 37 °C. After the specified time, samples were removed and dried at 37 °C for 24 h. Afterwards, the samples were weighed (w_2). The subsequent equation [288, 289] was used to estimate the deterioration rate of the composites.

$$\mathrm{Degradation} = \frac{w_1 - w_2}{w_1} \times 100 \qquad (3.2)$$

3.5.8 Statistical Analysis

The quantitative experimental results were expressed in terms of the average value ± standard deviation. At $p \leq 0.05$, the differences were deemed statistically significant. MS Excel 2016 was used to perform the statistical analysis.

3.6 Calculation of thermal activation energy

The thermal decomposition pattern of a substance with respect to temperature under a particular heating rate is determined by dynamic thermogravimetric analysis (TGA). The renowned techniques for predicting the thermal degradation parameters of the polymer composites are Coats-Redfern (Equation 3.3), Broido (Equation 3.4), and Horowitz-Metzger (Equation 3.5). These models were used to analyze the TGA data (temperature range; 560-600 ℃) of PEEK nanocomposites with and without ILs, and the activation energy for each component was determined from the slope of the graph. Figure 3.10 illustrates the procedure for using thermogravimetric data to determine the thermal activation energy.

$$\ln\left(\frac{-\ln(1-\alpha)}{T^2}\right) \text{ vs } 1000/T \qquad (3.3)$$

$$\ln \ln\left(\frac{1}{\alpha}\right) \text{ vs } 1000/T \qquad (3.4)$$

$$\ln\left\{\ln\left(\frac{w_0}{w_t}\right)\right\} \text{ vs } \theta \qquad (3.5)$$

Where α, T, w_0, w_t and θ are decomposition factor, temperature at any time t, weight at initial temperature, weight at final temperature and variable auxiliary temperature respectively.

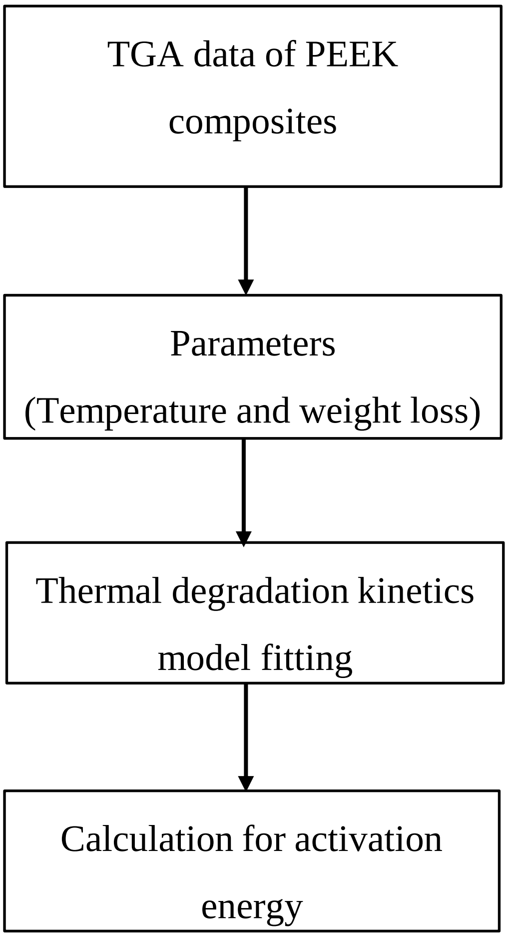

Figure 3.10: Procedure used to calculate activation energy of PEEK composites

3.7 Summary

PEEK/MWCNTs/nHA composites without ILs and PEEK/MWCNTs/nHA/ILs composites with different amounts of ILs [EMIM]Ac, [EMIM]$HS0_4$, [BMIM]Ac and [BMIM]HSO_4 were prepared under mild operating conditions (180 °C, 2 h). The weight percentage of IL to MWCNTs varies between 0:1 and 2:1. The PEEK composite pellets were obtained after melt mixing in the internal mixer (Madina engineering materials, Pakistan) at 350 ℃ and 80 rpm for 3 min. The final product was collected after the thermo molding of the PEEK pellets in the compression molding (Madina engineering materials, Pakistan) at 390 ℃ with 20 bars for 10 min. The final dimensions of the PEEK nanocomposite sheets were 7.62 cm × 7.62 cm × 0.2 cm with the target density of 1.2 gcm^{-3}.

The untreated and ILs treated PEEK composites were characterized for morphological, thermal stability, mechanical performance and biological properties by following standard analytical techniques. Optical microscope and FESEM were used to examine the MWCNTs dispersion in PEEK composites. DSC testing of the nanocomposite sheets was conducted to observe the melting and crystallization temperature. The decomposition temperature of the prepared PEEK nanocomposites was determined with the help of the TGA study. Nanoindentation and UTM experiments were used to measure the elastic modulus of the fabricated PEEK nanocomposites with and without ILs modifications and compared with those of pure PEEK and values of human cortical bone. The biological properties were assessed by the proliferation. Thermogravimetric profiles of the PEEK composites were modelled by using Coats-Redfern, Broido and Horowitz-Metzger methods to calculate the thermal activation energy of the materials.

CHAPTER 4

RESULTS AND DISCUSSION

4.1 Overview

This chapter describes a comprehensive evaluation of the characteristics of prepared composites. The comparative impact of organic solvent and different ionic liquids on the morphological, thermal and mechanical performance of the composites is studied. The biological study of pure polymer and its composites has also been presented. Moreover, the thermal degradation kinetics of ionic liquid assisted polymer composites with three existing methods, such as Coats-Redfern, Broido and Horowitz-Metzger, is determined.

4.2 Effect of organic solvent and ionic liquid on the properties of PEEK composites

4.2.1 The MWCNTs dispersion in PEEK composites

The Dino-lite microscope was used to examine the surface morphology of pure PEEK, PEEK/MWCNTs, and PEEK/MWCNTs/IL nanocomposites, as illustrated in Figure 4.1. As shown in Figure 4.1b, large-sized aggregates with an average size of 0.38 mm were observed in the PEEK/MWCNTs composites after the incorporation of DMF with MWCNTs. It demonstrates the poor MWCNTs dispersion in the PEEK matrix [58, 290]. However, when IL was employed to distribute MWCNTs into PEEK, a substantial decrease in MWCNTs agglomerates (0.20 mm) was found. This decrease in MWCNTs agglomerations could be attributed to the strong interactions among [EMIM]HSO_4 and MWCNTs than those of DMF and MWCNTs in PEEK/MWCNTs/IL nanocomposites [243].

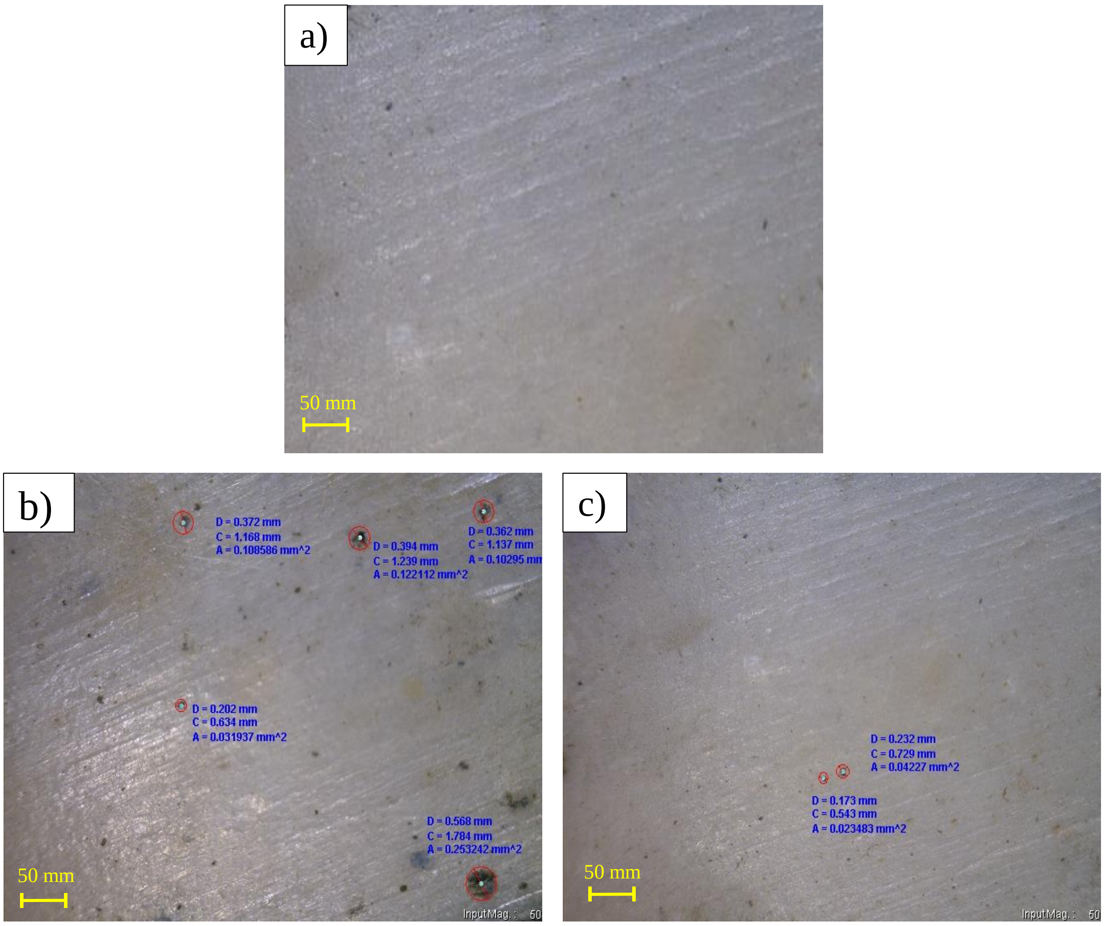

Figure 4.1: a) Optical micrographs of neat PEEK b) PEEK/MWCNTs c) PEEK/MWCNTs/IL at 50 mm magnification

To illustrate the role of [EMIM]HSO_4 as a distributing agent for MWCNTs, Figures 4.2 and 4.3 exhibit FESEM micrographs of pure PEEK and its nanocomposites. Figure 4.2 (c, d, e) confirms that the distribution of components in PEEK/MWCNTs composites (PEEK nanocomposites based on DMF) was not uniform. On the other side, when IL-modified MWCNTs were employed, mapping demonstrated a more homogeneous dispersion of components (C, O, and S) as shown in Figure 4.2 (f, g, h). Due to the large surface area and poor compatibility of MWCNTs [34, 291], thick agglomerates of MWCNTs were found in PEEK in the absence of IL, as displayed in Fig 4.3b. Additionally, these MWCNTs aggregates were formed in the composites due to the poor affinity of MWCNTs for the PEEK matrix [292]. On the other hand, IL-modified MWCNTs offered excellent dispersion and enhanced compatibility with the PEEK, as seen in Figure 4.3c. The uniform distribution and deagglomeration of

MWCNTs represented the existence of strong π–π interactions between the surface of the π-electronic nanotubes and the imidazolium ring of the IL [293, 294].

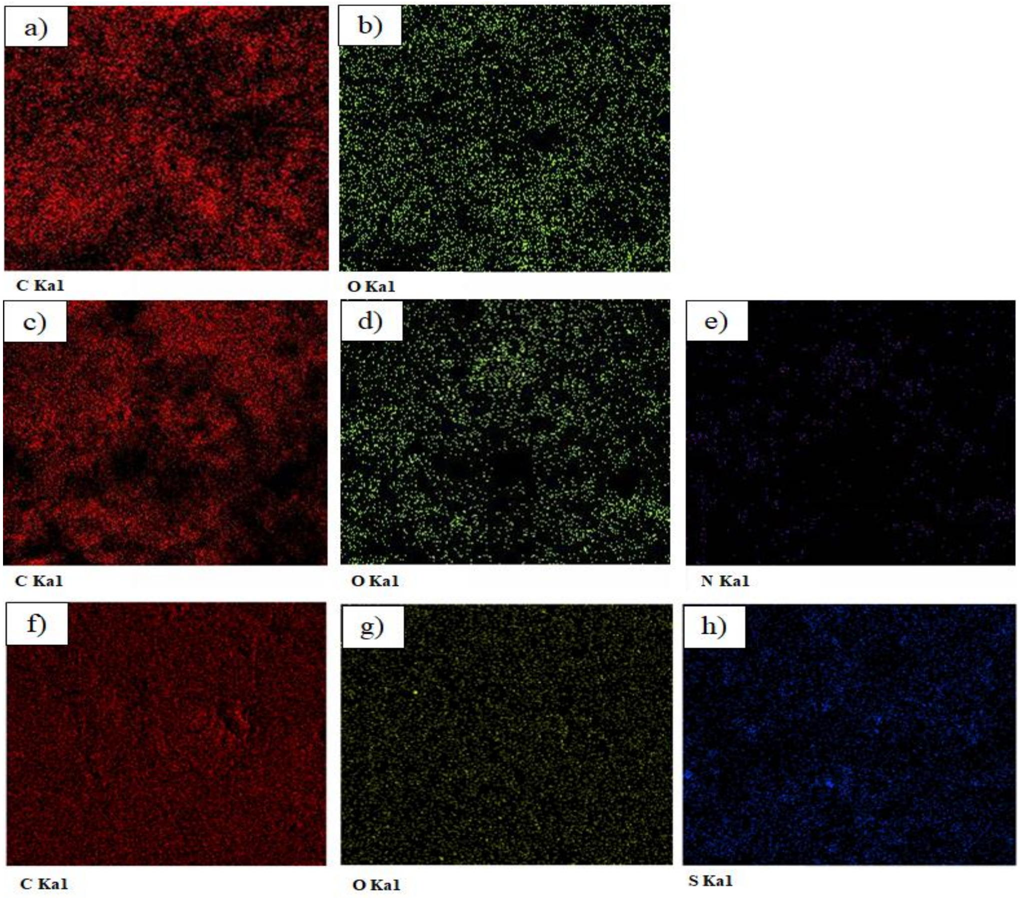

Figure 4.2: Mapping of pure PEEK (a, b), PEEK/MWCNTs (c, d, e), PEEK/MWCNTs/IL (f, g, h)

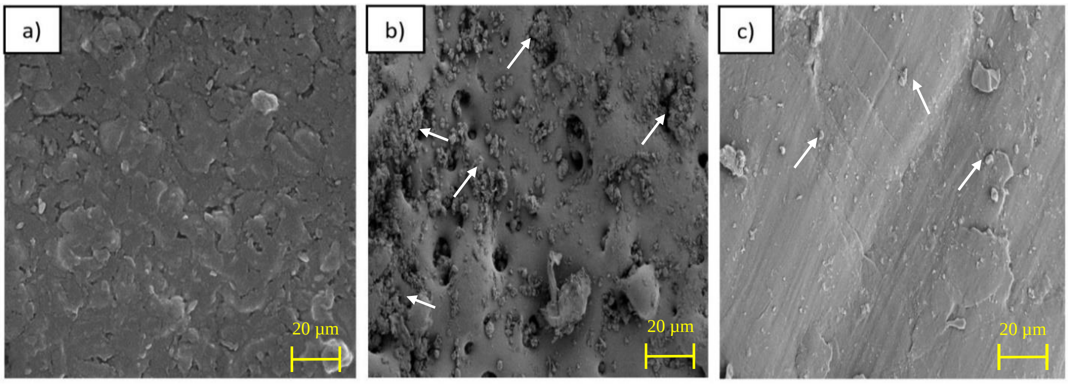

Figure 4.3: FESEM images of PEEK (a), PEEK/MWCNTs (b), PEEK/MWCNTs/IL (c) at X500

4.2.2 The thermal properties of PEEK composites

The tendency of a composite material to maintain necessary properties such as strength and hardness at the service temperature is referred to as thermal stability. Therefore, it is always necessary to investigate the thermal degradation properties of polymeric composites. Thermal characteristics of pure PEEK, PEEK/MWCNTs, and PEEK/MWCNTs/IL were evaluated using thermogravimetric analysis in an inert environment, as shown in Figure 4.4, and the parameters inferred from TGA profiles are given in Table 4.1. The thermogram of the PEEK/MWCNTs/IL composite indicated that it degraded in two phases. The first decomposition stage was due to the presence of IL, whereas the second stage was corroborated to polymer matrix. Similar degradation behavior for IL [227, 295], and PEEK polymer [74], have been described in the literature.

The T_{15} (15 % weight loss) of PEEK/MWCNTs/IL was 614 °C, which was considerably greater than the corresponding values for PEEK/MWCNTs (583 °C) and pure PEEK (570 °C). The enhanced thermal resilience shown by PEEK/MWCNTs/IL composites was due to the considerable interfacial interactions between IL-modified MWCNTs and PEEK polymer [242, 296] and restricting the molecular chain movement of polymer around MWCNTs [48]. Takassi et al. (2017) [244] found similar findings for poly(amide-imide-IL)/MWCNTs composites.

Takassi et al. (2017) [244] used a well-established synthetic method to create a novel salicylic acid-incorporating diacid monomer using widely accessible chemicals. The diacid produced was exploited to make a thermally resistant poly(amide-imide) through direct polycondensation using 4,4′-diphenylmethanediamine in an IL, 1,3-diisopropyl-imidazolium bromide as a green media. The manufactured polymer was served as the matrix for the formation of poly(amide-imide)/multiwalled carbon nanotube composites at three different MWCNTs concentrations (5, 10, and 15% wt). The microscopy methods revealed the uniform MWCNTs distribution in the poly(amide-imide) matrix. The decomposition temperature at 10 % (T_{d10}) weight loss of the composite containing 5% MWCNTs modified with IL was greater (41 °C) than that of pure PAI. It might be due to excellent dispersion and high heat transmission of MWCNTs, which prevented it from accumulating at specific locations and causing deterioration.

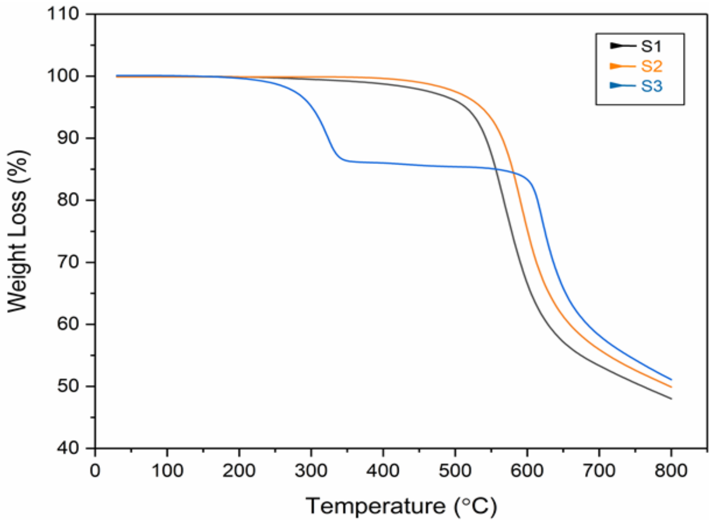

Figure 4.4: Thermogravimetric (TG) curves for the PEEK, PEEK/MWCNTs, PEEK/MWCNTs/IL at 10 °C/min

DSC is a commonly used industrial quality control method for observing the physical processes in polymeric composites such as crystallization, fusion, and glass transition temperature. The DSC heating and cooling profiles of pure PEEK and its nanocomposites are displayed in Figure 4.5, and the associated data are summarized in Table 4.1. The melting point (T_m) and crystallization temperature (T_c) of each sample were determined using these graphs. The T_m of pure PEEK was 342 °C, but it raised to 347 °C and 350 °C for PEEK/MWCNTs and PEEK/MWCNTs/IL composites. Likewise, for pure PEEK, PEEK/MWCNTs, and PEEK/MWCNTs/IL, the T_c values were 283 °C, 285 °C, and 290 °C, respectively. The enhanced T_m and T_c values revealed that the thermal stability of the produced nanocomposites has been improved.

Yang et al. (2018) [47] found a similar effect when poly (vinylidene fluoride) (PVDF) nanocomposites were fabricated with IL-modified CNTs for increased T_m and T_c because of the homogeneous dispersion of MWCNTs in the presence of IL. It demonstrated that CNTs treated with IL served as the most efficient nucleation sites for polymer crystallites [234, 293]. The enhanced PEEK matrix crystallization in PEEK/MWCNTs/IL could be due to the strong interactions between the PEEK polymer and the well-dispersed MWCNTs through IL [47], which promoted the nucleation density of the PEEK.

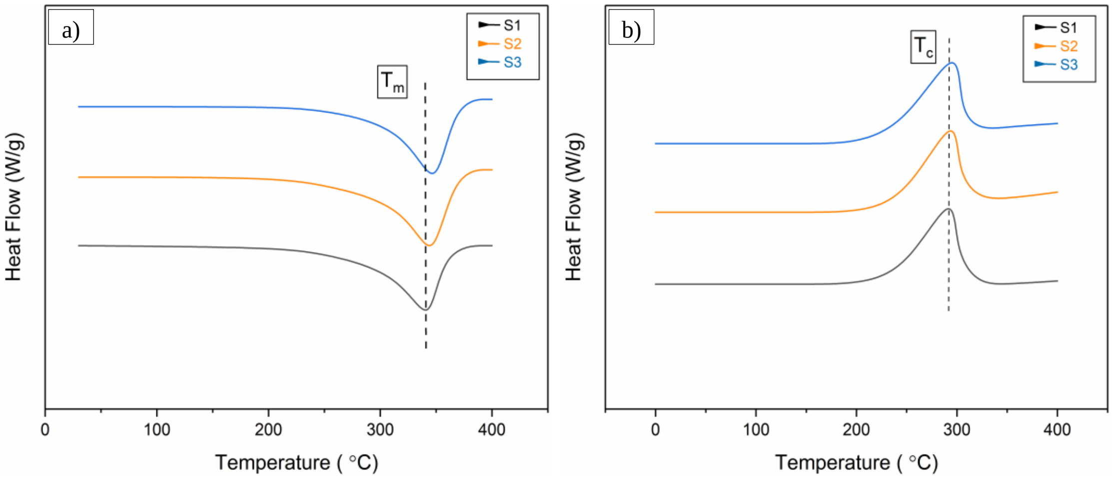

Figure 4.5: Heating (a) and cooling (b) curves of differential scanning calorimetry (DSC) for PEEK and its nanocomposites at 10 °C/min.

Table 4.1: The thermal properties of PEEK and its nanocomposites

Sample	Crystallization temperature T_c (°C)	Melting temperature T_m (°C)	Melting enthalpy ΔH_m (J/g)	Degree of crystallization X_c (%)	Decomposition temperature T_{15} (°C)
PEEK	283 ± 2.3	342 ± 1.2	48.62 ± 0.3	37.40 ± 2.1	570 ± 3.2
PEEK/ MWCNTs	285 ± 1.3	347 ± 0.8	50.03 ± 0.5	38.87 ± 1.3	583 ± 2.8
PEEK/ MWCNTs/IL	290 ± 2.9	350 ± 1.8	52.91 ± 0.5	41.11 ± 1.7	614 ± 3.5

4.2.3 The mechanical properties of PEEK composites

Nanoindentation is commonly used to study the nanomechanical characteristics of materials and may also be used to assess the machinability of polymeric materials. Figure 4.6 shows the typical loading and unloading profiles obtained from the nanoindenter for PEEK composites. The maximum indentation penetration of 80 µm was achieved at 100 mN of indentation force. From the Figure 4.6, when comparing the PEEK/MWCNTs composites to the neat PEEK, it was noticed that the PEEK/MWCNTs had a harder behaviour (2%). It may be attributed to the inclusion of

MWCNTs in the PEEK [297, 298]. Because of the nucleation actions between the PEEK matrix and the MWCNTs, the presence of MWCNTs in the composites enhanced the degree of crystallinity [299]. At the same indentation force, the curve of PEEK/MWCNTs/IL was considerably harder (5%) than that of neat PEEK due to the homogenous distribution of MWCNTs in the PEEK matrix via IL. Qiu et al. (2013) found similar findings on polyamide 66/MWCNTs composites [300].

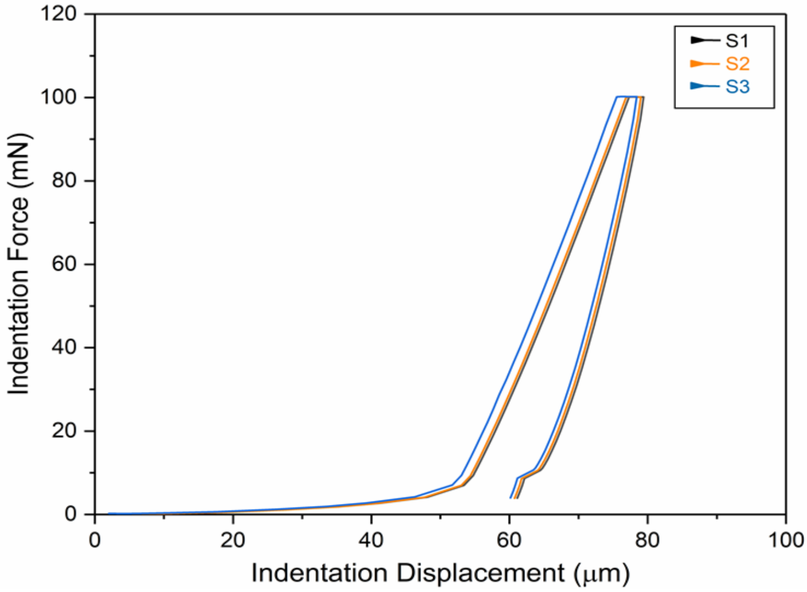

Figure 4.6: Indentation load-displacement curves for the PEEK, PEEK/MWCNTs, and PEEK/MWCNTs/IL

The elastic modulus is a fundamental mechanical property of the materials that has a significant effect on their stiffness and reliability. The elastic modulus of the manufactured laminates is described in terms of contact depth (μm), and typical PEEK nanocomposites curves are given in Figure 4.7. At low contact depths (5-20 μm), elevated modulus values were found as a result of minor changes in the polymer physical characteristics. As seen in the figure, the inclusion of MWCNTs and IL-modified MWCNTs increased the elastic modulus of the developed samples [298, 301]. However, owing to the uneven dispersion and agglomeration of MWCNTs, the required elastic modulus value was not achieved in the PEEK/MWCNTs. On the other hand, the modulus of the PEEK/MWCNTs/IL composite was raised to an acceptable level as a result of the MWCNTs being successfully dispersed inside the PEEK polymer via IL [300].

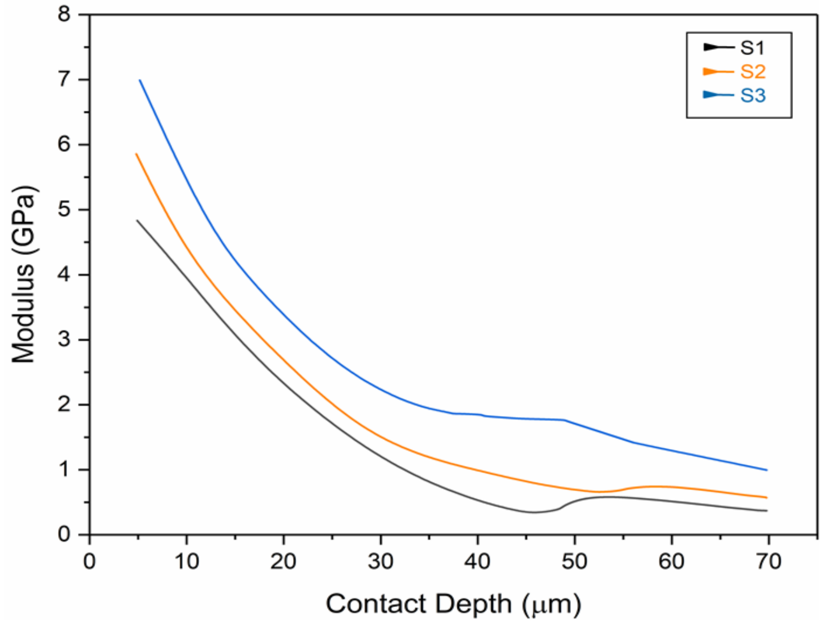

Figure 4.7: Elastic Modulus as a function of contact depth for PEEK nanocomposites.

Figure 4.8 illustrates the stain-stress behavior of pure PEEK, PEEK/MWCNTs, and PEEK/MWCNTs/IL composites and Table 4.2 summarizes the tensile characteristics of synthesized nanocomposites and human bone. The elastic modulus and tensile strength of pristine PEEK were estimated to be 4 GPa and 80 MPa, respectively, and were raised to 5.5 GPa and 83.4 GPa for PEEK/MWCNTs. PEEK/MWCNTs/IL, on the other hand, had elastic modulus (7.06 GPa) and tensile strength (88.7 MPa) and compared to human bone (7-12 GPa, 85-100 MPa) [1].

Liu et al. (2010) [247], found similar findings when they used IL-modified MWCNTs in poly(urethane) composites and revealed that mechanical characteristics of the composites were raised. The enhanced mechanical strength was suggested to be related to the efficient dispersion of MWCNTs in the composites by ILs. Moreover, the homogenous dispersion of MWCNTs constrained the amorphous phase by enhancing polymer crystallinity. Due to the restriction sites, the polymer was unable to deform, resulting in a reduction in ductility and improvements in stiffness and toughness [302]. Similar behavior was also observed by other researchers [49, 235, 240]. The uniform distribution of MWCNTs was critical in the load transfer between the matrix and the MWCNTs. Because of the stress being transferred from the composites to the MWCNTs, both the tensile strength and elastic modulus were enhanced.

Abraham et al. (2018) [49] synthesized well-dispersed, durable, and mechanically long-term reliable multiwalled carbon nanotube (MWCNT)-styrene-butadiene rubber (SBR) composites using a melt mixing method with the intervention of an ionic liquid (1-benzyl-3-methylimidazolium chloride) as a dispersant. The mechanical characteristics of MWCNTs/SBR vulcanizates were examined under a variety of loading conditions, and it was discovered that the uniform structure promoted mechanical performance with increased stiffness. It was discovered that the homogeneously dispersed MWCNTs immobilized the length of polymer chains, resulting in a significant increase in mechanical properties. Virgin SBR has elastic modulus of about 1.44 MPa, while 10 phr addition of ionic liquid modified MWCNTs resulted in elastic modulus of approximately 6.45 MPa (347 % improvements) owing to the addition of a stronger substance to the rubber matrix.

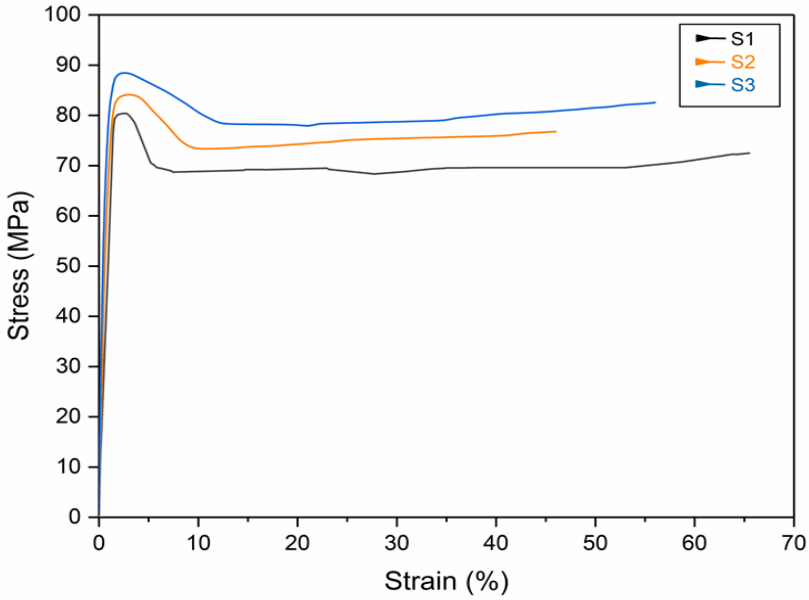

Figure 4.8: Stress-Strain curves of a) PEEK and its nanocomposites

The comparative impact of DMF-modified MWCNTs and IL-modified MWCNTs on PEEK nanocomposites clearly indicated that the composites fabricated with IL assisted MWCNTs have superior thermal and mechanical properties. FESEM and optical micrographs revealed that IL improved MWCNTs dispersion in PEEK/MWCNTs/IL when compared to the PEEK/MWCNTs composites. The decomposition temperature of PEEK/MWCNTs/IL was increased by 9.8% than that of neat PEEK. Additionally, the elastic modulus and tensile strength of PEEK/MWCNTs/IL composites were significantly greater than those of pristine PEEK and PEEK/MWCNTs composites and were equivalent to those of human cortical bone. Thus, it might be claimed that IL is an effective and environmentally benign reagent for the preparation of PEEK/MWCNTs nanocomposites with potential uses in the biomedical applications.

Table 4.2: The mechanical properties of PEEK and its nanocomposites

Sample Type	Tensile Strength (MPa)	Elastic Modulus (GPa)
PEEK	80.0 ± 0.30	4.00 ± 0.80
PEEK/MWCNTs	83.4 ± 1.80	5.30 ± 0.10
PEEK/MWCNTs/IL	88.7 ± 2.04	7.06 ± 0.40
Human Bone	85–100	7–12

4.3 Effect of ionic liquids with different amounts on the properties of PEEK composites

4.3.1 Effect of [EMIM]Ac and [BMIM]HSO$_4$ on the MWCNTs dispersion in PEEK composites

The homogeneous MWCNTs dispersion in a range of polymer matrices is considered essential for enhancing the thermomechanical properties of polymer composites employed in a wide variety of engineering applications. The micrographs of the produced PEEK nanocomposites in Figure 4.9 were taken using an optical microscope to determine the size of the nanofiller particles. Figures 4.9 (a) and 4.10 (f-i) show PEEK nanocomposites without ILs and PEEK nanocomposites with [BMIM]HSO$_4$. Because of the poor compatibility of the filler with PEEK, MWCNTs created very big agglomerates in sample S4, as seen in Figure 4.9 (a). While, when IL contained MWCNTs were employed, the compatibility and dispersion of MWCNTs in the PEEK polymer were significantly improved. For instance, the average size of the MWCNTs agglomeration in S4 nanocomposites was 250.57 µm, while in

S20, nanocomposites were significantly decreased to 73.63 μm. The strong cation-π or π-π stacking interactions among the π-electronic nanotubes surface and imidazolium cation are responsible for the decrease in the MWCNTs aggregation in the polymer matrix [303, 304].

The micrographs in Figure 4.9 (b-e) are of [EMIM]Ac-based PEEK composites obtained using optical microscopy. For sample S4, when MWCNTs were used in PEEK, the MWCNTs clusters were observed because of their strong Vander Waals forces. By contrast, it can be demonstrated that strong physical interactions between MWCNTs and PEEK supplied by IL greatly inhibited MWCNTs aggregation. The average size of MWCNTs agglomerates for samples S5, S6, S7 and S8 was observed as 140.89, 115.45, 103.61 and 89.72 μm, respectively. The improvement in the dispersion of MWCNTs after introducing [EMIM]Ac could be attributed to the strong interactions between PEEK and MWCNTs [305].

Therattil et al. (2020) [306] conducted similar experiments using IL, [BMIM][Cl] (1-butyl-3-methylimidazolium chloride) to distribute MWCNTs into natural rubber (NR). Both [BMIM][Cl] and MWCNTs were shown to have substantial synergetic effects on properly dispersing MWCNTs into NR. The morphological findings indicated that IL modified MWCNTs were uniformly spreaded without intertubular connections, with a good tube–tube contact and few aggregates. It was believed that the exfoliation of highly entangled MWCNTs bundles was resulted by the strong interactions between the cation of the imidazolium ring and π-electrons of the MWCNTs.

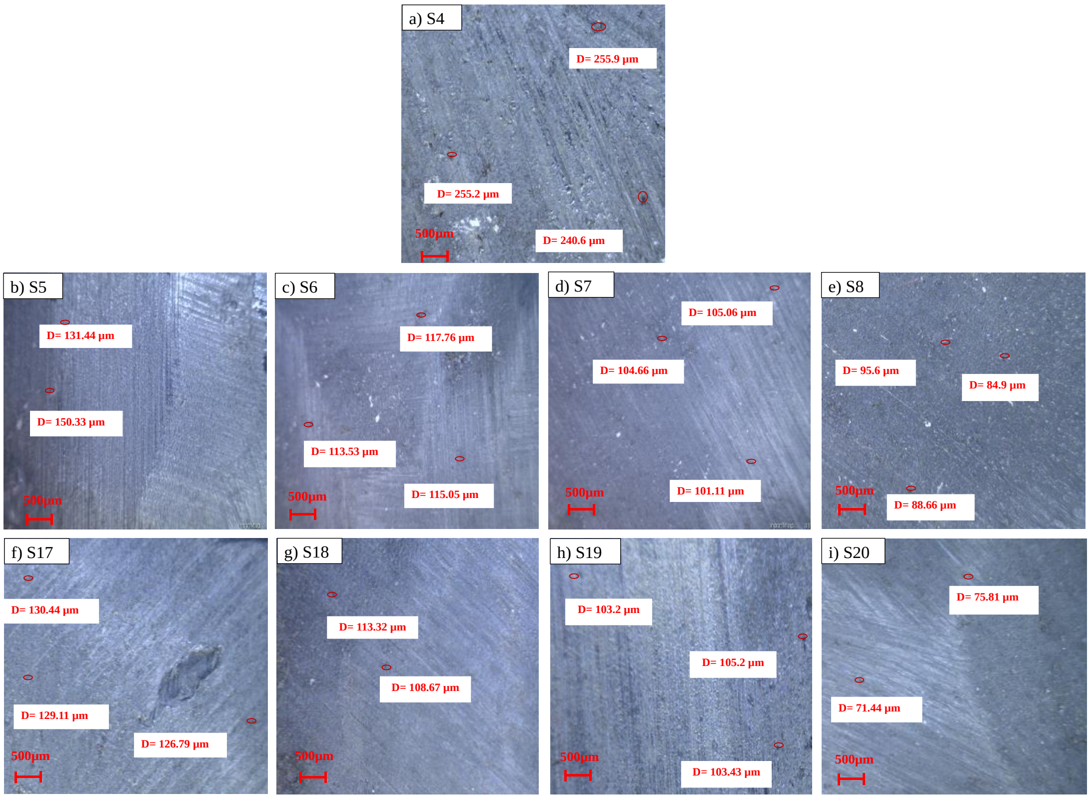

Figure 4.9: PEEK composites micrographs obtained from optical microscope a) Without IL, b-e) [EMIM]Ac based composites, f-i) [BMIM]HSO_4 based composites

The FESEM experiments were performed to evaluate further the effect of ILs and optical micrographs on the distribution of MWCNTs into PEEK. FESEM images and the comparisons of the non-IL and ILs based PEEK nanocomposites with varying IL loadings are provided in Figure 4.10. The distribution of elements (mapping) and the EDX analysis are illustrated in Figures 4.11 and 4.12. As shown in Figure 4.10 (a), low compatibility and the thick clumps of MWCNTs in PEEK were found as a result of the low dispersibility of MWCNTs in PEEK. Similar findings were reported by Ke et al. (2017) [233], in which the extrusion and compression molding techniques were used to prepare CNTs/PVDF (polyvinylidene fluoride) nanocomposites. It was discovered that extremely large CNTs agglomerates were formed in the produced composites as a result of the high aspect ratio and poor dispersion capability of MWCNTs in the polymer matrix. On the other hand, when [BMIM]HSO_4 with MWCNTs were used (Figure 4.10 f-i), the aggregation of MWCNTs was considerably reduced [307]. It was also noticed that the uniform MWCNTs distribution in PEEK composites were observed at higher concentrations of [BMIM]HSO_4.

The Figure 4.10 (b-e) shows the outcomes of FESEM images for 0.5 to 2.0 wt % of [EMIM]Ac-based PEEK composites respectively, whereas Figure 4.11 and Figure 4.12 depict the results of mapping and EDX, respectively. When contrasted to Figure 4.11 (a-d) (PEEK composites without [EMIM]Ac), the uniform distribution of the elements was seen in Figure 4.11 (e-h). The dispersion of MWCNTs in PEEK and their compatibility were enhanced when various amounts of [EMIM]Ac were utilized, as shown in Figure 4.10 (b-e).

Similarly, for both [EMIM]Ac and [BMIM]HSO_4, the use of IL to MWCNTs (2:1) substantially correlates to homogeneous MWCNTs dispersion in the PEEK matrix as presented in Figures 4.10 (e, i). These FESEM findings are in agreement with the optical micrographs. In addition, the good dispersion and disintegration of the MWCNTs are attributed to the strong π-π interactions between the π-electrons of the MWCNTs and the cation of ILs [233, 308]. Thus, it might be argued that exploiting ILs-modified MWCNTs may be a viable, environmentally friendly method for producing PEEK composites with homogeneous MWCNTs dispersion for use as a substitute for human bone in biomedical applications.

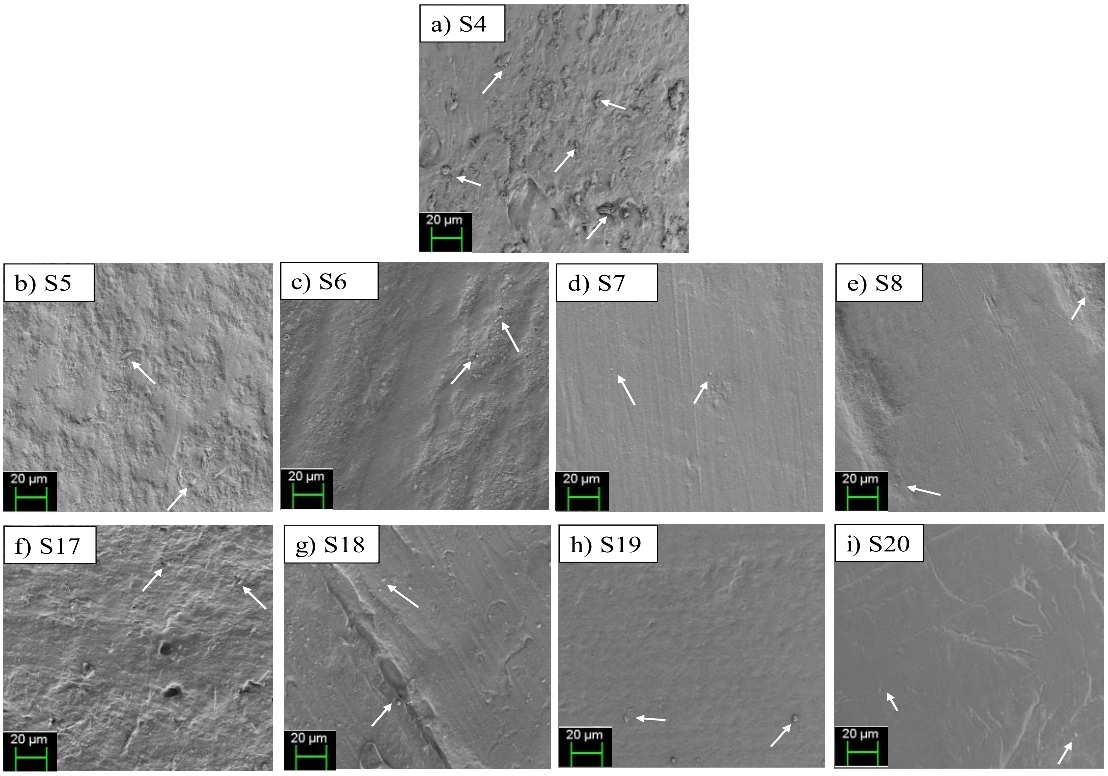

Figure 4.10: FESEM images of a) without IL, b-e) [EMIM]Ac based PEEK nanocomposites, f-i) [BMIM]HSO_4 based composites at 500X

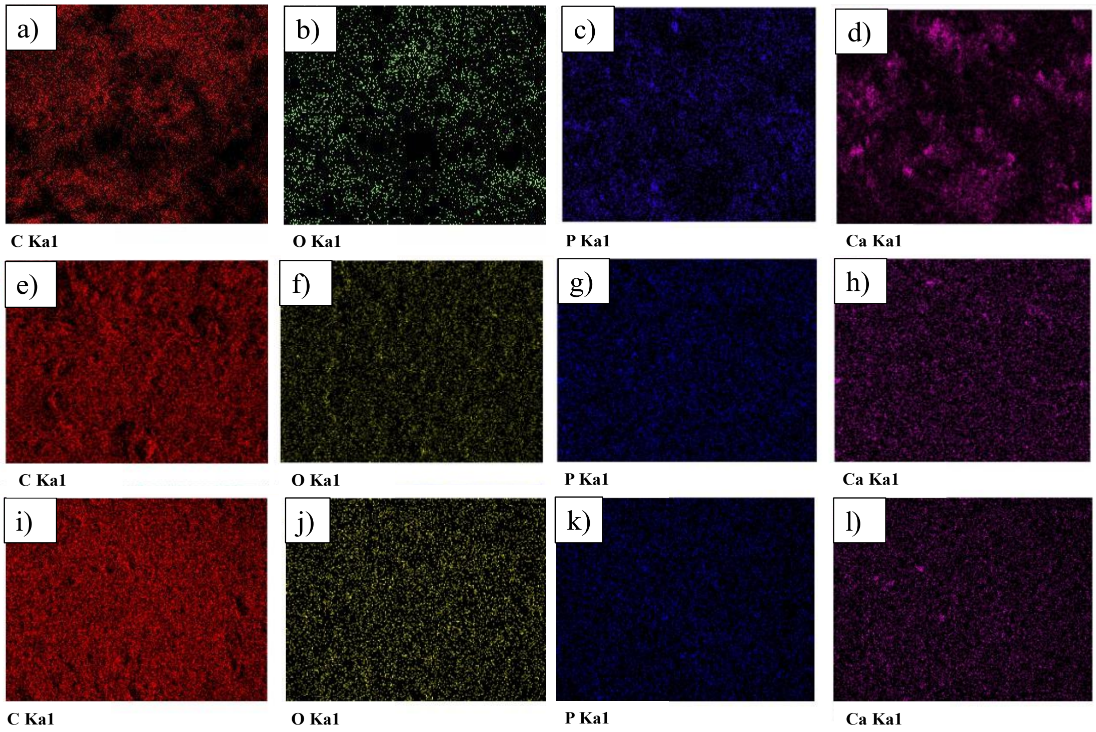

Figure 4.11: Mapping and EDX of PEEK nanocomposites a-d) Without IL e-h) [EMIM]Ac based PEEK nanocomposites, i-l) [BMIM]HSO$_4$ based PEEK composites

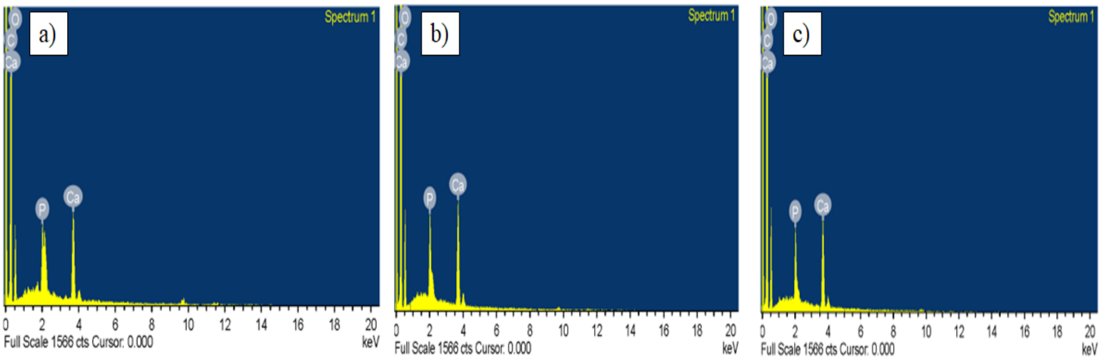

Figure 4.12: EDX images a) without IL b) [EMIM]Ac based PEEK nanocomposites c) [BMIM]HSO$_4$ based PEEK composites

4.3.2 Effect of [EMIM]HSO$_4$ and [BMIM]Ac on the MWCNTs dispersion in PEEK composites

The inclusion of ILs primarily seeks to enhance the filler dispersion by preventing the agglomeration of MWCNTs, thus encouraging a stronger interaction of the filler with the polymer matrix. As a result, composites composed of ILs-treated

MWCNTs often show better characteristics than those comprised of untreated MWCNTs. The effect of different quantities of [EMIM]HSO_4 (0.5 - 2 wt %) on the dispersion of MWCNTs in PEEK composites was explained in Figure 4.13 (b-e), respectively. These results clearly indicated that the thick clumps of MWCNTs (S4 $\cong$ 250.57 μm) were observed in PEEK composites without IL. However, ILs modified MWCNTs (0.5:1 to 2:1) exhibited the uniform structure with MWCNTs aggregates (90.3 μm). Le et al. (2016) [290] studied the effect of different amounts of ILs on the dispersion of CNTs in styrene-butadiene rubber composites. The macro dispersion (A/A_0) of CNTs in SBR composites without IL was found to be 13%, but decreased to 1.6% when IL was added, owing to the greater interactions among CNTs and SBR.

The optical microscope was used to assess the dispersion of MWCNTs in PEEK composites prepared without IL and with various [BMIM]Ac loadings, and the results are included in Figures 4.12 (a) and 4.12(f-i), respectively. The MWCNTs agglomeration was noted in sample S4 because of the poor compatibility between the MWCNTs and PEEK [28]. While after using ILs-modified MWCNTs, the MWCNTs aggregation was minimized with the average size 83.07 μm for S16 sample. Similar findings [309] were also noted in which the authors determined that ILs can provide the active surface sites for the possible stronger interactions between the filler and the polymer matrix.

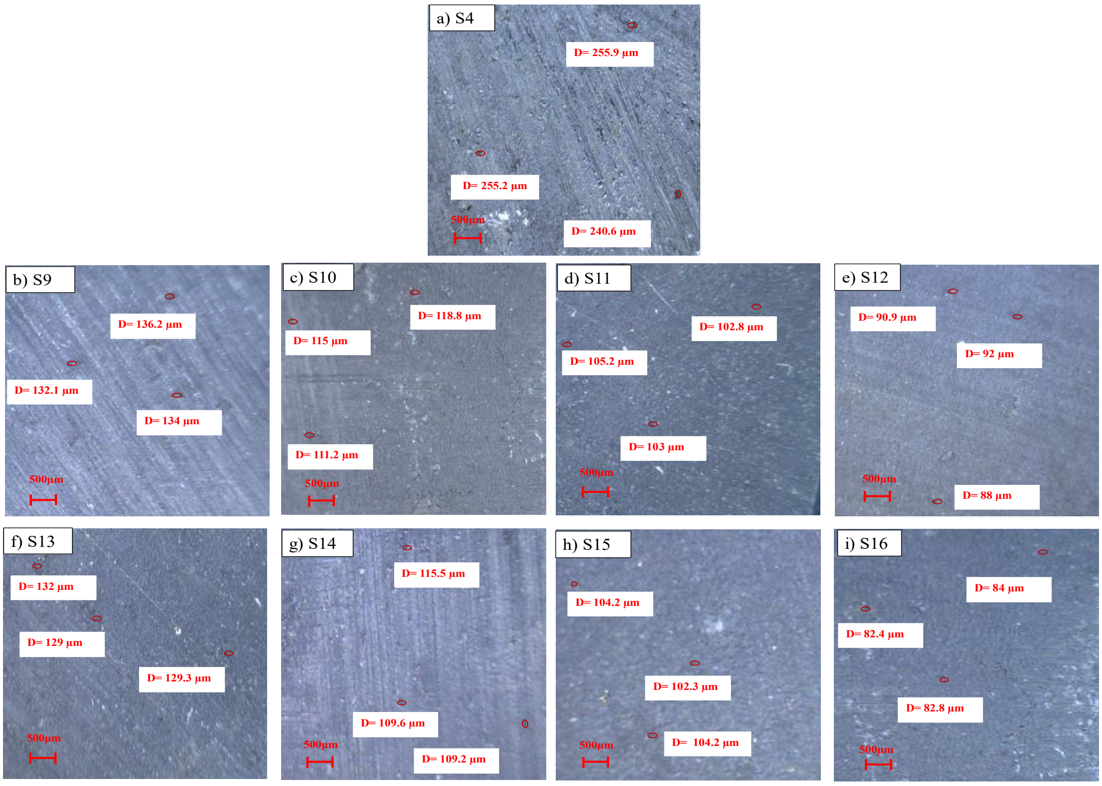

Figure 4.13: PEEK composites micrographs obtained from optical microscope a) Without IL, b-e) [EMIM]HSO_4 based composites, f-i) [BMIM]Ac based composites

The FESEM images, mapping and EDX analysis of PEEK composites fabricated without and with different concentrations of [EMIM]HSO_4 are displayed in Figure 4.14 (b-e), Figure 4.15 (e-h) and Figure 4.16 (b), respectively, to verify the outcomes of optical microscopy. The mapping confirmed that the elements were homogeneously distributed in the PEEK composites manufactured with IL-modified MWCNTs (Figure 4.15 e-h) than those to the PEEK composites without ILs (Figure 4.15 a-d). It can also be seen from Figure 4.14 (b-e) that the PEEK composites produced with various amounts of [EMIM]HSO_4 indicated the uniform MWCNTs dispersion when compared with sample S4 (without ILs). This change is attributed to the addition of ILs in PEEK composites which enhanced the MWCNTs dispersion by stronger π-π interactions among imidazolium ring and MWCNTs [43].

The impact of [BMIM]Ac on the dispersion of MWCNTs in PEEK composites is presented in Figure 4.14 (f-i), Figure 4.15 (i-l) and Figure 4.16 (c). The mapping (Figure 4.15 i-l) of these results evidenced that a uniform surface was observed when IL was employed in PEEK composites. However, when PEEK composites were fabricated without [BMIM]Ac, the MWCNTs aggregation was observed as depicted in S4 sample (Figure 4.14 a). After using IL-modified MWCNTs, the uniform MWCNTs distribution was divulged by using up to 2 wt % of IL. These FESEM results were corroborated with the optical micrographs.

The findings obtained for PEEK composites containing varying concentrations of ILs were consistent with the literature. For example, Fang et al. (2018) [58] synthesized poly(methyl methacrylate)/carbon nanotubes (PMMA/CNTs) composites employing two types of ILs, $[BMIM]PF_6$ and $[HMIM]PF_6$, using the internal mixer. The inclusion of ILs substantially improved the CNTs distribution in the PMMA matrix owing to the development of π-π stacking interactions among ILs and CNTs. This may limit the CNTs-CNTs interaction, thus reducing the CNTs aggregation in the fabricated composites.

A comparison of PEEK composites produced without and with various imidazolium-based ILs revealed that IL-modified MWCNTs were very efficient at enhancing the dispersion of MWCNTs in PEEK composites. The present study found that PEEK composites with a higher alkyl chain length decreased the aggregation of MWCNTs when compared to composites prepared with [EMIM] based ILs. These results are supporting the previously reported data [58, 290] in which the authors explained that ILs with higher alkyl chain promoted stronger interactions among the nanofiller and the polymer matrix.

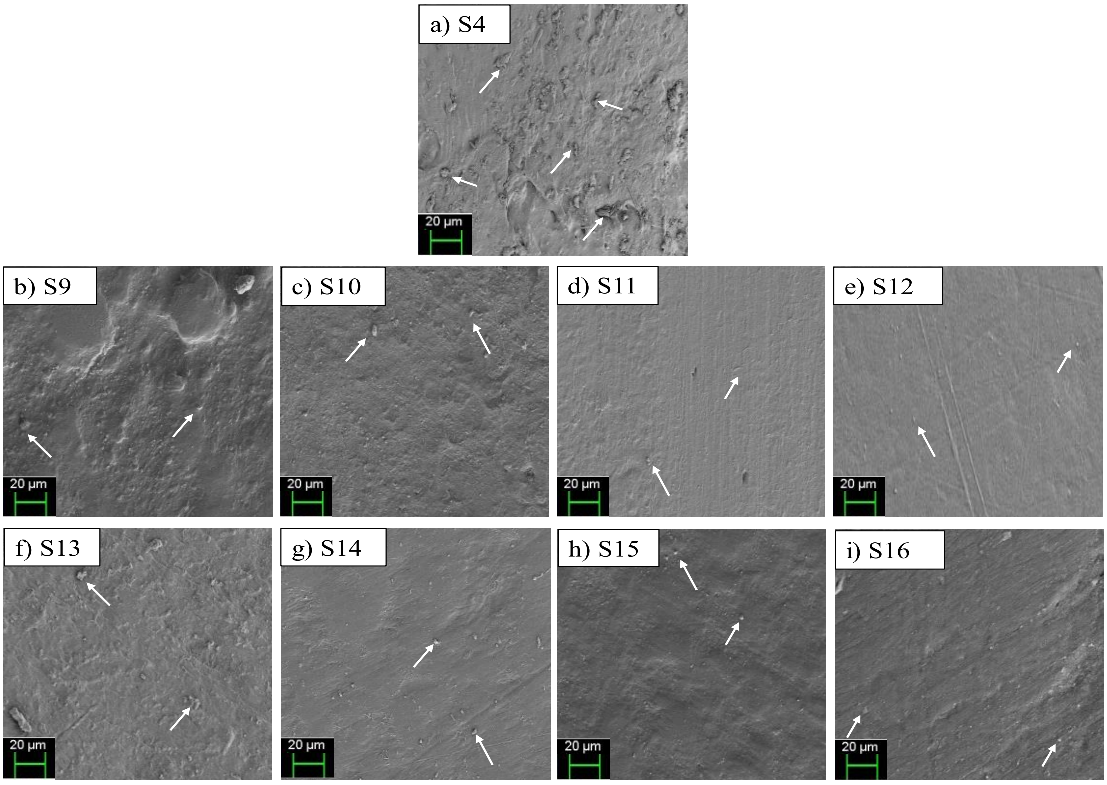

Figure 4.14: FESEM images of a) without IL, b-e) [EMIM]HSO_4 based composites, f-i) [BMIM]Ac based composites at 500X

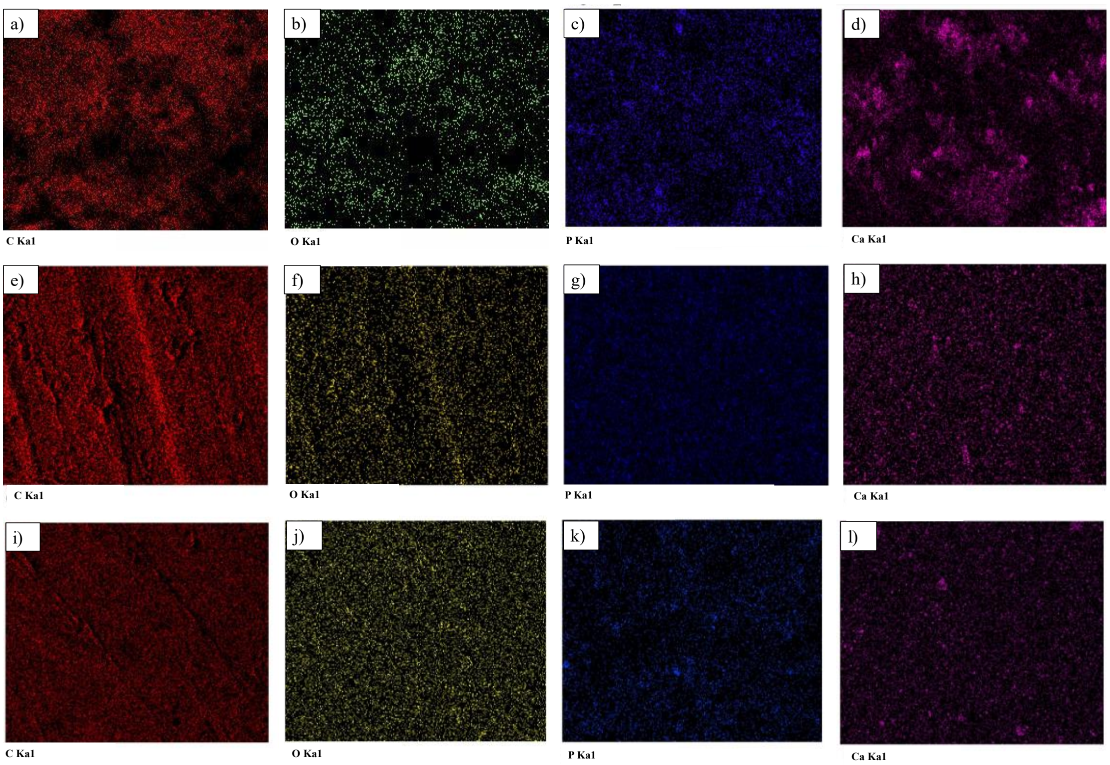

Figure 4.15: Mapping of PEEK nanocomposites a-d) Without IL e-h) [EMIM] HSO_4 based PEEK composites i-l) [BMIM]Ac based PEEK composites

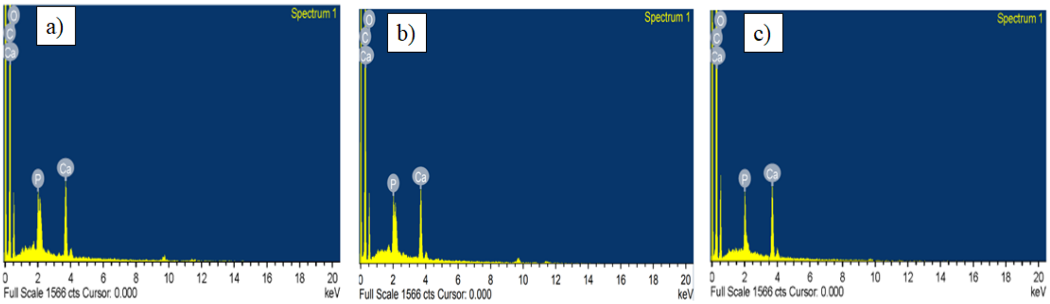

Figure 4.16: EDX analysis of PEEK nanocomposites a) Without IL b) [EMIM] HSO_4 based PEEK composites c) [BMIM]Ac based PEEK composites

4.3.3 Effect of [EMIM]Ac and [BMIM]HSO_4 on thermal properties of PEEK composites

The aggregation and unequal distribution of MWCNTs in numerous polymer matrices have a considerable effect on the thermal resilience and degradation temperature of composite materials, which becomes the basic restriction for their use in many applications. The results from the thermogravimetric study of untreated and ILs-treated PEEK-based composites are included in Figure 4.17 and Table 4.3. The Figure 4.17 (b) demonstrates the disintegration temperature of specimen S4, which was 570 °C. According to Figure 4.4, the decomposition temperature of pure PEEK was 560 °C. The addition of MWCNTs in the PEEK was responsible for the increase in thermal stability [310]. The inclusion of MWCNTs in PEEK has accelerated the crystallization of PEEK via the formation of nucleation sites [311]. In comparison, the degradation temperature of the S17 composite was 573 °C, which was increased to 581 °C for sample S18 due to the restriction of agglomeration, stronger nucleation actions, and π-π stacking interactions between the IL modified MWCNTs and PEEK. These results corroborated prior studies indicating that ILs were the primary driving factor for the strong π-π stacking interactions among MWCNTs and PEEK [312].

Furthermore, the breakdown temperatures of composites S19 and S20 were 578 and 576 °C, accordingly. This drop in thermal stability relative to sample S18 was a result of the plasticizing actions of ILs [293]. The synthesis of PMMA/IL/MWCNTs nanocomposites exhibited a similar performance [242]. The higher decomposition temperature for [BMIM]HSO_4 based PEEK composites was attributed to the stronger interactions between IL and filler due to the longer alkyl chain length of [BMIM]HSO_4 [58, 313]. The existence of longer alkyl chains ILs had improved the capacity of the imidazolium ring to lay parallel on the surface of CNTs, which was helpful for strong π-π interactions.

Figure 4.17 (a) displays the thermograms of the PEEK composites prepared without IL and with different [EMIM]Ac loadings. It was discovered that all PEEK composites degraded in a single stage in the nitrogen environment and the decomposition temperature of S4 was 570 °C and shifted to 572 °C and 580.12 °C for samples S5 and S6, respectively, and presented in Table 4.3. The incorporation of [EMIM]Ac in PEEK composites caused the nucleation effects and restricted the polymer chain movement with the cation-π or π-π strong interactions [236] between IL and MWCNTs, confirming the improved thermal stability of composites made with well-separated IL-modified MWCNTs. However, the decomposition temperature for samples S7 and S8 were 577 °C and 574.91 °C, which were less than S6 because of the plasticized nature of the IL [242] at higher concentrations.

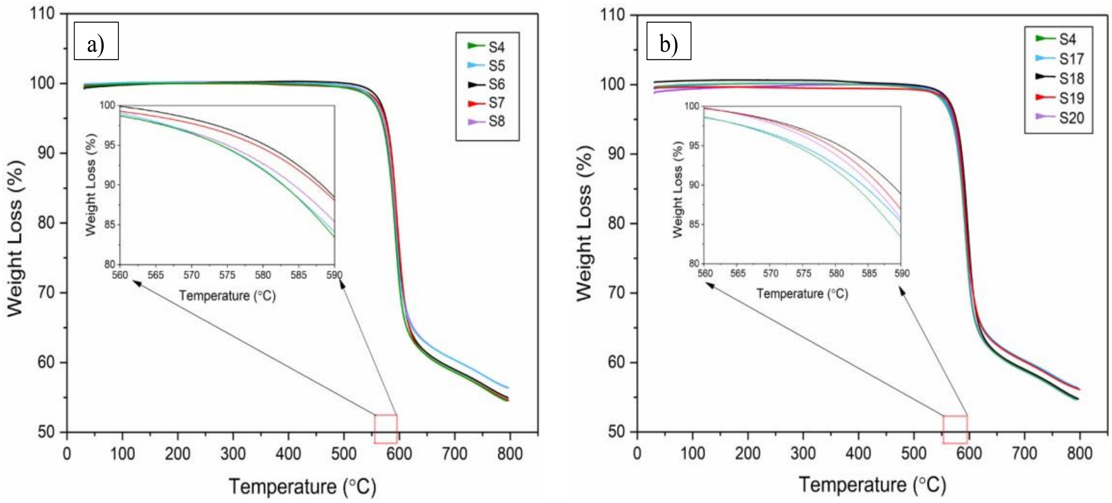

Figure 4.17: TGA curves of PEEK composites without and with different amounts of a) [EMIM]Ac and b) [BMIM]HSO_4 at 10 °C/min

The calculation of the phase transition temperature (melting point; T_m) and crystallinity (X_c) of thermoplastic polymer composites containing homogeneous MWCNTs dispersion is often recognized as a primary issue. The DSC curves of PEEK composites containing varying quantities of [BMIM]HSO_4 are shown in Figure 4.18 (b, d), and Table 4.3 provides the associated T_m and T_c values for the samples. As illustrated in Figure 4.18 (b), sample S4 had a T_c of 285 °C, which was significantly enhanced to 288 °C and 295 °C for samples S17 and S18, respectively. This improvement indicated that the PEEK polymer crystallized more rapidly in samples S17 and S18 than in samples S4 [314]. On the other hand, sample S18 had a T_m of 353 °C, which was greater than the T_m of the other samples, demonstrating that the optimal ratio of ILs to MWCNTs was (1:1), as described in Figure 4.18 (d). The increased thermal stability of the fabricated nanocomposites was a result of the improved T_m values. The findings revealed that efficiently dispersed MWCNTs acted as powerful nucleating agents [238, 314] and restricted the PEEK polymer chain to degrade [236], facilitating PEEK crystallization promptly.

A recent study demonstrated a similar effect in which polyvinylidene fluoride/multiwalled carbon nanotubes/ionic liquid (PVDF/MWCNTs/IL) composites were prepared with improved thermal characteristics [237]. In comparison to aggregated MWCNTs, the authors found that evenly distributed MWCNTs assisted by ILs provided effective PVDF nucleation sites. Additionally, the T_m and T_c values of composite materials S19 and S20 were diminished but not to the extent of composite S18, demonstrating that [BMIM]HSO_4 was plasticized [58, 242].

The crystallization (T_c) and melting temperature (T_m) of PEEK crystals as a measure of the [EMIM]Ac to MWCNTs ratio were determined by DSC profiles are depicted in Figure 4.18 (a, c). In Figure 4.5 (b), we demonstrated that the pure MWCNTs (S4) promoted the crystallization of PEEK. By including ILs-modified MWCNTs into PEEK composites, samples S5, S6, S7, and S8 quickly raised the crystallization temperature to 287 ℃, 293 ℃, 291 ℃, and 289 ℃, respectively, as shown in Figure 4.18 (a) and the deduced parameters are presented in Table 4.3. This indicated that modified MWCNTs containing varying concentrations of IL exhibit more effective nucleation effects than virgin MWCNTs. The particular interaction among the PEEK polymer and the imidazolium cation bound on MWCNTs surface was responsible for the synergetic nucleation actions of IL and MWCNTs [43]. Moreover, due to the plasticization interactions [315] of IL with PEEK, the overloading of IL culminated in the saturation of the surface of MWCNTs modification, and the free IL reduced the T_c of samples S7 and S8. As a result, raising the IL to MWCNTs proportion above 1:1, reduced the T_c of PEEK composites.

The ratio of IL to MWCNTs had a significant impact on the melting temperatures of the PEEK composites that were produced, as illustrated in Figure 4.18 (c). The melting temperature of S5 was raised by a lower quantity of IL-MWCNTs to 348 ℃. When the IL to MWCNTs ratio was raised from 1:1 to 2:1, PEEK crystallization intensified and the T_m rose to 351 ℃, 350 ℃, and 349 ℃ for S6, S7, and S8, respectively [43]. This is due to the strong interaction and nucleation centres between MWCNTs treated with IL and the PEEK polymer. However, it was important to note that the T_m values for S7 and S8 were lower than those for S6 because of the plasticization caused by greater IL concentrations [316, 317].

It was revealed that the highest T_c and T_m values were achieved at a 1:1 ratio of IL and MWCNTs, which resulted in enhanced PEEK crystallization. This may be linked to the crystalline phase and homogenous dispersion [43] of MWCNTs in the PEEK matrix.

The comparative study of PEEK composites manufactured using various amounts of [EMIM]Ac and [BMIM]HSO_4 demonstrated the superior thermal stability for [BMIM]HSO_4 based PEEK composites. This could be attributed to the longer alkyl chain length of the ILs, which resulted in stronger interactions between the filler and polymer matrix, which were necessary for enhancing polymer crystallization effects and delayed the thermal breakdown [318]. In contrast, the thermal properties were lowered at higher compositions (1.5 and 2 wt %) of employed ILs owing to their plasticizing nature [58].

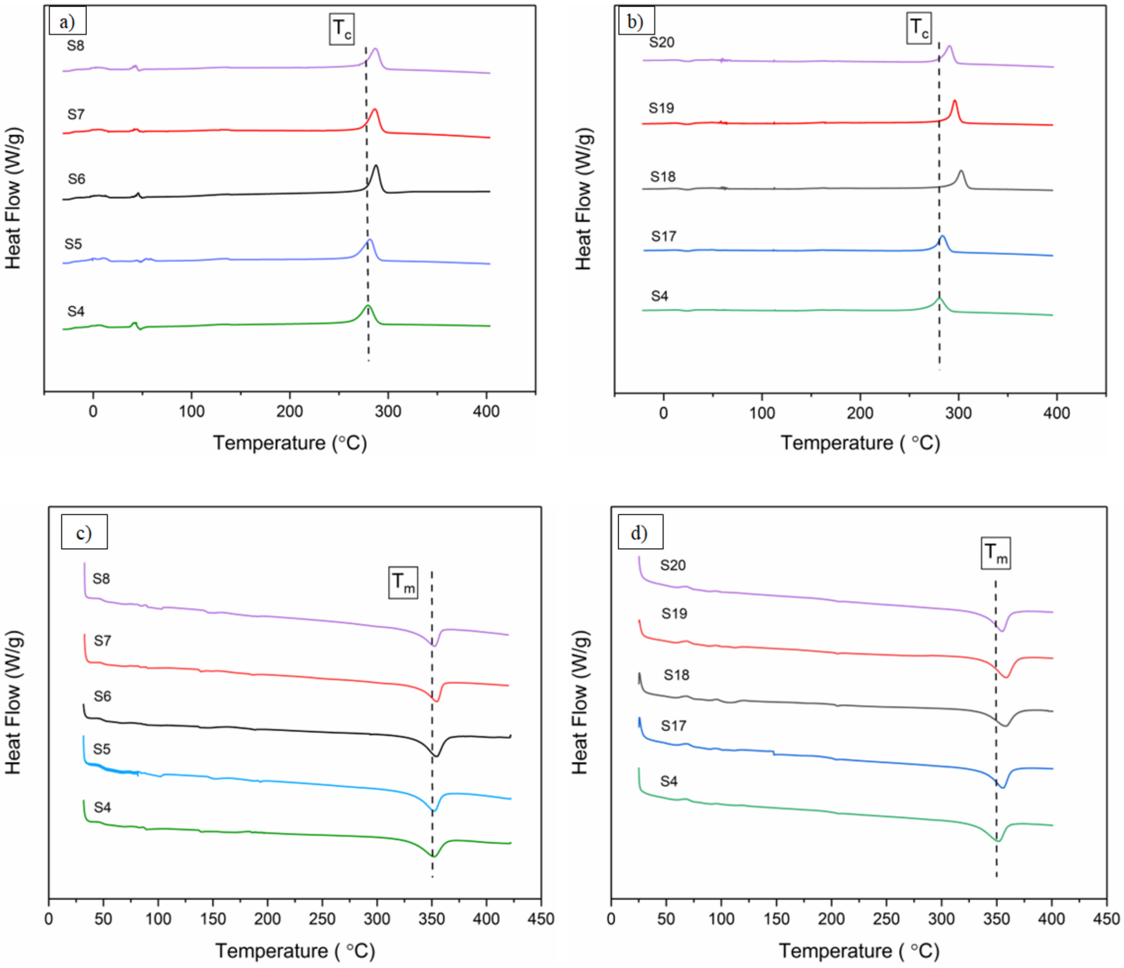

Figure 4.18: Cooling and heating curves of PEEK-based composites at 10 °C/min a) Cooling curves of [EMIM]Ac based composites b) Cooling curves of [BMIM]HSO_4 based composites c) Heating curves of [EMIM]Ac based composites d) Heating curves of [BMIM]HSO_4 based PEEK

Table 4.3: Thermal properties of [BMIM]HSO_4 and [EMIM]Ac based PEEK composites

Sample Name	Decomposition temperature T_d (°C)	Crystallization temperature T_c (°C)	Melting temperature T_m (°C)	Melting enthalpy ΔH_m (J/g)	Crystallinity X_c (%)
S4	570.00 ± 2.2	285 ± 1.2	347 ± 0.8	47.41±1.5	36.84±1.1
S5	572.00 ± 0.1	287 ± 2.1	348 ± 1.5	49.29±0.7	38.30±2.1
S6	580.12 ± 2.3	293 ± 1.6	351 ± 2.7	50.63±1.4	39.34±1.3
S7	577.00 ± 1.3	291 ± 1.4	350 ± 1.3	50.96±1.1	39.60±0.4
S8	574.91 ± 1.8	288 ± 0.9	349 ± 1.1	51.52±0.8	40.03±0.9
S17	573.00 ± 0.6	288 ± 1.4	349 ± 3.2	49.81±2.1	38.70±1.7
S18	581.09 ± 0.6	295 ± 3.2	353 ± 2.7	51.62±1.3	40.11±0.9
S19	578.00 ± 0.9	291 ± 2.3	352 ± 0.8	51.87±0.6	40.30±1.2
S20	576.12 ± 1.4	290 ± 1.5	351 ± 0.7	52.31±0.4	40.64±0.8

4.3.4 Effect of [EMIM]HSO_4 and [BMIM]Ac on thermal properties of PEEK composites

The findings of thermogravimetric analysis (TGA) using untreated and IL, [EMIM]HSO_4 modified MWCNTs at a continuous heating rate of 10 °C/min are presented in Figure 4.19. The outcome (Table 4.4) demonstrated unequivocally that the thermal stability of PEEK composites was greatly improved via the use of different compositions of ILs. It was worth noting that the S10 had a greater decomposition temperature (10.45 °C) than the untreated sample (S4). This improvement in thermal characteristics may be attributed to the proper distribution of MWCNTs in PEEK, which restricted the polymer ring mobility and retarded the breakdown of polymer composites. Additionally, the degradation temperatures of samples S11 and S12 (577.12°C and 575°C, respectively) were lower than those of S10 owing to the plasticizing effects of ILs (more than 1 wt %). Similar observations [319, 320] have been noted in the literature for greater loadings of IL.

Also, the thermal stability of PEEK composites formed with varying concentrations of [BMIM]Ac can be seen in Figure 4.19 (b). From Figure 4.19 (b) and

Table 4.4, it was elucidated that the inclusion of ILs-modified MWCNTs increased the disintegration temperature of the PEEK composites. Due to the substantial cluster of MWCNTs in PEEK, the decomposition temperature of S4 was found lower. On the other hand, the addition of [BMIM]Ac improved the compatibility of MWCNTs and PEEK which delayed the PEEK polymer to degrade. Also, the decomposition temperatures of samples S4, S13, S14, S15, and S16 were recorded as 570 °C, 572.30 °C, 580.89 °C, 577.49 °C, and 575.95 °C, respectively.

The results acquired for PEEK composites having different amounts of ILs are agreed with the previous literature. Sa et al. 2018 [236] investigated the thermal characteristics of PMMA/CNT composites employing IL, 1-butyl-3-methylimidazolium bis(trifluoromethyl sulfonyl)imide ([BMIM][TFSI]). The thermal properties of polymer nanocomposites were increased as a result of the strong interactions between the IL-MWCNTs and the polymer matrix. These interactions enhanced the dispersion of MWCNTs inside PMMA and immobilized the polymer ring.

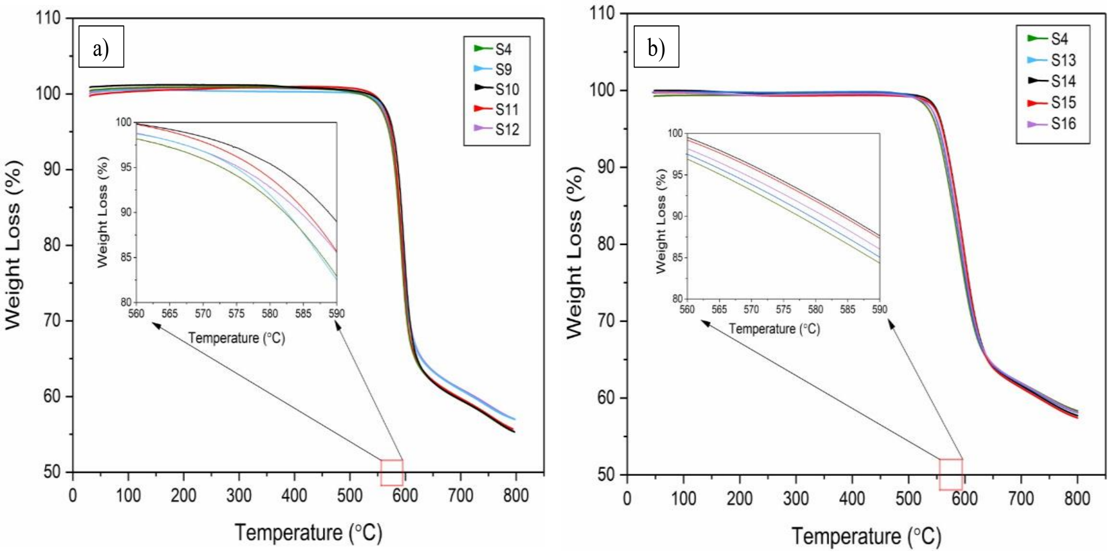

Figure 4.19: TGA curves of PEEK composites without and with different amounts of a) [EMIM]HSO_4 and b) [BMIM]Ac at 10 °C/min

Figure 4.20 (a, c) depicts the DSC cooling and heating curves of PEEK composites without and with $EMIMHSO_4$ for melt-blended samples, and the findings are listed in Table 4.4. As displayed in Figure 4.20 (a), sample S4 had a T_c of 285 °C, whereas samples S5 and S6 had a T_c of 287.4 °C and 294 °C. The increase in T_c is clearly due to the polymer improved compatibility and crystallization effects when combined with the IL modified filler. As shown in Figure 4.20 (c), the T_m value for PEEK composites without IL was 347 °C, which was raised to 348.5 °C and 352 °C for samples S9 and S10. The explanation for this result might be that homogenously dispersed IL modified MWCNTs acted as heterogeneous nucleation sites in the PEEK matrix, which encouraged the polymer crystallization [238, 314].

Furthermore, the impact of IL-modified MWCNTs on T_m and T_c of PEEK composites can also be observed from Figure 4.20 (a, c) when the amount of ILs was higher (more than 1 wt%). Both the T_m and T_c of samples comprising over 1 wt% [EMIM]HSO_4 (S11 and S12) were found to be lower than those containing 1% [EMIM]HSO_4 (S10). This shift might be attributed to the free space occupancy and the considerable plasticizing impacts [321, 322] of the IL in PEEK composites.

The cooling and heating patterns for [BMIM]Ac based PEEK composites are presented in Figure 4.20 (b, d), and their T_c and T_m are included in Table 4.4. The T_c and T_m of S4 were 285 °C and 347 °C, respectively, and were moved to 288 °C, 294.5 °C, and 348.8 °C, 352 °C for samples S13 and S14. As previously stated, this increase in thermal characteristics was due to the uniform dispersion of MWCNTs in PEEK and the polymer crystallization activities [234, 248]. Whereas the T_c and T_m readings for S15 and S16 were estimated to be 291 °C, 289.5 °C and 351 °C, 350 °C, respectively. The decrease in temperature values relative to S14 was ascribed to the plasticizing effects [317, 323] of [BMIM]Ac at larger loadings (more than 1 wt%) in polymer composites.

The T_c and T_m values obtained for PEEK composites containing varying quantities of ILs are consistent with prior literature. Zhao et al. (2012) [242] synthesized PMMA/MWCNTs composites using a facile melt blending technique with the addition of IL, 1-butyl-3-methyl-imidazolium hexafluorophosphate([BMIM][PF_6]). The IL was found to perform different features during the fabrication of the PMMA composites: it functioned as an efficient compatibilizer, significantly enhanced the distribution of MWCNTs in the PMMA matrix; and it also behaved as a plasticizer for the prepared composites, lowered the thermal characteristics in the PMMA matrix. The authors concluded that the approach was solvent-free and applicable to industrial applications, which offered new possibilities for the production of polymer/carbon nanotube composites on a large scale.

When the thermal properties of different concentrations of [EMIM]HSO_4 and [BMIM]Ac based PEEK composites were contrasted, it was analyzed that the PEEK composites fabricated with 1 wt % of [BMIM]Ac exhibited higher performance. It might be referred to higher alkyl chain length of the [BMIM]Ac, which led to stronger connections of filler-matrix. These interactions could be responsible for enhancing thermal stability of the prepared composites [236]. At higher concentrations (1.5 and 2 wt %) of used ILs, the thermal characteristics of the composites were reduced because of the plasticization effects [323].

Also, the comparative evaluation of the thermal performance of PEEK composites produced with ILs, [EMIM]Ac, [EMIM]HSO_4, [BMIM]HSO_4 and [BMIM]Ac revealed superior performance for [BMIM]HSO_4 in terms of crystallization and melting temperature. This justification became stronger in light of previously published research in which many authors [318, 324, 325] showed that ILs with a longer alkyl chain length could form stronger connections with the filler and polymer matrix, which were critical for enhancing polymer crystallization effects. Furthermore, owing to its high affinity and strong interactions with the filler and polymer matrix, the thermal stability of [BMIM]HSO_4-based PEEK composites were upgraded than other PEEK composites fabricated with other ILs [326].

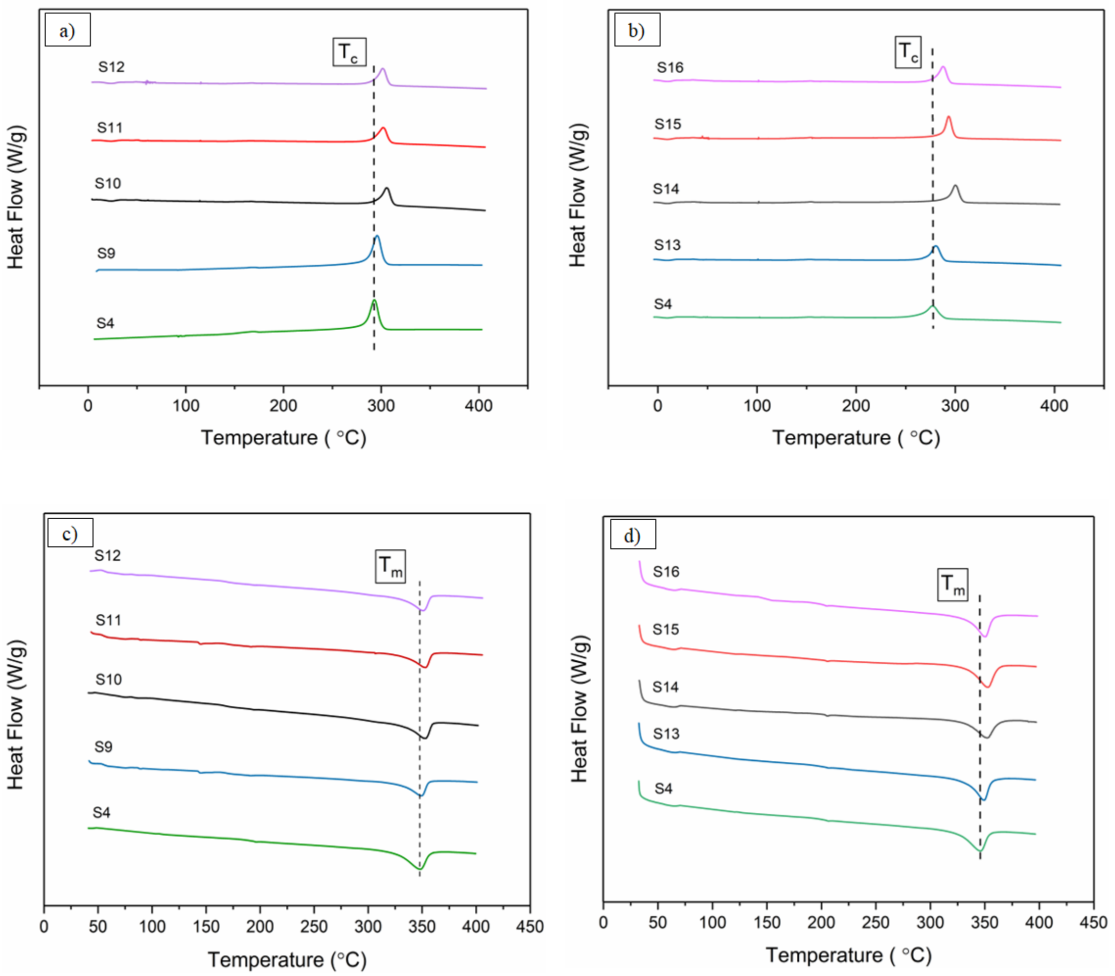

Figure 4.20: Cooling and heating curves of PEEK-based composites at 10 ℃/min a) Cooling curves of [EMIM]HSO_4 based composites b) Cooling curves of [BMIM]Ac based composites c) Heating curves of [EMIM]HSO_4 based composites d) Heating curves of [BMIM]Ac based PEEK composites

Table 4.4: Thermal properties of [EMIM]HSO_4 and [BMIM]Ac based PEEK composites

Sample Name	Decomposition temperature T_d (°C)	Crystallization temperature T_c (°C)	Melting temperature T_m (°C)	Melting enthalpy ΔH_m (J/g)	Crystallinity X_c (%)
S4	570.00 ± 2.2	285.00 ± 1.2	347.0 ± 0.8	47.41±1.5	36.47±1.1
S9	572.00 ± 1.2	287.71 ± 0.5	348.6 ± 1.1	49.51±0.9	38.47±1.2
S10	580.45 ± 1.5	294.00 ± 2.1	352.0 ± 2.2	50.87±0.4	39.53±0.4
S11	577.12 ± 1.2	291.00 ± 1.8	351.0 ± 1.1	51.09±0.2	39.70±0.2
S12	575.00 ± 0.8	289.40 ± 0.8	349.9 ± 1.7	51.74±1.3	40.20±0.5
S13	572.30 ± 3.1	288.00 ± 1.2	348.8 ± 1.4	49.75±1.2	38.66±1.1
S14	580.89 ± 2.3	294.50 ± 2.3	352.0 ± 1.7	50.97±0.2	39.60±0.4
S15	577.49 ± 1.1	291.00 ± 1.3	351.0 ± 2.8	51.42±1.3	39.95±0.9
S16	575.95 ± 1.9	289.53 ± 1.1	350.0 ± 1.2	51.89±0.2	40.32±0.6

4.3.5 Effect of [EMIM]Ac and [BMIM]HSO_4 on mechanical properties of PEEK composites

Polymeric composites could be used in a broad variety of engineering applications, if they exhibit good mechanical properties. For most applications, mechanical characteristics of polymer composites, especially tensile strength and elastic modulus, are the most essential of all the physicochemical properties of polymer composites. The load-displacement curves of nanoindentation investigations on PEEK nanocomposites at different [BMIM]HSO_4 compositions are shown in Figure 4.21 (b), using a maximum indentation depth of 70 μm, an indentation force of 100 mN, and a holding duration of 10 s. For non-IL composite (S4), the indentation displacement was 70 μm, which was reduced to 62 μm, 60.5 μm, 61 μm, and 61.55 μm for samples with IL (S17, S18, S19, and S20), respectively. This drop in indentation displacement suggested that the stiffness of composites was improved. Several studies have been conducted in the literature to substantiate these findings [327]. This change may be due to the uniform dispersion of MWCNTs inside PEEK and the enhanced π-interactions between the π-electrons of MWCNTs and the cation of the IL, as confirmed by FESEM and DSC. Additionally, the indentation displacement was increased at higher amounts of IL (1.5 wt % and 2 wt %) compared to 1 wt % of IL. This behavior was found, showing the existence of IL at higher concentrations in nanocomposites, which resulted in plasticization [236].

In Figure 4.21 (a), the nanoindentation curves are presented for various concentrations of [EMIM]Ac in PEEK composites. The maximal indentation load (100mN) and holding duration (10 sec) were applied, and the resultant indentation displacement (70 µm) was measured. From Figure 4.21 (a), it can be observed that the loading-unloading lines of samples were moved to the left, and the maximum depth was decreased with the addition of [EMIM]Ac-modified MWCNTs, suggesting that the mechanical resilience of PEEK composite to indentation load was enhanced. The indentation displacement for samples S4, S5, S6, S7, and S8 was 70 µm, 62.35 µm, 60.80 µm, 61.05 µm and 61.60 µm, respectively. This increase in mechanical stiffness of PEEK composites corroborated the effectively dispersed and strong interactions between MWCNTs and PEEK through [EMIM]Ac [241, 300]. However, the curves for S7 and S8 also demonstrated the impact of IL on the plasticity of PEEK composites [328].

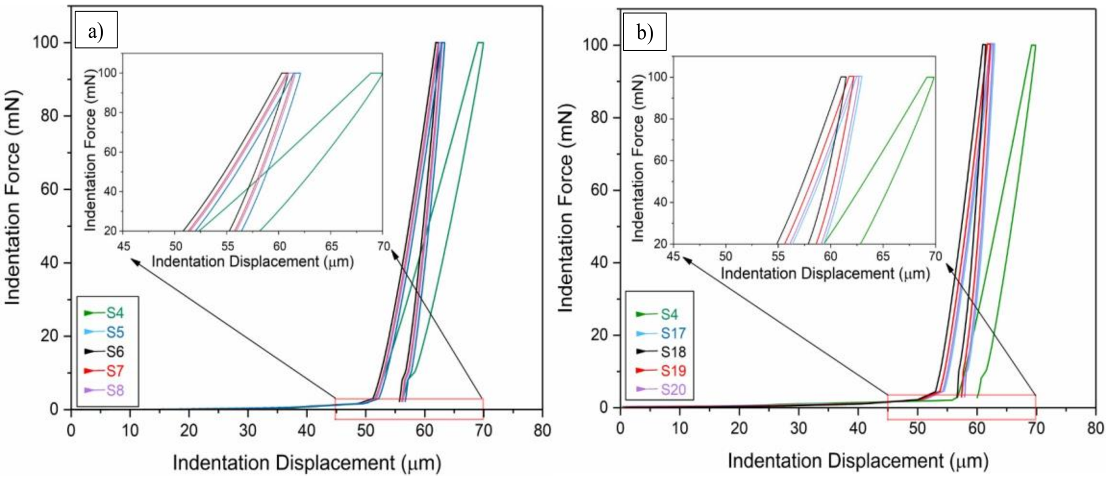

Figure 4.21: Load-displacement curves of PEEK-based composites with different loadings of a) [EMIM]Ac b) [BMIM]HSO_4

The elastic modulus is an essential attribute to examine when considering PEEK nanocomposites as a replacement for human bone fixation devices in biomedical engineering applications. The elastic modulus-contact depth patterns of PEEK nanocomposites are depicted in Figure 4.22 (b), and the corresponding parameters are reported in Table 4.5. As seen in Figure 4.7, the addition of MWCNTs to polymer matrices enhanced the elastic modulus relative to pure polymer [3]. Similarly, different IL compositions were added into PEEK nanocomposites, which significantly increased the mechanical properties of the composites. The elastic modulus of sample S18 was 37 % greater than that of sample S4, despite the fact that modulus values were lowered (not less than S17) at higher amounts of IL (1.5 wt % and 2 wt %). The crystallization and elastic modulus of PEEK composites were improved by deagglomerating and debundling MWCNT [249]. To support these findings, Boyer et al. (2012) [297] synthesized PEEK/CNTs composites with superior mechanical properties. This work proved that the homogeneous distribution of MWCNTs in PEEK enhanced nucleation sites, hence increasing the crystallinity and modulus values of the nanocomposites.

The elastic modulus of PEEK composites containing several quantities of [EMIM]Ac was determined using Figure 4.22 (a), and the findings are summarized in Table 4.5. The modulus of S4 was 5.5 GPa which was shifted to 7.01 GPa, 7.38 GPa, 7.22 GPa and 7.18 GPa for S5, S6, S7 and S8, respectively. It was noticed that the incorporation of IL with MWCNTs improved the modulus of the PEEK composites to a level comparable to that of human cortical bone (7-12 GPa) [1]. The improvements in mechanical characteristics confirmed that MWCNTs were distributed uniformly in PEEK [300]. In addition to that, PEEK composites fabricated with more than 1 wt % [EMIM]Ac (S7, S8) demonstrated the plasticization nature of the utilized IL. This phenomenon was commensurated with the previous findings [324] in the literature.

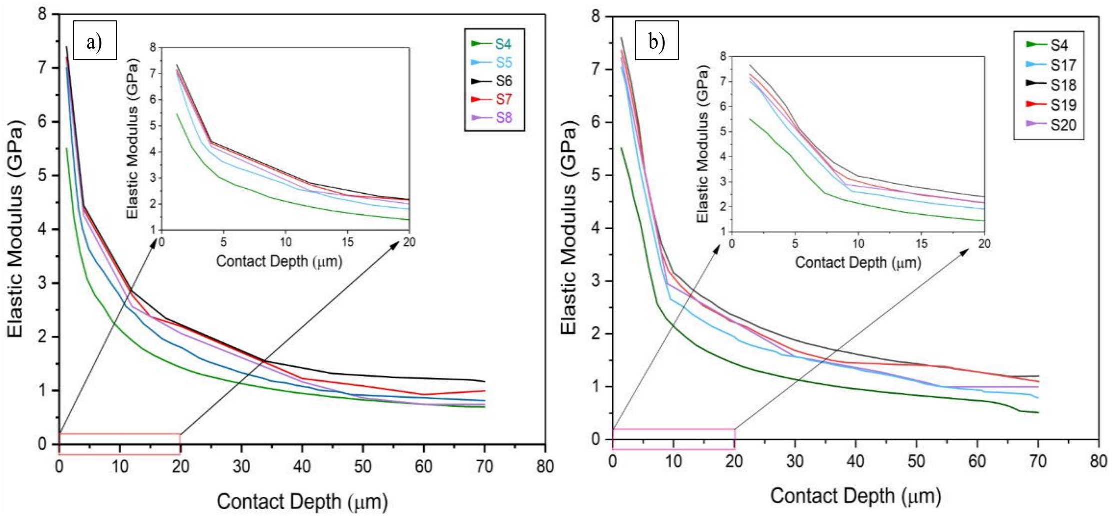

Figure 4.22: Elastic modulus profiles of PEEK-based composites with different loadings of a) [EMIM]Ac b) [BMIM]HSO$_4$

When inorganic fillers are incorporated into different polymer matrices, one of the primary concerns is the compromise in the mechanical performance (tensile strength). The stress-strain curves of PEEK composites with varying IL concentrations are shown in Figure 4.23. As observed in Figure 4.23 (b), the elastic modulus and tensile strength of specimen S4 were 5.5 GPa and 83 MPa, respectively, whereas these values were enhanced to 7.08 GPa and 84.5 MPa for S17. This shift occurred as a result of significant cation-π or π-π connections between the IL modified MWCNTs and the PEEK polymer [306, 329, 330]. The mechanical stability of S18 PEEK composites, including its elastic modulus and tensile strength, was determined to be the maximum. The elastic modulus and tensile strength of the composite S18 containing 1 wt % of IL were 7.65 GPa and 89 MPa, respectively, suggesting improvements of 37% and 7.2% over the non-IL PEEK nanocomposite (S4).

Also, a reduction in tensile characteristics (elastic modulus was 7.35 and 7.22 GPa for composites S19 and S20) was also seen with larger quantities of ILs (composites S19 and S20), although the reduction was not as significant as for composite S17, attributed to the plasticization effects of the ILs [233, 331]. As reported earlier, IL was used to develop styrene-butadiene rubber/multiwalled carbon nanotubes (SBR/MWCNTs) nanocomposites with enhanced MWCNTs dispersion and mechanical properties [49]. The tensile properties of the produced composites were found to be diminished because of the plasticization of ILs under higher loading.

The stress-strain curves of PEEK composites in which MWCNTs are modified without and with various amounts of [EMIM]Ac are presented in Figure 4.23 (a) and the obtained findings are mentioned in Table 4.5. The results revealed that the mechanical performance (elastic modulus and tensile strength) was improved (0.72 % and 27.45 %) for S5 when compared to PEEK composites comprising no IL. Also, these characteristics were modified (elastic modulus and tensile strength, 7.38 GPa, 7.22 GPa, 7.18 GPa and 87.9 MPa, 87 MPa, 86.9 MPa) for S6, S7 and S8 in contrast to S4 (7.01 GPa, 84.3 MPa), respectively. It was observed that maximum elastic modulus and tensile strength were measured for S6 due to strong cation-π or π-π interactions between equally dispersed MWCNTs and PEEK matrix [310, 332, 333], whereas the decline in the properties was also noticed for S7 and S8 owing to plasticizing behavior [306] of the IL employed.

Subramanian et al. (2011) [241] used an eco-friendly method to develop polychloroprene rubber/multi-walled carbon nanotubes (CR/MWCNTs) composites through the usage of ionic liquid, 1-butyl-3-methyl imidazolium bis(trifluoromethyl sulphonyl)imide via the hot press. The physical (cation-π/π-π) linkages between the cation of ionic liquid and π-electrons of MWCNTs were evidenced. In comparison to unmodified CR/MWCNTs composites, the author showed that the modulus of CR composites made using ILs-modified MWCNTs was enhanced by 50 %.

One potential explanation for the improved mechanical characteristics of the ILs-treated MWCNTs in PEEK composite was that MWCNTs entanglement and agglomeration were significantly decreased. The deagglomeration of MWCNTs had enhanced the cation-π or π-π interactions between the MWCNTs and PEEK matrix. This firm bond amongst the filler and the polymer matrix was thought to be the primary cause for the superior mechanical characteristics of the PEEK composites.

When the elastic modulus and tensile strength of PEEK composites manufactured with varied concentrations of [EMIM]Ac and [BMIM]HSO_4 were compared, it was discovered that the PEEK composites formed with 1 wt % of

[BMIM]HSO_4 performed better. This could be attributed to bigger alkyl chain length of [BMIM]HSO_4, which culminated in greater filler-matrix physical interactions. These connections might contributed to enhanced mechanical stability of the produced composites [300]. Also, due to the plasticization effects of the applied ILs at higher concentrations (1.5 and 2 wt %), the mechanical properties of the composites were diminished [328].

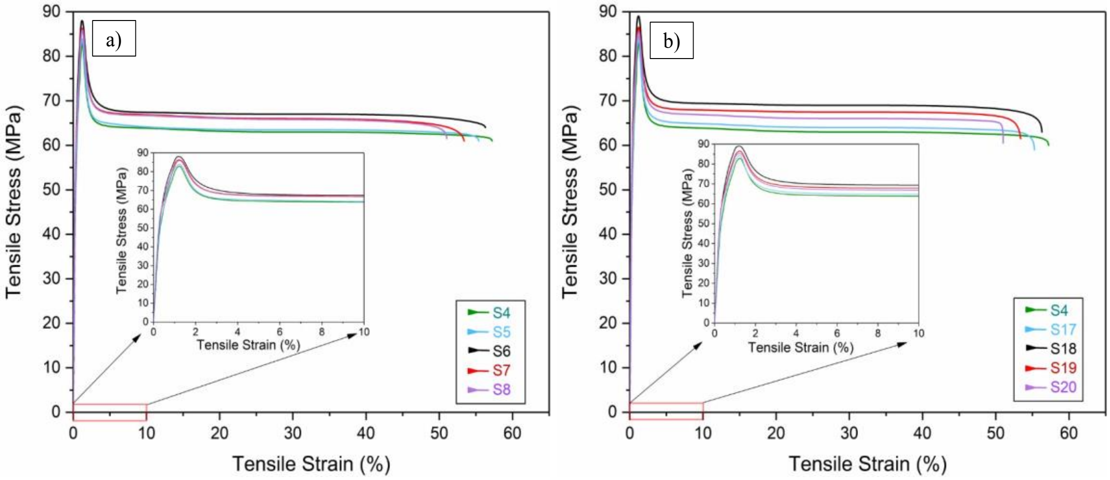

Figure 4.23: Stress-strain profiles of PEEK-based composites with different loadings of a) [EMIM]Ac b) [BMIM]HSO_4

Table 4.5: Mechanical properties of [BMIM]HSO_4 and [EMIM]Ac based PEEK composites

Sample Name	Tensile strength (MPa)	Elastic modulus (GPa)
S4	83.0 ± 2.2	5.50 ± 0.12
S5	84.3 ± 0.3	7.01 ± 0.02
S6	87.9 ± 1.2	7.38 ± 0.07
S7	87.0 ± 0.7	7.22 ± 0.12
S8	86.9 ± 0.8	7.18 ± 0.03
S17	84.5 ± 0.4	7.06 ± 0.14
S18	89.0 ± 0.2	7.65 ± 0.12
S19	88.2 ± 0.9	7.35 ± 0.12
S20	88.0 ± 1.3	7.22 ± 0.10

4.3.6 Effect of [EMIM]HSO_4 and [BMIM]Ac on mechanical properties of PEEK composites

It was clear from Figure 4.24 (a) that the load-displacement profiles of PEEK composites were influenced by the incorporation of $EMIMHSO_4$-modified MWCNTs. In particular, the curve for S9 was shifted left with the indentation displacement to 62.35 µm from 70 µm for untreated composite (S4). Likewise, the load-displacement curves moved to 60.60 µm, 61.20 µm and 61.70 µm for S10, S11, and S12, respectively. In fact, the stiffness of the composites was intensified by the compatibility and strong linkages provided by $EMIMHSO_4$ in PEEK/MWCNTs composites [297]. Besides, the improvements in the mechanical characteristics were affected by the plasticization and free movement of the polymer ring [236] for S11 and S12 when compared to those of S10.

In Figure 4.24 (b), the load-displacement curves of PEEK composites incorporated with different amounts of $BMIMHSO_4$ are briefly explained. The maximum indentation depth of 70 µm was observed for S4 when 100 mN load was applied with 10 s holding time. After the modification of MWCNTs with $BMIMHSO_4$ in PEEK composites, the resultant displacement was reduced to 12.54 %, 15 %, 14.6 % and 13.64 for S13, S14, S15 and S16 when compared to untreated PEEK composite (S4), respectively. It was because of the presence of IL-modified MWCNTs which increased the formation of PEEK crystal through nucleation sites among MWCNTs and PEEK [298]. As explained earlier, for PEEK composites prepared with other ILs, the stiffness of the composites S15 and S16 was also decreased owing to the plasticization behavior [334] of the used IL in PEEK composites. Qiu et al. (2013) [300] reported similar findings to improve the surface and mechanical properties of polyamide 66.

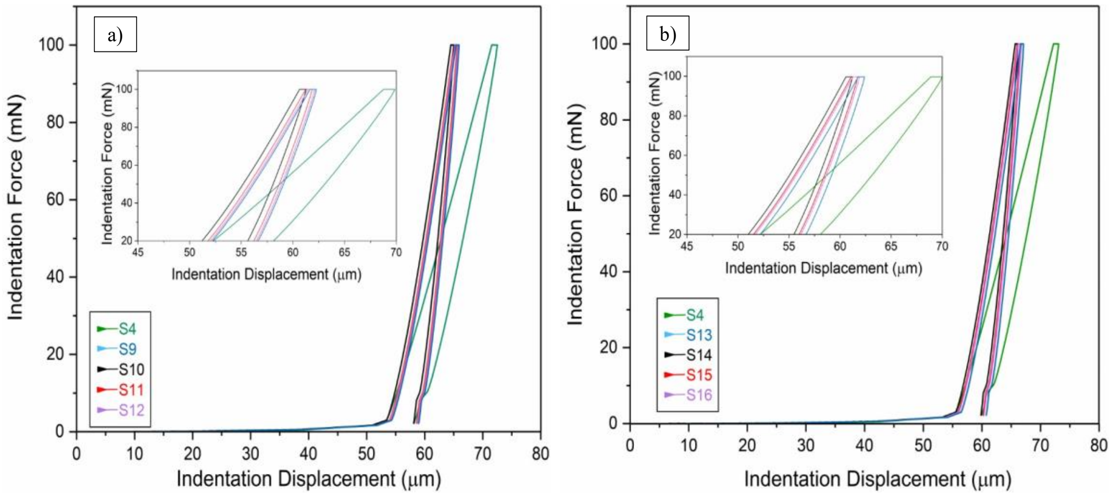

Figure 4.24: Load-displacement curves of PEEK-based composites with different loadings of a) [EMIM]HSO_4 b) [BMIM]Ac

The elastic modulus and contact depth curves of without and with [EMIM]HSO_4 treated PEEK composites were represented in Figure 4.25 (a), and their results are inferred in Table 4.6. The modulus of unmodified PEEK composites (S4) was 5.5 GPa and shifted to 7.31 GPa (32.9 % higher than S4) for S10 because of homogenous and precise dispersion of MWCNTs through [EMIM]HSO_4 in PEEK. The well-separated MWCNTs boosted the physical interactions [219, 245] between IL-modified MWCNTs and the PEEK polymer. Besides, these increments in elastic modulus were diminished for S11 and S12 owing to the higher concentrations of IL in PEEK composites and induced the plasticization behavior [243, 248].

PEEK composites containing various concentrations of [BMIM]Ac for indentation modulus is explained with contact depth of 70 μm (Figure 4.25 b). As illustrated in Figure 4.25 (b), it was interesting to note that the elastic modulus of PEEK composites varied in accordance with the IL loadings. The escalating trend with the values of 5.5 GPa, 7.02 GPa and 7.45 GPa was observed for S4, S13, and S14, respectively due to the strong π-π interactions between MWCNTs and PEEK provided by used IL [237]. This behavior was in agreement with the reported work by Sa et al. (2018) [236]. On the other hand, the depression in modulus readings was noticed for S15 and S16 when compared to those with S14 because of the higher amounts of ILs that produced plasticization effects [335] in the PEEK composites.

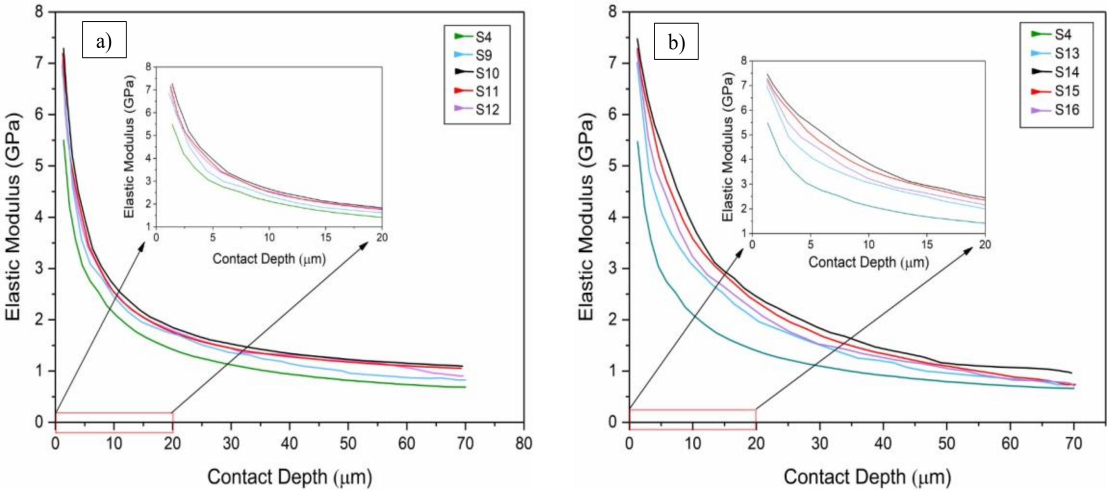

Figure 4.25: Elastic modulus profiles of PEEK-based composites with different loadings of a) [EMIM]HSO_4 b) [BMIM]Ac

The modulus and tensile strength values (listed in Table 4.6) were evaluated by tensile experiments for unmodified and modified PEEK composites with various quantities of [EMIM]HSO_4 (Figure 4.26 a). The modulus of S4 was 5.5 GPa, and rose to 6.95 GPa, 7.31 GPa, 7.20 GPa and 7.16 GPa, respectively, equivalent to an increase of 26 %, 32.9 %, 30.9 % and 30.18 % with respect to the unmodified PEEK composite. Also, the tensile strength of S9, S10, S11 and S12 was boosted by 0.72 %, 5%, 4.18 % and 4.06 % when compared to S4. This transition was witnessed due to robust cation-π or π-π interactions between the IL modified MWCNTs and PEEK polymer [290, 306, 329]. These linkages constrained the polymer ring free mobility and enhanced its mechanical resilience. At high concentrations (1.5 wt % and 2 wt % of [EMIM]HSO_4), the mechanical properties were diminished because of the free polymer ring movement induced by the plasticization effects [336, 337].

To provide an understandable representation of the mechanical characteristics, the stress-strain graphs of PEEK composites without and with [BMIM]Ac are described in Figure 4.26 (b), and the results are tabulated in Table 4.6. In comparison to S4, the tensile strength and elastic modulus of other composites were significantly elevated. The highest tensile strength and elastic modulus (88.8 MPa, 7.45 GPa) for S14 were observed. The increased mechanical stability was ascribed to the dispersion of the filler and strong interfacial interactions [49, 313] among modified filler and the matrix. The uniform distribution of the filler and the powerful interactions restricted the movement of the polymer chain. However, the mechanical attributes were faded for S15 and S16 in contrast to S14 owing to the softening behavior of employed IL in the PEEK composites. Similar observations were discussed in the hitherto published literature [338, 339].

Abraham et al. (2018) [49] produced well-dispersed, durable, and mechanically stable MWCNTs-styrene-butadiene rubber (SBR) composites using a melt mixing method with the use of an IL, 1-benzyl-3-methylimidazolium chloride as a dispersant. The authors thoroughly investigated the dispersion and mechanical characteristics of IL-assisted MWCNTs in SBR matrix. The tensile experiments demonstrated that the mechanical reinforcement was enhanced (tensile strength was 318 % higher than those of pure polymer) as a result of appropriate MWCNTs distribution in the SBR matrix which provoked the physical linkages (π-π interactions) among SBR and MWCNTs.

The comparative analysis of PEEK composites made with varying proportions of [EMIM]HSO_4 and [BMIM]Ac indicated that [BMIM]Ac-based PEEK composites had higher mechanical stability. This might be due to the ILs longer alkyl chains, which contributed in stronger interactions between the filler and the polymer matrix, which were important for boosted mechanical performance [237]. By contrast, the mechanical characteristics of the used ILs were degraded at larger amounts (1.5 and 2 wt %) due to their plasticizing tendency [338].

Overall, the mechanical characteristics of PEEK composites synthesized with ILs ([EMIM]Ac, [EMIM]HSO_4, [BMIM]Ac, and [BMIM]HSO_4) were evaluated and compared. It was noticed that [BMIM]Ac and [BMIM]HSO_4 based PEEK composites exhibited enhanced elastic modulus and tensile strength than other ILs. This explanation has become stronger in view of previous literature in which numerous authors [318, 324] demonstrated that ILs with a bigger alkyl chain might established significant interactions with both the filler and polymer matrix, that was critical for improving the MWCNTs distribution and mechanical stability. Further, the mechanical stability of 1 wt % of [BMIM]HSO_4-based PEEK composites was highest compared to other PEEK composites produced with other ILs, due to its high affinity and strong interactions with the filler and polymer matrix [326].

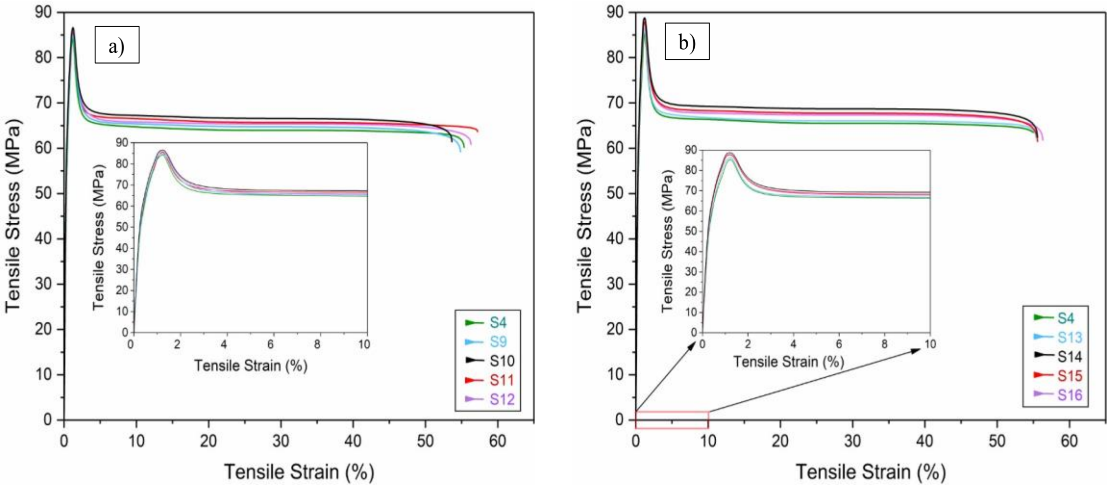

Figure 4.26: Stress-strain profiles of PEEK-based composites with different loadings of a) [EMIM]HSO_4 b) [BMIM]Ac

Table 4.6: Mechanical properties of [EMIM]HSO_4 and [BMIM]Ac based PEEK composites

Sample Name	Tensile strength (MPa)	Elastic modulus (GPa)
S4	83.0 ± 2.20	5.50 ± 0.12
S9	84.3 ± 0.22	6.95 ± 0.08
S10	87.9 ± 0.19	7.31 ± 0.10
S11	87.2 ± 0.17	7.20 ± 0.02
S12	87.1 ± 0.38	7.16 ± 0.08
S13	84.5 ± 0.20	7.02 ± 0.04
S14	88.8 ± 0.12	7.45 ± 0.11
S15	88.0 ± 0.49	7.28 ± 0.12
S16	87.8 ± 1.10	7.22 ± 0.09

4.3.7 Effect of [EMIM]Ac and [BMIM]HSO_4 on the biological properties of PEEK composites

The inclusion of HA into PEEK is deemed critical for its comprehension and assessment of biocompatibility in biological applications [340]. The viability of cells grown on pure PEEK (control), PEEK/MWCNTs/nHA (without ILs) and different amounts of [BMIM]HSO_4 and [EMIM]Ac based PEEK composites is demonstrated in

Figure 4.27 and tabulated in Table 4.7. The NIH3T3 cells were deposited onto the scaffolds and incubated with the cells for 24 h. As determined by absorbance tests, all composites containing varying concentrations of ILs were biocompatible with NIH3T3 cells. The biocompatibility and proliferation of cells in all samples were significantly greater than the permissible range (80 %) of control. It can be deduced that when HA was included in the composites, the absorbance values (cells viability and proliferation rate) were much larger than those for the control. The transformation of an oxidized (blue) redox indicator into a reduced (red) form due to the action of dehydrogenase enzyme inside metabolically active cells revealed the development of cells. The cell culture investigation established that the produced PEEK/MWCNTs composites with HA were nontoxic [341]. These findings were supported to earlier research demonstrating the increase in biocompatibility after the integration of HA in PEEK [63, 342]. The overall data suggested that PEEK as well as all the materials used in the fabrication of scaffolds for hard tissue regeneration were found to be biocompatible and nontoxic in vitro.

Rashidi et al. (2021) [178] investigated the impacts of carbon nanotubes and hydroxyapatite on the biological characteristics of PEEK. The melt blending at 400 °C was used to produce the PEEK composites for biological applications. The findings indicated that CNTs and HA improved the biological properties of PEEK composites. Additionally, it was shown that both fillers, CNTs and HA had a number of advantages in biological properties, including cell differentiation, protein absorption, and cell adhesion, and it was concluded that PEEK/HA/CNTs composites could offer the optimal circumstances for cell development.

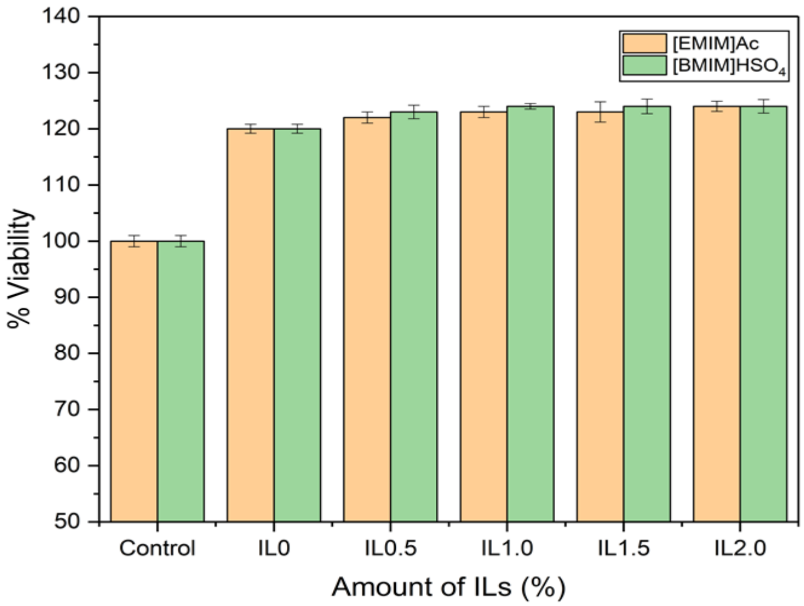

Figure 4.27: Cells viability of [EMIM]Ac and [BMIM]HSO$_4$ based PEEK composites

Table 4.7: Cells viability of PEEK composites made with [EMIM]Ac and [BMIM]HSO$_4$

Sample Name	Cells Viability (%)
Control	100
S4	120 ± 0.8
S5	122 ± 1.0
S6	123 ± 1.0
S7	123 ± 1.8
S8	124 ± 0.9
S17	123 ± 1.2
S18	124 ± 0.5
S19	124 ± 1.3
S20	124 ± 1.2

The EDX analysis was used to determine the calcium/phosphorous (Ca/P) ratio in the PEEK composites prior to their biological assessment. As seen in Figures 4.28 (b-d), the addition of HA to PEEK resulted in the presence of Ca and P peaks in the composites, as compared to pure PEEK (Figure 4.28 a). The composites are biologically compatible with the human bone if Ca/P ratio is 1.67. PEEK composites fabricated without IL and with ILs showed the value more than 1.67. Thus, it could be ascribed that the biocompatibility of prepared PEEK composites was considerably enhanced by the introduction of the bioactive material (HA). These findings are consistent with the previously reported literature [343].

Maheshwari et al. (2014) [126] fabricated and evaluated polycaprolactone/polyvinyl alcohol/hydroxyapatite nanoparticles (PCL/PVA/HAp) scaffolds for bone tissue regeneration application. The EDX analysis was conducted to determine the composition and ratio of Ca/P in the composites and concluded that the ratio value was 1.62, close to natural bone. This value showed that PCL/PVA/Hap nanocomposites were biocompatible and could be used as substitution for human bone.

The comparative investigation of PEEK composites comprising variable concentrations of [EMIM]Ac and [BMIM]HSO_4 revealed that PEEK composites incorporating [BMIM]HSO_4 had greater bioactivity. By using [BMIM]HSO_4, the dispersion and π-π interactions between HA and PEEK were enhanced, which were important for boosting biocompatibility [63, 342]. Additionally, the proliferation and absorbance of the cells were linearly related to the quantities of ILs applied. This suggested that the biological characteristics of PEEK composites were enhanced by increasing the quantity of ILs.

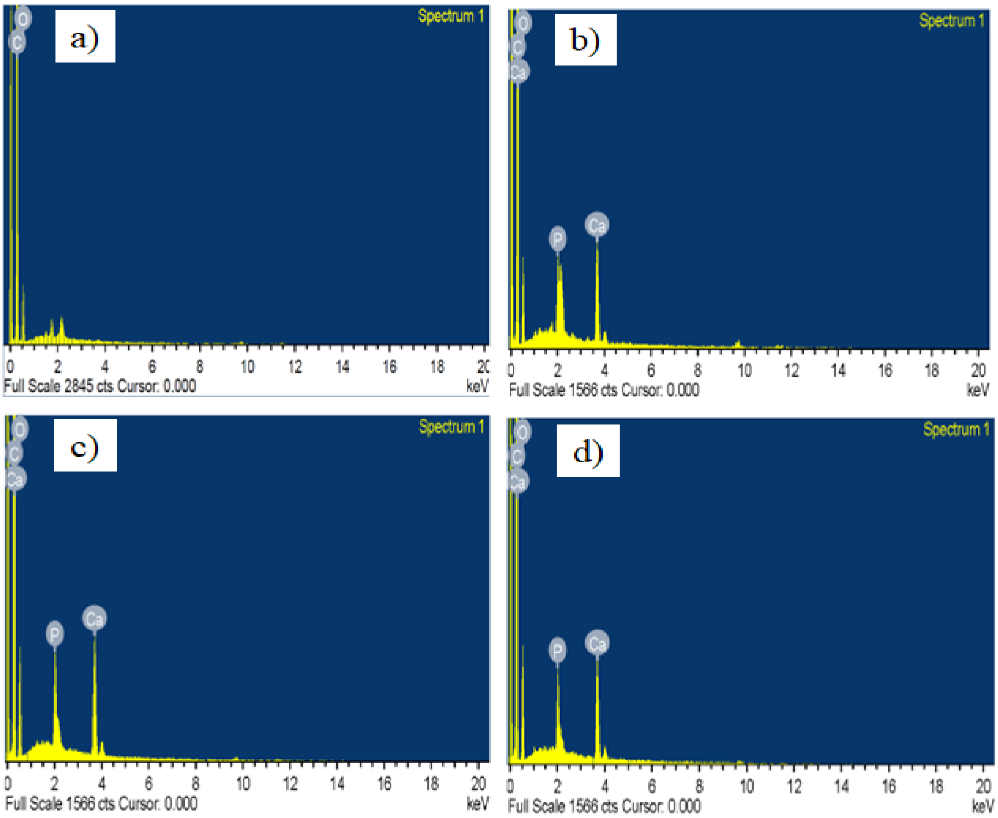

Figure 4.28: EDX analysis of a) pure PEEK b) without IL c) 1 wt % of [BMIM]HSO_4 d) 1 wt % of [EMIM]Ac

4.3.8 Effect of [EMIM]HSO_4 and [BMIM]Ac on the biological properties of PEEK composites

The Alamar blue assay (cells proliferation) was conducted to determine the viability of control and HA-induced PEEK/MWCNTs composites produced with [EMIM]HSO_4 and [BMIM]Ac, and the findings are shown in Figure 4.29 and Table 4.8. It was worth mentioning that the biological behavior of the PEEK composites was enhanced when contrasted to pure PEEK in terms of absorbance (µm). It revealed that PEEK composites were cytocompatible in terms of viability and proliferation, which could be credited to the incorporation of HA into PEEK [344]. Furthermore, the attachment of cells was augmented with the presence of various concentrations of both ILs [345, 346]. This might be ascribed to the homogeneous and evenly distributed MWCNTs and HA, which increased the potential of cells adhering to the PEEK surface.

The results obtained for composites of PEEK/MWCNTs/nHA/ILs with various quantities of ILs were similar with those found in the literature. For example, Sabir et al. (2020) [347] synthesized and characterized the cellulose/hydroxyapatite composites for dental restorations. Alamar blue compatibility experiments were used to determine the biological characteristics of the manufactured composites. The findings indicated that microwave irradiation method could be employed to effectively generate HA on cellulose fibres, thus enhancing the biological attributes (over 90% cell proliferation) of dental resin composite materials.

In another study, to determine the biocompatibility of PEEK tertiary composites, PEEK/nHA/CF (polyetheretherketone/nanohydroxyapatite/carbon fibre) were produced by melt blended technique. The cell culture investigation was carried out to analyze the cytocompatibility and cellular growth of these composites. The synthesized ternary composites were thought to be cell-compatible, with no cytotoxicity effects. Thus, the improved biological performance of the PEEK/nHA/CF ternary composite gave tremendous prospects as a bioactive implant substrate in dentistry and orthopedic applications [52].

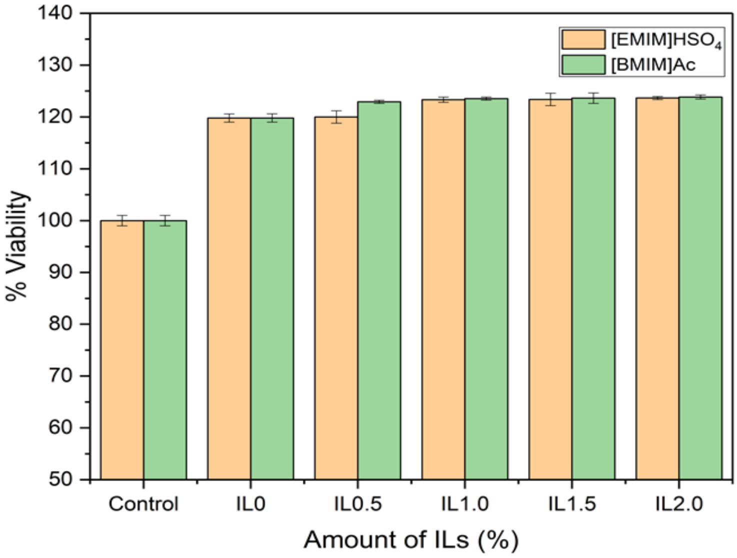

Figure 4.29: Cells viability of [EMIM]HSO$_4$ and [BMIM]Ac based PEEK composites

Table 4.8: Cells viability of PEEK composites with [EMIM]HSO_4 and [BMIM]Ac

Sample Name	Cells Viability (%)
Control	100
S4	120 ± 0.8
S9	120 ± 1.2
S10	123 ± 0.5
S11	123 ± 1.2
S12	124 ± 0.3
S13	123 ± 0.3
S14	124 ± 0.3
S15	124 ± 1.0
S16	124 ± 0.4

The biological evaluation and comparison of pure PEEK and PEEK composites prepared with HA by EDX analysis are presented in Figure 4.30. This study was carried out to determine the presence of Ca and P elements in the prepared composites. It was not only confirmed that Ca and P were presented in the prepared PEEK composites (Figures 4.30 b-d) but also the Ca/P ratio was more than the required value of human bone (1.67). It can be concluded that the introduction of HA had enhanced the biological properties of the PEEK composites.

The purpose of this study was to synthesize and characterize polylactic acid/nano-hydroxyapatite (PLLA/nHAP) composite scaffolds for bone regeneration [348]. The manufactured composites were examined for their morphological, biological, and mechanical characteristics. The composition and structural features of the manufactured nHAP were found to be identical to those of natural bone apatite. According to EDX analysis, the Ca/P molar ratios were about 1.6, which was near to the stoichiometric composition of nHAP (Ca/P = 1.67).

The degradability results of PEEK composites were evaluated after putting the samples in phosphate buffer solution (PBS) and lysozyme solution at 37 ℃ for 6 months. It was determined that there were no contaminants in the solution, confirming that the manufactured composites were not biodegraded. Similar results were obtained by Hahn et al. (2013) [349] for PEEK/HA composites.

The comparison of PEEK composites containing various concentrations of [BMIM]Ac and [EMIM]HSO_4 demonstrated that composites having [BMIM]Ac exhibited better bioactivity. The addition of [BMIM]Ac increased the dispersion and π-π interactions between HA and PEEK, which were significant for promoting biocompatibility [344]. Furthermore, cell growth and absorbance were directly proportional to the amount of ILs given. This showed that raising the concentration of ILs in PEEK composites improved their biological properties.

The biological assessment of PEEK/MWCNTs/nHA/ILs composites made with different ILs, [EMIM]Ac, [EMIM]HSO_4, [BMIM]Ac, [BMIM]HSO_4 recommended a green and ecologically friendly strategy by demonstrating no cytotoxic effects and improved cell proliferation. In this study, the biological characteristics of the composites increased linearly with the quantity of ILs present. Overall, the biocompatibility of PEEK composites with various ILs was almost same, however the addition of HA improved the bioactivity of PEEK composites significantly when compared with pure PEEK. Hence, the produced formulation can be exploited in the biomedical sector as a substitute for implant material.

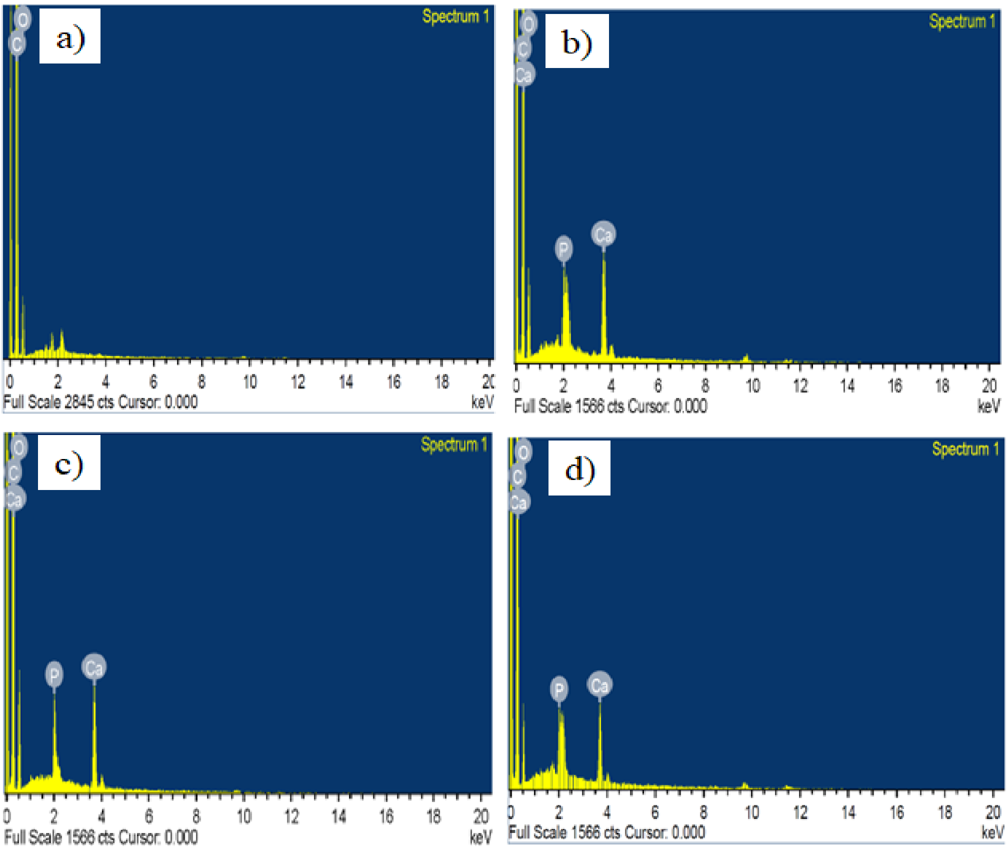

Figure 4.30:EDX analysis of a) pure PEEK b) without IL c) 1 wt % of $[EMIM]HSO_4$ d) 1 wt % of [BMIM]Ac

4.3.9 Effect of [EMIM]Ac and $[BMIM]HSO_4$ on thermal degradation kinetic of PEEK composites

It is essential to understand and anticipate the thermal degradation kinetics in order to develop efficient molding and thermoplastic processing methods for the manufacturing of PEEK composites using various ILs. The thermal decomposition kinetics of polymers are studied using a variety of integral and non-isothermal approaches. The Coats-Redfern method using a single heating rate is the most often used integral method for determining apparent activation energy (E_a) [274]. The temperature zone of 560 °C-600 °C was chosen as the temperature range with the quickest degradation rate since all samples degraded within this range [62]. Figure 4.31 (b) illustrates the Coats-Redfern plots with various concentrations of $[BMIM]HSO_4$ based PEEK nanocomposites, and Table 4.9 provides their calculated activation energy and regression coefficient. The parallel lines with R^2 (not less than 0.9987) for $[BMIM]HSO_4$ based PEEK nanocomposites were achieved. These findings suggested that the Coats-Redfern model can be used to evaluate the thermal degradation of PEEK composites. The E_a of sample S18 was 222.17 KJ/mol, which was greater than the activation energy of all other produced samples and revealed that these results are consistent with TGA and DSC data.

The Coats-Redfern data (Figure 4.31 a) for PEEK composites in which MWCNTs were modified through various concentrations of [EMIM]Ac are evaluated. The activation energies determined from the slope of these parallel lines in the temperature region 560 °C-600 °C where the quickest pyrolysis rate happened, are provided in Table 4.9. The activation energy calculation clearly demonstrated that treating MWCNTs with varying concentrations of [EMIM]Ac had a significant effect on their thermal breakdown rates. Interestingly, substantial enhancements in the activation energy of PEEK composites (made through IL) were found when contrasted to untreated composites. It was clear from Table 4.9 that the activation energy of S4 was 207.85 KJ/mol, which was enhanced to 209.62 KJ/mol, 222 KJ/mol, 218.15 KJ/mol and 218.01 KJ/mol.

The PEEK composites incorporated with [EMIM]Ac demonstrated a close resemblance to [BMIM]HSO_4 based composites. The thermal properties of polymer nanocomposites were discovered to have a linear relationship with the apparent activation energy [261, 350]. This demonstrated that the addition of IL-assisted MWCNTs into PEEK improved the MWCNTs dispersion and substantially hindered the thermal degradation of composites [258]. Also, the flexible polymer ring mobility and plasticizing effects of ILs decreased the activation energy and thermal stability of polymer composites when the amounts of ILs ([BMIM]HSO_4 and [EMIM]Ac) are more than 1 wt % [236, 351].

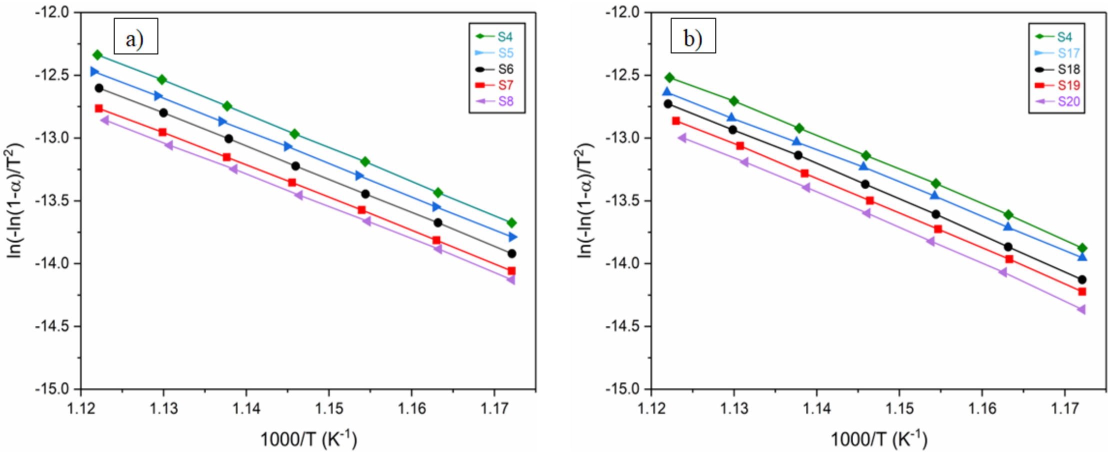

Figure 4.31: Coats-Redfern plots of PEEK composites with various amounts of ILs a) [BMIM]HSO$_4$ b) [EMIM]Ac

The thermo kinetic characteristics of PEEK composites without and with [BMIM]HSO$_4$ were obtained (Table 4.9) under constant heating rate using the non-isothermal Broido technique (Figure 4.32 b). In general, kinetic quantities, including activation energy (Ea; kJ/mol) and regression coefficient (R^2), were calculated from the linear plots of ln ln (1/α) and 1000/T (K^{-1}). As shown in Table 4.9, the Ea of S4 was measured as 192 KJ/mol, which was changed to 196.61 KJ/mol, 199.72 KJ/mol, 199.52 KJ/mol and 199.12 KJ/mol for S17, S18, S19, and S20, respectively, corresponding to 2.4 %, 4.02 %, 3.92 % and 3.7 % improvements than unmodified PEEK composite. This confirmed the increased crystallization of PEEK as a result of the strong physical contacts between the IL-treated filler and the polymer matrix [271]. While the Ea for PEEK composite materials with greater IL loadings (S19 and S20) was reduced when compared to those for S18, due to the plasticity of the used IL [236].

The parallel lines in Figure 4.32 (a) demonstrate the untreated and [EMIM]Ac-treated composite samples heated at a steady rate applying the Broido model, while Table 4.9 provides the average activation energies in the temperature region of 560 °C–600 °C as estimated using the slope of these segments. Table 4.9 displayed that 1 wt % of [EMIM]Ac treated composite had the highest activation energy of 197.91 kJ/mol, preceded by 1.5 wt % and 2 wt % of IL treated composite with values of 197.84 kJ/mol and 197.78 KJ/mol, respectively, whereas non-IL sample had the lowest activation energy of 192 kJ/mol. The higher activation energies of ILs-treated composites suggested that ILs loading had increased the attachment of MWCNTs to polymer, requiring a larger amount of energy to disrupt the composites bonds on a macroscale [352]. In addition to that, the values of kinetic parameters, including activation energy of PEEK composites (more than 1 wt % of IL) were reduced due to the softening effects [319] induced by IL.

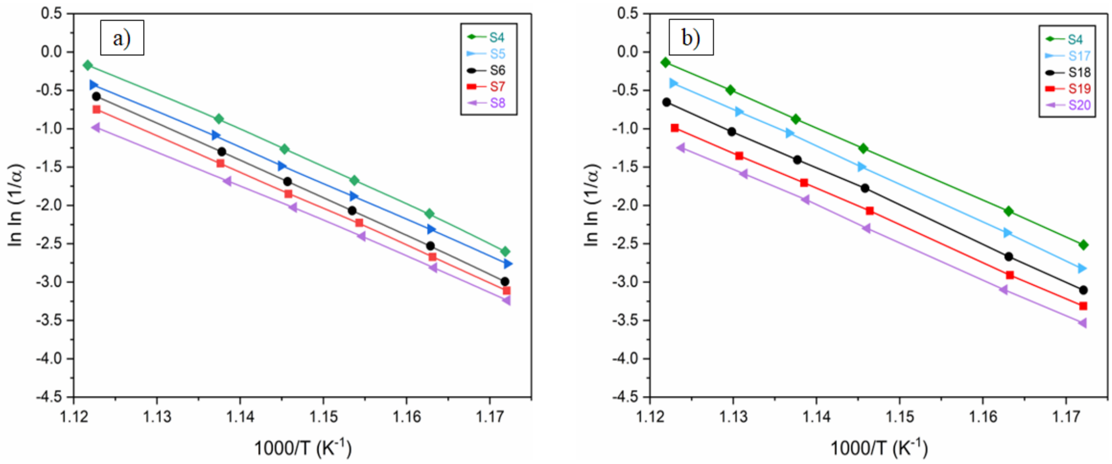

Figure 4.32: Broido plots of PEEK composites with various amounts of ILs a) [BMIM]HSO_4 b) [EMIM]Ac

The Horowitz-Metzger method calculated the activation energy for PEEK composite materials, including [BMIM]HSO_4 using TGA data collected with a heating rate of 10 °C/min as illustrated in Figure 4.33 (b) and their outcomes are listed in Table 4.9. The activation energy (Ea) and regression coefficient (R^2) of thermal disintegration of IL-modified MWCNTs in the PEEK composite sample (S18) were found to be 239 kJ/mol and 0.9983, which were greater than the non-IL PEEK composite (S4) and all the remaining specimens. The incorporation of IL-assisted filler nanoparticles to the polymer matrix increased the Ea significantly, indicating that the PEEK composites were more resistant to break as a consequence of the inclusion of evenly distributed IL-treated MWCNTs [296, 353]. Additionally, the computed Ea values had a high degree of reliability in representing the thermal decomposition kinetics of the PEEK composites, as the R^2 values were greater than 0.99. Conversely, the kinetic properties of the S19 and S20 composites were decreased slightly in contrasted to S18, suggesting a small shift in thermal stability. This could be because to the high concentration of IL [290, 354], which led to low thermal resilience.

The Ea can be calculated from the slope of the straight lines of Horowitz-Metzger plots (Figure 4.33 a) of PEEK composites manufactured with various loadings of [EMIM]Ac. The kinetics parameters after calculations are deduced in Table 4.9. By increasing the concentration of [EMIM]Ac to 1 wt%, the kinetic properties, including Ea, were augmented to 238.01 KJ/mol as compared to untreated PEEK composites (232 KJ/mol). These findings showed that IL-modified inhibited the breakdown of PEEK composites, indicating that more energy was needed for thermal decomposition [270, 272]. In addition to that, thermal properties were diminished for more than 1 wt % of [EMIM]Ac based PEEK samples because of the plasticization of used IL [354, 355].

Hamayoun et al. (2016) [356] investigated the flexural and thermal characteristics of the manufactured composite panels and observed significant enhancements after modification of OPF (oil palm frond) nanoparticles with the ILs [EMIM]Ac and [BMIM]Cl at high initial solid loading and comparatively moderate processing parameters. It was evidenced that composites modified with ILs had greater activation energies, which were ascribed to their increased thermal properties as a consequence of the ILs treatment. The improved activation energies of ILs-treated composites showed that pretreatment with ILs strengthened the adherence of OPF particles to the polymer binder, requiring a larger amount of energy to disrupt these interactions, which manifested in the composites better mechanical characteristics on a macroscale.

When the kinetic parameters including activation energies of PEEK composites fabricated with various amounts of [EMIM]Ac and [BMIM]HSO_4 were evaluated, it was revealed that PEEK composites formed with 1 wt % of [BMIM]HSO_4 presented the highest values. This might be due to the longer alkyl chain length of [BMIM]HSO_4, which led to strong physical interactions between the filler and matrix. These associations may have aided in prolonging thermal breakdown and resulting in higher Ea values [271]. Additionally, the Ea of the PEEK composites were dropped owing to the plasticizing effects of the added ILs at higher quantities (1.5 and 2 wt %) [236, 351].

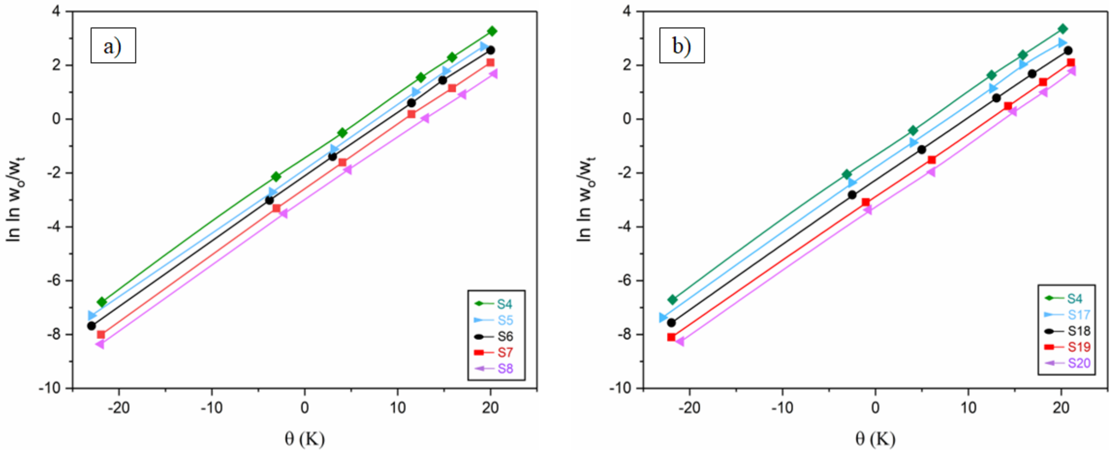

Figure 4.33: Horowitz-Metzger plots of PEEK composites with various amounts of ILs a) [BMIM]HSO_4 b) [EMIM]Ac

Table 4.9: Kinetic parameters of [BMIM]HSO_4 and [EMIM]Ac based PEEK composites

Sample	Coats-Redfern		Broido		Horowitz-Metzger	
	Ea	R^2	Ea	R^2	Ea	R^2
S4	207.85±0.9	0.9991	192.00±1.6	0.9990	232.00±2.3	0.9980
S5	209.67±1.2	0.9992	195.37±0.8	0.9991	233.17±2.1	0.9980
S6	222.11±0.8	0.9991	197.91±2.3	0.9982	238.01±2.1	0.9980
S7	218.15±3.2	0.9993	197.84±3.6	0.9988	237.42±2.4	0.9979
S8	218.01±2.2	0.9990	197.78±1.5	0.9986	237.32±0.8	0.9979
S17	211.25±2.4	0.9987	196.61±3.3	0.9991	234.12±2.4	0.9978
S18	225.19±1.1	0.9994	199.72±1.4	0.9992	239.00±1.6	0.9983
S19	220.44±2.2	0.9993	199.52±1.6	0.9989	238.11±2.1	0.9982
S20	219.45±1.7	0.9993	199.12±2.3	0.9988	237.92±2.2	0.9980

4.3.10 Effect of [EMIM]HSO_4 and [BMIM]Ac on thermal degradation kinetic of PEEK composites

It is noted from Figure 4.34 (a) that the parallel lines are derived from the TGA data of [EMIM]HSO_4 based PEEK composites using the Coats-Redfern model and Table 4.10 provides that the values of Ea and R^2, considering the first order of reaction with heating rate 10 °C/min. The values of Ea were 209.67 KJ/mol, 222.17 KJ/mol, 218.88 KJ/mol and 218.81 for S9, S10, S11 and S12, respectively, when compared to S4 (207.85 KJ/mol). It was noticed that the Ea values were boosted for IL-treated MWCNTs in PEEK composites due to the uniform MWCNTs dispersion [48] in PEEK that pervaded the polymer ring strongly during thermal breakdown. Zhao et al. (2012) [242] reported a similar assessment for PMMA/MWCNTs/IL composites. However, when more than 1% IL was applied, the PEEK composites exhibited a declining trend in terms of kinetic properties. This could be ascribed to the plasticization effects [357] and the free movement of the polymer in the composites.

The resilience to heat deterioration of PEEK composites with [BMIM]Ac treated filler is precisely described employing the Coats-Redfern technique in Figure 4.34 (b). The linear lines are obtained in the temperature range 560 °C-600 °C and the related kinetic parameters are summarized in Table 4.10. The Ea for S4 was 207.85 KJ/mol, which was enhanced to 209.62 KJ/mol, 222.11 KJ/mol, 218.15 KJ/mol and 218.01 KJ/mol for S13, S14, S15 and S16, respectively. Also, the maximum regression coefficient (R^2) value was 0.9999 for 1 wt % of IL, indicating the optimal ratio of IL to MWCNTs in PEEK composites. Yao et al. [358] reported similar findings for PEEK composites, including carbon fibre, where the filler increased the activation energy. When compared to S14, the Ea of S15 and S16 were reduced 1.82 % and 1.88 %, respectively, due to the greater concentrations and softening behaviour [359] of the IL.

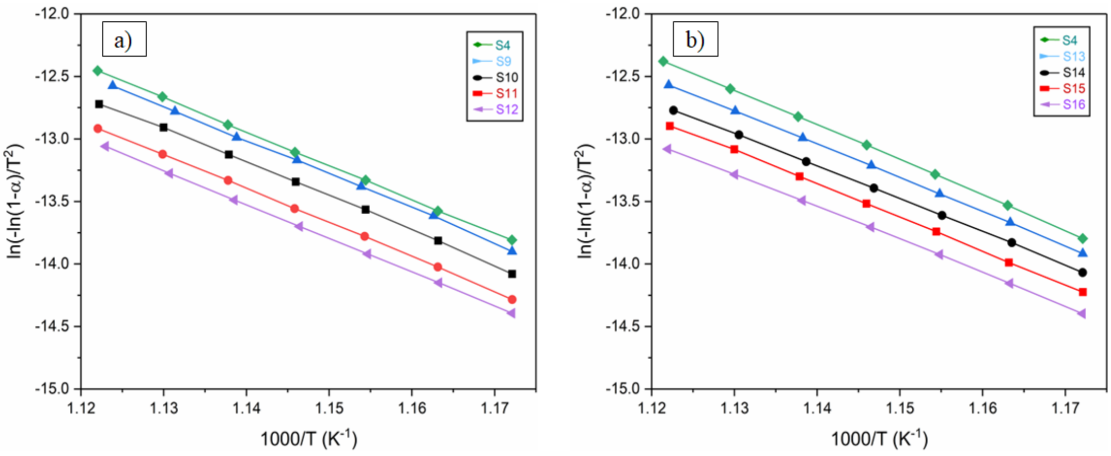

Figure 4.34: Coats-Redfern plots of PEEK composites with various amounts of ILs a) [EMIM]HSO_4 b) [BMIM]Ac

The linear graphs (Figure 4.35 a) of PEEK composites prepared without and with [EMIM]HSO_4 loadings between ln ln (1/α) and I/T are generated using the Broido model to establish the impact of IL on the thermal efficiency of PEEK composites, and the critical properties including activation energy is determined and presented in Table 4.10. According to Table 4.10, the Ea values for untreated PEEK composites were 192 KJ/mol and relocated to 198.92 KJ/mol, 198.82 KJ/mol, 198.08 KJ/mol and 198.06 KJ/mol for S9, S10, S11 and S12, respectively. The elevated Ea values demonstrated that IL modification was essential in postponing the breaking of polymer composites chains [48, 293]. Whereas, these values were dropped when the loading of applied IL exceeded 1% wt owing to the empty space occupied by IL and its plasticizing ability [360].

Figure 4.35 (b) displays the thermal decomposition kinetics of TGA data of PEEK composites containing MWCNTS modified with varying quantities of [BMIM]Ac and the straight lines are obtained for the Broido method (reaction order is 1). The findings summarized in Table 4.10 demonstrated that IL raised the activation energy and pre-exponentiation factor. The highest values of Ea and R^2 for samples S14 were determined as 198.86 KJ/mol and 0.9993 respectively when compared to other samples. The results revealed that the optimum ratio for IL: MWCNTs (wt %) was 1:1, at which the thermal breakdown was significantly delayed [43]. Also, the results clearly demonstrated that after modifying MWCNTs with various [BMIM]Ac concentrations, the Ea values were boosted.

The consequences of this study were in accordance with the previously published research. Jiang et al. (2017) [361] used an easy-to-use physical mixing method to create a new synergistic flame retardant by injecting IL, 1-butyl-3-methyl-imidazolium dibutyl phosphate ([BMIM][DBP]) as a synergist with the melamine. The author demonstrated that Ea was a critical criterion for determining the thermal stability of melamine and its derivatives. It was worth noting that the effective proportion of [BMIM][DBP] in melamine enhanced the thermal resilience, whereas its larger concentrations decreased the thermal properties.

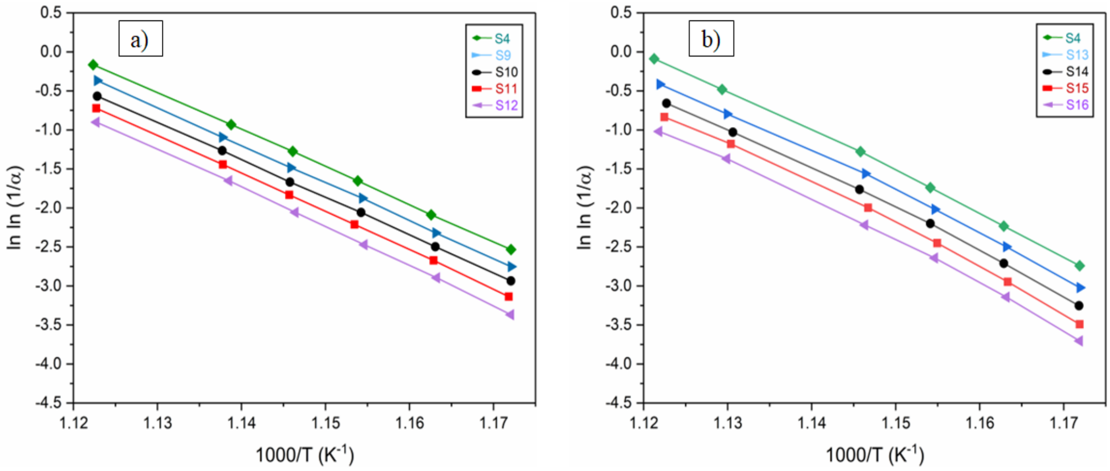

Figure 4.35: Broido plots of PEEK composites with various amounts of ILs a) [EMIM]HSO_4 b) [BMIM]Ac

Figure 4.36 (a) and Table 4.11 gives the results of the Horowitz-Metzger model for non and various proportions of [EMIM]HSO_4 based PEEK composites. It was elucidated from Table 4.10 that IL was critical in enhancing the Ea. The Ea of S10 was boosted by 2.79 % with R^2 (0.9976) than S4 (non-IL sample). The cause for this modification ascribed to the homogenous distribution of MWCNTs in PEEK as well as the strong physical π-π interactions [339, 362]. Although, the Ea for S11 and S12 was increased to 2.37 % and 2.33 % when contrasted to S4 but lower than S10 due to the suitable ratio of IL to MWCNTs [43] and the plasticity of IL [363] at higher amounts.

The consequence of different amounts of IL pretreatment on the PEEK/MWCNTs was investigated by the Horowitz-Metzger approach for thermal properties, especially in terms of activation energy. The parallel lines (Figure 4.36 b) were obtained from the TGA data (temperature range (560°C-600°C) of [BMIM]Ac treated MWCNTs in PEEK composites, and the related findings are summarized in Table 4.10. It was observed that maximum activation energy and regression coefficient was achieved for 1 wt % [BMIM]Ac and the corresponding values were 238.47 KJ/mol and respectively. The delayed thermal stability of S14 was linked to the strong adherence [333] of the IL-modified MWCNTs with the PEEK. Similar study was found in the literature to corroborate these facts. Additionally, the Ea for S15 and S16 was reduced owing to the higher amounts of the IL and its plasticization behavior [48, 235].

To study the thermal kinetics, Rajeshwari et al. (2014) [260] used melt mixing to produce high-density polyethylene (HDPE) enriched multi-walled carbon nanotubes

(MWCNTs) hybrids with various volume fractions. It was exciting to observe that the activation energies of the HDPE/MWCNTs composite rose (8 %) with MWCNTs vol % loading than the untreated HDPE composite. This improvement in Ea was correlated with a decrease in polymer chain mobility in the composites. Likewise, it was discovered that the Ea was constant at greater MWCNTs concentrations in HDPE composites.

A similar phenomenon [364] was found for Ea estimations using the Coats-Redfern technique. Therefore, Ea of the untreated fibre was determined to be 44.41 kJ/mol, which was increased to 54.01 kJ/mol and 55.81 kJ/mol for the [bmim][Cl] and [emim][dep] treated OPF fibres, respectively. Even though, it was worth noting that the premeditated Ea values based on linear regression analysis had coefficients of determination (R^2) ranging from 0.9930 to 0.9990, indicating that a higher R^2 provided more accurate kinetic variables for the temperature range under consideration.

The comparative evaluation of PEEK composites produced with different quantities of [EMIM]HSO_4 and [BMIM]Ac indicated that PEEK composites containing 1 wt % [BMIM]Ac had higher activation energies. This could be attributed to the longer alkyl chain length of the IL, which resulted in stronger interactions between the filler and polymer matrix, which were necessary for enhancing the thermal properties [43]. In comparison, the thermal characteristics of the PEEK composites were decreased at greater concentrations of ILs (1.5 and 2 wt %) due to their plasticizing nature [48, 235].

Moreover, the thermal kinetics of PEEK composites produced with four imidazolium ILs, including [BMIM]HSO_4, [EMIM]Ac, [BMIM]Ac and [EMIM]HSO_4 were evaluated and exhibited that [BMIM]HSO_4 and [BMIM]Ac showed superior performance. This explanation have become stronger in view of previous literature in which numerous authors [365, 366] demonstrated that ILs with a bigger alkyl chain might established significant correlations with both the filler and polymer matrix, that was critical for improving the MWCNTs distribution and delayed the thermal degradation. Further, the calculated activation energy of 1 wt % of [BMIM]HSO_4-based PEEK composites was highest compared to other PEEK composites produced with other ILs, due to its high affinity and strong interactions with the filler and polymer matrix [326]. At more than 1 wt % of ILs, the Ea values were reduced because of the plasticization effects of ILs in the composites as confirmed by DSC and TGA studies.

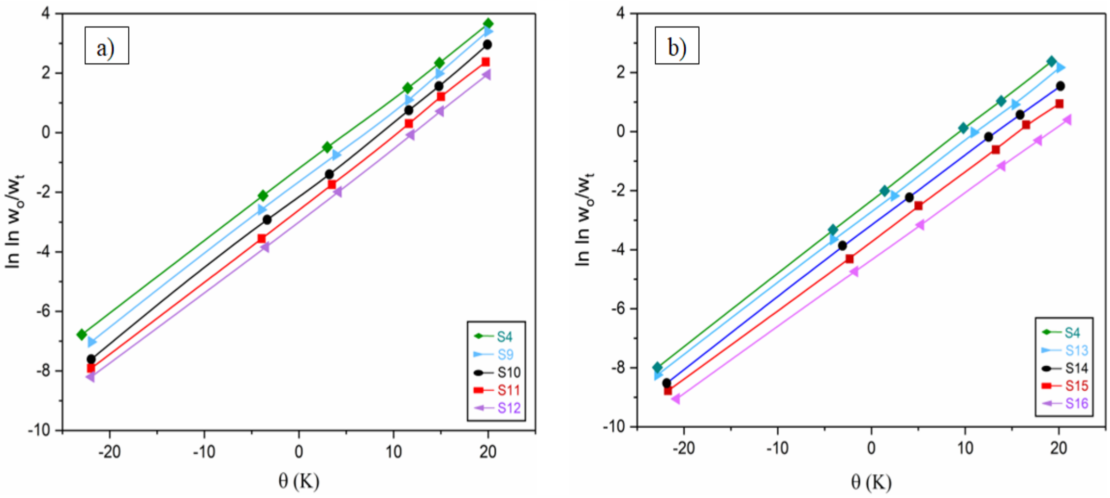

Figure 4.36: Horowitz-Metzger plots of PEEK composites with various amounts of ILs a) [EMIM]HSO$_4$ b) [BMIM]Ac

It must be stated that using several kinetic methods to investigate thermal breakdown trends using thermogravimetric data is a complementary strategy, not a competing one, as suggested by the International Confederation for Thermal Analysis and Calorimetry (ICTAC) Kinetics Project. Therefore, it is essential to understand and anticipate the thermal degradation kinetics in order to develop efficient molding and thermoplastic processing methods for the manufacturing of PEEK composites using various ILs. As a consequence, a useful activation energy range was determined by combining all of the findings from the Broido, Coats-Redfern, and Horowitz-Metzger approaches. According to the regression coefficient (R^2) values, the Coats-Redfern model was best linear fit to the data, which was consistent with the previous research [367]. Compared to Broido and Horowitz-Metzger models, Coats-Redfern model was most reliable and accurate [368]. The PEEK composites prepared with four employed ILs ([EMIM]Ac, [BMIM]HSO$_4$, ([BMIM]Ac, [EMIM]HSO$_4$) showed 3-8 % higher Ea than that of the untreated sample. Besides, the overall trend in the Ea measurements was Ea of [BMIM]HSO$_4$ > Ea of [BMIM]Ac > Ea of [EMIM]HSO$_4$ > Ea of [EMIM]Ac. The Ea values observed in this research were within the range of previous reports for PEEK-based composites.

Table 4.10: Kinetic parameters of [EMIM]HSO_4 and [BMIM]Ac based PEEK composites

Sample	Coats-Redfern		Broido		Horowitz-Metzger	
	Ea	R^2	Ea	R^2	Ea	R^2
S4	207.85±0.9	0.9991	192.00±1.6	0.9990	232.00±2.3	0.9980
S9	209.67±2.3	0.9991	195.92±1.1	0.9990	233.43±2.4	0.9983
S10	222.17±0.8	0.9990	198.32±1.3	0.9984	238.32±2.6	0.9984
S11	218.88±1.6	0.9991	198.08±1.5	0.9986	237.49±2.3	0.9982
S12	218.81±2.4	0.9989	198.08±1.8	0.9983	237.41±1.6	0.9980
S13	210.72±1.4	0.9988	196.24±2.2	0.9990	233.82±1.8	0.9982
S14	224.92±0.7	0.9993	198.86±1.4	0.9991	238.47±1.2	0.9986
S15	219.33±2.4	0.9991	198.74±1.3	0.9987	237.93±1.5	0.9985
S16	219.04±1.1	0.9990	198.41±2.1	0.9986	237.84±2.2	0.9984

The future development of additional classes of polymer composites in which IL modification technology on MWCNTs is a highly interesting feature. Furthermore, activation energy estimations using three commonly used thermo-kinetic models showed unequivocally that a technique based on ILs might be a very promising option for effective MWCNTs usage in PEEK composites.

4.4 Summary

The efficacy of ILs in PEEK/MWCNTs/nHA composites was tested, and it was discovered that IL significantly decreased MWCNTs agglomeration compared to non-IL PEEK composites. The decomposition temperature of PEEK/MWCNTs/nHA/IL composites was boosted, especially for 1 wt % of ILs. Similarly, the crystallinity and melting point of ILs-treated PEEK composites were increased. The mechanical properties of PEEK/MWCNTs/nHA/IL composites are in the required range (7.65 GPa for 1 wt % of [BMIM]HSO_4 corresponding to human cortical bone (7-12 GPa). Likewise, the incorporation of nHA has improved the biological performance of the

PEEK composites compared to pure PEEK. Also, the impact of ILs on thermal degradation kinetics of PEEK composites was determined, and the activation energy values are substantially raised. The highest thermomechanical properties were obtained for [BMIM]HSO_4 based PEEK/MWCNTs/nHA/ILs than the other employed ILs. The findings show that ILs pretreatment could be an effective and environmentally benign processing approach for MWCNTs dispersion in PEEK for enhanced mechanical performance in biological applications.

CHAPTER 5

CONCLUSIONS AND RECOMMENDATIONS

5.1 Conclusions

The purpose of this research was to determine the feasibility of utilizing ionic liquids (ILs) to distribute MWCNTs in PEEK/MWCNTs/nHA/ILs composite materials via a melt-blended method for biomedical uses, particularly for human bone substitution. The effect of modifying MWCNTs with four imidazolium ILs containing distinct anions, alkyl chain lengths and different amounts: 1-ethyl-3-methylimidazolium acetate ([EMIM]Ac), 1-ethyl-3-methylimidazolium hydrogen sulfate ([EMIM]HSO_4), 1-butyl-3-methylimidazolium acetate ([BMIM]Ac), and 1-butyl-3-methylimidazolium hydrogen sulfate ([BMIM]HSO_4) on the morphological, thermal and mechanical characteristics of the fabricated PEEK/MWCNTs/nHA/ILs composite was assessed. Besides, the role of nHA on the biological efficacy, and effect of ILs on thermal degradation kinetics of PEEK/MWCNTs/nHA/ILs were evaluated.

- The morphological characterization of PEEK/MWCNTs/ILs composites provoked that ILs-modified MWCNTs were homogenously distributed in PEEK as compared to PEEK composites fabricated without IL (DMF).

- When contrasted to pure PEEK and PEEK/MWCNTs/nHA composites, the thermomechanical properties of PEEK/MWCNTs/ILs/nHA were enhanced. Interestingly, the tensile strength and elastic modulus (89 MPa and 7.65 GPa for 1 wt % of [BMIM]HSO_4), were within the required range when compared to the values of human cortical bone (85-100 MPa and 7-12 GPa).

- Alamar Blue assay discovered that the incorporation of HA to PEEK/MWCNTs/ILs composites improved the biocompatibility when compared to pure polymer matrix. It was also found that cells viability of all PEEK/MWCNTs composites was more than the permissible range (80%) of the control.

- Based on calculated activation energy and regression coefficient values of PEEK/MWCNTs composites, the overall trend in the E_a measurements followed the trend; E_a of [BMIM]HSO_4 > E_a of [BMIM]Ac > E_a of [EMIM]HSO_4 > E_a of [EMIM]Ac.

The current findings can contribute to the recognition of ILs-assisted benign method to produce PEEK/MWCNTs/nHA/ILs composites for use as a substitute of human bone in biomedical field.

5.2 Recommendations

The following suggestions could be made focusing on the experimental and modelling assessment, and findings, in order to manufacture PEEK composites with optimal characteristics.

The future research should concentrate on the impact of hydroxyapatite (HA) on the mechanical characteristics of composites composed of PEEK/MWCNTs/nHA/ILs. Based on the current research, [BMIM]HSO_4 could be considered for this investigation.

The surface (bioactive layer) and antibacterial properties of the prepared composites should be examined in detail after immersing in the stimulated body fluid (SBF).

The future study should strongly encourage modelling of the ILs-facilitated pretreatment processes in predicting the other thermodynamic parameters.

A comprehensive and optimized screening and selection of ILs with the appropriate cations and anions, as well as consideration of processing limitations, would allow the design of ILs systems with desirable properties, possibly resulting effective for PEEK/MWCNTs composites.

The process and economic feasibility of PEEK/MWCNTs/nHA/ILs composites should be investigated via simulations tools in order for them to become commercially viable.

References

[1] C. Liu, K. W. Chan, J. Shen, C. Z. Liao, K. W. K. Yeung, S. Tjong, "Polyetheretherketone hybrid composites with bioactive nanohydroxyapatite and multiwalled carbon nanotube fillers," *Polymers*, vol. 8, no. 12, pp. 425, 2016.

[2] A. Ahmad, T. Iqbal, S. Yasin, R. Hanif, S. Riaz, P. F. Luckham, "Stability of Amorphous PEEK in Organic Solvents," *Journal- Chemical Society of Pakistan*, vol. 40, no. 4, pp. 810-818, 2018.

[3] S. E. Arevalo, L. Pruitt, "Nanomechanical analysis of medical grade PEEK and carbon fiber-reinforced PEEK composites," *Journal of the Mechanical Behavior of Biomedical Materials*, vol. 111, pp. 104008, 2020.

[4] T. Wei, J. Wang, X. Yu, Y. Wang, Q. Wu, C. Chen, "Mechanical and thermal properties and cytotoxicity of Al_2O_3 nano particle-reinforced poly (ether-ether-ketone) for bone implants," *RSC Advances*, vol. 9, no. 59, pp. 34642-34651, 2019.

[5] J. Zheng, J. Kang, C. Sun, C. Yang, L. Wang, D. Li, "Effects of printing path and material components on mechanical properties of 3D-printed polyether-ether-ketone/hydroxyapatite composites," *Journal of the Mechanical Behavior of Biomedical Materials*, p. 104475, 2021.

[6] R. Ma, Q. Li, L. Wang, X. Zhang, L. Fang, Z. Luo, B. Xue, S. Ma, "Mechanical properties and in vivo study of modified-hydroxyapatite/polyetheretherketone biocomposites," *Materials Science and Engineering: C*, vol. 73, pp. 429-439, 2017.

[7] J. Cao, Y. Lu, H. Chen, L. Zhang, C. Xiong, "Preparation, mechanical properties and in vitro cytocompatibility of multi-walled carbon nanotubes/poly (etheretherketone) nanocomposites," *Journal of Biomaterials Science, Polymer Edition*, vol. 29, no. 4, pp. 428-447, 2018.

[8] J. S. Lee, S. D. Baek, J. Venkatesan, I. Bhatnagar, H. K. Chang, H. T. Kim, S. Kim, "In vivo study of chitosan-natural nano hydroxyapatite scaffolds for bone tissue regeneration," *International Journal of Biological Macromolecules*, vol. 67, pp. 360-366, 2014.

[9] R. E. McMahon, L. Wang, R. Skoracki, A. Mathur, "Development of nanomaterials for bone repair and regeneration," *Journal of Biomedical Materials Research Part B Applied Biomaterials*, vol. 101, no. 2, pp. 387-397, 2013.

[10] L. L. Hench, An introduction to bioceramics. *World scientific*, 1993.

[11] J. H. Lee, H. L. Jang, K. M. Lee, H. Baek, K. Jin, K. S. Hong, J. Noh, H. Lee, "In vitro and in vivo evaluation of the bioactivity of hydroxyapatite-coated polyetheretherketone biocomposites created by cold spray technology," *Acta Biomaterialia*, vol. 9, no. 4, pp. 6177-6187, 2013.

[12] S. Ha, M. Kirch, F. Birchler, K. Eckert, J. Mayer, E. Wintermantel, C. Sittig, I. Pfund-Klingenfuss, M. Textor, N. Spencer, "Surface activation of polyetheretherketone (PEEK) and formation of calcium phosphate coatings by precipitation," *Journal of Materials Science: Materials in Medicine*, vol. 8, no. 11, pp. 683-690, 1997.

[13] M. A. Bakar, P. Cheang, K. J. Khor, "Tensile properties and microstructural analysis of spheroidized hydroxyapatite–poly (etheretherketone) biocomposites," *Materials Science and Engineering: A*, vol. 345, no. 1-2, pp. 55-63, 2003.

[14] A. M. Díez-Pascual, M. Naffakh, C. Marco, G. Ellis, M. A. Gómez-Fatou, "High-performance nanocomposites based on polyetherketones," *Progress in Materials Science*, vol. 57, no. 7, pp. 1106-1190, 2012.

[15] Z. Spitalsky, D. Tasis, K. Papagelis, C. J. Galiotis, "Carbon nanotube–polymer composites: chemistry, processing, mechanical and electrical properties," *Progress in Polymer Science*, vol. 35, no. 3, pp. 357-401, 2010.

[16] M. Masuelli, "Fiber Reinforced Polymers: The Technology Applied for Concrete Repair," BoD–Books on Demand, 2013.

[17] S. Bal, S. J. Samal, "Carbon nanotube reinforced polymer composites—a state of the art," *Bulletin of Materials Science*, vol. 30, no. 4, pp. 379, 2007.

[18] R. Ma, T. Tang, "Current strategies to improve the bioactivity of PEEK," *International Journal of Molecular Sciences*, vol. 15, no. 4, pp. 5426-5445, 2014.

[19] D. Almasi, N. Iqbal, M. Sadeghi, I. Sudin, M. R. Abdul Kadir, T. Kamarul, "Preparation methods for improving PEEK's bioactivity for orthopedic and dental application: a review," *International Journal of Biomaterials*, vol. 2016, 2016.

[20] P. Feng, S. Peng, P. Wu, C. Gao, W. Huang, Y. Deng, T. Xiao, C. Shuai, "A nano-sandwich construct built with graphene nanosheets and carbon nanotubes enhances mechanical properties of hydroxyapatite–polyetheretherketone scaffolds," *International Journal Nanomedicine*, vol. 11, pp. 3487, 2016.

[21] M. Sattari, A. Molazemhosseini, M. Naimi-Jamal, A. Khavandi, "Nonisothermal crystallization behavior and mechanical properties of PEEK/SCF/nano-SiO2 composites," *Materials Chemistry and Physics*, vol. 147, no. 3, pp. 942-953, 2014.

[22] S. He, H. Jia, Y. Lin, H. Qian, J. Lin, "Effect of clay modification on the structure and properties of sulfonated poly (ether ether ketone)/clay nanocomposites," *Polymer Composites*, vol. 37, no. 9, pp. 2632-2638, 2016.

[23] Y. Shi, S. Zhou, Z.-G. Heng, M. Liang, Y. Wu, Y. Chen, H.-W. Zou, E. C. Research, "Interlocking Structure Formed by Multiscale Carbon Fiber–Polytetrafluoroethylene Fiber Hybrid Significantly Enhances the Friction and Wear Properties of Polyphenylene Sulfide Based Composites," *Industrial & Engineering Chemistry Research*, vol. 58, no. 36, pp. 16541-16551, 2019.

[24] M. Remanan, S. Bhowmik, L. Varshney, K. Jayanarayanan, "Tungsten carbide, boron carbide, and MWCNT reinforced poly (aryl ether ketone) nanocomposites: Morphology and thermomechanical behavior," *Journal of Applied Polymer Science*, vol. 136, no. 5, pp. 47032, 2019.

[25] Y. Li, Z. Man, X. Lin, L. Wei, H. Wang, M. Lei, "Role of Well-dispersed Carbon Nanotubes and Limited Matrix Degradation on Tribological Properties of Flame Sprayed PEEK Nanocomposite Coatings," *Journal of Trbology*, vol. 144, pp. 1-36, 2021.

[26] A. Tewatia, J. Hendrix, Z. Dong, M. Taghon, S. Tse, G. Chiu, W. E. Mayo, B. Kear, T. Nosker, J. Lynch, "Characterization of melt-blended graphene–poly (ether ether ketone) nanocomposite," *Materials Science and Engineering: B*, vol. 216, pp. 41-49, 2017.

[27] M. Rinaldi, D. Puglia, F. Dominici, V. Cherubini, L. Torre, F. Nanni, "Melt processing and mechanical property characterization of high-performance poly (ether ether ketone)–carbon nanotube composite," *Polymer International*, vol. 66, no. 12, pp. 1731-1736, 2017.

[28] Y. Su, F. Zhou, X. Wei, D. Jing, X. Zhang, S. Zhang, "Enhanced mechanical and electrical properties of carbon fiber/poly (ether ether ketone) laminates via inserting carbon nanotubes interleaves," *Journal of Applied Polymer Science*, vol. 137, no. 19, pp. 48658, 2020.

[29] S. Smart, A. Cassady, G. Lu, D. J. C. Martin, "The biocompatibility of carbon nanotubes," *Carbon*, vol. 44, no. 6, pp. 1034-1047, 2006.

[30] Z. Cao, L. Qiu, Y. Yang, Y. Chen, X. Liu, "The surface modifications of multi-walled carbon nanotubes for multi-walled carbon nanotube/poly (ether ether ketone) composites," *Applied Surface Science*, vol. 353, pp. 873-881, 2015.

[31] S. Samie, A. Nejati, M. R. Avazfard, S. Amini, "Preparation and characterization of the modified PEEK/CNTs-nanocomposites," *AIP Conference Proceedings*, 2016, vol. 1779, no. 1, p. 040009: AIP Publishing LLC.

[32] N. G. Sahoo, S. Rana, J. W. Cho, L. Li, S. Chan, "Polymer nanocomposites based on functionalized carbon nanotubes," *Progress in Polymer Science*, vol. 35, no. 7, pp. 837-867, 2010.

[33] J. P. da-Silva, B. G. Soares, S. Livi, G. Barra, "Phosphonium–based ionic liquid as dispersing agent for MWCNT in melt-mixing polystyrene blends: Rheology, electrical properties and EMI shielding effectiveness," *Materials Chemistry and Physics*, vol. 189, pp. 162-168, 2017.

[34] J. Cao, Y. Lu, H. Chen, L. Zhang, C. Xiong, P. Biomaterials, "Preparation, properties and in vitro cellular response of multi-walled carbon nanotubes/bioactive glass/poly (etheretherketone) biocomposite for bone tissue engineering," *International Journal of Polymeric Materials and Polymeric Biomaterials*, vol. 68, no. 8, pp. 433-441, 2019.

[35] S. Li, J. Li, N. Ma, D. Liu, G. J. Sui, "Super-compression-resistant multiwalled carbon nanotube/nickel-coated carbonized loofah fiber/polyether ether ketone composite with excellent electromagnetic shielding performance," *ACS Sustainable Chemistry & Engineering*, vol. 7, no. 16, pp. 13970-13980, 2019.

[36] T. Rajmohan, R. Rangarajan, D. Seshadhri, L. Seshan, D. Kumar, "Synthesis and characterisation of Multi wall Carbon Nano Tubes (MWCNT) reinforced Poly-Ether-Ether-Ketone (PEEK) composites," *Applied Mechanics and Materials*, 2015, vol. 813, pp. 235-239: Trans Tech Publ.

[37] C. Rong, G. Ma, S. Zhang, L. Song, Z. Chen, G. Wang, P. Ajayan, "Effect of carbon nanotubes on the mechanical properties and crystallization behavior of poly (ether ether ketone)," *Composites Science and Technology*, vol. 70, no. 2, pp. 380-386, 2010.

[38] A. M. Diez-Pascual, M. Naffakh, M. Gómez-Fatou, "Mechanical and electrical properties of novel poly (ether ether ketone)/carbon nanotube/inorganic fullerene-like WS_2 hybrid

nanocomposites: Experimental measurements and theoretical predictions," *Materials Chemistry and Physics*, vol. 130, no. 1-2, pp. 126-133, 2011.

[39] L. Cao, S. Deng, Z. J. Lin, "Enhancement of carbon nanotube particle distribution in PPS/PEEK/Carbon nanotube ternary composites with sausage-like structure," *Polymers*, vol. 8, no. 2, pp. 50, 2016.

[40] H. Mahmood, M. Moniruzzaman, S. Yusup, N. Muhammad, T. Iqbal, H. Akil, "Ionic liquids pretreatment for fabrication of agro-residue/thermoplastic starch based composites: A comparative study with other pretreatment technologies," *Journal of Cleaner Production*, vol. 161, pp. 257-266, 2017.

[41] H. Mahmood, M. Moniruzzaman, S. Yusup, T. Welton, "Ionic liquids assisted processing of renewable resources for the fabrication of biodegradable composite materials," *Green Chemistry*, vol. 19, no. 9, pp. 2051-2075, 2017.

[42] S. Zhang, N. Sun, X. He, X. Lu, X. Zhang, "Physical properties of ionic liquids: database and evaluation," *AIP Journal of Physical and Chemical Reference Data*, vol. 35, no. 4, pp. 1475-1517, 2006.

[43] C. Xing, L. Zhao, J. You, W. Dong, X. Cao, Y. Li, "Impact of ionic liquid-modified multiwalled carbon nanotubes on the crystallization behavior of poly (vinylidene fluoride)," *The Journal of Physical Chemistry B*, vol. 116, no. 28, pp. 8312-8320, 2012.

[44] D. J. Couling, R. J. Bernot, K. M. Docherty, J. K. Dixon, E. Maginn, "Assessing the factors responsible for ionic liquid toxicity to aquatic organisms via quantitative structure–property relationship modeling," *Green Chemistry*, vol. 8, no. 1, pp. 82-90, 2006.

[45] X. X. Ma, J. Wei, Q. B. Zhang, F. Tian, Y. Y. Feng, W. J. Guan, "Prediction of thermophysical properties of acetate-based ionic liquids using semiempirical methods," *Industrial & Engineering Chemistry Research*, vol. 52, no. 27, pp. 9490-9496, 2013.

[46] F. J. Gschwend, C. L. Chambon, M. Biedka, A. Brandt-Talbot, P. S. Fennell, J. P. Hallett, "Quantitative glucose release from softwood after pretreatment with low-cost ionic liquids," *Green Chemistry*, vol. 21, no. 3, pp. 692-703, 2019.

[47] J. Yang, Y. Xiao, C. Yang, S. Li, X. Qi, Y. Wang, "Multifunctional poly (vinylidene fluoride) nanocomposites via incorporation of ionic liquid coated carbon nanotubes," *European Polymer Journal*, vol. 98, pp. 375-383, 2018.

[48] G. Jiang, S. Song, Y. Zhai, C. Feng, Y. Zhang, "Improving the filler dispersion of polychloroprene/carboxylated multi-walled carbon nanotubes composites by non-covalent functionalization of carboxylated ionic liquid," *Composites Science and Technology*, vol. 123, pp. 171-178, 2016.

[49] J. Abraham, J. Thomas, N. Kalarikkal, S. C. George, S. Thomas, "Static and dynamic mechanical characteristics of ionic liquid modified MWCNT-SBR composites: theoretical perspectives for the nanoscale reinforcement mechanism," *The Journal of Physical Chemistry B*, vol. 122, no. 4, pp. 1525-1536, 2018

[50] X. Han, D. Yang, C. Yang, S. Spintzyk, L. Scheideler, P. Li, D. Li, J. Geis-Gerstorfer, F. Rupp, "Carbon fiber reinforced PEEK composites based on 3D-printing technology for orthopedic and dental applications," *Journal of Clinical Medicine*, vol. 8, no. 2, pp. 240, 2019.

[51] F. Awaja, D. V. Bax, S. Zhang, N. James, D. McKenzie, "Cell adhesion to PEEK treated by plasma immersion ion implantation and deposition for active medical implants," *Plasma Processes and Polymers*, vol. 9, no. 4, pp. 355-362, 2012.

[52] Y. Deng, P. Zhou, X. Liu, L. Wang, X. Xiong, Z. Tang, J. Wei, S. Wei, "Preparation, characterization, cellular response and in vivo osseointegration of polyetheretherketone/nano-hydroxyapatite/carbon fiber ternary biocomposite," *Colloids and Surfaces B: Biointerfaces*, vol. 136, pp. 64-73, 2015.

[53] R. Ma, D. Guo, "Evaluating the bioactivity of a hydroxyapatite-incorporated polyetheretherketone biocomposite," *Journal of Orthopaedic Surgery and Research*, vol. 14, no. 1, pp. 1-13, 2019.

[54] C. Shuai, C. Shuai, P. Wu, F. Yuan, P. Feng, Y. Yang, W. Guo, X. Fan, T. Su, S. J. Peng, "Characterization and bioactivity evaluation of (polyetheretherketone/polyglycolicacid)-hydroyapatite scaffolds for tissue regeneration," *Materials*, vol. 9, no. 11, pp. 934, 2016.

[55] P. Swaminathan, M. Uddin, P. Wooley, R. Asmatulu, "Fabrication and biological analysis of highly porous PEEK bionanocomposites incorporated with carbon and hydroxyapatite nanoparticles for biological applications," *Molecules*, vol. 25, no. 16, pp. 3572, 2020.

[56] Z. Jiang, Q. Chen, Z. Zhu, C. Y. Tsai, M. Zhao, H. J. Sue, A. Chang, T. Bremner, L. P. DiSano, "Well-dispersed Poly (ether-ether-ketone)/Multi-Walled Carbon Nanotubes Nanocomposites Prepared via A Simple Solution Mixing Approach." *Polymer International*, pp. 1090-1098, 2021.

[57] S. Li, F. Wen, C. Sun, Z. Wang, R. Chen, Q. He, J. Mu, "A comparative study on the influences of whisker and conventional carbon nanotubes on the electrical and thermal conductivity of polyether ether ketone composites," *Journal of Applied Polymer Science*, pp. 50720, 2021.

[58] D. Fang, C. Zhou, G. Liu, G. Luo, P. Gong, Q. Yang, Y. Niu, G. Li, "Effects of ionic liquids and thermal annealing on the rheological behavior and electrical properties of poly (methyl methacrylate)/carbon nanotubes composites," *Polymer*, vol. 148, pp. 68-78, 2018.

[59] B. G. Soares, N. Riany, A. A. Silva, G. M. Barra, S. Livi, "Dual-role of phosphonium–based ionic liquid in epoxy/MWCNT systems: Electric, rheological behavior and electromagnetic interference shielding effectiveness," *European Polymer Journal*, vol. 84, pp. 77-88, 2016.

[60] L. Chen, M. Sharifzadeh, N. Mac Dowell, T. Welton, N. Shah, J. P. Hallett, "Inexpensive ionic liquids:$[HSO_4]^-$-based solvent production at bulk scale," *Green Chemistry*, vol. 16, no. 6, pp. 3098-3106, 2014.

[61] R. Peng, Y. Wang, W. Tang, Y. Yang, X. J. Xie, "Progress in imidazolium ionic liquids assisted fabrication of carbon nanotube and graphene polymer composites," *Polymers*, vol. 5, no. 2, pp. 847-872, 2013.

[62] P. Patel, A. A. Stec, T. R. Hull, M. Naffakh, A. M. Diez-Pascual, G. Ellis, N. Safronava, R. Lyon, "Flammability properties of PEEK and carbon nanotube composites," Polymer Degradation and Stability, vol. 97, no. 12, pp. 2492-2502, 2012.

[63] L. Wang, L. Weng, S. Song, Z. Zhang, S. Tian, R. J. Ma, "Characterization of polyetheretherketone–hydroxyapatite nanocomposite materials," *Materials Science and Engineering: A*, vol. 528, no. 10-11, pp. 3689-3696, 2011.

[64] K. Friedrich, "Polymer composites for tribological applications," *Advanced Industrial and Engineering Polymer Research*, vol. 1, no. 1, pp. 3-39, 2018.

[65] R. N. Johnson, A. G. Farnham, R. A. Clendinning, W. F. Hale, C. Merriam, "Poly (aryl ethers) by nucleophilic aromatic substitution. I. Synthesis and properties," *Journal of Polymer Science Part A-1: Polymer Chemistry*, vol. 5, no. 9, pp. 2375-2398, 1967.

[66] T. Attwood, P. Dawson, J. Freeman, L. Hoy, J. Rose, P. J. Staniland, "Synthesis and properties of polyaryletherketones," Polymer, vol. 22, no. 8, pp. 1096-1103, 1981.

[67] O. Searle, R.. Pfeiffer, "Victrex® poly (ethersulfone)(PES) and Victrex® poly (etheretherketone)(PEEK)," *Polymer Engineering and Science*, vol. 25, no. 8, pp. 474-476, 1985.

[68] H. Lyu, N. Jiang, Y. Li, D. Zhang, "Enhancing CF/PEEK interfacial adhesion by modified PEEK grafted with carbon nanotubes," *Composites Science and Technology*, vol. 210, pp. 108831, 2021.

[69] M. Mokhtari, E. Archer, N. Bloomfield, E. Harkin-Jones, A. McIlhagger, "A review of electrically conductive Poly (ether ether ketone) materials." *Polymer International*, pp. 1016-1025, 2021.

[70] X. Zhang, "Carbon nanotube/polyetheretherketone nanocomposites: mechanical, thermal, and electrical properties," *Journal of Composite Materials*, vol. 55, pp. 0021998320981134, 2020.

[71] S. Li, W. Li, J. Nie, D. Liu, G. Sui, "Synergistic effect of graphene nanoplate and carbonized loofah fiber on the electromagnetic shielding effectiveness of PEEK-based composites," *Carbon*, vol. 143, pp. 154-161, 2019.

[72] V. Mittal, "Polymer nanotubes nanocomposites: synthesis, properties and applications," John Wiley & Sons, 2014.

[73] A. Diez-Pascual, J. Gonzalez-Dominguez, Y. Martinez-Rubi, M. Naffakh, A. Ansón, M. Martínez, B. Simard, M. J. Gómez, "Synthesis and properties of PEEK/carbon nanotube nanocomposites," pp. 281-313, 2010.

[74] Y. Liu, S. Huang, J. Tan, Z. Wang, Z. Jiang, H. Zhang, "PEEK/diatomite composites by in situ polymerization: Synthesis, characterization and fundamental properties," *Journal of Applied Polymer Science*, vol. 136, no. 3, pp. 46983, 2019

[75] S. Ajami, M. Coathup, J. Khoury, G. Blunn, "Augmenting the bioactivity of polyetheretherketone using a novel accelerated neutral atom beam technique," *Journal of Biomedical Materials Research Part B: Applied Biomaterials*, vol. 105, no. 6, pp. 1438-1446, 2017.

[76] T. W. Wright, "Definitions in Biomaterials: DF Williams (Ed.), Elsevier, Amsterdam," 1987, 72 1989.

[77] N. Athanasou, J. Quinn, C. Bulstrode, "Resorption of bone by inflammatory cells derived from the joint capsule of hip arthroplasties," *The Journal of Bone and Joint Surgery*, vol. 74, no. 1, pp. 57-62, 1992.

[78] C. Maniatopoulos, R. Pilliar, D. Smith, "Threaded versus porous-surfaced designs for implant stabilization in bone-endodontic implant model," *Journal of Biomedical Materials Research*, vol. 20, no. 9, pp. 1309-1333, 1986.

[79] P. Robotti, G. Zappini, "Thermal plasma spray deposition of titanium and hydroxyapatite on polyaryletheretherketone implants," in *PEEK biomaterials handbook*: Elsevier, 2012, pp. 119-143.

[80] D. Buser, N. Broggini, M. Wieland, R. Schenk, A. Denzer, D. Cochran, B. Hoffmann, A. Lussi, and S. Steinemann, "Enhanced bone apposition to a chemically modified SLA titanium surface," *Journal of Dental Research*, vol. 83, no. 7, pp. 529-533, 2004.

[81] S. Hacking, P. Boyraz, B. Powers, E. Sen-Gupta, W. Kucharski, C. Brown, E. Cook, Surface roughness enhances the osseointegration of titanium headposts in non-human primates," *Journal of Neuroscience Methods*, vol. 211, no. 2, pp. 237-244, 2012.

[82] Y. Deng, X. Liu, A. Xu, L. Wang, Z. Luo, Y. Zheng, F. Deng, J. Wei, Z. Tang, S. J. Wei, "Effect of surface roughness on osteogenesis in vitro and osseointegration in vivo of carbon fiber-reinforced polyetheretherketone–nanohydroxyapatite composite," *International Journal of Nanomedicine*, vol. 10, p. 1425, 2015.

[83] K. B. Sagomonyants, M. L. Jarman-Smith, J. N. Devine, M. S. Aronow, G. Gronowicz, "The in vitro response of human osteoblasts to polyetheretherketone (PEEK) substrates compared to commercially pure titanium," *Biomaterials*, vol. 29, no. 11, pp. 1563-1572, 2008.

[84] D. Briem, S. Strametz, K. Schröoder, N. Meenen, W. Lehmann, W. Linhart, A. Ohl, J. Rueger, "Response of primary fibroblasts and osteoblasts to plasma treated polyetheretherketone (PEEK) surfaces," vol. 16, no. 7, pp. 671-677, 2005.

[85] E. Liston, "Plasma treatment for improved bonding: a review," *The Journal of Adhesion*, vol. 30, no. 1-4, pp. 199-218, 1989.

[86] J. Waser-Althaus, A. Salamon, M. Waser, C. Padeste, M. Kreutzer, U. Pieles, B. Müller, K. J. Peters, "Differentiation of human mesenchymal stem cells on plasma-treated polyetheretherketone," *Journal of Materials Science: Materials in Medicine*, vol. 25, no. 2, pp. 515-525, 2014.

[87] J. Khoury, S. R. Kirkpatrick, M. Maxwell, R. E. Cherian, A. Kirkpatrick, R. C. Svrluga, "Neutral atom beam technique enhances bioactivity of PEEK," *Nuclear Instruments and Methods in Physics Research Section B: Beam Interactions with Materials and Atoms,* vol. 307, pp. 630-634, 2013.

[88] J. Marchand-Brynaert, G. Pantano, O. Noiset, "Surface fluorination of PEEK film by selective wet-chemistry," *Polymer*, vol. 38, no. 6, pp. 1387-1394, 1997.

[89] M. Pino, N. Stingelin, K. Tanner, "Nucleation and growth of apatite on NaOH-treated PEEK, HDPE and UHMWPE for artificial cornea materials," *Acta Biomaterialia,* vol. 4, no. 6, pp. 1827-1836, 2008.

[90] Y. Zhao, H. M. Wong, W. Wang, P. Li, Z. Xu, E. Y. Chong, C. H. Yan, K. W. Yeung, P. K. Chu, "Cytocompatibility, osseointegration, and bioactivity of three-dimensional porous and nanostructured network on polyetheretherketone," *Biomaterials*, vol. 34, no. 37, pp. 9264-9277, 2013.

[91] D. Almasi, S. Izman, M. Assadian, M. Ghanbari, M. Kadir, "Crystalline ha coating on peek via chemical deposition," *Applied Surface Science*, vol. 314, pp. 1034-1040, 2014.

[92] A. A. Stratton-Powell, K. M. Pasko, C. L. Brockett, J. Tipper, R. Research®, "The biologic response to polyetheretherketone (PEEK) wear particles in total joint replacement: a systematic review," *Symposium: Advances in PEEK Technology*, vol. 474, no. 11, pp. 2394-2404, 2016.

[93] I. V. Panayotov, V. Orti, F. Cuisinier, J. Yachouh, "Polyetheretherketone (PEEK) for medical applications," *Journal of Materials Science: Materials in Medicine*, vol. 27, no. 7, pp. 1-11, 2016.

[94] Q. Li, Y. Zhang, D. Wang, H. Wang, G. He, "Porous polyether ether ketone: A candidate for hard tissue implant materials," *Materials & Design*, vol. 116, pp. 171-175, 2017.

[95] R. A. Surmenev, "A review of plasma-assisted methods for calcium phosphate-based coatings fabrication," *Surface and Coatings Technology,* vol. 206, no. 8-9, pp. 2035-2056, 2012.

[96] Y. Yang, K.-H. Kim, J. Ong, "A review on calcium phosphate coatings produced using a sputtering process—an alternative to plasma spraying," *Biomaterials*, vol. 26, no. 3, pp. 327-337, 2005.

[97] T. Shimizu, S. Fujibayashi, S. Yamaguchi, B. Otsuki, Y. Okuzu, T. Matsushita, T. Kokubo, S. Matsuda, "In vivo experimental study of anterior cervical fusion using bioactive polyetheretherketone in a canine model," *PLOS ONE*, vol. 12, no. 9, pp. e0184495, 2017.

[98] P. Johansson, "On hydroxyapatite modified peek implants for bone applications," Malmö University, Department of Prosthetic dentistry, 2017.

[99] R. B. Heimann, "Plasma-sprayed hydroxylapatite-based coatings: chemical, mechanical, microstructural, and biomedical properties," *Journal of Thermal Spray Technology*, vol. 25, no. 5, pp. 827-850, 2016.

[100] S. Tang, P. Cheang, M. AbuBakar, K. Khor, K. J. Liao, "Tension–tension fatigue behavior of hydroxyapatite reinforced polyetheretherketone composites," *International Journal of Fatigue*, vol. 26, no. 1, pp. 49-57, 2004.

[101] K. W. Chan, C. Z. Liao, H. M. Wong, K. W. Yeung, S. Tjong, "Preparation of polyetheretherketone composites with nanohydroxyapatite rods and carbon nanofibers having high strength, good biocompatibility and excellent thermal stability," *RSC Advances*, vol. 6, no. 23, pp. 19417-19429, 2016.

[102] L. Wang, L. Weng, S. Song, Q. Sun, "Mechanical properties and microstructure of polyetheretherketone–hydroxyapatite nanocomposite materials," *Materials Letters*, vol. 64, no. 20, pp. 2201-2204, 2010.

[103] H. Garg, G. Bedi, A. Garg, "Implant surface modifications: a review," *Journal of Clinical and Diagnostic Research*, vol. 6, no. 2, pp. 319-324, 2012.

[104] S. Nour, N. Baheiraei, R. Imani, N. Rabiee, M. Khodaei, A. Alizadeh, S. M. Moazzeni, "Bioactive materials: a comprehensive review on interactions with biological microenvironment based on the immune response," *Journal of Bionic Engineering*, vol. 16, no. 4, pp. 563-581, 2019.

[105] M. Jarcho, "Calcium phosphate ceramics as hard tissue prosthetics," *Clinical Orthopaedics and Related Research®*, vol. 157, pp. 259-278, 1981.

[106] T. Thamaraiselvi, S. Rajeswari, "Biological evaluation of bioceramic materials-a review," *Carbon*, vol. 24, no. 31, pp. 172, 2004.

[107] H.-D. Jung, H. S. Park, M.-H. Kang, S.-M. Lee, H.-E. Kim, Y. Estrin, Y.-H. Koh, "Polyetheretherketone/magnesium composite selectively coated with hydroxyapatite for enhanced in vitro bio-corrosion resistance and biocompatibility," *Materials Letters*, vol. 116, pp. 20-22, 2014.

[108] D. Adams, G. F. Malgas, R. Smith, S. Massia, T. Alford, J. Mayer, "Microwave annealing for preparation of crystalline hydroxyapatite thin films," *Journal of Materials Science*, vol. 41, no. 21, pp. 7150-7158, 2006.

[109] P. Smith, P. Carey, T. Sigmon, "Excimer laser crystallization and doping of silicon films on plastic substrates,"*Applied physics letters*, vol. 70, no. 3, pp. 342-344, 1997.

[110] C. W. Yang, T. S. Lui, E. Chang, "Low temperature crystallization and structural modification of plasma-sprayed hydroxyapatite coating with hydrothermal treatment," in *Advanced Materials Research*, 2007, vol. 15, pp. 147-152: Trans Tech Publ.

[111] W. Tong, J. Chen, Y. Cao, L. Lu, J. Feng, X. J. Zhang, "Effect of water vapor pressure and temperature on the amorphous-to-crystalline HA conversion during heat treatment of HA coatings," *Journal of Biomedical Materials Research*, vol. 36, no. 2, pp. 242-245, 1997.

[112] T. Kokubo, H.-M. Kim, M. J. Kawashita, "Novel bioactive materials with different mechanical properties," *Biomaterials*, vol. 24, no. 13, pp. 2161-2175, 2003.

[113] M. A. Bakar, P. Cheang, K. J. Khor, "Thermal processing of hydroxyapatite reinforced polyetheretherketone composites," *Journal of Materials Processing Technology*, vol. 89, pp. 462-466, 1999.

[114] K. Tan, C. Chua, K. Leong, C. Cheah, W. Gui, W. Tan, F. J. Wiria, "Selective laser sintering of biocompatible polymers for applications in tissue engineering," *2nd International Conference on New Biomedical Materials*, vol. 15, no. 1, 2, pp. 113-124, 2005.

[115] K. Tan, C. Chua, K. Leong, M. Naing, C. Cheah, "Fabrication and characterization of three-dimensional poly (ether-ether-ketone)/-hydroxyapatite biocomposite scaffolds using laser sintering," *Proceedings of the Institution of Mechanical Engineers, Part H: Journal of Engineering in Medicine*, vol. 219, no. 3, pp. 183-194, 2005.

[116] R. K. Roeder, S. M. Smith, T. L. Conrad, N. J. Yanchak, C. H. Merrill, G. Converse, "Porous and bioactive PEEK implants for interbody spinal fusion," *Advanced Materials & Processes* vol. 167, no. 10, pp. 46-48, 2009

[117] F. Awaja, S. Zhang, N. James, D. McKenzie, "Enhanced autohesive bonding of polyetheretherketone (PEEK) for biomedical applications using a methane/oxygen plasma treatment," *Plasma Proceses and Polymers*, vol. 7, no. 12, pp. 1010-1021, 2010.

[118] J. H. Lee, H. L. Jang, K. M. Lee, H. R. Baek, K. Jin, J. Noh, "Cold-spray coating of hydroxyapatite on a three-dimensional polyetheretherketone implant and its biocompatibility evaluated by in vitro and in vivo minipig model," *Journal of Biomedical Materials Research Part B Applied Biomaterials*, vol. 105, no. 3, pp. 647-657, 2017.

[119] K. Wong, C. Wong, W. Liu, H. Pan, M. Fong, W. Lam, W. Cheung, W. Tang, K. Chiu, K. J. Luk, "Mechanical properties and in vitro response of strontium-containing hydroxyapatite/polyetheretherketone composites," *Biomaterials*, vol. 30, no. 23-24, pp. 3810-3817, 2009.

[120] P. Johansson, R. Jimbo, Y. Kozai, T. Sakurai, P. Kjellin, F. Currie, A. J. Wennerberg, "Nanosized hydroxyapatite coating on PEEK implants enhances early bone formation: a histological and three-dimensional investigation in rabbit bone," *Materials*, vol. 8, no. 7, pp. 3815-3830, 2015.

[121] X. Liu, Y. Gao, Y. Shang, X. Zhu, Z. Jiang, C. Zhou, J. Han, H. J. Zhang, "Non-covalent modification of boron nitride nanoparticle-reinforced PEEK composite: Thermally conductive, interfacial, and mechanical properties," *Polymer*, vol. 203, pp. 122763, 2020.

[122] R. Ma, L. Weng, X. Bao, S. Song, Y. Zhang, "In vivo biocompatibility and bioactivity of in situ synthesized hydroxyapatite/polyetheretherketone composite materials,"*Journal of Applied Polymer Science*, vol. 127, no. 4, pp. 2581-2587, 2013.

[123] G. L. Converse, W. Yue, R. Roeder, "Processing and tensile properties of hydroxyapatite-whisker-reinforced polyetheretherketone," *Biomaterials*, vol. 28, no. 6, pp. 927-935, 2007.

[124] S. Yu, K. P. Hariram, R. Kumar, P. Cheang, K. Aik, "In vitro apatite formation and its growth kinetics on hydroxyapatite/polyetheretherketone biocomposites," *Biomaterials*, vol. 26, no. 15, pp. 2343-2352, 2005.

[125] Y. Zhang, L. Hao, M. Savalani, R. A. Harris, L. Di Silvio, K. Tanner, "In vitro biocompatibility of hydroxyapatite-reinforced polymeric composites manufactured by selective laser sintering," *Journal of Biomedical Materials Research Part A*, vol. 91, no. 4, pp. 1018-1027, 2009.

[126] S. U. Maheshwari, V. K. Samuel, N. Nagiah, "Fabrication and evaluation of (PVA/HAp/PCL) bilayer composites as potential scaffolds for bone tissue regeneration application," *Ceramics International*, vol. 40, no. 6, pp. 8469-8477, 2014.

[127] I. Y. Kim, A. Sugino, K. Kikuta, C. Ohtsuki, S. Cho, "Bioactive composites consisting of PEEK and calcium silicate powders,"*Journal of Biomaterials Applications*, vol. 24, no. 2, pp. 105-118, 2009.

[128] L. Petrovic, D. Pohle, H. Münstedt, T. Rechtenwald, K. Schlegel, S. Rupprecht, "Effect of βTCP filled polyetheretherketone on osteoblast cell proliferation in vitro,"*Journal of Biomedical Science*, vol. 13, no. 1, pp. 41-46, 2006.

[129] C. Wilmowsky, E. Vairaktaris, D. Pohle, T. Rechtenwald, R. Lutz, H. Münstedt, G. Koller, M. Schmidt, F. W. Neukam, K. A. Schlegel, "Effects of bioactive glass and β-TCP containing three-dimensional laser sintered polyetheretherketone composites on osteoblasts in vitro," *Journal of Biomedical Materials Research Part A*, vol. 87, no. 4, pp. 896-902, 2008.

[130] K. Li, C. Y. Yeung, K. Yeung, S. Tjong, "Sintered hydroxyapatite/polyetheretherketone nanocomposites: mechanical behavior and biocompatibility," *Advanced Engineering Materials*, vol. 14, no. 4, pp. B155-B165, 2012.

[131] G. Zhong, M. Vaezi, X. Mei, P. Liu, S. J. Yang, "Strategy for Controlling the Properties of Bioactive Poly-Ether-Ether-Ketone/Hydroxyapatite Composites for Bone Tissue Engineering Scaffolds," *ACS omega*, vol. 4, no. 21, pp. 19238-19245, 2019.

[132] R. Ma, S. Tang, H. Tan, W. Lin, Y. Wang, J. Wei, L. Zhao, T. Tang, "Preparation, characterization, and in vitro osteoblast functions of a nano-hydroxyapatite/polyetheretherketone biocomposite as orthopedic implant material," *International Journal of Nanomedicine*, vol. 9, pp. 3949, 2014.

[133] D. J. Chung, "Thermal analysis of carbon fiber polymer-matrix composites by electrical resistance measurement," *Thermochimica acta*, vol. 364, no. 1-2, pp. 121-132, 2000.

[134] D. Li, R. B. Kaner, "Graphene-based materials," *Science*, vol. 320, no. 5880, pp. 1170-1171, 2008.

[135] S. Stankovich, D. A. Dikin, G. H. Dommett, K. M. Kohlhaas, E. J. Zimney, E. A. Stach, R. D. Piner, S. T. Nguyen, R. S. Ruoff, "Graphene-based composite materials," *nature*, vol. 442, no. 7100, pp. 282-286, 2006.

[136] S. J. Iijima, "Helical microtubules of graphitic carbon," *nature*, vol. 354, no. 6348, pp. 56-58, 1991.

[137] R. Bacon, "Growth, structure, and properties of graphite whiskers," *Journal of applied physics*, vol. 31, no. 2, pp. 283-290, 1960.

[138] A. Oberlin, M. Endo, T. Koyama, "Filamentous growth of carbon through benzene decomposition," *Journal of crystal growth*, vol. 32, no. 3, pp. 335-349, 1976.

[139] E. T. Thostenson, Z. Ren, T.-W.Chou, "Advances in the science and technology of carbon nanotubes and their composites: a review," *Composites Science and Technology*, vol. 61, no. 13, pp. 1899-1912, 2001.

[140] D. D. Ganji, S. Kachapi, *Application of nonlinear systems in nanomechanics and nanofluids: analytical methods and applications*. William Andrew, 2015.

[141] N. Saifuddin, A. Raziah, A. Junizah, "Carbon nanotubes: a review on structure and their interaction with proteins," *Journal of Chemistry*, vol. 2013, 2013.

[142] M. Antunes, J. Velasco, "Multifunctional polymer foams with carbon nanoparticles," *Progress in Polymer Science*, vol. 39, no. 3, pp. 486-509, 2014.

[143] G. G. Tibbetts, M. L. Lake, K. L. Strong, B. Rice, "A review of the fabrication and properties of vapor-grown carbon nanofiber/polymer composites," *Composites Science and Technology*, vol. 67, no. 7-8, pp. 1709-1718, 2007.

[144] C. Q. Sun, H. Bai, B. Tay, S. Li, E. Jiang, "Dimension, strength, and chemical and thermal stability of a single C− C bond in carbon nanotubes," *The Journal of Physical Chemistry B*, vol. 107, no. 31, pp. 7544-7546, 2003.

[145] E. Pop, D. Mann, Q. Wang, K. Goodson, H. Dai, "Thermal conductance of an individual single-wall carbon nanotube above room temperature," Nano letters, vol. 6, no. 1, pp. 96-100, 2006.

[146] V. Sgobba, G. A. Rahman, C. Ehli, D. Guldi, "Covalent and non-covalent approaches toward multifunctional carbon nanotube materials," pp. 329-379, 2007.

[147] K. I. Tserpes, N. Silvestre, *Modeling of carbon nanotubes, graphene and their composites*. Springer, 2014.

[148] W. Khan, R. Sharma, P. Saini, "Carbon nanotube-based polymer composites: synthesis, properties and applications," 2016.

[149] R. Perveen, A. Nasar, "Multiwalled carbon nanotube-based nanocomposites for artificial bone grafting," *Applications of Nanocomposite Materials in Orthopedics*, pp. 111-126, 2019.

[150] P. Ajayan, O. Stephan, C. Colliex, D. J. Trauth, "Aligned carbon nanotube arrays formed by cutting a polymer resin—nanotube composite," *science*, vol. 265, no. 5176, pp. 1212-1214, 1994.

[151] J. Gonzalez-Dominguez, P. Castell, S. Bespin-Gascon, A. Anson-Casaos, A. Diez-Pascual, M. Gomez-Fatou, A. Benito, W. Maser, M. Martinez, "Covalent functionalization of MWCNTs with poly (p-phenylene sulphide) oligomers: a route to the efficient integration through a chemical approach," *Journal of Materials Chemistry*, vol. 22, no. 39, pp. 21285-21297, 2012.

[152] A. Nish, J.-Y. Hwang, J. Doig, R. Nicholas, "Highly selective dispersion of single-walled carbon nanotubes using aromatic polymers," *Nature nanotechnology*, vol. 2, no. 10, pp. 640-646, 2007.

[153] A. M. Díez-Pascual, G. Martínez, J. M. González-Domínguez, A. Ansón, M. T. Martínez, M. Gómez, "Grafting of a hydroxylated poly (ether ether ketone) to the surface of single-walled carbon nanotubes," *Journal of Materials Chemistry*, vol. 20, no. 38, pp. 8285-8296, 2010.

[154] G. Wang, Z. Qu, L. Liu, Q. Shi, J. Guo, "Study of SMA graft modified MWNT/PVC composite materials," *Materials Science and Engineering: A*, vol. 472, no. 1-2, pp. 136-139, 2008.

[155] D. T. Tasis, N. Bianco, " Chemistry of carbon nanotubes," *Chemical reviews*, vol. 106, pp. 1105, 2006.

[156] A. Shanmugharaj, J. Bae, R. R. Nayak, S. Ryu, "Preparation of poly (styrene-co-acrylonitrile)-grafted multiwalled carbon nanotubes via surface-initiated atom transfer radical polymerization," *Journal of Polymer Science Part A: Polymer Chemistry*, vol. 45, no. 3, pp. 460-470, 2007.

[157] E. Bormashenko, "Progress in understanding wetting transitions on rough surfaces," *Advances in Colloid and Interface Science*, vol. 222, pp. 92-103, 2015.

[158] T. Fujigaya, N. Nakashima, "Methodology for homogeneous dispersion of single-walled carbon nanotubes by physical modification," *Polymer journal*, vol. 40, no. 7, pp. 577-589, 2008.

[159] V. Moore, M. Strano, E. Haroz, " Individually Suspended Single-Walled Carbon Nanotubes in Various Surfactants," *Nano Letters,* vol. 3, pp. 1379-1382, 2003.

[160] V. Krstic, G. S. Duesberg, J. Muster, M. Burghard, S. Roth, "Langmuir− Blodgett films of matrix-diluted single-walled carbon nanotubes," *Chemistry of Materials*, vol. 10, no. 9, pp. 2338-2340, 1998.

[161] S. Bandow, A. Rao, K. Williams, A. Thess, R. Smalley, P. Eklund, "Purification of single-wall carbon nanotubes by microfiltration," *The Journal of Physical Chemistry B*, vol. 101, no. 44, pp. 8839-8842, 1997.

[162] E. T. Thostenson, C. Li, T. W. Chou, "Nanocomposites in context," *Composites science and technology*, vol. 65, no. 3-4, pp. 491-516, 2005.

[163] M. Moniruzzaman, K. Winey, "Polymer nanocomposites containing carbon nanotubes," *Macromolecules*, vol. 39, no. 16, pp. 5194-5205, 2006.

[164] J. N. Coleman, U. Khan, W. J. Blau, Y. Gunko, "Small but strong: a review of the mechanical properties of carbon nanotube–polymer composites," *Carbon*, vol. 44, no. 9, pp. 1624-1652, 2006.

[165] P. C. Ma, N. A. Siddiqui, G. Marom, J. K. Kim, "Dispersion and functionalization of carbon nanotubes for polymer-based nanocomposites: a review," *Composites Part A: Applied Science and Manufacturing*, vol. 41, no. 10, pp. 1345-1367, 2010.

[166] A. Gurses, *Introduction to polymer-clay nanocomposites*. Pan Stanford, 2019.

[167] L. C. Tang, L. Zhao, F. Qiang, Q. Wu, L. X. Gong, J. P. Peng, "Mechanical Properties of Rubber Nanocomposites Containing Carbon Nanofillers," *Carbon-Based Nanofiller and Their Rubber Nanocomposites*, pp. 367-423, 2019.

[168] A. V. Rane, K. Kanny, V. Abitha, S. Thomas, "Methods for synthesis of nanoparticles and fabrication of nanocomposites," *Synthesis of inorganic nanomaterials*, pp. 121-139, 2018.

[169] A. M. Díez-Pascual, M. Naffakh, J. M. González-Domínguez, A. Ansón, Y. Martínez-Rubi, M. T. Martínez, B. Simard, M. A. Gómez, "High performance PEEK/carbon nanotube composites compatibilized with polysulfones-I. Structure and thermal properties," *Carbon*, vol. 48, no. 12, pp. 3485-3499, 2010.

[170] M. Loos, "Chapter 6-Processing of Polymer Matrix Composites Containing CNTs," pp. 171-188, 2015.

[171] K. Lau, M. Lu, C. Lam, H. Cheung, F. Sheng, H. Li, "Thermal and mechanical properties of single-walled carbon nanotube bundle-reinforced epoxy nanocomposites: the role of solvent for nanotube dispersion," *Composites Science and Technology*, vol. 65, no. 5, pp. 719-725, 2005.

[172] P. Saini, "Electrical properties and electromagnetic interference shielding response of electrically conducting thermosetting nanocomposites," *Thermoset Nanocomposites*, 2013.

[173] M. L. De La Chapelle, C. Stephan, T. Nguyen, S. Lefrant, C. Journet, P. Bernier, E. Munoz, A. Benito, W. Maser, M. J. Martinez, "Raman characterization of singlewalled carbon nanotubes and PMMA-nanotubes composites," *Synthetic Metals*, vol. 103, no. 1-3, pp. 2510-2512, 1999.

[174] J. Benoit, B. Corraze, S. Lefrant, W. Blau, P. J. Bemier, "Transport properties of PMMA-carbon nanotubes composites," *Pascal and Francis Bibliographic Databases*, vol. 121, no. 1-3, pp. 1215-1216, 2001.

[175] A. B. Dalton, S. Collins, E. Munoz, J. M. Razal, V. H. Ebron, J. P. Ferraris, J. N. Coleman, B. G. Kim, R. Baughman, "Super-tough carbon-nanotube fibres," *Nature*, vol. 423, no. 6941, pp. 703-703, 2003.

[176] F. Du, J. E. Fischer, K. Winey, "Coagulation method for preparing single-walled carbon nanotube/poly (methyl methacrylate) composites and their modulus, electrical conductivity, and thermal stability," *Journal of Polymer Science Part B*, vol. 41, no. 24, pp. 3333-3338, 2003.

[177] K. Kim, "Thermal Conductivity Improvement of PEEK/ZrO2 Coated MWCNT Nanocomposites." *Advances in Nanocomposites*, 2011.

[178] E. Rashidi, H. Rezaie, H. J. Ghassai, "The effect of carbon nanotube addition on the mechanical properties and biological functionality of poly-ether-ether-ketone–hydroxyapatite composites," *Polymer Composites*, 2021.

[179] R. Na, J. Liu, G. Wang, S. J. Zhang, "Light weight and flexible poly (ether ether ketone) based composite film with excellent thermal stability and mechanical properties for wide-band electromagnetic interference shielding," *RSC advances*, vol. 8, no. 6, pp. 3296-3303, 2018.

[180] L. Lin, Y. Han, X. Zhao, Y. Wang, H. Zhang, Z. Jiang, Z. J. Chen, "Effectively improving the performance of MWNT/PEEK composite by choosing PAK-Cz as the solubilizer," *High Performance Polymers*, vol. 31, no. 8, pp. 875-884, 2019.

[181] Y. Du, N. Hu, H. Zhou, P. Li, P. Zhang, X. Zhao, G. Dang, C. J. Chen, "Dispersion of multi-walled carbon nanotubes in poly (aryl ether ketone) obtained by in situ polymerization," *Polymer*, vol. 58, no. 7, pp. 832-837, 2009.

[182] S. H. Modi, K. B. Dikovics, H. Gevgilili, G. Mago, S. F. Bartolucci, F. T. Fisher, D. M. Kalyon, "Nanocomposites of poly (ether ether ketone) with carbon nanofibers: Effects of dispersion and thermo-oxidative degradation on development of linear viscoelasticity and crystallinity," *Polymer*, vol. 51, no. 22, pp. 5236-5244, 2010.

[183] V. Tishkova, P.-I. Raynal, P. Puech, A. Lonjon, M. Le Fournier, P. Demont, E. Flahaut, W. J. C. S. Bacsa, "Electrical conductivity and Raman imaging of double wall carbon nanotubes in a polymer matrix," *Composites Science and Technology*, vol. 71, no. 10, pp. 1326-1330, 2011.

[184] C. Han, M. Chi, Y. Zheng, L. Jiang, C. Xiong, L. Zhang, "Mechanical properties and bioactivity of high-performance poly (etheretherketone)/carbon nanotubes/bioactive glass biomaterials," vol. 20, no. 8, pp. 1-8, 2013.

[185] Y. Hwang, M. Kim, J. Kim, "Improvement of the mechanical properties and thermal conductivity of poly (ether-ether-ketone) with the addition of graphene oxide-carbon nanotube hybrid fillers," *Composites Part A: Applied Science and Manufacturing*, vol. 55, pp. 195-202, 2013.

[186] M. Bryning, D. Milkie, M. Islam, J. Kikkawa, A. J. Yodh, "Thermal conductivity and interfacial resistance in single-wall carbon nanotube epoxy composites," *AIP Applied Physics Letters*, vol. 87, no. 16, p. 161909, 2005.

[187] D. Carroll, P. Redlich, P. Ajayan, J. Charlier, X. Blase, A. De Vita, R. J. Car, "Electronic structure and localized states at carbon nanotube tips," *Physical Review Letters*, vol. 78, no. 14, pp. 2811, 1997.

[188] P. Verma, P. Saini, V. J. Choudhary, "Designing of carbon nanotube/polymer composites using melt recirculation approach: Effect of aspect ratio on mechanical, electrical and EMI shielding response," *Materials & Design*, vol. 88, pp. 269-277, 2015.

[189] C. A. Cooper, D. Ravich, D. Lips, J. Mayer, H. Wagner, "Distribution and alignment of carbon nanotubes and nanofibrils in a polymer matrix," *Composites Science and Technology*, vol. 62, no. 7-8, pp. 1105-1112, 2002.

[190] O. Meincke, D. Kaempfer, H. Weickmann, C. Friedrich, M. Vathauer, H. J. Warth, "Mechanical properties and electrical conductivity of carbon-nanotube filled polyamide-6 and its blends with acrylonitrile/butadiene/styrene," *Polymer*, vol. 45, no. 3, pp. 739-748, 2004.

[191] Z. Jin, K. Pramoda, G. Xu, S. Goh, "Dynamic mechanical behavior of melt-processed multi-walled carbon nanotube/poly (methyl methacrylate) composites," *Chemical Physics Letters*, vol. 337, no. 1-3, pp. 43-47, 2001.

[192] W. Tang, M. H. Santare, S. Advani, "Melt processing and mechanical property characterization of multi-walled carbon nanotube/high density polyethylene (MWNT/HDPE) composite films," *Carbon*, vol. 41, no. 14, pp. 2779-2785, 2003.

[193] R. Andrews, D. Jacques, D. Qian, T. Rantell, "Multiwall carbon nanotubes: synthesis and application," *Accounts of Chemical Research*, vol. 35, no. 12, pp. 1008-1017, 2002

[194] A. R. Bhattacharyya, T. Sreekumar, T. Liu, S. Kumar, L. M. Ericson, R. H. Hauge, R. E. Smalley, "Crystallization and orientation studies in polypropylene/single wall carbon nanotube composite," *Polymer*, vol. 44, no. 8, pp. 2373-2377, 2003.

[195] R. Ma, B. Zhu, Q. Zeng, P. Wang, Y. Wang, C. Liu, C. J. Shen, "Melt-processed poly (ether ether ketone)/carbon nanotubes/montmorillonite nanocomposites with enhanced mechanical and thermomechanical properties," *Materials*, vol. 12, no. 3, pp. 525, 2019.

[196] M. N. Uddin, P. S. Dhanasekaran, R. Asmatulu, "Mechanical properties of highly porous PEEK bionanocomposites incorporated with carbon and hydroxyapatite nanoparticles for scaffold applications," *Progress in biomaterials*, vol. 8, no. 3, pp. 211-221, 2019.

[197] D. Bangarusampath, H. Ruckdäschel, V. Altstädt, J. K. Sandler, D. Garray, M. Shaffer, "Rheology and properties of melt-processed poly (ether ether ketone)/multi-wall carbon nanotube composites," *Polymer*, vol. 50, no. 24, pp. 5803-5811, 2009.

[198] F. Deng, T. Ogasawara, N. Takeda, "Tensile properties at different temperature and observation of micro deformation of carbon nanotubes–poly (ether ether ketone) composites," *Composites Science and Technology*, vol. 67, no. 14, pp. 2959-2964, 2007.

[199] A. Diez-Pascual, M. Naffakh, M. Gómez, C. Marco, G. Ellis, J. Gonzalez-Dominguez, A. Ansón, M. Martinez, Y. Martinez-Rubi, B. J. Simard, "The influence of a compatibilizer on the thermal and dynamic mechanical properties of PEEK/carbon nanotube composites," *Nanotechnology*, vol. 20, no. 31, pp. 315707, 2009.

[200] D. Bangarusampath, H. Ruckdäschel, V. Altstädt, J. K. Sandler, D. Garray, M. Shaffer, "Rheological and electrical percolation in melt-processed poly (ether ether ketone)/multi-wall carbon nanotube composites," vol. 482, no. 1-3, pp. 105-109, 2009.

[201] J. Li, L. Q. Zhang, "The research on the mechanical and tribological properties of carbon fiber and carbon nanotube-filled PEEK composite," *Polymer composites*, vol. 31, no. 8, pp. 1315-1320, 2010.

[202] A. M. Díez-Pascual, M. Naffakh, J. M. González-Domínguez, A. Ansón, Y. Martínez-Rubi, M. T. Martinez, B. Simard, M. A. Gómez, "High performance PEEK/carbon nanotube composites compatibilized with polysulfones-II. Mechanical and electrical properties," *Carbon*, vol. 48, no. 12, pp. 3500-3511, 2010.

[203] M. Naffakh, A. M. Díez-Pascual, M. Gómez-Fatou, "New hybrid nanocomposites containing carbon nanotubes, inorganic fullerene-like WS_2 nanoparticles and poly (ether ether ketone)(PEEK)," *Journal of Materials Chemistry*, vol. 21, no. 20, pp. 7425-7433, 2011.

[204] T. Tsuda, T. Ogasawara, F. Deng, N. Takeda, "Direct measurements of interfacial shear strength of multi-walled carbon nanotube/PEEK composite using a nano-pullout method," *Composites Science and Technology*, vol. 71, no. 10, pp. 1295-1300, 2011.

[205] A. M. Diez-Pascual, M. Naffakh, C. Marco, G. Ellis, "Rheological and tribological properties of carbon nanotube/thermoplastic nanocomposites incorporating inorganic fullerene-like WS_2 nanoparticles," *The Journal of Physical Chemistry B*, vol. 116, no. 27, pp. 7959-7969, 2012.

[206] Y. J. Lin, S. Qin, B. Han, C. Gao, S. Zhang, "Preparation of poly (ether ether ketone)-based composite with high electrical conductivity, good mechanical properties and thermal stability," *High Performance Polymers*, vol. 29, no. 2, pp. 205-210, 2017.

[207] A. M. Gohn, J. Seo, R. H. Colby, R. P. Schaake, R. Androsch, A. Rhoades, "Crystal nucleation in poly (ether ether ketone)/carbon nanotube nanocomposites at high and low supercooling of the melt," *Polymer*, vol. 199, pp. 122548, 2020.

[208] L. Dai, J. Sun, "Mechanical properties of carbon nanotubes-polymer composites," pp. 155-194, 2016.

[209] A. Wang, H. Xu, Q. Zhou, X. Liu, Z. Li, R. Gao, X. Liu, L. J. Zhang, "Electrochemical performances of a new solid composite polymer electrolyte based on hyperbranched star polymer and ionic liquid for lithium-ion batteries," *Journal of Solid State Electrochemistry*, vol. 21, no. 8, pp. 2355-2364, 2017.

[210] K. Dong, X. Liu, H. Dong, X. Zhang, S. Zhang, "Multiscale studies on ionic liquids," *Chemical reviews*, vol. 117, no. 10, pp. 6636-6695, 2017.

[211] D. M. Correia, L. C. Fernandes, P. M. Martins, C. García-Astrain, C. M. Costa, J. Reguera, S. J. Lanceros-Méndez, "Ionic liquid–polymer composites: a new platform for multifunctional applications," *Advanced Functional Materials*, vol. 30, no. 24, pp. 1909736, 2020.

[212] A. Chapeaux, L. D. Simoni, M. A. Stadtherr, J. Brennecke, E. Data, "Liquid phase behavior of ionic liquids with water and 1-octanol and modeling of 1-octanol/water partition coefficients," *Journal of Chemical & Engineering Data*, vol. 52, no. 6, pp. 2462-2467, 2007.

[213] A. Marciniak, "The solubility parameters of ionic liquids," *International journal of molecular sciences*, vol. 11, no. 5, pp. 1973-1990, 2010.

[214] M. Diedenhofen, F. Eckert, A. Klamt, "Prediction of infinite dilution activity coefficients of organic compounds in ionic liquids using COSMO-RS," *Journal of Chemical & Engineering Data*, vol. 48, no. 3, pp. 475-479, 2003.

[215] S. Spange, D. Keutel, F. Simon, "Approaches to empirical donor-acceptor and polarity-parameters of polymers in solution and at interfaces," *The Journal of Chemical Physics*, vol. 89, pp. 1615-1622, 1992.

[216] S. Zhang, Q. Zhuang, M. Zhang, H. Wang, Z. Gao, J. Sun, J. Yuan, "Poly (ionic liquid) composites," *Chemical Society Reviews*, vol. 49, no. 6, pp. 1726-1755, 2020.

[217] P. Bonhote, A. Dias, N. Papageorgiou, K. Kalyanasundaram, M. Grätzel, "Hydrophobic, highly conductive ambient-temperature molten salts," *Inorganic Chemistry*, vol. 35, no. 5, pp. 1168-1178, 1996.

[218] A. Brandt, J. Gräsvik, J. P. Hallett, T. Welton, "Deconstruction of lignocellulosic biomass with ionic liquids," Green Chemistry, vol. 15, no. 3, pp. 550-583, 2013.

[219] A. A. Shamsuri, S. Jamil, K. J. Abdan, "Processes and Properties of Ionic Liquid-Modified Nanofiller/Polymer Nanocomposites—A Succinct Review," *Processes*, vol. 9, no. 3, pp. 480, 2021.

[220] F. Endres, S. El Abedin, "Air and water stable ionic liquids in physical chemistry," *Physical Chemistry Chemical Physics*, vol. 8, no. 18, pp. 2101-2116, 2006.

[221] T. L. Greaves, C. Drummond, "Protic ionic liquids: properties and applications," *Chemical Reviews*, vol. 108, no. 1, pp. 206-237, 2008.

[222] S. Nazari, S. Cameron, M. B. Johnson, K. Ghandi, "Physicochemical properties of imidazo-pyridine protic ionic liquids," vol. 1, no. 38, pp. 11570-11579, 2013.

[223] D. Irge, "Ionic liquids: A review on greener chemistry applications, quality ionic liquid synthesis and economical viability in a chemical processes," *The Journal of Physical Chemistry*, vol. 5, pp. 74-79, 2016.

[224] K. N. Marsh, J. A. Boxall, R. Lichtenthaler, "Room temperature ionic liquids and their mixtures—a review," *Fluid Phase Equilibria*, vol. 219, no. 1, pp. 93-98, 2004.

[225] G. Yu, D. Zhao, L. Wen, S. Yang, X. Chen, "Viscosity of ionic liquids: Database, observation, and quantitative structure-property relationship analysis," *AIChE Journal*, vol. 58, no. 9, pp. 2885-2899, 2012.

[226] B. Wang, L. Qin, T. Mu, Z. Xue, G. Gao, "Are ionic liquids chemically stable?," *Chemical Reviews*, vol. 117, no. 10, pp. 7113-7131, 2017.

[227] A. Grząbka-Zasadzińska, A. Skrzypczak, S. Borysiak, "The influence of the cation type of ionic liquid on the production of nanocrystalline cellulose and mechanical properties of chitosan-based biocomposites," *Cellulose*, vol. 26, no. 8, pp. 4827-4840, 2019.

[228] Y. Shimizu, Y. Ohte, Y. Yamamura, S. Tsuzuki, K. J. Saito, "Comparative study of imidazolium-and pyrrolidinium-based ionic liquids: thermodynamic properties," *The Journal of Physical Chemistry B*, vol. 116, no. 18, pp. 5406-5413, 2012.

[229] N. Sathitsuksanoh, K. M. Holtman, D. J. Yelle, T. Morgan, V. Stavila, J. Pelton, H. Blanch, B. A. Simmons, A. J. George, "Lignin fate and characterization during ionic liquid biomass pretreatment for renewable chemicals and fuels production," *Green Chemistry*, vol. 16, no. 3, pp. 1236-1247, 2014.

[230] A. Xu, J. Wang, H. J. Wang, "Effects of anionic structure and lithium salts addition on the dissolution of cellulose in 1-butyl-3-methylimidazolium-based ionic liquid solvent systems," *Green Chemistry*, vol. 12, no. 2, pp. 268-275, 2010.

[231] J. Vitz, T. Erdmenger, C. Haensch, U. S. Schubert, "Extended dissolution studies of cellulose in imidazolium based ionic liquids," *Green Chemistry*, vol. 11, no. 3, pp. 417-424, 2009.

[232] S. H. Lee, T. V. Doherty, R. J. Linhardt, J. Dordick, "Ionic liquid-mediated selective extraction of lignin from wood leading to enhanced enzymatic cellulose hydrolysis," *Biotechnology and Bioengineering*, vol. 102, no. 5, pp. 1368-1376, 2009.

[233] K. Ke, P. Pötschke, S. Gao, B. Voit, "An ionic liquid as interface linker for tuning piezoresistive sensitivity and toughness in poly (vinylidene fluoride)/carbon nanotube composites," *ACS Applied Materials & Interfaces*, vol. 9, no. 6, pp. 5437-5446, 2017.

[234] Y. Wang, C. Xing, J. Guan, Y. Li, "Towards flexible dielectric materials with high dielectric constant and low loss: PVDF nanocomposites with both homogenously dispersed CNTs and ionic liquids nanodomains," *Polymers*, vol. 9, no. 11, pp. 562, 2017.

[235] K. Subramaniam, A. Das, D. Steinhauser, M. Klüppel, G. J. Heinrich, "Effect of ionic liquid on dielectric, mechanical and dynamic mechanical properties of multi-walled carbon nanotubes/polychloroprene rubber composites," *European Polymer Journal*, vol. 47, no. 12, pp. 2234-2243, 2011.

[236] K. Sa, P. C. Mahakul, K. K. Nanda, P. Mahanandia, "Effect of ionic liquid functionalized carbon nanotubes on mechanical, thermal and electrical properties of carbon nanotubes-reduced graphene oxide/PMMA nanocomposites," *Chemical Physics Letters*, vol. 706, pp. 76-81, 2018.

[237] A. Mandal, A. Nandi, "Ionic liquid integrated multiwalled carbon nanotube in a poly (vinylidene fluoride) matrix: formation of a piezoelectric β-polymorph with significant reinforcement and

conductivity improvement," *ACS Applied Materials & Interfaces*, vol. 5, no. 3, pp. 747-760, 2013.

[238] X. Lv, C. Liu, D. Wu, S. Song, Z. Shao, S. Sun, "Epoxy-based ionic liquid towards multi-walled carbon nanotubes/polybutylene terephthalate composite with excellent dispersion and conductivity behaviors," *Journal of Polymer Research*, vol. 27, no. 8, pp. 1-9, 2020.

[239] J. Sanes, N. Saurín, F. Carrión, G. Ojados, M. Bermúdez, "Synergy between single-walled carbon nanotubes and ionic liquid in epoxy resin nanocomposites," *Composites Part B: Engineering*, vol. 105, pp. 149-159, 2016.

[240] K. Subramaniam, A. Das, F. Simon, G. Heinrich, "Networking of ionic liquid modified CNTs in SSBR," *European Polymer Journal*, vol. 49, no. 2, pp. 345-352, 2013.

[241] K. Subramaniam, A. Das, G. Heinrich, "Development of conducting polychloroprene rubber using imidazolium based ionic liquid modified multi-walled carbon nanotubes," *Composites Science and Technology*, vol. 71, no. 11, pp. 1441-1449, 2011.

[242] L. Zhao, Y. Li, X. Cao, J. You, W. Dong, "Multifunctional role of an ionic liquid in melt-blended poly (methyl methacrylate)/multi-walled carbon nanotube nanocomposites," *Nanotechnology*, vol. 23, no. 25, p. 255702, 2012.

[243] F. Carrión, C. Espejo, J. Sanes, M. Bermúdez, "Single-walled carbon nanotubes modified by ionic liquid as antiwear additives of thermoplastics," *Composites Science and Technology*, vol. 70, no. 15, pp. 2160-2167, 2010.

[244] M. A. Takassi, A. Zadehnazari, "Green Synthesis of Salicylic Acid-Based Poly (amide-imide) in Ionic Liquid and Composite Formation with Multiwalled Carbon Nanotube," *Polymer-Plastics Technology and Engineering*, vol. 56, no. 12, pp. 1358-1365, 2017.

[245] A. Das, K. Stöckelhuber, R. Jurk, J. Fritzsche, M. Klüppel, G. Heinrich, "Coupling activity of ionic liquids between diene elastomers and multi-walled carbon nanotubes," *Carbon*, vol. 47, no. 14, pp. 3313-3321, 2009.

[246] J. Abraham, P. Xavier, S. Bose, S. C. George, N. Kalarikkal, S. J. Thomas, "Investigation into dielectric behaviour and electromagnetic interference shielding effectiveness of conducting styrene butadiene rubber composites containing ionic liquid modified MWCNT," *Polymer*, vol. 112, pp. 102-115, 2017.

[247] L. Liu, Z. Zheng, C. Gu, X. Wang, "The poly (urethane-ionic liquid)/multi-walled carbon nanotubes composites," *Composites Science and Technology*, vol. 70, no. 12, pp. 1697-1703, 2010.

[248] M. Sharma, S. Sharma, J. Abraham, S. Thomas, G. Madras, S. Bose, "Flexible EMI shielding materials derived by melt blending PVDF and ionic liquid modified MWNTs," *Materials Research Express*, vol. 1, no. 3, pp. 035003, 2014.

[249] R. Meira, D. M. Correia, S. Ribeiro, P. Costa, A. C. Gomes, F. Gama, S. Lanceros-Méndez, C. J. Ribeiro, "Ionic-liquid-based electroactive polymer composites for muscle tissue engineering," *ACS Applied Polymer Materials*, vol. 1, no. 10, pp. 2649-2658, 2019.

[250] H. P. Bloch, C. Soares, *Process plant machinery*. Elsevier, 1998.

[251] N. Tabassi, M. Moghbeli, I. Ghasemi, "Thermoplastic starch/cellulose nanocrystal green composites prepared in an internal mixer," *Iranian Polymer Journal*, vol. 25, no. 1, pp. 45-57, 2016.

[252] H. Y. Kordkheili, M. Farsi, Z. Rezazadeh, "Physical, mechanical and morphological properties of polymer composites manufactured from carbon nanotubes and wood flour," *Composites Part B: Engineering*, vol. 44, no. 1, pp. 750-755, 2013.

[253] Y. Nakaramontri, C. Kummerlöwe, C. Nakason, N. Vennemann, "The effect of surface functionalization of carbon nanotubes on properties of natural rubber/carbon nanotube composites," *Polymer*, vol. 36, no. 11, pp. 2113-2122, 2015.

[254] R. Salehiyan, M. Nofar, S. S. Ray, V. Ojijo, "Kinetically controlled localization of carbon nanotubes in polylactide/poly (vinylidene fluoride) blend nanocomposites and their influence on electromagnetic interference shielding, electrical conductivity, and rheological properties," *The Journal of Physical Chemistry C*, vol. 123, no. 31, pp. 19195-19207, 2019.

[255] V. Romhányi, D. Kun, B. Pukánszky, "Correlations among miscibility, structure, and properties in thermoplastic polymer/lignin blends," *ACS Sustainable Chemistry & Engineering*, vol. 6, no. 11, pp. 14323-14331, 2018.

[256] T. I. Hamad, M. M. Jassim, "Assessment of (PEEK) Composite as A Dental Implant (in Vitro Physical Properties)," *Indian Journal of Forensic Medicine*, vol. 13, no. 4, 2019.

[257] Y. Shih, M. Chou, H. Lian, L. Hsu, S. Chen-Wei, "Highly transparent and impact-resistant PMMA nanocomposites reinforced by cellulose nanofibers of pineapple leaves modified by eco-friendly methods," *Express Polymer Letters*, vol. 12, no. 9, pp. 844-854, 2018.

[258] M. Remanan, M. Kannan, R. S. Rao, S. Bhowmik, L. Varshney, M. Abraham, K. J. Jayanarayanan, O. Polymers, "Microstructure development, wear characteristics and kinetics of thermal decomposition of hybrid nanocomposites based on poly aryl ether ketone, boron carbide and multi walled carbon nanotubes," *Journal of Inorganic and Organometallic Polymers and Materials*, vol. 27, no. 6, pp. 1649-1663, 2017.

[259] G. C. Vasconcelos, R. L. Mazur, B. Ribeiro, E. C. Botelho, M. Costa, "Evaluation of decomposition kinetics of poly (ether-ether-ketone) by thermogravimetric analysis," *Materials Research*, vol. 17, pp. 227-235, 2014.

[260] P. Rajeshwari, T. Dey, "Thermogravimetric kinetics of degradation of HDPE based MWCNTs reinforced composites," *International Journal of Plastics Technology*, vol. 18, no. 2, pp. 294-320, 2014.

[261] S. A. Al-Bayaty, R. A. Al-Uqaily, N. Jubier, "Using the Coats-Redfern Method during Thermogravimetric Analysis and Differential Scanning Calorimetry Analysis of the Thermal Stability of Epoxy and Epoxy/Silica Nanoparticle Nanocomposites," J*ournal of Southwest Jiaotong*, vol. 55, no. 4, 2020.

[262] J. Li, H. Wang, Z. H. Li, T. T. Zhao, T. T. Wang, R. N. Wang, B. W. Cao, X. L. Zhang, W. Zheng, L. B. Li, "Study on Thermal Degradation and Kinetic of Microencapsulated Red Phosphorus (MRP)/High Density Polyethylene (HDPE) Composite," *Key Engineering Materials*, vol. 842, pp. 98-104, 2020.

[263] M. K. Pitchan, S. Bhowmik, M. Balachandran, M. Abraham, "Effect of surface functionalization on mechanical properties and decomposition kinetics of high performance polyetherimide/MWCNT nano composites," *Composites Part A: Applied Science and Manufacturing*, vol. 90, pp. 147-160, 2016.

[264] H. Mahmood, M. Moniruzzaman, T. Iqbal, S. Yusup, "Effect of ionic liquids pretreatment on thermal degradation kinetics of agro-industrial waste reinforced thermoplastic starch composites," *Journal of Molecular Liquids*, vol. 247, pp. 164-170, 2017.

[265] X. Xiong, J. Wang, H. Jia, E. Fang, L. Ding, "Structure, thermal conductivity, and thermal stability of bromobutyl rubber nanocomposites with ionic liquid modified graphene oxide," *Polymer Degradation and Stability*, vol. 98, no. 11, pp. 2208-2214, 2013.

[266] Z. Kovacevic, S. Bischof, M. Fan, "The influence of Spartium junceum L. fibres modified with montmorrilonite nanoclay on the thermal properties of PLA biocomposites," *Composites Part B: Engineering*, vol. 78, pp. 122-130, 2015.

[267] A. W. Coats, J. Redfern, "Kinetic parameters from thermogravimetric data," *Nature*, vol. 201, no. 4914, pp. 68-69, 1964.

[268] A. Broido, "A simple, sensitive graphical method of treating thermogravimetric analysis data," *Journal of Polymer Science Part A-2: Polymer Physics*, vol. 7, no. 10, pp. 1761-1773, 1969.

[269] H. H. Horowitz, G. J. Metzger, "A new analysis of thermogravimetric traces," *Analytical Chemistry*, vol. 35, no. 10, pp. 1464-1468, 1963.

[270] M. Ambika, N. Nagaiah, K. Prashantha, "Thermal resistance and mechanical stability of tungsten oxide filled polymer composite radiation shields," *International Journal of Polymer Analysis and Characterization*, vol. 25, no. 6, pp. 431-443, 2020.

[271] M. Soheilmoghaddam, P. Pasbakhsh, M. U. Wahit, H. C. Bidsorkhi, R. H. Pour, W. T. Whye, and R. T. De Silva, "Regenerated cellulose nanocomposites reinforced with exfoliated graphite nanosheets using BMIMCL ionic liquid," *Polymer*, vol. 55, no. 14, pp. 3130-3138, 2014.

[272] J. H. Lee, S. H. Park, S. H. Kim, H. Ito, "Replication and surface properties of micro injection molded PLA/MWCNT nanocomposites," *Polymer Testing*, vol. 83, pp. 106321, 2020.

[273] S. Lal, V. Kumar, S. J. Arora, "Eco-friendly synthesis of biodegradable and high strength ternary blend films of PVA/starch/pectin: Mechanical, thermal and biodegradation studies," *Polymers and Polymer Composites*, pp. 0967391120972881, 2020.

[274] M. I. Khan, H. U. Khan, K. Azizli, S. Sufian, Z. Man, A. A. Siyal, N. Muhammad, M. Rehman, "The pyrolysis kinetics of the conversion of Malaysian kaolin to metakaolin," *Applied Clay Science*, vol. 146, pp. 152-161, 2017.

[275] V. K. Rangari, G. M. Mohammad, S. Jeelani, Y. V. Butenko, V. Dhanak, "Synthesis and characterization of diamond-coated CNTs and their reinforcement in Nylon-6 single fiber," *ACS Applied Materials & Interfaces*, vol. 2, no. 7, pp. 1829-1834, 2010.

[276] L. Gomez-Coma, A. Garea, A. Irabien, "Hybrid solvent ([emim][Ac]+ water) to improve the CO_2 capture efficiency in a PVDF hollow fiber contactor," *ACS Sustainable Chemistry & Engineering*, vol. 5, no. 1, pp. 734-743, 2017.

[277] L. Gomez-Coma, A. Garea, J.-C. Rouch, T. Savart, J.-F. Lahitte, J.-C. Remigy, A. J. Irabien, "Membrane modules for CO_2 capture based on PVDF hollow fibers with ionic liquids immobilized," *Journal of Membrane Science*, vol. 498, pp. 218-226, 2016.

[278] D. M. Correia, C. M. Costa, E. Lizundia, R. Sabater i Serra, J. A. Gómez-Tejedor, L. T. Biosca, J. M. Meseguer-Dueñas, J. L. Gomez Ribelles, S. J. Lanceros-Méndez, "Influence of cation and anion type on the formation of the electroactive β-phase and thermal and dynamic mechanical properties of poly (vinylidene fluoride)/ionic liquids blends," *The Journal of Physical Chemistry C*, vol. 123, no. 45, pp. 27917-27926, 2019.

[279] H. Palmgren, "Processing conditions in the batch-operated internal mixer," *Rubber Chemistry and Technology*, vol. 48, no. 3, pp. 462-494, 1975.

[280] P. Freakley, S. Patel, "Internal mixing: a practical investigation of the flow and temperature profiles during a mixing cycle," *Rubber Chemistry and Technology*, vol. 58, no. 4, pp. 751-773, 1985.

[281] J. Funt, "Rubber mixing," vol. 53, no. 3, pp. 772-779, 1980.

[282] I. Manas-Zloczower, A. Nir, Z. Tadmor, "Dispersive mixing in rubber and plastics," *Rubber Chemistry and Technology*, vol. 57, no. 3, pp. 583-620, 1984.

[283] Z. Tadmor, C. Gogos, "Modeling of processing machines with elementary steps," *Principles of Polymer Processing*: Wiley-Interscience New York, pp. 465-518, 1979.

[284] K. Chen, Q. Tian, C. Tian, G. Yan, F. Cao, S. Liang, X. J. Wang, "Mechanical reinforcement in thermoplastic polyurethane nanocomposite incorporated with polydopamine functionalized graphene nanoplatelet," *Industrial & Engineering Chemistry Research*, vol. 56, no. 41, pp. 11827-11838, 2017.

[285] R. Ajdary, N. Kretzschmar, H. Baniasadi, J. Trifol, J. V. Seppälä, J. Partanen, O. J. Rojas, "Selective Laser Sintering of Lignin-Based Composites," *ACS Sustainable Chemistry & Engineering*, vol. 9, no. 7, pp. 2727-2735, 2021.

[286] A. R. Sanadi, D. F. Caulfield, R. Jacobson, "Agro-fiber thermoplastic composites," pp. 377-401, 1997.

[287] Y. Sun, Y. Ma, L. Wang, F. Wang, Q. Wu, G. Pan, "Physicochemical properties of corn stalk after treatment using steam explosion coupled with acid or alkali," *Carbohydrate Polymers*, vol. 117, pp. 486-493, 2015.

[288] S. Ahtzaz, M. Nasir, L. Shahzadi, W. Amir, A. Anjum, R. Arshad, F. Iqbal, A. A. Chaudhry, M. Yar, M. ur Rehman, "A study on the effect of zinc oxide and zinc peroxide nanoparticles to enhance angiogenesis-pro-angiogenic grafts for tissue regeneration applications," *Materials & Design*, vol. 132, pp. 409-418, 2017.

[289] H. Khalid, H. Iqbal, R. Zeeshan, M. Nasir, F. Sharif, M. Akram, M. Irfan, F. A. Khan, A. A. Chaudhry, A. F. Khan, "Silk fibroin/collagen 3D scaffolds loaded with TiO_2 nanoparticles for skin tissue regeneration," *Polymer Bulletin*, pp. 1-20, 2020.

[290] H. Le, A. Das, S. Basak, M. Tahir, S. Wießner, D. Fischer, U. Reuter, K. Stöckelhuber, A. Bhowmick, Q. J. Do, "Effect of different ionic liquids on the dispersion and phase selective wetting of carbon nanotubes in rubber blends," *Polymer*, vol. 105, pp. 284-297, 2016.

[291] L. V. Sigolaeva, T. V. Bulko, M. S. Kozin, W. Zhang, M. Köhler, I. Romanenko, J. Yuan, F. H. Schacher, D. V. Pergushov, V. Shumyantseva, "Long-term stable poly (ionic liquid)/MWCNTs inks enable enhanced surface modification for electrooxidative detection and quantification of dsDNA," *Polymer*, vol. 168, pp. 95-103, 2019.

[292] X. Zheng, D. Li, C. Feng, X. Chen, "Thermal properties and non-isothermal curing kinetics of carbon nanotubes/ionic liquid/epoxy resin systems," *Thermochimica Acta*, vol. 618, pp. 18-25, 2015.

[293] Y. Ge, Q. Zhang, Y. Zhang, F. Liu, J. Han, C. Wu, "High-performance natural rubber latex composites developed by a green approach using ionic liquid-modified multiwalled carbon nanotubes," *Journal of Applied Polymer Science*, vol. 135, no. 38, pp. 46588, 2018.

[294] W. Du, Y. Jin, S. Lai, L. Shi, Y. Shen, H. J. Yang, "Multifunctional light-responsive graphene-based polyurethane composites with shape memory, self-healing, and flame retardancy properties," *Composites Part A: Applied Science and Manufacturing*, vol. 128, pp. 105686, 2020.

[295] K. Subramaniam, A. Das, L. Haubler, C. Harnisch, K. W. Stockelhuber, G. Heinrich, "Enhanced thermal stability of polychloroprene rubber composites with ionic liquid modified MWCNTs," *Polymer Degradation and Stability*, vol. 97, no. 5, pp. 776-785, 2012.

[296] P. Xu, H. Gui, Y. Hu, A. Bahader, Y. J. Ding, "Dielectric properties of polypropylene-based nanocomposites with ionic liquid-functionalized multiwalled carbon nanotubes," *Journal of Electronic Materials*, vol. 43, no. 7, pp. 2754-2758, 2014.

[297] F. Boyer, P. Olivier, F. Pons, P. Cadaux, "Mechanical and electrical behavior of a peek/carbon nanotubes composite," *ECCM15-15th European conference on composite materials, Venice, Italy*, 2012.

[298] S. Ji, C. Sun, J. Zhao, F. J. Liang, "Comparison and analysis on mechanical property and machinability about polyetheretherketone and carbon-fibers reinforced polyetheretherketone," *Materials*, vol. 8, no. 7, pp. 4118-4130, 2015.

[299] W. Huang, K. Edenzon, L. Fernandez, S. Razmpour, J. Woodburn, P. Cebe, "Nanocomposites of poly (vinylidene fluoride) with multiwalled carbon nanotubes," *Journal of Applied Polymer Science*, vol. 115, no. 6, pp. 3238-3248, 2010.

[300] L. Qiu, Y. Chen, Y. Yang, L. Xu, X. Liu, "A study of surface modifications of carbon nanotubes on the properties of polyamide 66/multiwalled carbon nanotube composites," *Journal of Nanomaterials*, vol. 2013, 2013.

[301] S. Gao, S. Gao, B. Xu, H. J. Yu, "Effects of different pH-values on the nanomechanical surface properties of PEEK and CFR-PEEK compared to dental resin-based materials," *Materials*, vol. 8, no. 8, pp. 4751-4767, 2015.

[302] S. Vidhate, A. Shaito, J. Chung, N. D'Souza, "Crystallization, mechanical, and rheological behavior of polyvinylidene fluoride/carbon nanofiber composites," *Journal of Applied Polymer Science*, vol. 112, no. 1, pp. 254-260, 2009.

[303] T. Fukushima, A. Kosaka, Y. Ishimura, T. Yamamoto, T. Takigawa, N. Ishii, T. J. Aida, "Molecular ordering of organic molten salts triggered by single-walled carbon nanotubes," *Science*, vol. 300, no. 5628, pp. 2072-2074, 2003.

[304] S. Bellayer, J. W. Gilman, N. Eidelman, S. Bourbigot, X. Flambard, D. M. Fox, H. C. De Long, P. C. Trulove, "Preparation of homogeneously dispersed multiwalled carbon nanotube/polystyrene nanocomposites via melt extrusion using trialkyl imidazolium compatibilizer,"*Advanced Functional Materials*, vol. 15, no. 6, pp. 910-916, 2005.

[305] T. J. Simmons, S. H. Lee, J. Miao, M. Miyauchi, T.-J. Park, S. S. Bale, R. Pangule, J. Bult, J. G. Martin, J. S. Dordick, "Preparation of synthetic wood composites using ionic liquids," *Wood Science and Technology*, vol. 45, no. 4, pp. 719-733, 2011.

[306] J. Therattil, K. S. Anil, L. A. Pothan, D. Rouxel, H. J. Maria, N. Kalarikal, S. J. Thomas, "Cure acceleration and plasticizing effect of imidazolium ionic liquid on the properties of natural rubber/carbon nanotube composites," *Functional Composites and Structures*, vol. 2, no. 3, pp. 035003, 2020.

[307] M. Tunckol, E. Z. Hernandez, J.-R. Sarasua, J. Durand, P. Serp, "Polymerized ionic liquid functionalized multi-walled carbon nanotubes/polyetherimide composites," *European Polymer Journal*, vol. 49, no. 12, pp. 3770-3777, 2013.

[308] V. Bugatti, G. Viscusi, A. Di Bartolomeo, L. Iemmo, D. C. Zampino, V. Vittoria, G. J. Gorrasi, "Ionic liquid as dispersing agent of LDH-carbon nanotubes into a biodegradable vinyl alcohol polymer," *Polymers*, vol. 12, no. 2, pp. 495, 2020.

[309] L. T. Trinh, Y. J. Lee, J.-W. Lee, B. Lee, "Characterization of ionic liquid pretreatment and the bioconversion of pretreated mixed softwood biomass," *Biomass and Bioenergy*, vol. 81, pp. 1-8, 2015.

[310] X. Yuan, H. Liu, H. Yu, W. Ding, Y. Li, J. Wang, "High-performance sodium polyacrylate nanocomposites developed by using ionic liquid covalently modified multiwalled carbon nanotubes," *Journal of Applied Polymer Science*, vol. 137, no. 39, pp. 49161, 2020.

[311] S. Arun, S. J. Kanagaraj, "Mechanical characterization and validation of poly (methyl methacrylate)/multi walled carbon nanotube composite for the polycentric knee joint," *Journal of the Mechanical Behavior of Biomedical Materials*, vol. 50, pp. 33-42, 2015.

[312] J. Sonamuthu, S. Samayanan, A. R. Jeyaraman, B. Murugesan, B. Krishnan, S. J. Mahalingam, E. C, Influences of ionic liquid and temperature on the tailorable surface morphology of F-apatite nanocomposites for enhancing biological abilities for orthopedic implantation," *Materials Science and Engineering: C*, vol. 84, pp. 99-107, 2018.

[313] A. I. Frolov, K. Kirchner, T. Kirchner, M. Fedorov, "Molecular-scale insights into the mechanisms of ionic liquids interactions with carbon nanotubes," *Faraday Discussions*, vol. 154, pp. 235-247, 2012.

[314] G. Han, Z. Wang, K. Liu, S. Li, X. Du, W. Du, "Synthesis of CNT-reinforced AZ31 magnesium alloy composites with uniformly distributed CNTs," *Materials Science and Engineering: A*, vol. 628, pp. 350-357, 2015.

[315] C. Xing, J. You, Y. Li, J. Li, "Nanostructured poly (vinylidene fluoride)/ionic liquid composites: formation of organic conductive nanodomains in polymer matrix," *The Journal of Physical Chemistry C*, vol. 119, no. 36, pp. 21155-21164, 2015.

[316] M. P. Scott, C. S. Brazel, M. G. Benton, J. W. Mays, J. D. Holbrey, R. Rogers, "Application of ionic liquids as plasticizers for poly (methyl methacrylate)," *Chemical Communications*, no. 13, pp. 1370-1371, 2002.

[317] C. Xing, J. Guan, Y. Li, J. Li, "Effect of a room-temperature ionic liquid on the structure and properties of electrospun poly (vinylidene fluoride) nanofibers," *ACS Applied Materials & Interfaces*, vol. 6, no. 6, pp. 4447-4457, 2014.

[318] P. Samanta, P. Halder, P. Bahadur, S. Dutta Choudhury, H. Pal, "Effect of ionic liquids as cosurfactants on photoinduced electron transfer in tetronic micelles," *The Journal of Physical Chemistry B*, vol. 122, no. 44, pp. 10190-10201, 2018.

[319] A. Tsurumaki, S. Tajima, T. Iwata, B. Scrosati, H. Ohno, "Evaluation of ionic liquids as novel antistatic agents for polymethacrylates," *Electrochimica Acta*, vol. 248, pp. 556-561, 2017.

[320] P. Chen, F. Xie, F. Tang, T. McNally, "Unexpected plasticization effects on the structure and properties of polyelectrolyte complexed chitosan/alginate materials," *ACS Applied Polymer Materials*, vol. 2, no. 7, pp. 2957-2966, 2020.

[321] Z. Liu, W. Wang, F. J. Stadler, Z.-C. Yan, "Rheology of concentrated polymer/ionic liquid solutions: an anomalous plasticizing effect and a universality in nonlinear shear rheology," *Polymers*, vol. 11, no. 5, pp. 877, 2019.

[322] A. Vashchuk, A. Fainleib, O. Starostenko, D. Grande, "Application of ionic liquids in thermosetting polymers: Epoxy and cyanate ester resins," *Express Polymer Letters*, vol. 12, no. 10, pp. 898-917, 2018.

[323] C. Wong, A. Y. Yap, C. Liew, "The effect of ionic liquid on the development of poly (vinyl alcohol)(PVA)-based ion conductors for electric double layer capacitors application," *Journal of Electroanalytical Chemistry*, vol. 886, pp. 115146, 2021.

[324] R. Mejri, J. Dias, A. Lopes, S. B. Hentati, M. M. Silva, G. Botelho, A. M. De Ferro, J. Esperança, A. Maceiras, J. Laza, "Effect of ionic liquid anion and cation on the physico-chemical properties of poly (vinylidene fluoride)/ionic liquid blends," *European Polymer Journal*, vol. 71, pp. 304-313, 2015.

[325] H. L. Ngo, K. Lecompte, L. Hargens, A. McEwen, "Thermal properties of imidazolium ionic liquids," *Thermochimica Acta*, vol. 357, pp. 97-102, 2000.

[326] D. Kundu, G. Pugazhenthi, T. Banerjee, "Low-to Room-Temperature Dehydrogenation of Dimethylamine Borane Facilitated by Ionic Liquids: Molecular Modeling and Experimental Studies," *Energy & Fuels*, vol. 34, no. 10, pp. 13167-13178, 2020.

[327] J. Song, H. Shi, Z. Liao, S. Wang, Y. Liu, W. Liu, Z. Peng, "Study on the Nanomechanical and Nanotribological Behaviors of PEEK and CFRPEEK for Biomedical Applications," *Polymers*, vol. 10, no. 2, pp. 142, 2018.

[328] M. Yousfi, S. Livi, J. Duchet-Rumeau, "Ionic liquids: A new way for the compatibilization of thermoplastic blends," *Chemical Engineering Journal*, vol. 255, pp. 513-524, 2014.

[329] L. Zhou, F. Pan, S. Zeng, Q. Li, L. Bai, Y. Liu, Y. J. Nie, "Ionic liquid assisted fabrication of cellulose-based conductive films for Li-ion battery," *Journal of Applied Polymer Science*, vol. 137, no. 35, pp. 49430, 2020.

[330] A. R. Kim, J. C. Gabunada, D. Yoo, "Amelioration in physicochemical properties and single cell performance of sulfonated poly (ether ether ketone) block copolymer composite membrane using sulfonated carbon nanotubes for intermediate humidity fuel cells," *International Journal of Energy Research*, vol. 43, no. 7, pp. 2974-2989, 2019.

[331] J. Pernak, F. Walkiewicz, M. Maciejewska, M. Zaborski, "Ionic liquids as vulcanization accelerators," *Industrial & Engineering Chemistry Research*, vol. 49, no. 10, pp. 5012-5017, 2010

[332] C. Yang, J. Xu, Y. Xing, S. Hao, Z. Ren, "Covalent polymer functionalized graphene oxide/poly (ether ether ketone) composites for fused deposition modeling: improved mechanical and tribological performance," *RSC Advances*, vol. 10, no. 43, pp. 25685-25695, 2020.

[333] G. Sahu, M. Das, C. Sethy, R. Wazalwar, C. N. Kundu, A. M. Raichur, J. Tripathy, and Physics, "Ionic liquid-assisted fabrication of poly (vinyl alcohol)/nanosilver/graphene oxide composites and their cytotoxicity/antimicrobial activity," *Materials Chemistry and Physics*, vol. 266, pp. 124524, 2021.

[334] D. Correia, L. Fernandes, N. Pereira, J. Barbosa, J. Serra, R. Pinto, C. Costa, and S. Lanceros-Méndez, "All printed soft actuators based on ionic liquid/polymer hybrid materials," *Applied Materials Today*, vol. 22, pp. 100928, 2021.

[335] I. Vázquez-Fernández, A. Bouzina, M. Raghibi, L. Timperman, J. Bigarré, M. Anouti, "Influence of hydrophilic/hydrophobic protic ionic liquids (PILs) on the poly (vinylidene fluoride)(PVDF-ionic liquid) membrane properties," *Journal of Materials Science*, vol. 55, no. 35, pp. 16697-16717, 2020.

[336] K. Park, J. Xanthos, "Ionic liquids as plasticizers/lubricants for polylactic acid," *Polymer Engineering & Science*, vol. 50, no. 6, pp. 1105-1110, 2010.

[337] H. Ruan, Q. Zhang, W. Liao, Y. Li, X. Huang, X. Xu, S. J. Lu, "Enhancing tribological, mechanical, and thermal properties of polyimide composites by the synergistic effect between graphene and ionic liquid," *Materials & Design*, vol. 189, pp. 108527, 2020.

[338] H. Le, S. Wießner, A. Das, D. Fischer, M. Auf der Landwehr, Q. Do, K.-W. Stöckelhuber, G. Heinrich, H.-J. Radusch, "Selective wetting of carbon nanotubes in rubber compounds–Effect of the ionic liquid as dispersing and coupling agent," *European Polymer Journal*, vol. 75, pp. 13-24, 2016.

[339] C. Xing, M. Zhao, L. Zhao, J. You, X. Cao, Y. Li, "Ionic liquid modified poly (vinylidene fluoride): crystalline structures, miscibility, and physical properties," *Polymer Chemistry*, vol. 4, no. 24, pp. 5726-5734, 2013.

[340] B. I. Oladapo, S. Zahedi, "Improving bioactivity and strength of PEEK composite polymer for bone application," *Materials Chemistry and Physics*, vol. 266, pp. 124485, 2021.

[341] F. Zarif, S. Tabassum, A. Jamal, U. Gul, M. A. Gilani, F. Sharif, S. Zahid, A. Asif, A. A. Chaudhry, I. Rehman, "Surface-grafted remedial hydroxyapatite nanoparticles to avoid operational infections," *Monatshefte für Chemie - Chemical Monthly*, vol. 150, no. 4, pp. 605-615, 2019.

[342] F. Zarif, F. Sharif, M. Batool, A. Haider, U. Gul, M. A. Gilani, A. Idrees, S. J. Tabassum, "Enhanced Surface Properties of Hydroxyapatite by Grafting Tartaric Acid for Sustained Release of Moxifloxacin," *ChemistrySelect*, vol. 4, no. 14, pp. 4105-4111, 2019.

[343] H. El-Maghraby, O. Gedeon, D. Rohanova, Y. Greish, "Compressive strength and preliminary in vitro evaluation of gypsum and gypsum–polymer composites in protein-free SBF at 37° C," *Ceramics International*, vol. 36, no. 5, pp. 1561-1569, 2010.

[344] F. Sharif, S. Roman, A. Asif, G. Gigliobianco, S. Ghafoor, M. Tariq, S. A. Siddiqui, F. Mahmood, N. Muhammad, I. Rehman, "Developing a synthetic composite membrane for cleft palate repair," *Journal of Tissue Engineering and Regenerative Medicine*, vol. 13, no. 7, pp. 1178-1189, 2019.

[345] Z. Tayyab, S. Z. Safi, A. Rahim, A. S. Khan, F. Sharif, Z. U. H. Khan, F. Rehman, Z. Ullah, J. Iqbal, N. Muhammad, Polymer Edition, "Preparation of cellulosic Ag-nanocomposites using an ionic liquid," *Journal of Biomaterials Science, Polymer Edition*, vol. 30, no. 9, pp. 785-796, 2019.

[346] B. Iqbal, N. Muhammad, A. Rahim, F. Iqbal, F. Sharif, S. Z. Safi, A. S. Khan, G. Gonfa, M. Uroos, I. Rehman, "Development of collagen/PVA composites patches for osteochondral defects using a green processing of ionic liquid," *International Journal of Polymeric Materials and Polymeric Biomaterials*, vol. 68, no. 10, pp. 590-596, 2019.

[347] M. Sabir, A. Ali, U. Siddiqui, N. Muhammad, A. S. Khan, F. Sharif, F. Iqbal, A. T. Shah, A. Rahim, I. Rehman, Polymer Edition, "Synthesis and characterization of cellulose/hydroxyapatite based dental restorative composites," *Journal of Biomaterials Science, Polymer Edition*, vol. 31, no. 14, pp. 1806-1819, 2020.

[348] E. Nejati, H. Mirzadeh, M. Zandi, "Synthesis and characterization of nano-hydroxyapatite rods/poly (l-lactide acid) composite scaffolds for bone tissue engineering," *Composites Part A: Applied Science and Manufacturing*, vol. 39, no. 10, pp. 1589-1596, 2008.

[349] B. Hahn, D. Park, J. Choi, J. Ryu, W. Yoon, J. Choi, J. Kim, C. Ahn, H. Kim, B. Yoon, "Osteoconductive hydroxyapatite coated PEEK for spinal fusion surgery," *Applied Surface Science*, vol. 283, pp. 6-11, 2013.

[350] B. Palai, S. Mohanty, S. Nayak, "Synergistic effect of polylactic acid (PLA) and Poly (butylene succinate-co-adipate)(PBSA) based sustainable, reactive, super toughened eco-composite blown films for flexible packaging applications," *Polymer Testing*, vol. 83, pp. 106130, 2020.

[351] Y. F. Shih, "Thermal degradation and kinetic analysis of biodegradable PBS/multiwalled carbon nanotube nanocomposites," *Journal of Polymer Science Part B: Polymer Physics*, vol. 47, no. 13, pp. 1231-1239, 2009.

[352] S. Oza, H. Ning, I. Ferguson, N. Lu, "Effect of surface treatment on thermal stability of the hemp-PLA composites: correlation of activation energy with thermal degradation," *Composites Part B: Engineering*, vol. 67, pp. 227-232, 2014.

[353] J. H. Lee, S. H. Park, S. Kim, "Surface alkylation of cellulose nanocrystals to enhance their compatibility with polylactide," *Polymers*, vol. 12, no. 1, pp. 178, 2020.

[354] F. Xie, B. M. Flanagan, M. Li, R. W. Truss, P. J. Halley, M. J. Gidley, T. McNally, J. L. Shamshina, R. D. Rogers, "Characteristics of starch-based films with different amylose contents plasticised by 1-ethyl-3-methylimidazolium acetate," *Carbohydrate Polymers*, vol. 122, pp. 160-168, 2015.

[355] B. Zhang, F. Xie, T. Zhang, L. Chen, X. Li, R. W. Truss, P. J. Halley, J. L. Shamshina, T. McNally, R. D. Rogers, "Different characteristic effects of ageing on starch-based films plasticised by 1-ethyl-3-methylimidazolium acetate and by glycerol," *Carbohydrate Polymers*, vol. 146, pp. 67-79, 2016.

[356] H. Mahmood, M. Moniruzzaman, S. Yusup, H. Akil, "Ionic liquid pretreatment at high solids loading: A clean approach for fabrication of renewable resource based particulate composites," *Polymer Composites*, vol. 39, no. 6, pp. 1994-2003, 2018.

[357] F. Ren, J. Wang, F. Xie, K. Zan, S. Wang, S. J. Wang, "Applications of ionic liquids in starch chemistry: A review," *Green Chemistry*, vol. 22, no. 7, pp. 2162-2183, 2020.

[358] F. Yao, J. Zheng, M. Qi, W. Wang, Z. Qi, "The thermal decomposition kinetics of poly (ether-ether-ketone)(PEEK) and its carbon fiber composite," *Thermochimica acta*, vol. 183, pp. 91-97, 1991.

[359] B. Zhang, F. Xie, J. L. Shamshina, R. D. Rogers, T. McNally, D. K. Wang, P. J. Halley, R. W. Truss, S. Zhao, L. Chen, "Facile preparation of starch-based electroconductive films with ionic liquid," *ACS Sustainable Chemistry & Engineering*, vol. 5, no. 6, pp. 5457-5467, 2017.

[360] A. Sankri, A. Arhaliass, I. Dez, A. C. Gaumont, Y. Grohens, D. Lourdin, I. Pillin, A. Rolland-Sabaté, E. Leroy, "Thermoplastic starch plasticized by an ionic liquid," *Carbohydrate Polymers*, vol. 82, no. 2, pp. 256-263, 2010.

[361] H.-C. Jiang, W.-C. Lin, M. Hua, X.-H. Pan, C.-M. Shu, J.-C. Jiang, "Analysis of kinetics of thermal decomposition of melamine blended with phosphorous ionic liquid by green approach," *Journal of Thermal Analysis and Calorimetry*, vol. 131, no. 3, pp. 2821-2831, 2018.

[362] J. Le Bideau, L. Viau, A. Vioux, "Ionogels, ionic liquid based hybrid materials," *Chemical Society Reviews*, vol. 40, no. 2, pp. 907-925, 2011.

[363] E. Leroy, P. Jacquet, G. Coativy, A. laure Reguerre, D. Lourdin, "Compatibilization of starch–zein melt processed blends by an ionic liquid used as plasticizer," *Carbohydrate Polymers*, vol. 89, no. 3, pp. 955-963, 2012.

[364] C. Gai, Y. Dong, T. Zhang, "The kinetic analysis of the pyrolysis of agricultural residue under non-isothermal conditions," *Bioresource Technology*, vol. 127, pp. 298-305, 2013.

[365] R. Markiewicz, A. Klimaszyk, M. Jarek, M. Taube, P. Florczak, M. Kempka, Z. Fojud, S. Jurga, "Influence of Alkyl Chain Length on Thermal Properties, Structure, and Self-Diffusion Coefficients of Alkyltriethylammonium-Based Ionic Liquids," *International Journal of Molecular Sciences*, vol. 22, no. 11, pp. 5935, 2021.

[366] A. T. Hoz, U. G. Brauer, K. M. Miller, "Physicochemical and Thermal Properties for a Series of 1-Alkyl-4-methyl-1, 2, 4-triazolium Bis (trifluoromethylsulfonyl) imide Ionic Liquids," *The Journal of Physical Chemistry B*, vol. 118, no. 33, pp. 9944-9951, 2014.

[367] S. Gopalakrishnan, R. Sujatha, "Comparative thermoanalytical studies of polyurethanes using Coats-Redfern, Broido and Horowitz-Metzger methods," *Der Chemica Sinica*, vol. 2, no. 5, pp. 103-117, 2011.

[368] S. Sankhla, H. H. Sardar, S. J. Neogi, "Greener extraction of highly crystalline and thermally stable cellulose micro-fibers from sugarcane bagasse for cellulose nano-fibrils preparation," *Polymers*, vol. 251, pp. 117030, 2021.

PUBLICATIONS

1. Aqeel Ahmad, Hamayoun Mahmood, Nurlidia Mansor, Tanveer Iqbal, Muhammad Moniruzzaman, “Ionic liquid assisted polyetheretherketone-multiwalled carbon nanotubes nanocomposites: An environmentally friendly approach” Journal of Applied Polymer Science, Wiley, (Q1, Impact Factor = 3.125) (2021)

2. Aqeel Ahmad, Hamayoun Mahmood, Nurlidia Mansor, Tanveer Iqbal, Muhammad Moniruzzaman, “Ionic liquid modified PEEK-MWCNTs nanocomposites with enhanced thermomechanical properties,” Journal of Physics: Conference Series (Q4, Impact Factor = 0.547) (2021)

3. Aqeel Ahmad, Nurlidia Mansor, Hamayoun Mahmood, Tanveer Iqbal, Muhammad Moniruzzaman, “Effect of ionic liquids on thermomechanical properties of polyetheretherketone-multiwalled carbon nanotubes nanocomposites” Journal of Applied Polymer Science, Wiley, (Q1, Impact Factor = 3.125) (2021)

CONFERENCES:

4. Paper presented at (ICACES-2021)” virtually held at University of Engineering and Technology, New Campus, Lahore, Pakistan, Malaysia. Title: Role of Ionic liquid on the mechanical properties of polyetheretherketone-multiwalled carbon nanotubes (PEEK-MWCNTs) nanocomposites.
5. Paper presented at IRTTEC, Kuala Lumpur on September 30, 2020 virtually.
   Title: Ionic liquid modified PEEK-MWCNTs nanocomposites with enhanced thermomechanical properties
   Conference Details: The 1st International Recent Trends in Technology Engineering and Computing Conference 2020 (IRTTEC 2020)
   Journal: Journal of Physics: Conference Series
   Indexing: Scopus

APPENDIX A

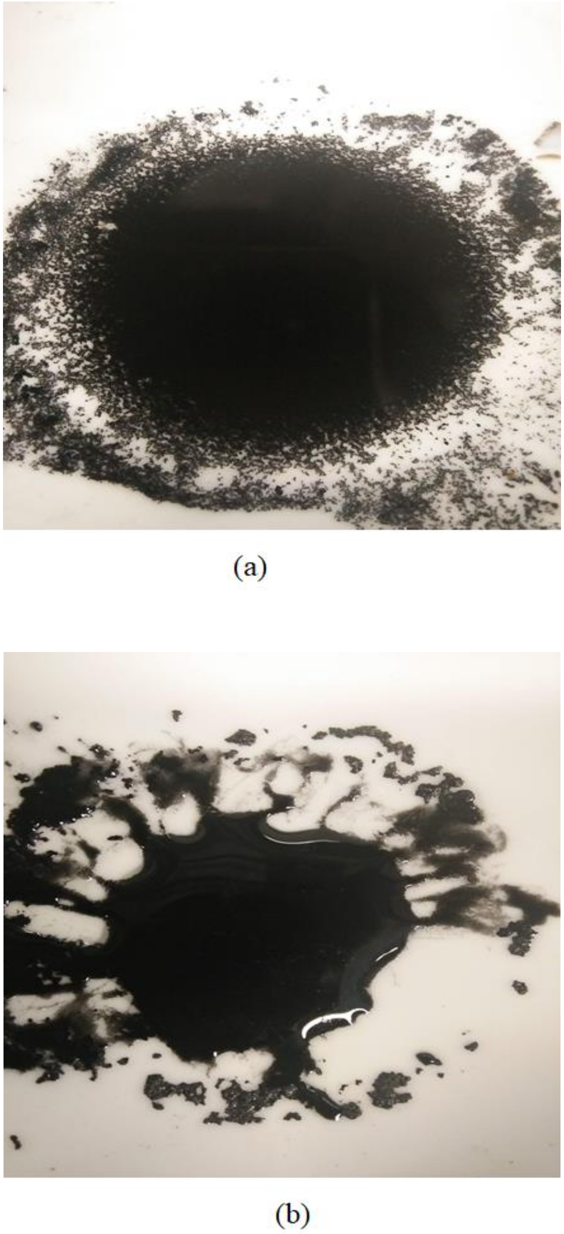

Figure A. 1: (a) DMF-modified MWCNTs (b) IL modified MWCNTs

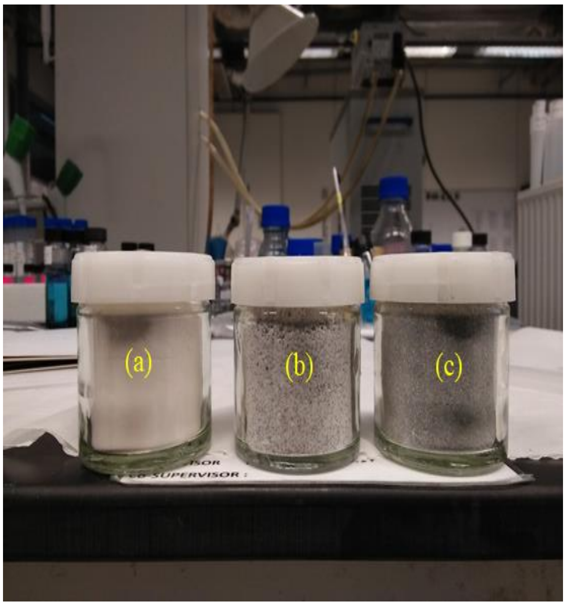

Figure A. 2: (a) Pure PEEK powder (b) PEEK./MWCNTs/DMF (c) PEEK./MWCNTs/IL before melt-blending

Figure A. 3: PEEK composites after heating at 350 ℃ in internal mixer

Figure A. 4: PEEK composites after heating at 390 °C in compression molding

Figure A. 5: PEEK composites for cells viability and cytotoxicity

Table A.1: Literature on mechanical properties of PEEK composites

Authors	Composite Materials	Elastic Modulus	Ref.
Jianfei Cao et al.	PEEK/MWCNTs/BG	6.10	[34]
Chen Liu et al.	PEEK/MWCNTs/HA	6.83	[1]
Bo Wang et al.	PEEK/CNTs	4.9	[226]
Ruixue Ma et al.	PEEK/CNTs/MMT	5.7	[195]
Md. Nizam Uddin et al.	PEEK/CNTs/HA	5.1	[196]

APPENDIX B

Calculations for Coats-Redfern Model

$\ln\left(\frac{-\ln(1-\alpha)}{T^2}\right)$ vs $1000/T$

First of all, calculate α

$$\alpha = \frac{m_0 - m_t}{m_0 - m_f}$$

We are taking only one value for the understanding.

m_o = 100 wt %, m_t = 92 wt % and m_f = 60 wt %

$\alpha = \frac{100-92}{100-60}$

$\alpha = 0.2$

then,

$1 - \alpha = 1 - 0.2 = 0.8$,

ln (1-α) = -0.2231

-ln (1-α) = 0.2231

For T = 580 ℃ = 580 +273.15 =853.15 K

T^2 = 727864.9225

$\frac{1}{T}$ = 0.001172 K

$\frac{1000}{T}$ = 1.172 K

Now,

$\frac{-\ln(1-\alpha)}{T^2}$ = 3.06 × 10^{-7}

$\ln\left(\frac{-\ln(1-\alpha)}{T^2}\right)$ = -14.84

Calculations for Broido Model

$\ln\ln\left(\frac{1}{\alpha}\right)$ vs 1000/T

$$\alpha = \frac{w_t - w_f}{w_0 - w_f}$$

We are taking only one value for the understanding.

w_0 = 93 wt %, w_t = 85 wt % and w_f = 62 wt %

$w_t - w_f = 23$

$w_0 - w_f = 31$

So

α = 0.74

$\frac{1}{\alpha}$ = 1.35

$\ln\left(\frac{1}{\alpha}\right)$ = 0.3

$\ln\ln\left(\frac{1}{\alpha}\right)$ = -1.2

For T = 590 ℃ = 590 +273.15 =863.15 K

T^2 = 744993.3969

$\frac{1}{T}$ = 0.001159 K

$\frac{1000}{T}$ = 1.159 K

Calculations for Horowitz-Metzger Model

$\ln\left\{\ln\left(\frac{w_0}{w_t}\right)\right\}$ vs θ

First of all, calculate $\frac{w_0}{w_t}$

We are taking only one value for the understanding.

w_0 = 93 wt %, w_t = 85 wt %

$\frac{w_0}{w_t}$ = 1.09

$\ln \frac{w_0}{w_t}$ = 0.08617

$\ln\{\ln (\frac{w_0}{w_t})\}$ = -2.4514

For θ,

$\theta = T - T_s$

Take T= 860 K and T_S = 877 K

So,

$\theta = T - T_s$

θ= 860-877 = -17 K